

Cover Page



Universiteit Leiden



The handle <http://hdl.handle.net/1887/29981> holds various files of this Leiden University dissertation

Author: Maaden, Koen van der

Title: Microneedle-mediated vaccine delivery

Issue Date: 2014-12-10

MICRONEEDLE-MEDIATED VACCINE DELIVERY

Koen van der Maaden

The research described in this thesis was performed at the division of Drug Delivery Technology of the Leiden Academic Centre for Drug Research (LACDR), Leiden University, Leiden, the Netherlands.

ISBN/EAN: 978-94-6108-831-4

© 2014, Koen van der Maaden. All rights reserved. No parts of this thesis may be reproduced or transmitted in any form or by any means without permission of the author.

About the cover: The image on the cover shows an electron micrograph of a cutting plane of a microneedle that has been modified with APTES. The round shapes on the microneedle surface are APTES molecules that have been reacted into nanoparticles, which occurs at the intersection of non parallel planes.

Thesis design by: Tim Ruterink

Printed by: Gildeprint

MICRONEEDLE-MEDIATED VACCINE DELIVERY

Proefschrift

ter verkrijging van
de graad van Doctor aan de Universiteit Leiden,
op gezag van Rector Magnificus prof. mr. C.J.J.M. Stolker,
volgens besluit van het College voor Promoties
te verdedigen op woensdag 10 december 2014
klokke 11.15 uur

door

Koen van der Maaden
Geboren te Bergen op Zoom
in 1985

Promotiecommissie

Promotoren:

Prof. Dr. Joke A. Bouwstra

Prof. Dr. Wim Jiskoot

Overige leden:

Dr. A. Moore, University College Cork, Ierland

Dr. Ir. C.W.J.Oomens, Universiteit Eindhoven

Prof. Dr. H.W. Frijlink, Universiteit Groningen

Prof. Dr. W.E. Hennink, Universiteit Utrecht

Prof. Dr. P.H. van der Graaf, Universiteit Leiden

OUTLINE

Chapter 1: General introduction, aim and outline of this thesis	p 7
Chapter 2: Microneedle technologies	p 13
• Microneedle technologies for (trans)dermal drug and vaccine delivery	p 14
Chapter 3: Microneedle pretreatment	p 39
• 3.1- Impact-insertion applicator improves reliability of skin penetration by solid microneedle arrays	p 40
• 3.2- Parameter optimization toward optimal microneedle-based dermal vaccination	p 48
Chapter 4: Coated microneedles	p 65
• 4.1- Fluorescent nanoparticle adhesion assay: a novel method for surface pKa determination of self-assembled monolayers on silicon surfaces	p 66
• 4.2- Nanolayered chemical modification of silicon surfaces with ionizable surface groups for pH-triggered protein adsorption and release: application to microneedles	p 84
• 4.3- Ovalbumin-coated pH-sensitive microneedle arrays effectively induce ovalbumin-specific antibody and T-cell responses in mice	p 104
• 4.4- Chemical modifications of silicon surfaces for the generation of a tunable isoelectric point	p 116
• 4.5- Layer-by-layer assembly of inactivated poliovirus and N-trimethyl chitosan on pH-sensitive microneedles for dermal vaccination	p 130
Chapter 5: Hollow microneedles	p 143
• Novel hollow microneedle technology for depth controlled microinjection-mediated dermal vaccination: a study with polio vaccine in rats	p 144
Chapter 6: Summary, general discussion and conclusion	p 159
Appendix	p 171
• Nederlandse samenvatting	p 172
• Curriculum vitae	p 184
• List of publications	p 185
• Dankwoord	p 186
• Abbreviations	p 188

CHAPTER 1

GENERAL INTRODUCTION,
AIM AND OUTLINE
OF THIS THESIS

GENERAL INTRODUCTION, AIM AND OUTLINE OF THIS THESIS

General introduction

Vaccination

Vaccination is the one of the greatest achievements in medicine. It prevents approximately 6 million deaths per year according to the World Health Organization, and has resulted in high-income countries that infectious diseases are not the most common cause of death anymore [1, 2]. Important pioneers who greatly contributed to the concept of vaccination and its introduction to protect humans against infectious diseases were Edward Jenner (1749-1823) and Louis Pasteur (1822-1895). In 1796 Jenner extracted the content of pustules from a cowpox infected milk maid and injected it in an 8 year old boy. Subsequently, he inoculated this boy with the smallpox virus and the boy did not show any symptoms of the disease. Pasteur introduced the use of live attenuated microorganisms for vaccination. He discovered that pathogenic bacteria became less pathogenic when they were cultured for a few months, while retaining their immunogenicity and thereby their ability to induce protective immunity upon vaccination. Since then vaccination has been highly improved and became available against multiple infectious diseases, such as hepatitis B, diphtheria, pertussis, and poliomyelitis. Moreover, therapeutic vaccines, such as vaccines against cancer and cardiovascular diseases, are under development [3-5].

Despite the efforts and success of vaccination campaigns, in low-income countries infectious diseases still are the main cause of death [6]. Besides, vaccination is very expensive, which is not only because of the production costs. Factors such as transport, cold-chain requirements and the need for trained medical personnel to administer the vaccine contribute to the vaccination costs [7, 8]. Furthermore, vaccination does not always induce sufficient immune responses. For example, despite enormous efforts made during several decades, there are still no effective vaccines available against infectious diseases such as HIV, malaria and tuberculosis. Finally, since most vaccines are administered subcutaneously or intramuscularly by using hypodermic needles, vaccination causes pain, fear and stress in children and their parents, resulting in a reduction of the vaccination coverage [8-10]. To overcome these hurdles alternative minimally-invasive vaccination strategies have been considered and studied. One of the alternative administration routes is the dermal route.

Dermal vaccination

As the skin is constantly challenged by foreign substances such as pathogens trying to enter the body, the skin has evolved into an outstanding protective barrier. The first barrier is the stratum corneum, which is a physical barrier that is impermeable for most compounds. Besides, the skin is immunologically very active and contains specialized cells that prevent incoming pathogens from causing systemic infections. Reversely, the stratum corneum complicates the dermal route for minimally-invasive vaccine delivery [8, 9]. Therefore, it was until the mid 90's that non- and minimally-invasive vaccination *via* the skin, also called dermal vaccination, was first successfully applied. In this study Paul *et al.* obtained high antigen-specific antibody titers against gap junction protein and bovine serum albumin upon topical application of transfersomes in mice [11]. Later, Glen *et al.* confirmed the applicability of the dermal route for non- and minimally-invasive vaccination in mice [12] and in humans [13] by applying cholera toxin-containing formulations onto intact skin. Another method for minimally-invasive dermal vaccination is by using microneedles that were firstly described in 1998 by Henry *et al.* [14].

Microneedles

Microneedles are micron-sized structures with a length of less than 1 mm that are used to deliver a drug, including vaccines, into the skin in a minimally-invasive and potentially pain free manner [9, 15, 16]. Therefore, microneedles could lead to an increased vaccination coverage. Moreover, since microneedles allow self administration of vaccines [8, 9] and can circumvent the cold-chain [17], their use could contribute to a significant reduction of vaccination costs. Finally, dermal vaccination has a dose-sparing potential, as the skin is a potent immune organ. In general, microneedles can be used by four different approaches to deliver a drug into the skin:

1. *'Poke and flow'*. Hollow microneedles are pierced into the skin after which a drug formulation is delivered through the bore of the microneedle.
2. *'Poke and patch'*. Solid microneedles are used to pierce the skin, creating microchannels in the skin. Subsequently, a patch containing a drug formulation is applied onto the microchannels through which a drug can diffuse into the skin.
3. *'Poke and release'*. A drug is encapsulated into dissolving or porous solid microneedles and is released upon piercing them into the skin.
4. *'Coat and poke'*. The microneedle surface is coated with a drug that is released upon piercing of the microneedles into the skin.

Although microneedles have great potential for application in dermal vaccine delivery, microneedles do not always successfully and/or reproducibly pierce the skin and therefore often insertion devices (microneedle applicators) are required. These devices reduce the required insertion forces of skin penetration by microneedles.

Aim and outline of this thesis

The main goals of this research were to:

1. Investigate skin-penetrating ability of microneedles with and without using an applicator;
2. Prepare and characterize nanolayered pH-sensitive surfaces to improve the coating and delivery efficiency of microneedles with vaccines without impairing microneedle sharpness and penetration ability;
3. Fabricate and characterize hollow microneedles for depth controlled microinjections into skin;
4. Evaluate the application of the ‘poke and patch’, the ‘coat and poke’, and the ‘poke and flow’ approach for vaccination in animal studies.

In *Chapter 2* an overview of microneedle technologies for (trans)dermal drug delivery is provided whereby the four ways of drug delivery *via* microneedles with their advantages and disadvantages are described. Furthermore, this chapter describes production methods of microneedles as well as conditions that influence skin penetration. Finally, the use of microneedles for the delivery of vaccines and therapeutic proteins is discussed.

The research described in *Chapter 3* focuses on solid microneedles that are applied by the ‘poke and patch’ method. In *Chapter 3.1* the necessity of an impact-insertion applicator was tested for reproducible microneedle insertion of high-density microneedle arrays into the skin. *Chapter 3.2* describes different types of solid microneedles that were evaluated for their ability to pierce the stratum corneum and to deliver a model vaccine, ovalbumin, into the skin. Subsequently, mice were vaccinated with ovalbumin to investigate the induction of antigen-specific IgG responses upon the application of the different microneedle arrays. Moreover, the effect of several parameters, such as the effect of an impact-insertion applicator, the microneedle application area, site of microneedle application, and the delivered antigen dose, on the antibody responses was investigated to optimize microneedle-based immunization.

Chapter 4 describes a novel method to coat solid microneedle arrays that are modified with pH-sensitive groups. To this end, first a novel surface characterization tool was developed for determining the pK_a of modified silicon surfaces by using fluorescently labeled nanoparticles, as described in *Chapter 4.1*. Subsequently, in the research described in *Chapter 4.2* this technology was used to prepare and analyze surfaces that were modified with pH-sensitive surface groups, a weak base, to coat surfaces with a model vaccine and to trigger the release upon contact with physiological pH. Next, microneedle surfaces were modified with pH-sensitive surface groups and were tested for pH-dependent ovalbumin binding and subsequent ovalbumin release into *ex vivo* human skin. To evaluate the *in vivo* applicability of these antigen-coated pH-sensitive microneedles, in *Chapter 4.3* the ovalbumin-coated microneedles were used to immunize mice for the induction of antigen-specific antibody and T-cell responses. To further extend the applicability of pH-sensitive coatings, surfaces with a surface isoelectric point (sIEP) were developed in *Chapter 4.4*. These surfaces aid

electrostatic adsorption of positively charged (bio)polymers at a pH value above the pI and their repulsion from the surface at a pH value below the pI. It is demonstrated that negatively charged (bio)polymers can be reversely coated and released. Finally, Chapter 4.5 describes the preparation of microneedles with a pH-sensitive surface onto which polyelectrolyte multilayers consisting of negatively charged inactivated polio vaccine and positively charged trimethyl chitosan were coated. The release of inactivated polio vaccine and trimethyl chitosan from the microneedles was evaluated in *ex vivo* human skin and the immunogenicity was assessed after topical application of the coated microneedles in rats.

In Chapter 5 the preparation and usage of hollow microneedles for dermal drug delivery by the ‘poke and flow’ approach is described. These hollow microneedles were prepared by etching fused silica capillaries by hydrofluoric acid. Furthermore, this chapter describes a novel applicator for depth controlled microinjections into skin. Finally, the potential of the newly developed applicator and hollow microneedles for dermal vaccination was studied in an immunization study in rats with inactivated poliovirus vaccine.

Chapter 6 summarizes the results and conclusions of this thesis. Besides, the prospects of microneedle-based immunization and drug delivery are discussed.

References

- [1] F. Andre, R. Booy, H. Bock, J. Clemens, S. Datta, T. John, B. Lee, S. Lolekha, H. Peltola, T. Ruff, M. Santosham, H. Schmitt, Vaccination greatly reduces disease, disability, death and inequity worldwide. *Bulletin of the World Health Organization* 86 (2008) 140-146.
- [2] CDC, Vaccines & Immunizations, available from: <http://www.cdc.gov/vaccines/>.
- [3] M.G. Carstens, Opportunities and challenges in vaccine delivery. *European Journal of Pharmaceutical Sciences* 36 (2009) 605-608.
- [4] Janeway, *Immunobiology*, 2005.
- [5] J. Chen, G. Ni, X.S. Liu, Papillomavirus virus like particle-based therapeutic vaccine against human papillomavirus infection related diseases: Immunological problems and future directions. *Cellular Immunology* 269 (2011) 5-9.
- [6] WHO, The top 10 causes of death, available from: <http://www.who.int/mediacentre/factsheets/fs310/en/index2.html>.
- [7] WHO, Controlled Temperature Chain (CTC); available from: <http://www.who.int/biologicals/areas/vaccines/controlledtemperaturechain/en/>.
- [8] S.M. Bal, Z. Ding, E. van Riet, W. Jiskoot, J. Bouwstra, Advances in transcutaneous vaccine delivery: do all ways lead to Rome? *Journal of Controlled Release* 148 (2010) 266-282.
- [9] Y.-C. Kim, J.-H. Park, M.R. Prausnitz, Microneedles for drug and vaccine delivery. *Advanced Drug Delivery Reviews* 64 (2012) 1547-1568.
- [10] T. Warger, H. Schild, G. Rechtsteiner, Initiation of adaptive immune responses by transcutaneous immunization. *Immunology Letters* 109 (2007) 13-20.
- [11] A. Paul, G. Cevc, B.K. Bachhawat, Transdermal immunization with large proteins by means of ultradeformable drug carriers. *European Journal of Immunology* 25 (1995) 3521-3524.
- [12] G.M. Glenn, M. Rao, G.R. Matyas, C.R. Alving, Skin immunization made possible by cholera toxin. *Nature* 391 (1998) 851.
- [13] G.M. Glenn, D.N. Taylor, X. Li, S. Frankel, A. Montemarano, C.R. Alving, Transcutaneous immunization: A human vaccine delivery strategy using a patch. *Nature Medicine* 6 (2000) 1403-1406.
- [14] S. Henry, D.V. McAllister, M.G. Allen, M.R. Prausnitz, Microfabricated microneedles: A novel approach to transdermal drug delivery. *Journal of Pharmaceutical Sciences* 87 (1998) 922-925.
- [15] M.I. Haq, E. Smith, D.N. John, M. Kalavala, C. Edwards, A. Anstey, A. Morrissey, J.C. Birchall, Clinical administration of microneedles: skin puncture, pain and sensation. *Biomed Microdevices* 11 (2009) 35-47.
- [16] S.M. Bal, J. Caussin, S. Pavel, J.A. Bouwstra, In vivo assessment of safety of microneedle arrays in human skin. *Journal of Controlled Release* 35 (2008) 193-202.
- [17] H.S. Gill, M.R. Prausnitz, Coated microneedles for transdermal delivery. *Journal of Controlled Release* 117 (2007) 227-237.

CHAPTER 2

MICRONEEDLE TECHNOLOGIES FOR (TRANS)DERMAL DRUG AND VACCINE DELIVERY

MICRONEEDLE TECHNOLOGIES FOR (TRANS)DERMAL DRUG AND VACCINE DELIVERY

Koen van der Maaden
Wim Jiskoot
Joke Bouwstra

[Journal of Controlled Release](#),
[161 \(2012\) 645-655](#)

Abstract

Microneedles have been used for the dermal and transdermal delivery of a broad range of drugs, such as small molecular weight drugs, oligonucleotides, DNA, peptides, proteins and inactivated viruses. However, until now there are no microneedle-based (trans) dermal drug delivery systems on the market. In the past decade various types of microneedles have been developed by a number of production processes. Numerous geometries of microneedles have been designed from various materials. These microneedles have been used for different approaches of microneedle-based (trans) dermal drug delivery. Following a brief introduction about dermal and transdermal drug delivery, this review describes different production methods for solid and hollow microneedles as well as conditions that influence skin penetration. Besides, the four microneedle-based (trans)dermal drug delivery approaches are discussed: 'poke and flow', 'poke and patch', 'poke and release', and 'coat and poke'. A separate section of this review is devoted to the use of microneedles for the delivery of therapeutic proteins and vaccines. Finally, we give our view on research and development that is needed to render microneedle-based (trans)dermal drug delivery technologies clinically useful in the near future.

1. Introduction

The field of microelectronics and micromachinery is becoming more and more applicable for medical purposes, because nowadays it is possible to accurately make nano-scaled geometries by techniques developed for the computer industry. One application of these techniques is the production of microneedles for dermal and transdermal drug delivery, i.e., the delivery of drugs into and through the skin, respectively (see table 1 for terminology). Microneedles are needle-like structures with diameters in the size order of microns and lengths up to one millimeter. These structures are used to pierce the upper layer of the skin to enable (trans)dermal drug delivery. Scientists are now able to produce microneedles made of different materials with different geometries and sizes, and with or without a bore. Microneedles have been used for (trans)dermal drug delivery and for taking biological samples *via* the skin. The major advantage of microneedles is their ability to pierce the skin in a minimally-invasive and potentially painless way. Furthermore, microneedles can be integrated into “lab-on-a-chip” systems, whereby hollow microneedles are combined with either microsensors, micropumps, or both. Such systems can be used as health monitoring systems for diseases, such as diabetes. The ultimate goal of “lab-on-a-chip” approaches is to create minimally-invasive, fully automated modules for constantly extracting and analyzing biological fluid and directly responding on the analytical results by the delivery of drugs [1-5]. However, until now there are no microneedle-based drug delivery systems on the market for (trans)dermal delivery.

After a short introduction about (trans)dermal drug delivery, this review describes different production methods for microneedles as well as factors that influence skin penetration, such as microneedle geometry and the use of an applicator. Then different (trans)dermal drug delivery approaches by microneedles are described for solid and hollow microneedles. Subsequently, the (trans)dermal delivery of specific drug categories, namely vaccines and therapeutic proteins, by microneedles is discussed. Finally, perspectives are given for the clinical application of microneedle-based (trans)dermal drug delivery.

2. The skin and its implications for drug delivery

The skin is the largest organ in the human body and is of great importance for the protection of the body against excessive water loss and to offer a protective barrier against unwanted influences, such as pathogens. The skin owes its protective function to its efficient physical barrier, the stratum corneum, which is 15-20 μm thick and is indispensable for a proper barrier function as it complicates foreign compounds, including drugs, to penetrate the skin [6, 7]. The viable epidermis is located below the stratum corneum and has a thickness of 130-180 μm . Below the epidermis lies the dermis, which is about 2000 μm thick and contains nerves, blood vessels, nociceptors, lymph vessels, hair follicles and sweat glands [8-10], as depicted in figure 1.

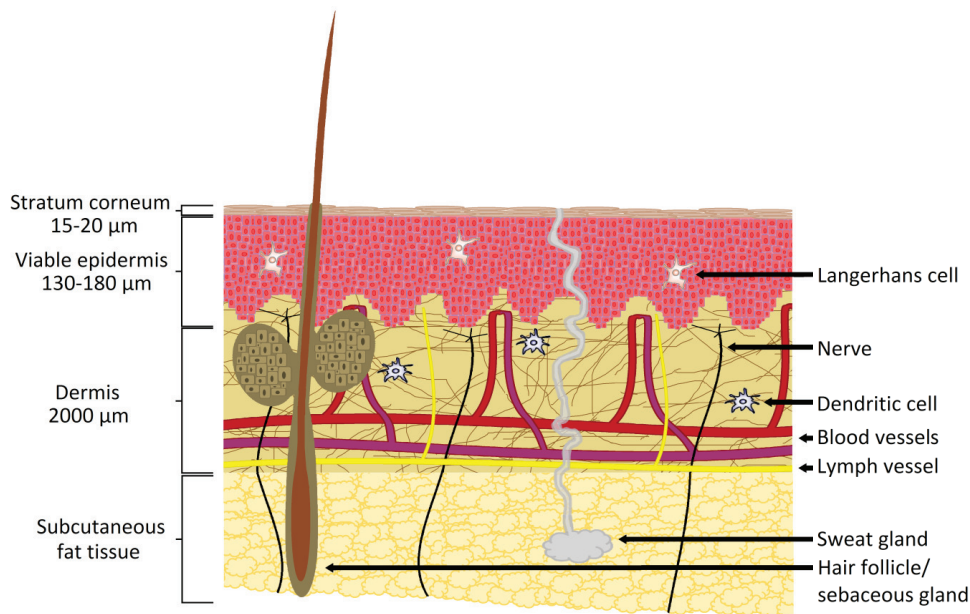


Figure 1: Representation of the skin microanatomy.

Table 1: Terminology

Term	Definition
Microneedle	Micron-scaled needle-like structure with a maximum length of 1 mm ¹
Dermal drug delivery	Delivery of drugs into the skin with the skin as the target (local delivery)
Transdermal drug delivery	Delivery of drugs through the skin, thus where the skin is not the target (systemic delivery)

Many drugs are delivered into the body by using conventional hypodermic needles and metal lancets for, e.g., subcutaneous and intramuscular injections, whereby the needles are used to pierce through the skin in order to reach the target site of injection. However, these procedures cause pain and carry the risk of transmitting various biohazardous pathogens [10-12]. The skin, however, has a great potential for non- or minimally-invasive drug delivery. First of all, the skin has a large surface area for drug application and the (trans)dermal route bypasses the first-pass effect of the liver. Besides, steady blood concentrations of a pharmacoin can be reached by the transdermal route, thereby avoiding fluctuations of the drug concentration in the blood, associated toxicity and inefficacy. Furthermore, swallowing problems and drug absorption and stability problems in the gastrointestinal tract can be circumvented [9, 13-17]. Also, because of the large number of immune cells, the skin offers a great potential for vaccination [10-12]. Altogether, drug delivery *via* the skin has multiple benefits over both the oral route and conventional injections. However, the dense structure of the stratum

¹ Longer needles have been used (up to 3 mm), which are however not microneedles in the strictest sense

corneum and the limited number of hair follicles and sebaceous glands complicates the delivery of therapeutic doses *via* the skin. Therefore, several methods have been developed for (trans)dermal drug delivery, such as chemical and lipid enhancers, and electric fields for iontophoresis [6, 14-17]. About 40 (trans)dermal products (20 drug molecules) are on the market, however, they are all low-molecular-weight drugs with a high potency [16, 18, 19]. This illustrates that it is difficult to overcome the skin barrier. As it is even more difficult to deliver high-molecular-weight drugs, such as proteins, polypeptides, oligonucleotides, and DNA, and even larger entities such as vaccines, novel methods have been developed to deliver such drugs *via* the skin. Among these methods are various microneedle approaches, which are the focus of our review. Microneedles are very promising for the (trans)dermal delivery of high-molecular-weight drugs because they enabling large molecules to pass the stratum corneum *via* micropores.

3. Microneedle production, geometry, and application technology

3.1 Production of microneedles

Numerous types of microneedles composed of various materials have been used for the (trans)dermal delivery of a broad range of compounds in a potentially painless manner, a selection of which is shown in figure 2. The first produced microneedles for drug delivery were made from silicon wafers by photolithography and deep reactive ion etching [13, 20, 21]. The used microfabrication technologies were initially developed for the production of integrated circuits and turned out to be very suitable for the highly-reproducible mass production of microneedles. Furthermore, these technologies enable the integration of, e.g., microsensors, micropumps, electrical circuits, and microneedles into one device [1, 13, 21-26]. Another benefit of silicon microneedles is that they are usually much sharper than polymeric and metal microneedles [27]. However, the production process for silicon microneedles requires expensive micro-fabrication processes and clean room processing. Another drawback of silicon needles is that they may break and stay behind in the skin due to the fragile nature of silicon [28-35].

Microneedles produced from silicon wafers have been developed with multiple geometries and can be divided into two major groups: *in-plane* and *out-of-plane* microneedles, as shown in figure 3. *In-plane* microneedles are formed in parallel with the machined surface of the silicon wafer, enabling the production of needles with various lengths over a large range. *In-plane* production techniques are state-of-the-art techniques, including surface micromachining and a variety of etching methods. Furthermore, they offer flexibility regarding needle design and shape, and are beneficial for the integration of microneedles with biosensors and micropumps [1, 22, 40-43]. *Out-of-plane* microneedles are formed perpendicular to the silicon wafer and are more easily produced in arrays than *in-plane* microneedles. Furthermore, *out-of-plane* microneedles have the major advantage of arranging the single microneedles of an array in

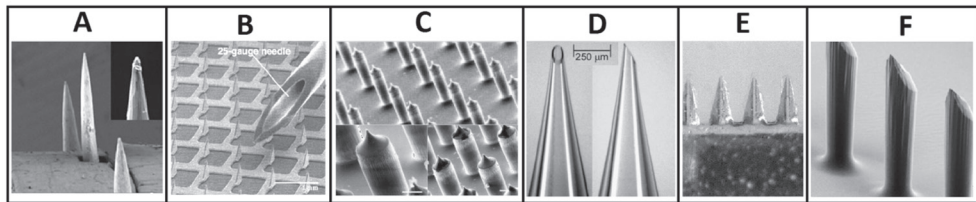


Figure 2: Microneedles made of different materials. (A) 770 μm long stainless steel microneedles from Dermaroller® [36], 330 μm long Macroflux® microneedles made of titanium [37], (C) silicon microneedles with a length of 150 μm [38], (D) microneedles of pulled glass capillary [39], (E) 500 μm long microneedles made of maltose [30], and (F) PLGA microneedles of 600 μm [32].

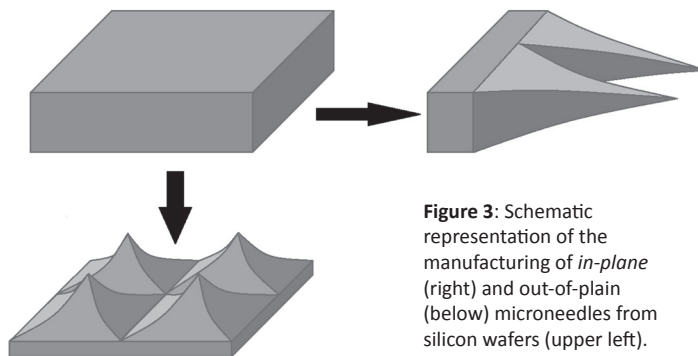


Figure 3: Schematic representation of the manufacturing of *in-plane* (right) and *out-of-plane* (below) microneedles from silicon wafers (upper left).

such a way that the drug can be delivered over a larger surface area of the skin. However, out-of-plane hollow microneedles are more difficult to integrate with lab-on-a-chip technologies than *in-plane* hollow microneedles [1, 20, 22, 24, 25, 42, 43].

More recently, other microneedle production processes have been introduced for the generation of cheaper and biocompatible microneedles, including metal, polymer and sugar-based microneedles. Solid metal microneedles can be produced by laser cutting them out of sheet metal and subsequently bending them out-of-plane [37, 44, 45]. Furthermore, solid microneedle arrays with a length of 300 μm have been made from the tip of 30 G needles, molded in a plastic backplate [46, 47], and stainless steel 34 G hollow microneedles have been developed for insulin delivery [48]. Hollow metal microneedles are often made from metal tubing by laser machining, electrochemical etching or by electrode discharge machining [22]. Another technology to produce metal microneedles is laser patterning. This is a technique whereby liquid particles, containing the microneedle material of interest, are deposited on a substrate in order to produce an out-of-plane 3-dimensional structure [49]. Laser patterning may be a versatile method to create microneedles from a broad range of materials.

Polymeric microneedles could have important benefits over microneedles made of other materials, because polymers are inexpensive, can be biocompatible, and they are amenable to mass production. Furthermore, because of their viscoelastic properties polymeric microneedles may be less sensitive to shear-induced breakage, and drugs may be incorporated

into biodegradable polymeric microneedles for controlled drug delivery [22, 25, 28, 32, 34, 35]. Furthermore, polymeric microneedles are extremely suited for the development of an all-in-one drug delivery system, whereby the microneedle is the drug delivery device as well as the drug formulation [50-55].

3.2 Microneedle geometry

Several factors may prevent microneedles from penetrating the skin. In particular, the elastic nature of skin can prevent microneedles from penetration by folding around the needles during microneedle application, especially in case of blunt and short microneedles. Due to the robustness of the skin, microneedle insertion forces may exceed the ultimate tensile forces of the microneedle and thereby damage the microneedles, especially for longer microneedles and microneedles made of relatively weak materials [34, 43, 46, 47, 54, 56-58]. Therefore, microneedle geometry is crucial for efficient microneedle-based (trans) dermal drug delivery, because it influences the strength of the microneedles, their ability to pierce the skin, the drug flow (through hollow microneedles), and therefore the rate of drug delivery. Various different microneedle shapes have been developed, ranging from cylindrical, rectangular, pyramidal, conical, octagonal, to quadrangular, with different needle lengths and widths. The sharpness of the microneedle tip is a very important factor for skin penetration, as sharper microneedles have higher potential for sufficiently penetrating the skin at a certain insertion force [13, 28, 29, 32, 34, 59, 60], i.e., larger tip diameters need higher insertion forces [61].

For hollow microneedles it is important that a sufficient and constant flow rate is generated for delivering drugs into the skin, without affecting the microneedle strength. The main factor affecting the flow rate is the compression of the dense dermal tissue at the needle tip during insertion [39]. Therefore, the shape of the tip is of great importance for the flow rate, e.g., the flow from a blunt-tip microneedle supports less flow than a bevel-tip microneedle, because a blunt-tip microneedle compresses the skin more extensively and thereby has an increased risk of clogging [25, 59]. Hence, it could be beneficial to have very sharp microneedles with the bore of the microneedle off-centered or on the side of the microneedle [25, 39, 42, 59]. Increasing the microneedle bore may increase the flow rate, however, this results in a decreased microneedle strength and a reduction in sharpness [42]. A way to increase the microneedle strength is by applying a metal coating on the microneedles [62, 63], which however, may decrease their sharpness.

For both hollow and solid microneedles, a low density of microneedle arrays may be beneficial for piercing the skin because they can pull the skin taut between the needles. Conversely, very dense microneedle arrays may be less efficient in piercing the skin because they can cause a 'bed of nails' effect [10, 28, 43]. Therefore, designing microneedles involves making compromises and using microneedle insertion devices [25, 47, 56, 59, 60], as described below.

3.3 Microneedle application devices

For medical application reproducible piercing is crucial, which demands the use of an applicator, even in the case of sharp microneedle arrays. However, the importance of using microneedle applicators has been underestimated for a long time.

Applicators for microneedles should meet certain requirements to be suitable for clinical use. Since microneedles are developed for decreasing patient discomfort and eliminating pain sensation, the applicator itself should not induce any pain. Furthermore, the use of an applicator should lead to a more effective, reproducible and depth-controlled penetration of microneedles into the skin, without increasing the risk of microneedle fracture [10, 28, 44, 47, 56-58]. Several microneedle application devices have been developed, for example an applicator based upon the reduction of insertion forces by a hand-operated rotary application for single hollow microneedles, which drills individual microneedles into the skin to a predetermined depth [57]. Furthermore, a hand-held microneedle applicator was developed to apply microneedles in a single rolling motion from an angle of 45° to 135° with the skin [56] and vibration-based microneedle insertion devices have been used to reduce the insertion forces [57, 64]. Partial retraction of hollow microneedles is beneficial for the flow rate, because this leads to less clogging at the tip opening [57]. However, most application devices are based upon impact-insertion, which mainly reduce the insertion forces by circumventing the skin's elasticity. These impact-insertion devices range from simple hand-held applicators, by which microneedles are either manually punched into the skin [56] or *via* a mechanically-driven applicator [37, 46, 65, 66], to more sophisticated electrically-driven microneedle applicators [47, 67]. The latter are preferable for multiple use (e.g. repeated dose, multiple patients) because the easily adjustable forces are more stable over time than manually or spring-induced forces. However, for a single administration a mechanically-driven applicator may be beneficial from an economic point of view. In conclusion, there is no universal applicator for microneedles and therefore the requirement of the applicator is dependent on the geometry, sharpness and density of the relevant microneedle and the intended use.

4. Drug delivery methods via the skin by microneedles

There are four general approaches of (trans)dermal drug delivery by microneedles, as schematically depicted in figure 4. The limitations, advantages and disadvantages of each of these approaches are summarized in table 2.

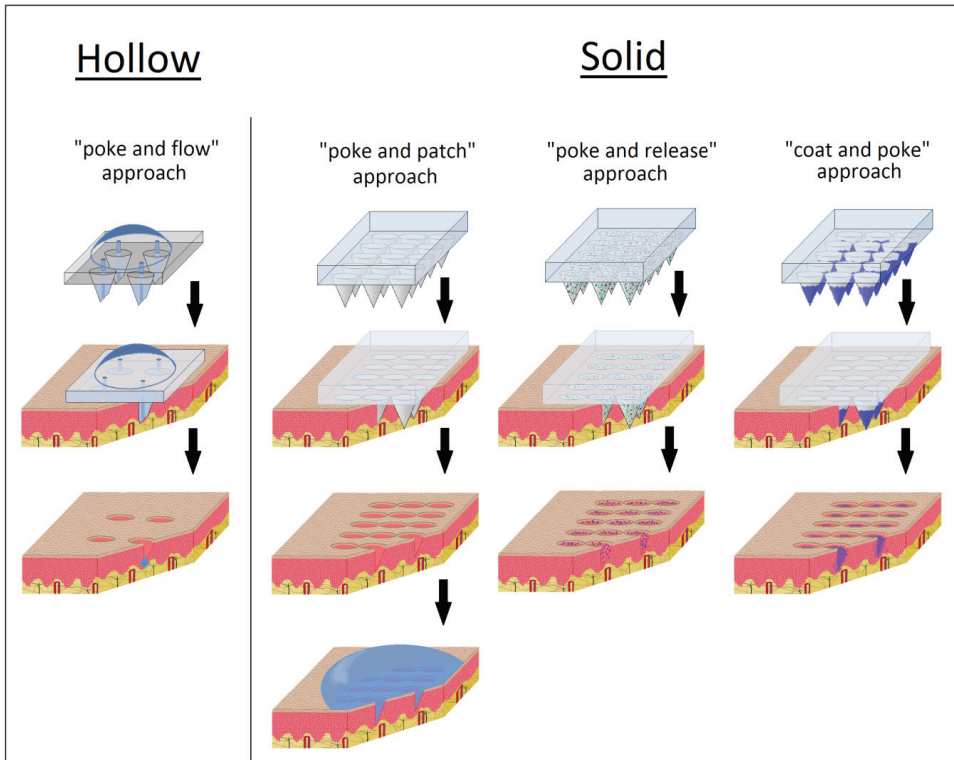


Figure 4: Different approaches of drug delivery by hollow and solid microneedles. Hollow microneedles are used with the 'poke and flow' approach, whereby a drug in solution is actively or passively delivered through the bore of the microneedle. Solid microneedles are used in three different manners. By the 'poke and patch' approach micropores are generated in the skin by microneedles, and after removal of the microneedles a patch is applied on top of these micropores, allowing the drug in the patch to diffuse through the skin. The 'poke and release' approach uses either dissolving microneedles or porous microneedles, which respectively release the drug by dissolution of the microneedles in the skin, or by diffusion of the drug in solution from the pores into the skin. Finally, with the 'coat and poke' method microneedles are pierced through the skin, and then the drug-containing coating is released into the skin through hydration of the coating.

Table 2: Main features of the different approaches of drug delivery by microneedles.

Drug delivery approach	Rate-limiting step of drug delivery	Main advantages	Main disadvantages
'poke and flow'	Solvent flow through microneedle bore Or, at higher volumes: Pressure resistance of the skin	Rate of drug delivery can be regulated, e.g., <i>via</i> a pump, if solvent flow is rate-limiting Delivery of high volumes Integration into lab-on-a-chip systems possible Precise dosing No or limited reformulation of the drug needed	Risk of clogging Impaired microneedle strength Increased risk of leakage for arrays More complex device
'poke and patch'	Diffusion of the drug through the micropores generated by microneedles into the skin, dependent on the pore size and number, and concentration of the drug in the patch	Technically simple No pump or encapsulation/coating process is required Extended release	Low fraction of the drug may be delivered (only of interest for drugs with high potency) Two-step administration process No precise dosing Reformulation of the drug needed
'poke and release'	Dissolving microneedles: dissolution rate Porous microneedles: diffusion of drug from the pores	Small amount of drug may be lost during the encapsulation/absorption process No patch or pump is required No sharps waste (dissolving microneedles) Precise dosing	Impaired microneedle strength (increased fracture and deformation of microneedle geometry) Often less sharp microneedles (decreased penetration ability) Small dose Reformulation of the drug needed
'coat and poke'	Detachment of the coating from microneedle surface Or, at thicker coatings: Dissolution rate of the coating	Microneedle strength is retained after coating No patch or pump is required Precise dosing	Requires an efficient coating procedure Small dose Reformulation of the drug needed Reduction of microneedle sharpness/penetration ability

4.1 Hollow microneedles

Hollow microneedles deliver drugs *via* the 'poke and flow' approach. An important benefit of hollow microneedles over solid microneedles is the possibility to facilitate force-driven fluid flow, thereby allowing faster rates of drug delivery [10, 14, 27, 28]. Furthermore, the dose of the desired drug in solution can be more easily controlled according to the need of the patient. This method of drug delivery can be achieved *via* passive diffusion through the bore of the microneedle [31, 68]. Other methods are also possible whereby the drug in solution is actively delivered through the bore of the microneedle. The latter requires a driving force through pressure, e.g., by combining a microneedle injection applicator with a syringe, a pump, or pressurized gas [10, 39, 41, 57, 69]. Furthermore, a microneedle array may

include the incorporation of a microfluidic chip [40] or a micropump to direct the content of the drug reservoir into the skin in a controlled way [70]. Another possibility is combining a drug reservoir with a heater, whereby the drug solution is pressed into the skin through fluid expansion or bubble formation [22]. Also, drug delivery can be accomplished by hand-pressing a flexible drug reservoir and thereby releasing the drug solution into the skin [42]. This is the most promising system for the market because it is fairly easy and relatively cheap to produce.

A disadvantage the ‘poke and flow’ approach is that the infusion rates are normally quite low (50-300 nL/min) [39, 57, 68]. However, this can be overcome by partial retraction or adding hyaluronidase to the infusion solution, which breaks down hyaluronic acid within skin collagen fibers, allowing infusion rates up to 18.8 $\mu\text{L}/\text{min}$ [39]. The inclusion of hyaluronidase in microneedle-based (trans)dermal drug delivery systems holds promise, because it has been approved by the FDA and has been co-administered with insulin in a clinical trial [71]. Finally, hollow microneedles can be combined with iontophoresis which allows the active displacement of charged particles and drugs through the bore of the hollow microneedles in a controlled way, whereby the drug delivery efficiency can be increased [28]. However, this leads to skin irritation due to a high current density at the site of the lowest resistance (i.e., at the micropores) when a constant current is used [72].

4.2 Solid microneedles

There are three main mechanisms by which solid microneedles can be used to deliver drugs into the skin, which include the ‘poke and patch’ approach, the ‘poke and release’ approach, and the ‘coat and poke’ approach, as schematically shown in figure 4.

4.2.1 Poke and patch

Solid microneedles for (trans)dermal drug delivery were first used in the ‘poke and patch’ approach [20]. In this method microneedles are applied onto the skin. Subsequently, the microneedles are removed and a patch containing the drug formulation is applied onto the site of microneedle application so that the drug can diffuse through the formed microchannels into the skin [14, 27, 28, 43]. Microneedle-based skin penetration studies have shown that the permeability for different compounds in *in vitro* skin was increased by solid microneedles up to four orders in magnitude [20, 38, 41, 46]. However, passive transport of drugs through microchannels does not always lead to a high bioavailability of drugs. The ‘poke and patch’ approach has been studied *in vitro* and *in vivo* for the (trans)dermal delivery of multiple types of compounds and for the sustained delivery of drugs [28, 36, 73-75]. For the ‘poke and patch’ approach it is very important that the micropores stay open during the drug application period [36, 67]. It has been reported that micropores in *in vivo* rat skin generated by microneedles were opened until at least 72 h after microneedle treatment when they are held under occlusive conditions [73], e.g., using occlusive tape or by exposure to a buffered solution [28, 36]. However, micropores close shortly after microneedle application when

micropores are not occluded or after patch removal [28, 74]. Furthermore, it has been shown that micropore opening can be extended up to seven days when diclofenac is added to the patch formulation [75]. However, this approach may not be viable/generally applicable, because longer opening times increase the risk of infection. The ‘poke and patch’ approach has been combined with iontophoresis, which leads to an increase in uptake of charged drugs by several orders in magnitude compared to iontophoresis or microneedles alone [76-80]. A disadvantage of this approach is that iontophoresis may cause skin irritation (also described in section 4.1). Also dissolving microneedles have been used in the ‘poke and patch’ approach [73].

A variation on the ‘poke and patch’ approach is the ‘scrape and patch’ approach, whereby microneedles, microprojections, or microblades are first scraped over the skin to generate micro-abrasions, whereon subsequently a patch with a drug solution is applied [81-84]. Mikszta *et al.* (2002) used blunt ended microneedles, named microenhancer arrays (MEAs), with the ‘scrape and patch’ approach for the delivery of Coomassie blue in the epidermis [81]. This “scrape and patch” approach with MEAs was later used for the dermal delivery of an attenuated chimeric flavivirus vaccine in primates [82] and for dermal delivery of an anthrax vaccine in mice and rabbits [85]. Finally, the ‘scrape and patch’ approach was used with Onvax™ (BD) microneedles for the delivery of a rabies vaccine into the epidermis in healthy volunteers, however, no protective immune responses were observed [86]. Therefore, for vaccination purposes more efficient approaches are needed.

4.2.2 Poke and release

The second mechanism for (trans)dermal drug delivery by solid microneedles is *via* the ‘poke and release’ approach. This approach features a controlled release of the drug from the microneedles by using materials which serve as a drug depot. This implies that, unlike the ‘poke and patch’ approach the microneedles must remain on the skin after their application until the drug is released. This method makes use of either porous, biodegradable, or dissolving microneedles from which a drug is slowly released into the skin. However, also hybrid microneedles have been made, e.g. solid non-dissolvable silicon microneedles with a biodegradable tip [87] or a stainless steel electrode pillar with a dissolvable tip [88].

4.2.2.1 Porous microneedles

Porous microneedles absorb a drug solution into their pores which is released after the microneedles are applied onto the skin. Porous microneedles can be made of non-biodegradable materials such as porous silicon [89, 90]. Furthermore, porous microneedles have been made of silicon from which only the tips of the microneedles were made porous by electrochemically etching in acetonitrile/HF [91]. However, because porous structures are generally more fragile than solid structures [92], porous silicon microneedles can break more easily in the skin and remain in the skin after removing the microneedle patch. This may give problems because silicon is not a biodegradable material. Therefore, porous

microneedles made of biodegradable materials are preferred, such as stainless steel solid microneedles electrochemically coated with micro-porous calcium phosphate, which serve as a biodegradable drug reservoir [93]. Furthermore, porous microneedles have been made of polylactic acid microparticles, but these microneedles were not able to penetrate human cadaver skin after manual application because of insufficient microneedle strength [92]. Finally, stainless steel microneedles have been made with pockets through the needle shaft, whereby these pockets were coated with one or more drugs. Such microneedles enable sustained release of different drugs from microneedles [94-96].

4.2.2.2 Dissolving microneedles

Another way of delivering drugs by the 'poke and release' approach is by using dissolving/degrading microneedles. These microneedles have a drug encapsulated in their matrix and are made of polymers or sugars. Biodegradable microneedles degrade in the skin after application, whereby the release of incorporated drugs can be sustained up to months by choosing the proper polymer [92]. Furthermore, these microneedles have the advantage that they eventually disappear and thereby leave no biohazardous sharps waste, enabling a safe disposal of the remaining device [27, 50, 51]. However, for the fabrication of the first drug-encapsulated dissolving microneedles UV photo-curing, organic solvents or elevated temperatures were often needed, which could impair drug stability in case of biomacromolecular drugs such as proteins and DNA [34, 50-52]. Besides, residual organic solvents and biodegradable materials itself may lead to skin irritation [67]. Biodegradable trimethylene glycol microneedles fabricated by UV stereo lithography can be used as a slow release (trans)dermal delivery system [97]. Microneedles made of maltose dissolve in less than 10 minutes in human skin after insertion. However, these microneedles need fabrication temperatures above 100°C to transit the maltose into the glassy phase [30, 55]. Another disadvantage of dissolving is the limited drug loading, e.g., bovine serum albumin (BSA) and calcein encapsulated polymeric microneedles have been made, however, a drug loading of more than 10% led to insufficient mechanical strength of the microneedles [34].

In the development of dissolving microneedles much research has been focused on improving drug stability. Methods to achieve this include the use of mild temperatures and circumventing the use of organic solvents during the microneedle manufacturing process [33, 50, 51, 53, 54, 98]. Protein-encapsulated dissolving microneedles from carboxymethylcellulose (CMC) and amylopectin have been produced, which were shown to dissolve completely in porcine cadaver skin within one hour [51]. Furthermore, protein-encapsulated dissolving microneedles have been produced from chondroitin sulfate or dextran, which release almost all the drug within one hour [33, 54]. Dissolving microneedles made by photopolymerization of vinyl pyrrolidone, were able to efficiently deliver insulin within several minutes into porcine cadaver skin [50, 53]. Finally, polymeric dissolving microneedles have been produced from Gantrez® AN 139, which deliver 83% of the encapsulated theophylline into porcine skin within 24 h [98].

4.2.3 Coat and poke

The fourth current approach of using solid microneedles to enhance the uptake of drugs into the viable skin is *via* the ‘coat and poke’ approach, whereby drug-coated microneedle arrays are, just as in the ‘poke and release’ approach, a single-unit drug delivery system [99]. Microneedles have been coated with a broad range of drugs, such as hydrophilic and hydrophobic low-molecular-weight drugs, DNA, RNA, proteins, peptides, inactivated pathogens, and particles [10, 27, 44, 94, 95, 100, 101]. Coating of microneedles can often be performed at ambient conditions [44, 45, 66, 94, 95, 102-104] and a dry coating may be more stable than a liquid formulation [66, 94, 95]. However, a drawback from this approach is that solid microneedles can only be coated with small quantities of drugs as thick coatings lead to a very low skin delivery efficiency [37, 44, 45, 102], likely because of a decreased sharpness of microneedles [100]. Therefore, coated microneedles for (trans)dermal drug delivery are only applicable for very potent drugs, such as vaccines [10, 27, 28]. One of the challenges to overcome with this approach is the relatively high loss of drug during coating. Over the past decade multiple methods of coating and coating devices have been developed for manufacturing drug-coated microneedle arrays. The first coating methods consisted of simple coating procedures/solutions, whereas later coating approaches became more sophisticated, as exemplified below.

Microneedles have been coated by (partial) immersion in aqueous solutions to coat up to 238 μg ovalbumin per cm^2 (10 μg ovalbumin per cm^2 leads to a coating thickness of about 3 μm). However, coating by immersion leads to a relatively high loss of drug, and variable coating thicknesses per microneedle [37, 44]. Therefore, a dip-coating procedure may be advantageous, which is a two-step procedure, involving a “dipping and withdrawal” step, leading to the formation of a liquid film on the microneedle, and a “drying” step, leading to the conversion of the liquid layer into a solid coating. Because the first step is fluid mechanically controlled, the microneedle withdrawal speed is important (faster=thicker) and has to be above the critical withdrawal speed. The critical withdrawal speed depends on the combination of the solid substrate and coating solution, the viscosity (higher=thicker), and surface tension (lower=thicker). For a uniform coating the “drying” step is important and depends on the rate of solvent evaporation, wettability, viscosity of the coating solution, and de-wetting [94, 95]. Therefore, it is important to decrease the surface tension and increase the viscosity of the coating solution to develop a microneedle coating [94]. This approach was extensively researched by Gill and Prausnitz [94], who as well have developed a coating apparatus that requires small volumes of only 100 μL coating solution [95]. The combination of the micro-scale dip-coating device whereby the microneedles were dipped 6 times into an aqueous surfactant-viscosity enhanced coating solution, composed of 1% CMC and 0.1% Lutrol F-68, was used in later studies to coat microneedles with an influenza vaccine [84, 105-113], and was further improved by the addition of 15% trehalose to the coating solution to increase vaccine stability [108-110, 113].

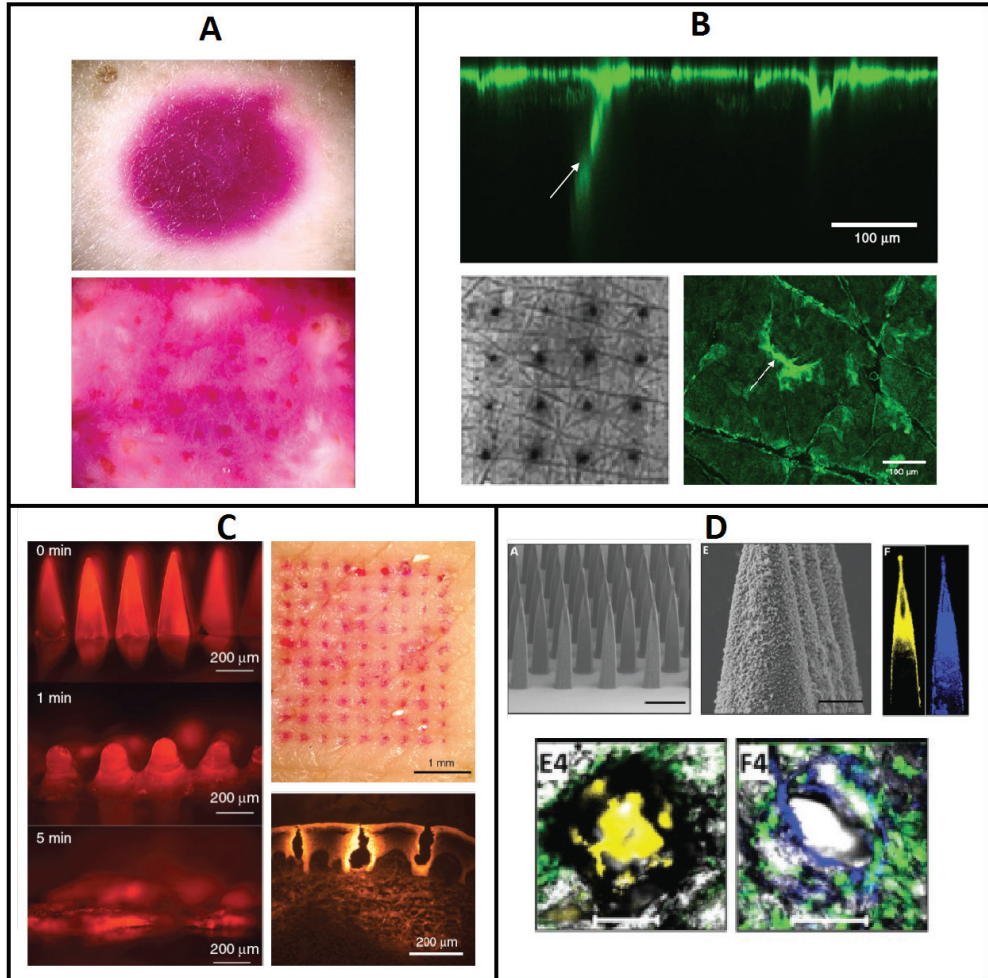


Figure 5: Examples of microneedle-based (trans)dermal delivery of model drugs into the skin. (A) Infusion of sulforhodamine in human cadaver skin by using hollow microneedles by the ‘poke and flow’ approach. The upper picture is the stratum corneum side and the lower picture is the bottom side of the skin [39]. (B) Drug delivery by the ‘poke and patch’ approach in *ex vivo* human skin of FITC labeled 200 nm polystyrene nanoparticles (upper and lower right picture, which are respectively an in depth scan and top view of nanoparticle penetrated skin by confocal microscopy) and trypan blue (lower left picture) [47]. The delivery of sulforhodamine in *ex vivo* pig skin by the ‘poke and release’ approach. On the left picture sulforhodamine encapsulated dissolving microneedles are shown before and after insertion in the skin. The right pictures show *ex vivo* pig skin after treatment with sulforhodamine encapsulated microneedles (the upper shows a top view by light microscopy, the lower shows a cross section by fluorescence microscopy) [53]. (D) Drug delivery by the ‘coat and poke’ approach of Cy3 labeled DNA (yellow) and Dil labeled PLGA nanoparticles (blue). The upper left picture shows uncoated microneedles and the middle picture shows microneedles coated by a nanolayered coating method. The lower pictures show the delivery of DNA (left) and PLGA nanoparticles (right) [120].

Other microneedle coating technologies have been developed, such as aerosol coating of microneedles [114], a roller drum approach whereby coatings of 100 μm thick were produced without coating the tip, to circumvent it from becoming blunt [115]. Furthermore, a conventional film coating process with hydroxypropyl methylcellulose and CMC for coating microneedles has been developed [99]. Also, a gas-jet drying device has been developed to coat microneedles with a coating solution, containing a drug, viscosity enhancer and a surfactant to generate coatings of 5 μm thick. However, during this procedure the backplate of the microneedle array is coated as well, resulting in a drug delivery efficiency of less than 33% [65, 66, 100].

Methods to increase the coating efficiency are the pre-coating of the surface of microneedles (e.g., with SiO_2 , PLGA, polyvinylpyrrolidone [94], chitosan [102]) or by the generation of polyelectrolyte coatings with microencapsulation properties (e.g., poly[di(carboxylatophenoxy)phosphazene] (PCPP) [116, 117], chitosan and CMC [118]). It has been shown that some of these pre-coatings lead to improved delivery into the skin, adjuvant effect, and improved vaccine stability [116, 117]. Furthermore, a recently developed sophisticated method to coat microneedle arrays is a layer-by-layer (LbL) coating approach, whereby nanolayers are formed by alternate coating of positively and negatively charged polyelectrolytes [119]. LbL coatings for microneedles have been developed by generating polyelectrolyte multilayers (PEM) for the (trans)dermal delivery of DNA [120] and proteins [104]. LbL PEMs are thin layers which enable nanometer-scale control over film structure and composition, provide control over multiple encapsulated agents, and give a robust control over the released material. Furthermore, they stabilize the encapsulated materials by occlusion and protect them against environmental influences. Finally, because these coatings are very thin (~100 nm) the microneedle geometry and sharpness are better preserved [100, 102, 104, 115, 120].

A variation on the ‘coat and poke’ method is the ‘dip and scrape’ approach, whereby the solid microneedles are first coated and are subsequently scraped over the skin. This approach leads to the delivery of drugs and vaccines in the formed micro-abrasions, which has the benefit that blunt tip solid microneedles can be used [81]. However, scraping induces more disruption of the epidermis than poking and may therefore induce more skin irritation. Moreover, this method most likely suffers from variable, less controlled delivery of the drug into the skin.

5. Vaccine and protein delivery by microneedles

In this review we dedicate a separate section to the delivery of therapeutic proteins and antigenic proteins for vaccination by microneedles, because these types of drugs are more difficult to deliver (trans)dermally and because of stability challenges. The different methods of drug delivery by microneedles, as described above, all have their own advantages and disadvantages with respect to (trans)dermal protein delivery. This is dependent on the type

of protein that needs to be delivered, e.g., therapeutic proteins have different requirements than protein antigens for immunization. For instance, whereas vaccines should be targeted to immune cells, for therapeutic proteins the opposite is true. The skin is an excellent organ for vaccination because of the large number of immune cells. Not surprisingly, protein delivery by microneedles has been studied mainly for the dermal delivery of antigens, as reviewed by Bal *et al.* (2010) [10]. For (trans)dermal vaccine delivery, preservation of protein integrity is important because a change in protein structure can lead to impaired vaccination efficacy and an altered immune response [109, 111, 112].

There have been several different proteins delivered by microneedles for vaccination and therapeutic purposes in both human and animals. Ovalbumin is a frequently used model protein antigen for studying the suitability of microneedles for dermal immunization [37, 45, 121-126]. Bovine serum albumin (BSA) [32, 34, 41, 51, 95, 102] and insulin [31, 41, 48, 50, 57, 94, 127-130] have been used as model proteins for transdermal delivery of therapeutic proteins by microneedles. BSA is a 66 kDa protein, which has been delivered by the ‘poke and flow’ approach [41], the ‘poke and patch’ approach [32], the ‘poke and release’ approach [34, 51], and the ‘coat and poke’ approach [102]. Though all different approaches of drug delivery by microneedles have been used for insulin as well as BSA, the ‘poke and flow’ approach by hollow microneedles has been employed most frequently, both *in vitro* and in animal studies [31, 41, 48, 50, 57, 94, 127-130]. Besides, insulin has been delivered by microneedles in human studies by the ‘poke and flow’ approach [128, 131-133]. Other model proteins, therapeutic proteins, and peptides have been delivered by microneedles, such as erythropoietin [33], lysozyme [51], parathyroid hormone (PTH) [115], recombinant human growth hormone (rhGH) [48, 54], and etanercept [48]. However, only a few limited studies have been performed on the stability of therapeutic proteins (trans)dermally delivered by microneedles (see below). Protein stability definitely requires more attention in order to give (trans)dermal protein delivery a chance to reach the clinic.

Different approaches of drug delivery by microneedles may induce different types of protein degradation, as summarized in table 3. Park *et al.* (2006) produced BSA-containing dissolving microneedles by filling a drug containing microneedle mold with a melted polymer at 135°C; BSA was kept in the solid state to limit protein degradation. They studied the stability of microneedle encapsulated BSA by measuring protein solubility, dynamic light scattering (DLS), and circular dichroism (CD). After heating BSA in the solid state for 10 min at 135°C no significant difference was found by DLS, whereas heating for 20 and 30 minutes led to aggregates in the size order of tens of nanometers. Furthermore, they observed little or no changes in the secondary structure after thermal processing of the protein in the solid state. However, 10% BSA was irreversibly aggregated after 10 min exposure to the polymer melt, and BSA was completely denatured after 1 h exposure to 135°C [34], which shows that this approach is not viable for the delivery of BSA and most likely other proteins. Lee *et al.* (2008) generated dissolving microneedles for BSA and lysozyme at ambient temperature conditions. They studied the structural and functional integrity of microneedle encapsulated lysozyme by

CD and enzymatic activity, respectively, and found that according to these methods lysozyme was not substantially degraded after two months of storage at room temperature [51]. However, one should keep in mind that lysozyme is a relatively stable model protein that may not be representative for relevant therapeutic proteins. Migalska *et al.* (2011) generated insulin encapsulated dissolving microneedles and found no chemical changes of denatured insulin by reversed-phase (rp) high-performance liquid chromatography (HPLC) and no changes of the secondary structure of insulin by CD [50]. Finally, Fukushima *et al.* (2011) produced rhGH encapsulated in dissolving microneedles and reported that the encapsulated rhGH was stable for one month, by an enzyme immunoassay and LC/MS/MS [54].

Ameri *et al.* (2009) studied the stability of PTH coated on microneedles by rp-HPLC and size exclusion-HPLC. They observed that aggregation and oxidation were the primary degradation processes of coated PTH, and found that the addition of sucrose to the coating decreased the aggregation of PTH from 7% to <0.5%. They reported that solid state aggregation (7%) is the main degradation process, and that the oxidation of PTH (1%) may be metal catalyzed by metal contamination from excipients or by the titanium microneedles themselves [115]. As several studies have demonstrated that protein aggregates induced by metal catalyzed oxidation are particularly immunogenic in immune tolerant mouse models [134-136], the presence of these degradation products may pose serious immunogenicity concerns.

6. Perspectives

Microneedle technologies offer a way to deliver drugs *via* the skin in a minimally-invasive and potentially painless manner and have been used to deliver drugs (trans)dermally by several approaches. However, “the microneedle” does not exist, and the ideal one is yet to be determined and may depend on the type of drug and the type of application.

Microneedles have been produced by different production methods from a variety of materials with a broad range of geometries and have been produced as solid and hollow microneedles. Furthermore, microneedles with different lengths have been used with or without a microneedle application device. However, all microneedles have restraints based on the type of microneedle. An important factor for microneedle-based drug delivery is the strength of the microneedles, i.e., they must not break during insertion into the skin. Hollow microneedles have a risk of clogging at the tip opening and are usually weaker than solid microneedles. This poses constraints on the design and the insertion methods of these needles. Furthermore, single hollow microneedles may be preferred over hollow microneedle arrays, because with the former there is a lower risk of leakage. However, if hollow microneedle arrays are made in such a way that each microneedle has its own drug reservoir, they may be preferred over single hollow microneedles because they can deliver a larger amount of drug.

Table 3: Hypotheses of microneedle induced protein degradation mechanisms, which may occur during protein delivery by microneedles.

Stress factor	Type of protein degradation	Type of microneedles	Factors involved
Interface induced	Aggregation Adsorption Unfolding	Hollow microneedles, coated microneedles and drug patch for the 'poke and flow' approach	Microneedle bore, applied pressure on microneedle, materials/surface properties, formulation (e.g., presence of a surfactant)
High protein concentration	Aggregation	Coated/dissolving microneedles	Microneedle coating/molding solution
Temperature induced	Aggregation Unfolding Chemical degradation	Dissolving microneedles	Microneedle polymerization/transition temperature, dissolving microneedle after application
Metal catalyzed	Aggregation Oxidation	Hollow and solid metal microneedles	Formulation impurities
Air exposure	Aggregation Adsorption Oxidation Unfolding	Coated/dissolving microneedles and drug patch for 'poke and flow' approach	Storage conditions of microneedles
pH induced	Aggregation Unfolding Chemical degradation	Coated/dissolving microneedles and drug patch for 'poke and flow' approach	Dissolving microneedle after application, pH of coating solution/patch solution/molding solution

To ensure that patients obtain the same and required dose during each administration microneedles should be able to pierce the skin in a reproducible manner. However, in order to obtain a reproducible penetration and a reproducible penetration depth an applicator is necessary. It has been shown that successful and reproducible skin penetration by microneedles can be reached by different approaches. For example, impact-insertion applicators are beneficial for high-density microneedle arrays and blunt microneedles to reach sufficient penetration; however, as the microneedle tip becomes sharper, a manual hand-held applicator may be sufficient.

There have been several clinical trials performed for the (trans)dermal delivery of various drugs in humans by using microneedles. Zosano Pharma performed a phase I/II study on the delivery of parathyroid hormone by using coated Macroflux® microneedles [137] and NanoPass Technologies have used their Micronjet® hollow microneedles for the delivery of insulin, influenza vaccine, and lidocaine (for local anesthesia) in clinical studies [138]. Also other clinical studies have been performed for the delivery of local anesthetics by microneedles. Gupta *et al.* used pulled hollow microneedles to deliver lidocaine to the skin [139] and Li *et al.* used solid microneedles from Nanomed Devices for dermal delivery of dyclonine [140]. BD Medical-Pharmaceutical systems tested a rabies vaccine in a clinical trial

by using the BD 34G hollow microneedles [86], and Wermeling *et al.* used solid microneedles for the transdermal delivery of naltrexone [141]. Finally, Gupta *et al.* used pulled microneedles to deliver insulin in a clinical study [128, 131], and Pettis *et al.* used steel microneedles in a clinical trial to administer insulin intradermally [132, 133].

In order to move microneedles to the market for (trans)dermal drug delivery, it is very important to properly choose the type of microneedle (e.g., hollow, solid, geometry, material, density, length). Furthermore, in order to obtain sufficient and reproducible penetration, and the possibility of self-administration, microneedle application devices should be used. Therefore, new microneedle-based products for (trans)dermal drug delivery should be one complete package for each type of drug; including the drug, a stable drug formulation, appropriate microneedles, and a microneedle application device.

Microneedle-based dermal immunization has been shown to be more dose effective than conventional intramuscular and subcutaneous immunization in both human and animal studies [66, 142-144]. Therapeutic proteins have been delivered by the different approaches of microneedle-based drug delivery, however, in the papers cited above protein structure was at best partially studied and still little is known about unwanted immunological effects of microneedle-based protein delivery. For therapeutic proteins, preservation of protein structure during manufacture, storage and use is considered even more important than for vaccines. Importantly, a change in the structure of therapeutic proteins does not only lead to a decrease of drug efficacy, it may also affect safety and induce unwanted immunogenicity. Furthermore, unwanted immunogenicity can lead to total loss of the therapeutic effect of a protein by neutralizing antibodies, and may even lead to depletion of endogenous proteins or breaking the immune-tolerance to self-antigens [145-150]. Since the skin is a potent immune organ, the latter is perhaps the biggest safety concern. This also underscores the need for extensive characterization of protein aggregates and subvisible particles that may be present and released from transdermal microneedle-based formulations, as these are considered important risk factors for unwanted protein immunogenicity [145, 151, 152]. However, to our knowledge no reports on unwanted immunogenicity of therapeutic protein delivery by microneedles have been published and research in this area is urgently needed to move this field forward. This implies a rigorous analysis of protein structure to ensure its integrity during manufacture and release [153], as well as immunogenicity studies in relevant animal models [154].

With the advance of microfluidics and microneedle technologies, microfabrication techniques are becoming more sophisticated. These techniques enable, in combination with hollow microneedles, the development of delivery and analysis devices on one chip (lab-on-a-chip). Lab-on-a-chip devices are promising tools for single-cell analysis, diagnostic and treatment purposes. Devices can be developed, e.g., for diabetics, whereby microneedles may be integrated with a microsensor for glucose detection, a micropump for delivering insulin, and a microchip which regulates the blood glucose value by observing it and adjusting the delivery of insulin accordingly [1-3, 21, 22, 42, 155].

Altogether, microneedle-based (trans)dermal drug delivery may have a great impact in future medicine, both for vaccination purposes and for the delivery of therapeutic drugs.

References

- [1] H.J.G.E. Gardeniers, R. Luttgge, E.J.W. Berenschot, M.J. de Boer, S.Y. Yeshurun, M. Hefetz, R.v.t. Oever, A.v.d. Berg, Silicon Micromachined Hollow Microneedles for Transdermal Liquid Transport, *J. Microelectromech. Syst.* 12 (2003) 855-862.
- [2] C.D. Chin, V. Linder, S.K. Sia, Lab-on-a-chip devices for global health: Past studies and future opportunities, *Lab Chip* 7 (2007) 41-57.
- [3] J.G.E. Gardeniers, A. van den Berg, Lab-on-a-chip systems for biomedical and environmental monitoring, *Anal. Bioanal. Chem.* 378 (2004) 1700-1703.
- [4] K. Tsuchiya, N. Nakanishi, Y. Uetsuji, E. Nakamachi, Development of blood extraction system for health monitoring system, *Biomed. Microdevices* 7 (2005) 347-353.
- [5] H.W. Vesper, P.M. Wang, E. Archibold, M.R. Prausnitz, G.L. Myers, Assessment of Trueness of a Glucose Monitor Using Interstitial Fluid and Whole Blood as Specimen Matrix, *Diabetes Technol. & Ther.* 8 (2006) 76-80.
- [6] J.T. Huzil, S. Sivaloganathan, M. Kohandel, M. Foldvari, Drug delivery through the skin: molecular simulations of barrier lipids to design more effective noninvasive dermal and transdermal delivery systems for small molecules, biologics, and cosmetics, *Wiley Interdiscip. Rev. Nanomed. Nanobiotechnol.* doi: 10.1002/wnan.147 (2011).
- [7] J.A. Bouwstra, M. Ponc, The skin barrier in healthy and diseased state, *Biochim. Biophys. Acta* 1758 (2006) 2080-2095.
- [8] J. Kanitakis, Anatomy, histology and immunohistochemistry of normal human skin, *Eur. J. Dermatol.* 12 (2002) 390-399.
- [9] E.N. Marieb, *Human Anatomy & Physiology*, Dayl Fox, 2004.
- [10] S.M. Bal, Z. Ding, E. van Riet, W. Jiskoot, J. Bouwstra, Advances in transcutaneous vaccine delivery: do all ways lead to Rome?, *J. Control. Release* 148 (2010) 266-282.
- [11] B. Combadiere, B. Mahe, Particle-based vaccines for transcutaneous vaccination, *Comp. Immunol. Microbiol. Infect. Dis.* 31 (2008) 293-315.
- [12] T. Warger, H. Schild, G. Rechtsteiner, Initiation of adaptive immune responses by transcutaneous immunization, *Immunol. Lett.* 109 (2007) 13-20.
- [13] D.V. McAllister, M.G. Allen, M.R. Prausnitz, Microfabricated microneedles for gene and drug delivery, *Annu. Rev. Biomed. Eng* 02 (2000) 289-313.
- [14] M.R. Prausnitz, Microneedles for transdermal drug delivery, *Adv. Drug Deliv. Rev.* 56 (2004) 581-587.
- [15] M.R. Prausnitz, R. Langer, Transdermal drug delivery, *Nat. Biotechnol.* 26 (2008) 1261 - 1268
- [16] T. Tanner, R. Marks, Delivering drugs by the transdermal route: review and comment, *Skin Res. Technol.* 14 (2008) 249-260.
- [17] A.M. Ball, K.M. Smith, Optimizing transdermal drug therapy, *Am. J. Health Syst. Pharm.* 65 (2008) 1337-1346.
- [18] G. Chopda, *Transdermal Drug Delivery Systems: A Review*, 2006, available from: <http://www.pharmainfo.net/reviews/transdermal-drug-delivery-systems-review>
- [19] R.K. Subedi, S.Y. Oh, M.-K. Chun, H.-K. Choi, Recent Advances in Transdermal Drug Delivery, *Arch. Pharm. Res.* 33 (2010) 339-351.
- [20] S. Henry, D.V. McAllister, M.G. Allen, M.R. Prausnitz, Microfabricated microneedles: a novel approach to transdermal drug delivery, *J. Pharm. Sci.* 87 (1998) 922-925.
- [21] W.H. Smart, K. Subramanian, The Use of Silicon Microfabrication Technology in Painless Blood Glucose Monitoring, *Diabetes Technol. Ther.* 2 (2000) 549-559.
- [22] M.L. Reed, W.-K. Lye, Microsystems for Drug and Gene Delivery, *Proc. IEEE* 92 (2004) 56-75.
- [23] J.D. Zahn, D. Trebotich, D. Liepmann, Microdialysis Microneedles for Continuous Medical Monitoring, *Biomed. Microdevices* 7 (2005) 59-69.
- [24] E.V. Mukerjee, S.D. Collins, R.R. Isseroff, R.L. Smith, Microneedle array for transdermal biological fluid extraction and in situ analysis, *Sens. Actuators A Phys.* 114 (2004) 267-275.
- [25] R. Luttgge, E.J.W. Berenschot, M.J. de Boer, D.M. Altpeter, E.X. Vrouwe, A. van den Berg, M. Dwenspoek, Integrated Lithographic Molding for Microneedle-Based Devices, *J. Microelectromech. Sys.* 16 (2007) 872-884.
- [26] A. Rodriguez, D. Molinero, E. Valera, T. Trifonov, L.F. Marsal, J. Pallares, R. Alcubilla, Fabrication of silicon oxide microneedles from macroporous silicon, *Sens. Actuators B* 109 (2005) 135-140.
- [27] M.R. Prausnitz, H.S. Gill, J.-H. Park, *Modified Release Drug Delivery*, Vol. 2nd ed New York: Healthcare, 2008, pp. 295-309.
- [28] A.K. Banga, Microporation applications for enhancing drug delivery, *Expert Opin. Drug Deliv.* 6 (2009) 343-354.
- [29] A. Arora, M.R. Prausnitz, S. Mitragotri, micro-scale devices for transdermal drug delivery, *Int. J. Pharm.* 364 (2008) 227-236.
- [30] T. Miyano, Y. Tobinaga, T. Kanno, Y. Matsuzaki, H. Takeda, M. Wakui, K. Hanada, Sugar Micro Needles as Transdermic Drug Delivery System, *Biomed. Microdevices* 7 (2005) 185-188.
- [31] S.P. Davis, W. Martanto, M.G. Allen, M.R. Prausnitz, Hollow metal microneedles for insulin delivery to diabetic rats, *IEEE Trans. Biomed. Eng.* 52 (2005) 909-915.
- [32] J.-H. Park, M.G. Allen, M.R. Prausnitz, Biodegradable polymer microneedles: Fabrication, mechanics and transdermal drug delivery, *J. Control. Release* 104 (2005) 51-66.
- [33] Y. Ito, J.-I. Yoshimitsu, K. Shiroyama, N. Sugioka, K. Takada, Self-dissolving microneedles for the percutaneous absorption of EPO in mice, *J. Drug Target.* 14 (2006) 255-261.
- [34] J.-H. Park, M.G. Allen, M.R. Prausnitz, Polymer Microneedles for Controlled-Release Drug Delivery, *Pharm. Res.* 23 (2006) 1008-1019.
- [35] S.-C. Kuo, Y. Chou, A Novel Polymer Microneedle Arrays and PDMS Micromolding Technique, *Tamkang J. Sci. Engineering* 7 (2004) 95-98.
- [36] H. Kalluri, C.S. Kolli, A.K. Banga, Characterization of Microchannels Created by Metal Microneedles: Formation and Closure, *The AAPS Journal* DOI:

- 10.1208/s12248-011-9288-3 (2011).
- [37] J.A. Matriano, M. Cormier, J. Johnson, W.A. Young, M. Butterly, K. Nyam, P.E. Daddona, Macroflex microprojection array patch technology: a new and efficient approach for intracutaneous immunization, *Pharm. Res.* 19 (2002) 63-70.
- [38] F. Chabri, K. Bouris, T. Jones, D. Barrow, A. Hann, C. Allender, K. Brain, J. Birchall., Microfabricated silicon microneedles for nonviral cutaneous gene delivery, *Br. J. Dermatol.* 150 (2004) 869-877.
- [39] W. Martanto, J.S. Moore, O. Kashlan, R. Kamath, P.M. Wang, J.M. O'Neal, M.R. Prausnitz, Microinfusion using hollow microneedles, *Pharm. Res.* 23 (2006) 104-113.
- [40] S.-J. Paik, S. Byun, J.-M. Lim, Y. Park, A. Lee, S. Chung, J. Chang, K. Chun, D.D. Cho, In-plane single-crystal-silicon microneedles for minimally-invasive microfluid systems, *Sens. Actuators A Phys.* 2004 (2004) 276-284.
- [41] D.V. McAllister, P.M. Wang, S.P. Davis, J.-H. Park, P.J. Canatella, M.G. Allen, M.R. Prausnitz, Microfabricated needles for transdermal delivery of macromolecules and nanoparticles: Fabrication methods and transport studies, *Proc. Natl. Acad. Sci. U. S. A.* 100 (2003) 13755-13760.
- [42] B. Stoerber, D. Liepmann, Design, fabrication and testing of a MEMS syringe, presented at the Solid-State Sensor, Actuator and Microsystems Workshop, Hilton Head, SC, 2002 (2002).
- [43] R. Sivamani, D. Liepmann, H. Maibach, Microneedles and transdermal applications, *Expert Opin. Drug Deliv.* 4 (2007) 19-25.
- [44] M. Cormier, B. Johnson, M. Ameri, K. Nyam, L. Libiran, D.D. Zhang, P. Daddona, Transdermal delivery of desmopressin using a coated microneedle array patch system, *J. Control. Release* 97 (2004) 503-511.
- [45] G. Widera, J. Johnson, L. Kim, L. Libiran, K. Nyam, P.E. Daddona, M. Cormier, Effect of delivery parameters on immunization to ovalbumin following intracutaneous administration by a coated microneedle array patch system, *Vaccine* 24 (2006) 1653-1664.
- [46] F.J. Verbaan, S.M. Bal, D.J. van den Berg, W.H.H. Groenink, H. Verpoorten, R. Lüttge, J.A. Bouwstra, Assembled microneedle arrays enhance the transport of compounds varying over a large range of molecular weight across human dermatomed skin, *J. Control. Release* 117 (2007) 238-245.
- [47] F.J. Verbaan, S.M. Bal, D.J. van den Berg, J.A. Dijkman, M.v. Hecke, H. Verpoorten, A. van den Berg, R. Lüttge, J.A. Bouwstra, Improved piercing of microneedle arrays in dermatomed human skin by an impact insertion method, *J. Control. Release* 128 (2008) 80-88.
- [48] A.J. Harvey, S.A. Kaestner, D.E. Sutter, N.G. Harvey, J.A. Mikszta, R.J. Pettis, Microneedle-based intradermal delivery enables rapid lymphatic uptake and distribution of protein drugs, *Pharm. Res.* 28 (2011) 107-116.
- [49] E.M. Nadgorny, J. Drelich, Laser-Based Deposition Technique: Patterning Nanoparticles into Microstructures, *Dekker Encyclopedia of Nanoscience and Nanotechnology* (2004) 1565-1579.
- [50] K. Migalska, D.I.J. Morrow, M.J. Garland, R. Thakur, A.D. Woolfson, R.F. Donnelly, Laser-engineered dissolving microneedle arrays for transdermal macromolecular drug delivery, *Pharm. Res.* 28 (2011) 1919-1930.
- [51] J.W. Lee, J.-H. Park, M.R. Prausnitz, Dissolving microneedles for transdermal drug delivery, *Biomaterials* 29 (2008) 2113-2124.
- [52] L.Y. Chu, S.-O. Choi, M.R. Prausnitz, Fabrication of dissolving polymer microneedles for controlled drug encapsulation and delivery: Bubble and pedestal microneedle designs, *J. Pharm. Sci.* 99 (2010) 4228-4238.
- [53] S.P. Sullivan, D.G. Koutsonanos, M.d.P. Martin, J.W. Lee, V. Zarnitsyn, S.-O. Choi, N. Murthy, R.W. Compans, I. Skountzou, M.R. Prausnitz, Dissolving polymer microneedle patches for influenza vaccination, *Nat. Med.* 16 (2010) 915-929.
- [54] K. Fukushima, A. Ise, H. Morita, R. Hasegawa, Y. Ito, N. Sugioka, K. Takada, Two-layered dissolving microneedles for percutaneous delivery of peptide/protein drugs in rats, *Pharm. Res.* 28 (2011) 7-21.
- [55] K. Lee, C.Y. Lee, H. Jung, Dissolving microneedles for transdermal drug administration prepared by stepwise controlled drawing of maltose, *Biomaterials* 32 (2011) 3134-3140.
- [56] M.I. Haq, E. Smith, D.N. John, M. Kalavala, C. Edwards, A. Anstey, A. Morrissey, J.C. Birchall, Clinical administration of microneedles: skin puncture, pain and sensation, *Biomed. Microdevices* 11 (2009) 35-47.
- [57] P.M. Wang, M. Cornwell, J. Hill, M.R. Prausnitz, Precise microinjection into skin using hollow microneedles, *J. Invest. Dermatol.* 126 (2006) 1080-1087.
- [58] R.F. Donnelly, T.R.R. Singh, A.D. Woolfson, Microneedle-based drug delivery systems: microfabrication, drug delivery, and safety, *Drug Delivery* 17 (2010) 187-207.
- [59] D.W. Bodhale, A. Nisar, N. Afzulpurkar, Structural and microfluidic analysis of hollow side-open polymeric microneedles for transdermal drug delivery applications, *Microfluid. Nanofluid.* 8 (2010) 373-392.
- [60] A.L. Teo, C. Shearwood, K.C. Nga, J. Lua, S. Moochhala, Transdermal microneedles for drug delivery applications, *Mat. Sci. Eng. B* 132 (2006) 151-154.
- [61] S.P. Davis, B.J. Landis, Z.H. Adams, M.G. Allen, M.R. Prausnitz, Insertion of microneedles into skin: measurement and prediction of insertion force and needle fracture force, *J. Biomech.* 37 (2004) 1155-1163.
- [62] J.D. Zahn, N.H. Talbot, D. Liepmann, A.P. Pisano, Microfabricated polysilicon microneedles for minimally-invasive biomedical devices, *Biomed. Microdevices* 2 (2000) 295-303.
- [63] S.-O. Choi, Y.C. Kim, J.-H. Park, J. Hutcheson, H.S. Gill, Y.-K. Yoon, M.R. Prausnitz, M.G. Allen, An electrically active microneedle array for electroporation, *Biomed. Microdevices* 12 (2010) 263-273.
- [64] M. Yang, J.D. Zahn, Microneedle insertion force reduction using vibratory actuation, *Biomed. Microdevices* 6 (2004) 177-182.
- [65] M.L. Crichton, A. Ansaldo, X. Chen, T.W. Prow, G.J.P. Fernando, M.A.F. Kendall, The effect of strain rate on the precision of penetration of short densely-packed microprojection array patches coated with vaccine, *Biomaterials* 31 (2010) 4562-4572.
- [66] X. Chen, G.J.P. Fernando, M.L. Crichton, C. Flaim, S.R. Yukiko, E.J. Fairmaid, H.J. Corbett, C.A. Primiero, A.B. Ansaldo, I.H. Frazer, L.E. Brown, M.A.F. Kendall, Improving the reach of vaccines to low-resource regions, with a needle-free vaccine delivery device and long-term thermostabilization, *J. Control. Release* 152 (2011) 349-355.

- [67] S.M. Bal, J. Caussin, S. Pavel, J.A. Bouwstra, In vivo assessment of safety of microneedle arrays in human skin, *J. Control. Release* 35 (2008) 193-202.
- [68] N. Roxhed, B. Samel, L. Nordquist, P. Griss, G. Stemme, Painless drug delivery through microneedle-based transdermal patches featuring active infusion, *IEEE Trans. Biomed. Eng.* 55 (2008) 1063 - 1071.
- [69] S. Chandrasekaran, A.B. Frazier, Mechanical characterization of surface micromachined hollow metallic microneedles, *IEEE The Sixteenth Annual International Conference on Micro Electro Mechanical Systems*, 2003. MEMS-03 Kyoto (2002) 363 - 366.
- [70] Q. Cui, C. Liu, X.F. Zha, Study on a piezoelectric micropump for the controlled drug delivery system, *Microfluid. Nanofluid.* 3 (2007) 377-390.
- [71] M. E. Tucker, Recombinant Human Hyaluronidase Accelerates Insulin Absorption, *Internal Medicine News* 2011, January 10 2012, Available from: <http://www.internalmedicineneeds.com/search/search-single-view/recombinant-human-hyaluronidase-accelerates-insulin-absorption/978d75e015.html>
- [72] G.L. Li, T.J.V. Steeg, H. Putter, J.V.D. Spek, S. Pavel, M. Danhof, J.A. Bouwstra, Cutaneous side-effects of transdermal iontophoresis with and without surfactant pretreatment: a single-blinded, randomized controlled trial, *Br. J. Dermatol.* 153 (2005) 404-412.
- [73] H. Kalluri, A.K. Banga, Formation and closure of microchannels in skin following microporation, *Pharm. Res.* 28 (2011) 82-94.
- [74] J. Gupta, H.S. Gill, S.N. Andrews, M.R. Prausnitz, Kinetics of skin resealing after insertion of microneedles in human subjects, *J. Control. Release* doi:10.1016/j.jconrel.2011.05.021 (2011).
- [75] S.L. Banks, K.S. Paudel, N.K. Brogden, C.D. Loftin, A.L. Stinchcomb, Diclofenac Enables Prolonged Delivery of Naltrexone Through Microneedle-Treated Skin, *Pharm. Res.* 28 (2011) 1211-1219.
- [76] H. Chen, H. Zhu, J. Zheng, D. Mou, J. Wan, J. Zhang, T. Shi, Y. Zhao, H. Xu, X. Yang, Iontophoresis-driven penetration of nanovesicles through microneedle-induced skin microchannels for enhancing transdermal delivery of insulin, *J. Control. Release* 139 (2009) 63-72.
- [77] X.-M. Wu, H. Todo, K. Sugibayashi, Enhancement of skin permeation of high molecular compounds by a combination of microneedle pretreatment and iontophoresis, *J. Control. Release* 118 (2007) 189-195.
- [78] A.V. Badkar, A.M. Smith, J.A. Eppstein, A.K. Banga, Transdermal delivery of interferon alpha-2B using microporation and iontophoresis in hairless rats, *Pharm. Res.* 24 (2007) 1389-1395.
- [79] S. Katikaneni, A. Badkar, S. Nema, A.K. Banga, Molecular charge mediated transport of a 13 kD protein across microporated skin, *Int. J. Pharm.* 378 (2009) 93-100.
- [80] W. Lin, M. Cormier, A. Samiee, A. Griffin, B. Johnson, C.-L. Teng, G.E. Hardee, P.E. Daddona, Transdermal delivery of antisense oligonucleotides with microprojection patch (Macroflux) technology, *Pharm. Res.* 18 (2001).
- [81] J.A. Mikszta, J.B. Alarcon, J.M. Brittingham, D.E. Sutter, R.J. Pettis, N.G. Harvey, Improved genetic immunization via micromechanical disruption of skin-barrier function and targeted epidermal delivery, *Nat. Med.* 8 (2002) 415-419.
- [82] C.H. Dean, J.B. Alarcon, A.M. Waterston, K. Draper, R. Early, F. Guirakhoo, T.P. Monath, J.A. Mikszta, Cutaneous delivery of a live, attenuated chimeric flavivirus vaccine against Japanese encephalitis (ChimeriVax)-JE) in non-human primates, *Hum. Vaccin.* 1 (2005) 106-111.
- [83] H.S. Gill, S.N. Andrews, S.K. Sakthivel, A. Fedanov, I.R. Williams, D.A. Garber, F.H. Priddy, S. Yellin, M.B. Feinberg, S.I. Staprans, M.R. Prausnitz, Selective removal of stratum corneum by microdermabrasion to increase skin permeability, *Eur. J. Pharm. Sci.* 38 (2009) 95-103.
- [84] M. Pearton, S.-M. Kang, J.-M. Song, Y.-C. Kim, F.-S. Quan, A. Anstey, M. Ivory, M.R. Prausnitz, R.W. Compans, J.C. Birchall, Influenza virus-like particles coated onto microneedles can elicit stimulatory effects on Langerhans cells in human skin, *Vaccine* 28 (2010) 6104-6113.
- [85] J.A. Mikszta, V.J. Sullivan, C. Dean, A.M. Waterston, J.B. Alarcon, J.P.D. III, J.M. Brittingham, J. Huang, C.R. Hwang, M. Ferriter, G. Jiang, K. Mar, K.U. Saikh, B.G. Stiles, C.J. Roy, Robert G. Ulrich, N.G. Harvey, Protective Immunization against Inhalational Anthrax: A Comparison of Minimally-invasive Delivery Platforms, *J. Infect. Dis.* 191 (2005) 278-288.
- [86] P.E. Laurent, H. Bourhy, M. Fantino, P. Alchas, J.A. Mikszta, Safety and efficacy of novel dermal and epidermal microneedle delivery systems for rabies vaccination in healthy adults, *Vaccine* 28 (2010) 5850-5856.
- [87] B. Chen, J. Wei, F.E.H. Tay, Y.T. Wong, C. Iliescu, Silicon microneedle array with biodegradable tips for transdermal drug delivery, *Microsyst. Technol.* 14 (2007) 1015-1019.
- [88] K. Lee, J.D. Kim, C.Y. Lee, S. Her, H. Jung, A high-capacity, hybrid electro-microneedle for in-situ cutaneous gene transfer, *Biomaterials* doi:10.1016/j.biomaterials.2011.06.058 (2011b).
- [89] D. Scholten, M. Stumber, F. Laermer, A. Feyh, Manufacturing method for a porous microneedle array and corresponding porous microneedle array and corresponding substrate composite, *United States Patent Application* 20110137254 (2011).
- [90] M.G. Allen, M.R. Prausnitz, D.V. McAllister, F.P.M. Cros, *Microneedle Devices and Methods of Manufacture and Use Thereof*, US 2010/0312191 A1 (2010).
- [91] J. Ji, F.E.H. Tay, J. Miao, C. Iliescu, Microfabricated microneedle with porous tip for drug delivery, *J. Micromech. Microeng.* 16 (2006) 958-964.
- [92] J.-H. Park, S.-O. Choi, R. Kamath, Y.-K. Yoon, M.G. Allen, M.R. Prausnitz, Polymer particle-based micromolding to fabricate novel microstructures, *Biomed. Microdevices* 9 (2007) 223-234.
- [93] M. Shirkhanzadeh, Microneedles coated with porous calcium phosphate ceramics: effective vehicles for transdermal delivery of solid trehalose, *J. Mater. Sci. Mater. Med.* 16 (2005) 37-45.
- [94] H.S. Gill, M.R. Prausnitz, Coating formulations for microneedles, *Pharm. Res.* 24 (2007) 1369-1380.
- [95] H.S. Gill, M.R. Prausnitz, Coated microneedles for transdermal delivery, *J. Control. Release* 117 (2007) 227-237.
- [96] H.S. Gill, M.R. Prausnitz, Pocketed Microneedles for Drug Delivery to the Skin, *J. Phys. Chem. Solids* 69 (2008) 1537-1541.
- [97] T. Matsuda, M. Mizutani, Liquid acrylate-ended capped biodegradable poly(ϵ -caprolactone-co-trimethylene carbonate). II. Computer-aided stereolithographic microarchitectural surface photoconstructs, *J. Biomed. Mater. Res.* 62 (2002) 395-403.

- [98] R.F. Donnelly, R. Majithiya, T.R.R. Singh, D.I.J. Morrow, M.J. Garland, Y.K. Demir, K. Migalska, E. Ryan, D. Gillen, C.J. Scott, A.D. Woolfson, Design, optimization and characterisation of polymeric microneedle arrays prepared by a novel laser-based micromoulding technique, *Pharm. Res.* 28 (2011) 41-57.
- [99] M.G. McGrath, A. Vrdoljak, C. O'Mahony, J.C. Oliveira, A.C. Moore, A.M. Crean, Determination of parameters for successful spray coating of silicon microneedle arrays, *Int. J. Pharm.* 415 (2011) 140-149.
- [100] X. Chen, T.W. Prow, M.L. Crichton, D.W.K. Jenkins, M.S. Roberts, I.H. Frazer, G.J.P. Fernando, M.A.F. Kendall, Dry-coated microprojection array patches for targeted delivery of immunotherapeutics to the skin, *J. Control. Release* 139 (2009) 212-220.
- [101] Y. Zhang, K. Brown, K. Siebenaler, A. Determan, D. Dohmeier, K. Hansen, Development of Lidocaine-Coated Microneedle Product for Rapid, Safe, and Prolonged Local Analgesic Action, *Pharm. Res.* DOI 10.1007/s11095-011-0524-4 (2011).
- [102] Y. Xie, B. Xu, Y. Gao, Controlled transdermal delivery of model drug compounds by MEMS microneedle array, *Nanomedicine* 1 (2005) 184-190.
- [103] H.S. Gill, J. Soderholm, M.R. Prausnitz, M. Salberg, Cutaneous vaccination using microneedles coated with hepatitis C DNA vaccine, *Gene Therapy* 17 (2010) 811-814.
- [104] E.M. Saurer, R.M. Flessner, S.P. Sullivan, M.R. Prausnitz, D.M. Lynn, Layer-by-Layer Assembly of DNA- and Protein-Containing Films on Microneedles for Drug Delivery to the Skin, *Biomacromolecules* 11 (2010) 3136-3143.
- [105] D.G. Koutsonanos, M.d.P. Martin, V.G. Zarnitsyn, S.P. Sullivan, R.W. Compans, M.R. Prausnitz, I. Skountzou, Transdermal influenza immunization with vaccine-coated microneedle arrays, *PLoS One* 4 (2009) e4773.
- [106] F.-S. Quan, Y.-C. Kim, D.-G. Yoo, R.W. Compans, M.R. Prausnitz, S.-M. Kang, Stabilization of influenza vaccine enhances protection by microneedle delivery in the mouse skin, *PLoS One* 4 (2009) e7215.
- [107] Q. Zhu, V.G. Zarnitsyn, L. Ye, Z. Wen, Y. Gao, L. Pan, I. Skountzou, H.S. Gill, M.R. Prausnitz, C. Yang, R.W. Compans, Immunization by vaccine-coated microneedle arrays protects against lethal influenza virus challenge, *Proc. Natl. Acad. Sci. U. S. A.* 106(19) (2009) 7968-7973.
- [108] F.-S. Quan, Y.-C. Kim, A. Vunnavu, D.-G. Yoo, J.-M. Song, M.R. Prausnitz, R.W. Compans, S.-M. Kang, Intradermal vaccination with influenza virus-like particles by using microneedles induces protection superior to that with intramuscular immunization, *Journal of Virol.* 84 (2010) 7760-7769.
- [109] Y.-C. Kim, F.-S. Quan, R.W. Compans, S.-M. Kang, M.R. Prausnitz, Formulation and coating of microneedles with inactivated influenza virus to improve vaccine stability and immunogenicity, *J. Control. Release* 142 (2010) 187-195.
- [110] Y.-C. Kim, F.-S. Quan, R.W. Compans, S.-M. Kang, M.R. Prausnitz, Formulation of microneedles coated with influenza virus-like particle vaccine, *AAPS PharmSciTech* 11 (2010) 1193-1201.
- [111] Y.-C. Kim, F.-S. Quan, D.-G. Yoo, R.W. Compans, S.-M. Kang, M.R. Prausnitz, Enhanced memory responses to seasonal H1N1 influenza vaccination of the skin with the use of vaccine-coated microneedles, *J. Infect. Dis.* 201 (2010) 190-198.
- [112] Y.-C. Kim, F.-S. Quan, R.W. Compans, S.-M. Kang, M.R. Prausnitz, Stability kinetics of influenza vaccine coated onto microneedles during drying and storage, *Pharm. Res.* 28 (2010) 135-144.
- [113] Y.-C. Kim, F.-S. Quan, D.-G. Yoo, R.W. Compans, S.-M. Kang, M.R. Prausnitz, Improved influenza vaccination in the skin using vaccine coated microneedles, *Vaccine* 27 (2009) 6932-6938.
- [114] C.J.B.G.T.J.C. Martin, Aerosol coating of microneedles, *WO/2009/081125* (2009).
- [115] M. Ameri, P.E. Daddona, Y.-F. Maa, Demonstrated Solid-State Stability of Parathyroid Hormone PTH(1-34) Coated on a Novel Transdermal Microprojection Delivery System, *Pharm. Res.* 26 (2009) 2454-2463.
- [116] A.K. Andrianov, A. Marin, D.P. DeCollibus, Microneedles with Intrinsic Immunoadjuvant Properties: Microfabrication, Protein Stability, and Modulated Release, *Pharm. Res.* 28 (2011) 58-65.
- [117] A.K. Andrianov, D.P. DeCollibus, H.A. Gillis, H.H. Kha, A. Marin, M.R. Prausnitz, L.A. Babiuk, H. Townsend, G. Mutwiri, Poly[di(carboxylatophenoxy) phosphazene] is a potent adjuvant for intradermal immunization, *Proc. Natl. Acad. Sci. U. S. A.* 106 (2009) 18936-18941.
- [118] A. Marin, A.K. Andrianov, Carboxymethylcellulose-Chitosan-Coated Microneedles with Modulated Hydration Properties, *J. Appl. Polymer Sci.* 121 (2011) 395-401.
- [119] X. Su, B.-S. Kim, S.R. Kim, P.T. Hammond, D.J. Irvine, Layer-by-Layer-Assembled Multilayer Films for Transcutaneous Drug and Vaccine Delivery, *ACS nano* 3 (2009) 3719-3729.
- [120] P.C. DeMuth, X. Su, R.E. Samuel, P.T. Hammond, D.J. Irvine, Nano-Layered Microneedles for Transcutaneous Delivery of Polymer Nanoparticles and Plasmid DNA, *Adv. Mater.* 22 (2010) 4851-4856.
- [121] R.J. Verheul, B. Slütter, S.M. Bal, J.A. Bouwstra, W. Jiskoot, W.E. Hennink, Covalently stabilized trimethyl chitosan-hyaluronic acid nanoparticles for nasal and intradermal vaccination, *J. Control. Release* doi:10.1016/j.jconrel.2011.07.014 (2011).
- [122] S.M. Bal, B. Slütter, W. Jiskoot, J.A. Bouwstra, Small is beautiful: N-trimethyl chitosan-ovalbumin conjugates for microneedle-based transcutaneous immunisation, *Vaccine* 29 (2011) 4025-4032.
- [123] S.M. Bal, B. Slütter, E. van Riet, A.C. Kruihof, Z. Ding, G.F.A. Kersten, W. Jiskoot, J.A. Bouwstra, Efficient induction of immune responses through intradermal vaccination with N-trimethyl chitosan containing antigen formulations, *J. Control. Release* 142 (2010) 374-383.
- [124] B. Slütter, S.M. Bal, D. Zhi, W. Jiskoot, J.A. Bouwstra, Adjuvant effect of cationic liposomes and CpG depends on administration route, *J. Control. Release* doi:10.1016/j.jconrel.2011.02.007 (2011).
- [125] A.P. Raphael, T.W. Prow, M.L. Crichton, X. Chen, G.J.P. Fernando, M.A.F. Kendall, Targeted, needle-free vaccinations in skin using multilayered, densely-packed dissolving microprojection arrays, *Small* 6 (2010) 1785-1793.
- [126] A. Kumar, X. Li, M.A. Sandoval, B.L. Rodriguez, B.R. Sloat, Z. Cui, Permeation of antigen protein-conjugated nanoparticles and live bacteria through microneedle-treated mouse skin, *Int. J. Nanomed.* 6 (2011) 1253-1264.
- [127] L. Nordquist, N. Roxhed, P. Griss, G. Stemme, Novel Microneedle Patches for Active Insulin Delivery are Efficient in Maintaining Glycaemic Control: An Initial Comparison with Subcutaneous Administration, *Pharm. Res.* 24 (2007) 1381-1388.

- [128] J. Gupta, E.I. Felner, M.R. Prausnitz, Minimally-invasive insulin delivery in subjects with type 1 diabetes using hollow microneedles, *Diabetes Technol. Ther.* 11 (2009) 329-337.
- [129] W. Martanto, S.P. Davis, N.R. Holiday, J. Wang, H.S. Gill, M.R. Prausnitz, Transdermal Delivery of Insulin Using Microneedles in Vivo, *Pharm. Res.* 21 (2004) 947-952.
- [130] Y. Wu, Y. Gao, G. Qin, S. Zhang, Y. Qiu, F. Li, B. Xu, Sustained release of insulin through skin by intradermal microdelivery system, *Biomed. Microdevices* 12 (2010) 665-671.
- [131] J. Gupta, E.I. Felner, M.R. Prausnitz, Rapid pharmacokinetics of intradermal insulin administered using microneedles in type 1 diabetes subjects, *Diabetes Technol. Ther.* 13 (2011) 451-456.
- [132] R.J. Pettis, B. Ginsberg, L. Hirsch, D. Sutter, S. Keith, E. McVey, N.G. Harvey, M. Hompesch, L. Nosek, C. Kapitza, L. Heinemann, Intradermal microneedle delivery of insulin lispro achieves faster insulin absorption and insulin action than subcutaneous injection, *Diabetes Technol. Ther.* 13 (2011) 435-442.
- [133] R.J. Pettis, L. Hirsch, C. Kapitza, L. Nosek, U. Hövelmann, H.-J. Kurth, D.E. Sutter, N.G. Harvey, L. Heinemann, Microneedle-based intradermal versus subcutaneous administration of regular human insulin or insulin lispro: pharmacokinetics and postprandial glycaemic excursions in patients with type 1 diabetes, *Diabetes Technol. Ther.* 13 (2011) 443-450.
- [134] S. Hermeling, L. Aranha, J.M.A. Damen, M. Slijper, H. Schellekens, D.J.A. Crommelin, W. Jiskoot, Structural characterization and immunogenicity in immune tolerant mice of recombinant human interferon alpha2b, *Pharm. Res.* 22 (2005) 1997-2006.
- [135] S. Hermeling, H. Schellekens, C. Maas, M.F.B.G. Gebbink, D.J.A. Crommelin, W. Jiskoot, Antibody response to aggregated human interferon alpha2b in wildtype and transgenic immune tolerant mice depends on type and level of aggregation, *J. Pharm. Sci.* 95 (2006) 1084-1096.
- [136] M.M.C.V. Beers, M. Sauerborn, F. Gilli, V. Brinks, H. Schellekens, W. Jiskoot, Oxidized and aggregated recombinant interferon beta is immunogenic in human interferon beta transgenic mice. *Pharm. Res.* 28 (2011) 2393-2402.
- [137] Zosano-Pharma, 29-09-2011, available from: http://zosanopharma.com/index.php?option=com_content&task=view&id=99&Itemid=139
- [138] NanoPass-Technologies, 2011-09-28, available from: <http://www.nanopass.com/content-c.asp?cid=22>
- [139] J. Gupta, D.D. Denson, E.I. Felner, M.R. Prausnitz, Rapid Local Anesthesia in Humans Using Minimally-invasive Microneedles, *Clin. J. Pain* doi: 10.1097/AJP.0b013e318225d9e9 (2011).
- [140] X. Li, R. Zhao, Z. Qin, J. Zhang, S. Zhai, Y. Qiu, Y. Gao, B. Xu, S.H. Thomas, Microneedle pretreatment improves efficacy of cutaneous topical anesthesia, *Am. J. Emerg. Med.* 28 (2010) 130-134.
- [141] D.P. Wermeling, S.L. Banks, D.A. Hudson, H.S. Gill, J. Gupta, M.R. Prausnitz, A.L. Stinchcomb, Microneedles permit transdermal delivery of a skin-impermeant medication to humans, *Proc. Natl. Acad. Sci. U. S. A.* 105 (2008) 2058-2063.
- [142] I. Leroux-Roels, E. Vets, R. Freese, M. Seiberling, F. Weber, C. Salamand, G. Leroux-Roels, Seasonal influenza vaccine delivered by intradermal microinjection: A randomised controlled safety and immunogenicity trial in adults, *Vaccine* 26 (2008) 6614-6619.
- [143] J. Beran, A. Ambrozaitis, A. Laikonis, N. Mickuviene, P. Bacart, Y. Calozet, E. Demanet, S. Heijmans, P.V. Belle, F. Weber, C. Salamand, Intradermal influenza vaccination of healthy adults using a new microinjection system: a 3-year randomised controlled safety and immunogenicity trial, *BMC Med.* 7 (2009).
- [144] P. van Damme, F. Oosterhuis-Kafeja, M. van der Wielen, Y. Almagor, O. Sharon, Y. Levin, Safety and efficacy of a novel microneedle device for dose sparing intradermal influenza vaccination in healthy adults, *Vaccine* 27 (2009) 454-459.
- [145] S. Hermeling, D.J.A. Crommelin, H. Schellekens, W. Jiskoot, Structure-immunogenicity relationships of therapeutic proteins, *Pharm. Res.* 21 (2004) 897-903.
- [146] H. Schellekens, Factors influencing the immunogenicity of therapeutic proteins, *Nephrol. Dial. Transplant. [Suppl 6]: vi3-vi9* (2005).
- [147] H. Schellekens, How to predict and prevent the immunogenicity of therapeutic proteins, *Biotechnol. Annu. Rev.* 14 (2008) 191-202.
- [148] M. Sauerborn, V. Brinks, W. Jiskoot, H. Schellekens, Immunogenic mechanism underlying the immune response to recombinant human protein therapeutics, *Trends Pharmacol. Sci.* 31 (2010) 53-59.
- [149] S.K. Singh, Impact of product-related factors on immunogenicity of biotherapeutics, *J. Pharm. Sci.* 100 (2011) 354-387.
- [150] T. Arakawa, J.S. Philo, D. Ejima, K. Tsumoto, F. Arisaka, Aggregation Analysis of Therapeutic Proteins, Part 1. *BioProcess International* 4(10(42-43)) (2006).
- [151] A.S. Rosenberg, Effects of protein aggregates: an immunologic perspective, *The AAPS Journal* 8 (2006) E501-E507.
- [152] S.K. Singh, N. Afonina, M. Awwad, K. Bechtold-Peters, J.T. Blue, D. Chou, M. Cromwell, H.-J. Krause, H.-C. Mahler, B.K. Meyer, L. Narhi, D.P. Nesta, T. Spitznagel, An industry perspective on the monitoring of subvisible particles as a quality attribute for protein therapeutics, *J. Pharm. Sci.* 99 (2010) 3302-3321.
- [153] J. den Engelsman, P. Garidel, R. Smulders, H. Koll, B. Smith, S. Bassarab, A. Seidl, O. Hainzl, W. Jiskoot, Strategies for the assessment of protein aggregates in pharmaceutical biotech product development, *Pharm. Res.* 28 (2011) 920-933.
- [154] V. Brinks, W. Jiskoot, H. Schellekens, Immunogenicity of Therapeutic Proteins: The Use of Animal Models, *Pharm. Res.* 28 (2011) 2379-2385.
- [155] J.D. Zahn, D. Trebotich, D. Liepmann, Microfabricated microdialysis microneedles for continuous medical monitoring, *Biomed. Microdevices* 7 (2005) 59-69.

CHAPTER 3

MICRONEEDLE PRETREATMENT

IMPACT-INSERTION APPLICATOR IMPROVES RELIABILITY OF SKIN PENETRATION BY SOLID MICRONEEDLE ARRAYS

Koen van der Maaden
Emine Sekerdag
Wim Jiskoot
Joke Bouwstra

[The AAPS Journal, 16
\(2014\) 681-684](#)

1. Introduction

Microneedles are needle-like structures shorter than 1 mm that have been advocated as devices for enabling potentially pain free intradermal delivery of biomacromolecules [1-5]. To permit a reproducible delivery of the drug, microneedles should be inserted into the skin in a controlled and reproducible manner [4, 6]. Obviously, one of the factors that influence the penetration ability of microneedles is the insertion process itself, e.g., microneedles can be inserted manually or by using insertion devices [3, 4, 6-9]. Recently, the penetration ability of low-density arrays (42 microneedles/cm²) with 750 µm long microneedles, applied manually or by using a snap-based applicator, was investigated [10]. However, no studies have been reported on the efficiency and reproducibility of the insertion of high-density microneedles into human skin. Therefore, the aim of this study was to investigate the effect of the type of application on *inter* and *intra* individual variability of microneedle insertion into human skin by microneedle users.

We show that participants using an impact-insertion applicator inserted high-density microneedles into *ex vivo* human skin with high efficiency and with a low *inter* and *intra* individual variation. However, when the same microneedle arrays were inserted by using a manual insertion device, the penetration efficiency was reduced by approximately 40% with a considerably lower reproducibility. Finally, the applicability of an impact-insertion applicator/microneedle arrays was confirmed in a vaccination study in mice.

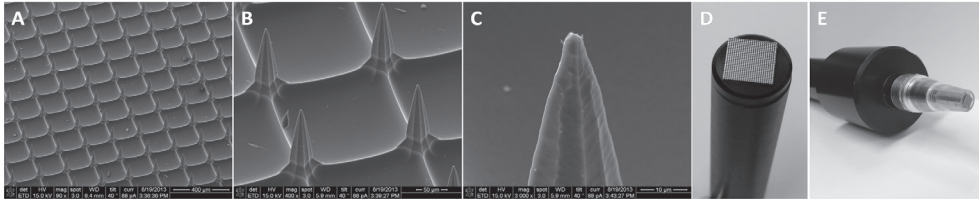


Figure 1: Electron micrographs of a high-density array of 200 µm long silicon microneedles with a magnification of 90x (A), 400x (B), and 3000x (C), mounted on a manual insertion device (D) or an impact-insertion applicator (E).

2. Materials and methods

2.1 Microneedle application

In this study high-density arrays (576 microneedles on a 5x5 mm backplate, gifted by Bosch, Germany, Stuttgart) with a microneedle length of 200 µm were used (figure 1). The microneedles were applied onto *ex vivo* human abdominal skin that was obtained from hospitals within 24 hours after cosmetic surgery and dermatomed to a thickness of 600 µm [11]. To investigate factors that influence the penetration efficiency, microneedles were applied onto the skin for 10 seconds with different forces (3.43-22.1 N) by applying weight rods (350-2250 g) onto the insertion device for manual application. Also, the effect of application time (5-60 seconds) with a constant force (7.36 N) was investigated. Next, 15 participants (21-57 year; 10 male and 5 female) volunteered to apply a microneedle array three times onto *ex vivo* human skin, in a direction perpendicular to the skin surface, by using either a manual application device (figure 1D), or an impact-insertion applicator at a velocity of 3 m/s (figure 1E) [12]. The type of microneedle application was randomly performed.

2.2 Penetration ability of microneedles

To determine the penetration ability, 70 µL of an aqueous 0.4% trypan blue (Sigma Aldrich) solution was applied and left for one hour at the site of prior microneedle application. Subsequently, the skin surface was washed two times with water and once with 70% ethanol. Next, the stratum corneum (SC) was removed by tape-stripping (Scotch tape) until no SC residue was visually observed on the tape and the skin appeared shiny. Finally, the penetration efficiency (PE) was calculated as follows:

$$PE = (\text{number of blue spots} / 576) * 100\%$$

2.3 Safranin staining

To visualize the SC removal efficiency, 10 µm thick cryosections of control and tape-stripped skin were made on a Leica cryostat (CM 3050S) and stained for 1 minute in a 1% (w/v) Safranin O solution (Sigma Aldrich). Next, the number of layers was visualized by swelling the SC in a 2% (w/v) KOH solution for 20 minutes (n=3).

2.4 Immunization of mice with ovalbumin

Eight-week old female BALB/c mice (Charles River) were immunized thrice with intervals of three weeks by the ‘poke and patch’ approach (100 µg ovalbumin /70 µL PBS (pH 7.4) for two hours, as previously described [13]), by using the impact-insertion applicator to apply either the high-density microneedle arrays or our first-generation LU-microneedles. The latter are made of 30 G needle tips, 300 µm long, and fixed in a backplate as a 4x4 microneedle array. They were previously shown to penetrate the skin when using the impact-insertion applicator [12]. A subcutaneous injection of 5 µg ovalbumin in 100 µL PBS was used as positive control. Ovalbumin-specific serum IgG responses were determined by a sandwich ELISA, as described previously [13]. Antibody titers were expressed as the log value of the serum dilution at the mid-point of a complete S-shaped absorbance-dilution curve. The study was carried out under the guidelines complied by the animal ethic committee of the Netherlands, and was approved by the “Dierexperimentencommissie Universiteit Leiden (UDEEC)” under number 13065.

3. Results and discussion

3.1 Assessment of piercing efficiency after stratum corneum removal

The application of dyes at the site of microneedle application is commonly used to assess microneedle penetration in the skin [12, 14-16]. However, when observing the complete skin following microneedle application, the resulting spots are not always penetrations, but could be indentations of the SC (see supplemental information). Indeed, our study made clear that without SC removal the penetration efficiency is overestimated. When microneedle arrays were applied with a manual insertion device onto *ex vivo* human skin, blue spots were visible (figure 2A), suggesting successful skin piercing with an efficiency of 81% (figure 2C). However, after removal of the SC less blue spots were visible (figure 2B), showing that only 46% of the microneedles pierced the skin (figure 2A). The SC consists of 20 layers of corneocytes (figure 2D), and after tape-stripping most of the SC was removed (figure 2E), which allowed a reliable assessment of the piercing efficiency. Therefore, this approach was used in the study described below.

3.2 Penetration ability of high-density microneedle arrays

First, two factors, application force and time, that potentially influence the penetration efficiency of manual microneedle application were investigated (figure 3). Increasing the applied force (at a constant application time of 10 seconds) up to 7.36 N greatly improved the penetration ability (3A), which is in agreement with the literature [9]. Further increase of the force or prolonging the application time of the microneedles at a constant force (7.36 N) only minimally increased the penetration efficiency but improved the reproducibility (3B).

Next, to investigate whether persons without microneedle experience are able to successfully and reproducibly penetrate skin, 15 participants were instructed to apply

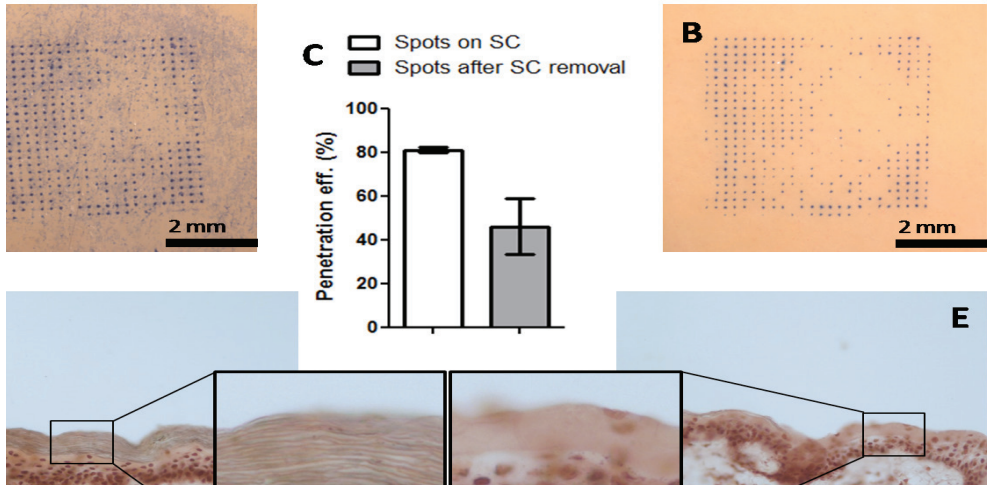


Figure 2: Representative examples of microneedle-pierced trypan blue stained *ex vivo* human skin before (A) and after stratum corneum (SC) removal (B). Calculated penetration efficiency before and after SC removal (mean \pm SD, n=3) (C). Representative examples of Safranin O stained freeze coupes of non-stripped (D) and tape-stripped (E) *ex vivo* human skin.

microneedles onto *ex vivo* human skin by using a manual insertion device or an impact-insertion applicator (figure 3C and 3D). Using a manual application device resulted in low penetration efficiencies (56%) and relative high *inter* and *intra* individual variation, which was probably caused by variations in applied force and that the microneedle application conditions were below the optimum insertion conditions. However, when using the impact-insertion applicator, all participants pierced the skin with significantly lower *inter* and *intra* individual variation. These results show that using a microneedle applicator is essential for efficient and reproducible penetration of skin by a high-density microneedle array.

3.3 Vaccination study in mice

To demonstrate that the use of the impact-insertion applicator can lead to reproducible immune responses following microneedle-mediated immunization, we performed a vaccination study in mice, using ovalbumin as a model antigen. Figure 4 shows that microneedle-based vaccination leads to the induction of reproducible ovalbumin-specific IgG responses. Interestingly, using high-density microneedles resulted in up to ten-fold higher IgG responses as compared to our first-generation LU-microneedles. As both microneedle arrays result in reproducible piercing, the difference is probably caused by differences in microneedle density, number (576 versus 16 microneedles/array) and geometry [12]. Furthermore, a comparison between microneedle-based and subcutaneous administration revealed that vaccination by using high-density microneedles initially led to significantly lower IgG responses than subcutaneous vaccination, but the differences became negligible after the 2nd boost. This shows that microneedle-based vaccination can lead to comparable immune responses as

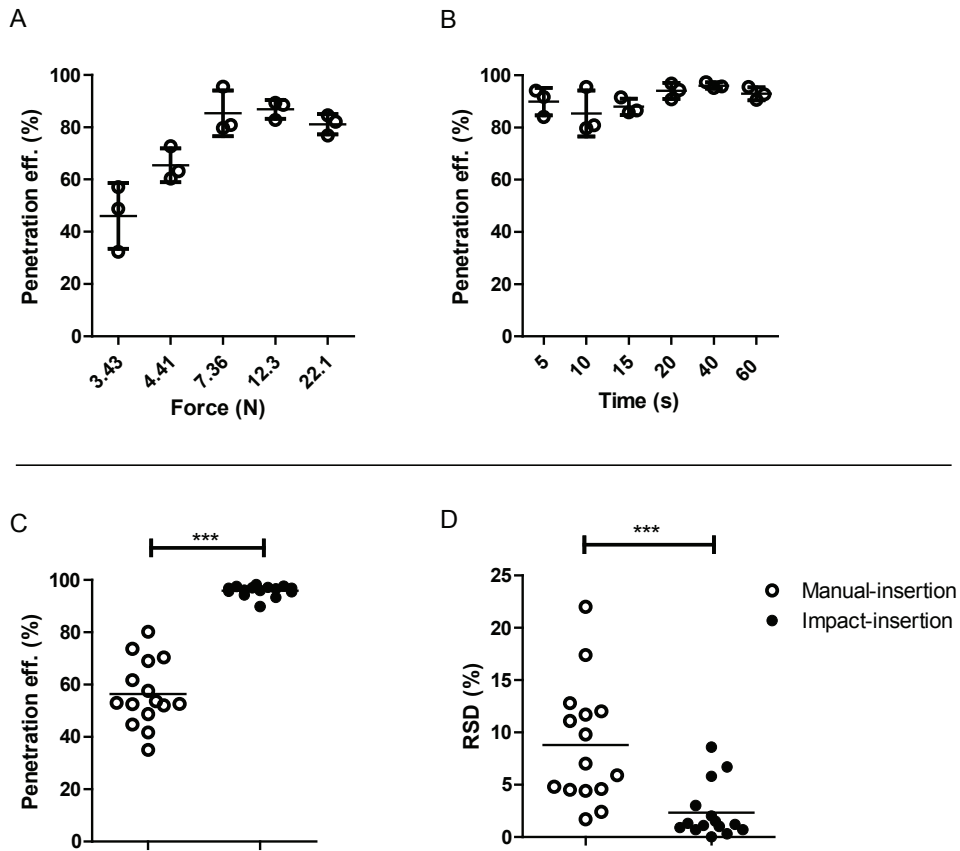


Figure 3: Penetration efficiency after application of a high-density microneedle array onto *ex vivo* human skin with different forces for 10 seconds (A) and at a constant force (7.36 N) with varying application times (B). The application of microneedles onto *ex vivo* human skin by non-experienced microneedle users (C and D). 15 participants pierced the skin with 200 μ m long microneedles by a manual insertion device (open circles) or an impact-insertion applicator (closed circles). Each point represents the average penetration efficiency of three individual microneedle applications by one individual (C) and the relative standard deviation (RSD) of the penetration efficiency for each participant (D). Significance (** $p < 0.001$) was determined by an unpaired two-tailed T-test.

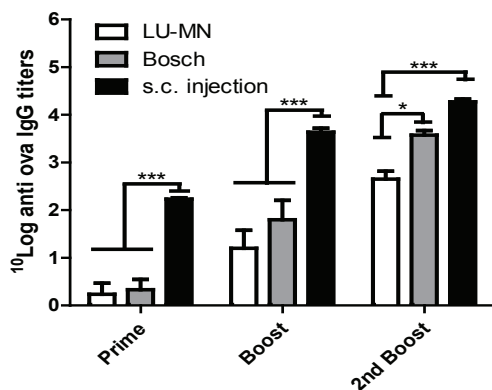


Figure 4: Ovalbumin-specific IgG responses upon microneedle-based (n=8) immunization by using an impact-insertion applicator with first-generation (LU-MN) or high-density (Bosch) microneedles, and subcutaneous (s.c.) injection (n=5). Each bar represents the mean \pm SEM. Non-responders were given an arbitrary titer of 1 and significance (* $p < 0.05$, ** $p < 0.001$) was determined by a two-way ANOVA with a Bonferroni post test.

compared to conventional immunization. Similar or slightly lower responses of microneedle-mediated vaccination with ovalbumin, as compared to subcutaneous/intramuscular injection, has been observed before [17, 18]. In conclusion, these data show the potential of using high-density microneedles with an impact-insertion applicator for vaccination.

4. Conclusion

This study shows that using an impact-insertion applicator improves the efficiency and reproducibility of high-density microneedle insertion, enabling reliable self-application of microneedle arrays onto the skin. Moreover, it was demonstrated that the impact-insertion applicator can be used for microneedle-mediated antigen delivery, yielding robust antigen-specific IgG responses, which depend on microneedle density and/or geometry.

Acknowledgements

We thank Dr. Michael Stumber (Robert Bosch GmbH) for the supply of microneedles and Eleni Maria Varypataki and Stefan Romeijn for their help with the immunization study.

References

- [1] M.I. Haq, E. Smith, D.N. John, M. Kalavala, C. Edwards, A. Anstey, A. Morrissey, J.C. Birchall, Clinical administration of microneedles: skin puncture, pain and sensation. *Biomed Microdevices* 11 (2009) 35-47.
- [2] N. Roxhed, B. Samel, L. Nordquist, P. Griss, G. Stemme, Painless drug delivery through microneedle-based transdermal patches featuring active infusion. *IEEE transactions on bio-medical engineering* 55 (2008) 1063 - 1071.
- [3] Y.-C. Kim, J.-H. Park, M.R. Prausnitz, Microneedles for drug and vaccine delivery. *Advanced Drug Delivery Reviews* 64 (2012) 1547-1568.
- [4] K. van der Maaden, W. Jiskoot, J. Bouwstra, Microneedle technologies for (trans)dermal drug and vaccine delivery. *Journal of controlled release* 161 (2012) 645-655.
- [5] M.R. Prausnitz, H.S. Gill, J.-H. Park, *Modified Release Drug Delivery*, Vol. 2nd ed New York: Healthcare, 2008, pp. 295-309.
- [6] T.R.R. Singh, N.J. Dunne, E. Cunningham, R.F. Donnelly, Review of Patents on Microneedle Applicators. *Recent Patents on Drug Delivery & Formulation* 5 (2011) 11-23.
- [7] M. Cormier, B. Johnson, M. Ameri, K. Nyam, L. Libiran, D.D. Zhang, P. Daddona, Transdermal delivery of desmopressin using a coated microneedle array patch system. *Journal of Controlled Release* 97 (2004) 503-511.
- [8] M.L. Crichton, A. Ansaldo, X. Chen, T.W. Prow, G.J.P. Fernando, M.A.F. Kendall, The effect of strain rate on the precision of penetration of short densely-packed microprojection array patches coated with vaccine. *Biomaterials* 31 (2010) 4562-4572.
- [9] R.F. Donnelly, M.J. Garland, D.I.J. Morham, K. Migalska, T.R.R. Singh, R. Majithiya, A.D. Woolfson, Optical coherence tomography is a valuable tool in the study of the effects of microneedle geometry on skin penetration characteristics and in-skin dissolution. *Journal of controlled release* 147 (2010) 333-341.
- [10] J.J. Norman, J.M. Arya, M.A. McClain, P.M. Frew, M.I. Meltzer, M.R. Prausnitz, Microneedle patches: Usability and acceptability for self-vaccination against influenza. *Vaccine* 32 (2014) 1856-1862.
- [11] K. van der Maaden, H. Yu, K. Sliedregt, R. Zwier, R. Lebourg, M. Oguri, A. Kros, W. Jiskoot, J.A. Bouwstra, Nanolayered chemical modification of silicon surfaces with ionizable surface groups for pH-triggered protein adsorption and release: application to microneedles. *Journal of Materials Chemistry B* 1 (2013) 4466-4477.
- [12] F.J. Verbaan, S.M. Bal, D.J. van den Berg, J.A. Dijkstra, M. van Hecke, H. Verpoorten, A. van den Berg, R. Luttge, J.A. Bouwstra, Improved piercing of microneedle arrays in dermatomed human skin by an impact insertion method. *Journal of Controlled Release* 128 (2008) 80-88.
- [13] Z. Ding, E. van Riet, S. Romeijn, G.F.A. Kersten, W. Jiskoot, J.A. Bouwstra, Immune modulation by adjuvants combined with diphtheria toxin administered topically in BALB/c mice after microneedle array pretreatment. *Pharmaceutical Research* 26 (2009) 1635-1643.
- [14] H. Kalluri, C.S. Kolli, A.K. Banga, Characterization of Microchannels Created by Metal Microneedles: Formation and Closure. *The AAPS Journal* 3 (2011) 473-481.
- [15] J.A. Matriano, M. Cormier, J. Johnson, W.A. Young, M. BATTERY, K. Nyam, P.E. Daddona, Macroflux microprojection array patch technology: a new and efficient approach for intracutaneous immunization. *Pharmaceutical Research* 19 (2002) 63-70.
- [16] D.P. Wermeling, S.L. Banks, D.A. Hudson, H.S. Gill, J. Gupta, M.R. Prausnitz, A.L. Stinchcomb, Microneedles permit transdermal delivery of a skin-impermeant medication to humans. *Proc Natl Acad Sci*

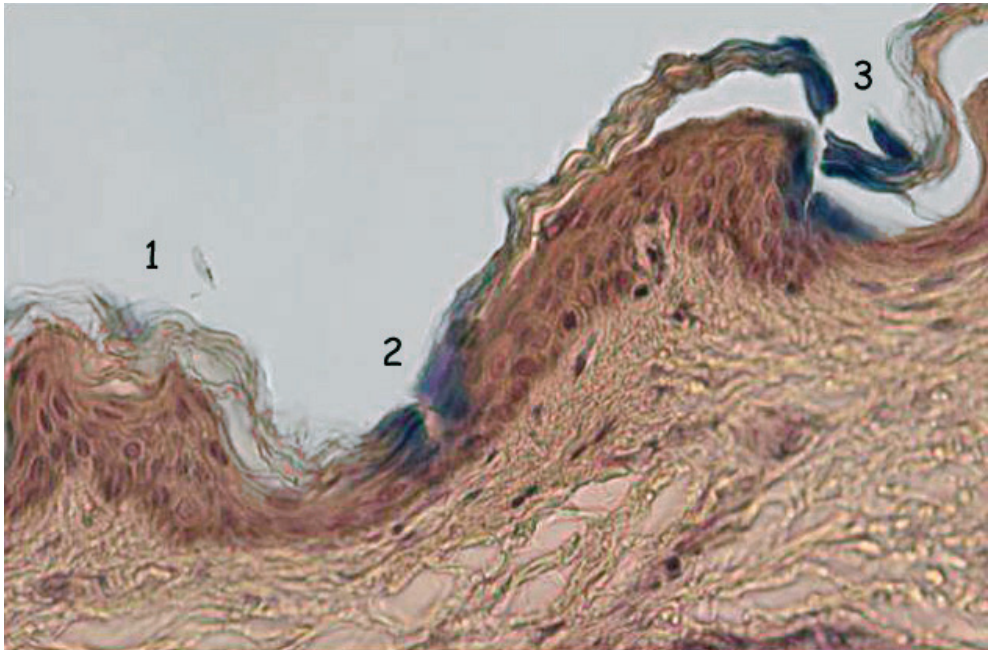
U S A 105 (2008) 2058-2063.

[17] L. Guo, J. Chen, Y. Qiu, S. Zhang, B. Xu, Y. Gao, Enhanced transcutaneous immunization via dissolving microneedle array loaded with liposome encapsulated antigen and adjuvant. *International Journal of Pharmaceutics* 447 (2013) 22-30.

[18] A. Kumar, X. Li, M.A. Sandoval, B.L. Rodriguez, B.R. Sloat, Z. Cui, Permeation of antigen protein-conjugated nanoparticles and live bacteria through microneedle-treated mouse skin. *International Journal of Nanomedicine* 6 (2011) 1253-1264.

Supplemental Information

Cryosection of microneedle treated *ex vivo* human skin with a manual application device, showing three blue stains on the stratum corneum (1-3). In this example two out of three (2 and 3) blue stains are penetrations of the skin and one blue stain is an indentation of the stratum corneum.



PARAMETER OPTIMIZATION TOWARD OPTIMAL MICRONEEDLE-BASED DERMAL VACCINATION

Koen van der Maaden
Eleni Maria Varypataki
Huixin Yu
Stefan Romeijn
Wim Jiskoot
Joke Bouwstra

[European Journal of
Pharmaceutical Sciences,](#)
[64 \(2014\) 18-25](#)

Abstract

Microneedle-based vaccination has several advantages over vaccination by using conventional hypodermic needles. Microneedles are used to deliver a drug into the skin in a minimally-invasive and potentially pain free manner. Besides, the skin is a potent immune organ that is highly suitable for vaccination. However, there are several factors that influence the penetration ability of the skin by microneedles and the immune responses upon microneedle-based immunization. In this study we assessed several different microneedle arrays for their ability to penetrate *ex vivo* human skin by using trypan blue and (fluorescently or radioactively labeled) ovalbumin. Next, these different microneedles and several factors, including the dose of ovalbumin, the effect of using an impact-insertion applicator, skin location of microneedle application, and the area of microneedle application, were tested *in vivo* in mice. The penetration ability and the dose of ovalbumin that is delivered into the skin were shown to be dependent on the use of an applicator and on the microneedle geometry and size of the array. Besides microneedle penetration, the above described factors influenced the immune responses upon microneedle-based vaccination *in vivo*. It was shown that the ovalbumin-specific antibody responses upon microneedle-based vaccination could be increased up to 12 fold when an impact-insertion applicator was used, up to 8 fold when microneedles were applied over a larger surface area, and up to 36 fold dependent on the location of microneedle application. Therefore, these influencing factors should be considered to optimize microneedle-based dermal immunization technologies.

1. Introduction

Microneedles are needle like structures with a length of less than 1 mm. Microneedles are used for the delivery of drugs, including vaccines, into the skin in a minimally-invasive and potentially pain free manner [1, 2]. In order to deliver a drug, however, microneedles should meet certain criteria. Primarily, microneedles should be long enough to pierce the stratum corneum but preferably short enough not to reach blood vessels and nerve endings. Even though microneedles have been developed with a sufficient length (300 μm) to penetrate human stratum corneum (15-20 μm), they often require an insertion device to overcome the skin's elasticity [3, 4].

Microneedles are used by four different approaches to deliver a drug into the skin, as reviewed elsewhere [5, 6]. One of these approaches is the 'poke and patch' approach, whereby microneedles are first used to pierce conduits into the skin and subsequently a patch that contains a drug formulation is applied on the site of microneedle application. The drug will diffuse through the conduits into skin [5, 6]. Logically, microneedles should penetrate the stratum corneum to enhance drug delivery into the viable skin. However, there are several factors that affect the penetration ability of microneedles, such as the microneedle density, the length of microneedles, the sharpness of the microneedle tip, the site of microneedle application, and the use of an applicator [4-6]. All of these factors may influence the immune responses upon microneedle-based vaccination. For example, it has been reported that the microneedle length influences the antigen-specific immune responses, e.g., 200-300 μm long microneedles induce lower responses than 800-1000 μm long microneedles [7, 8]. However, microneedles longer than 400 μm are more likely to induce pain [5]. A better insight into the influence of these factors on the immune responses could help to improve microneedle-based immunization in general.

In this study we investigated several of the above-mentioned factors on microneedle-based vaccine delivery by the poke and patch approach using ovalbumin as a model antigen and using microneedles with a length of 300 μm . First, the penetration ability of *ex vivo* human skin by several different microneedles was determined. Subsequently, the depth of ovalbumin delivery and the ovalbumin dose into *ex vivo* human skin was quantified. Finally, the effect of multiple parameters on the ovalbumin-specific immune responses was investigated. This study shows that antigen-specific IgG responses are dependent on the usage of an impact-insertion applicator, the microneedle application area, and the site of microneedle application.

2. Materials and methods

2.1 Chemicals

Sulfuric acid 96-98% was obtained from BOOM lab equipment, and sterile phosphate buffered saline (PBS) (140.3 mM Cl⁻, 163.9 mM Na⁺, 8.7 mM HPO₄²⁻, and H₂PO₄⁻; pH 7.4) was obtained from Braun. Chicken egg ovalbumin conjugated with Alexa-Fluor® 555 and stabilized Chromogen TMB were purchased from Invitrogen. Chicken egg ovalbumin grade VII was purchased from CALBIOCHEM®. Flat bottomed black 96-well plates and MICROLON® ELISA-plates were obtained from Greiner Bio-One. Bovine serum albumin fraction V was obtained from Roche. Pierce® Iodination Beads and goat anti-mouse IgG-horseradish peroxidase (HRP) (γ chain specific) was obtained from SouthernBiotech. Nimatek® (100 mg/mL ketamine, Eurovet Animal Health B.V., Bladel, the Netherlands), Rompun® (20 mg/mL xylazine, Bayer B.V., Mijdrecht, the Netherlands), and Oculentum Simplex were obtained from a local pharmacy. Iodine-125 radionuclide, 2 mCi (74 MBq), specific activity: ~17 Ci (629 GBq)/mg, in 10⁻⁵ M NaOH (pH 8-11) (reductant free), concentration: 100 mCi/mL was obtained from Perkin-Elmer. Amicon® Ultra centrifugal filter units with a molecular weight cut off of 30 kDa were obtained from Millipore™. VectaSheld® mounting medium with 4',6-diamidino-2-phenylindole (DAPI) was obtained from Vector Lab, Tissue-Tek® O.C.T. compound was obtained from Sakura Finetek, and trypan blue was from Sigma Aldrich.

2.2 Mice

Female BALB/c mice (H2^d) were obtained from Charles River (Maastricht, the Netherlands) and were maintained under standardized conditions in the animal facility of the Leiden Academic Centre for Drug Research, Leiden University. The mice were 8 weeks old at the start of the vaccination study and the study was carried out under the guidelines complied by the animal ethic committee of the Netherlands, and was approved by the "Dierexperimentencommissie Universiteit Leiden (UDEEC)" under number 11127 and 13065.

2.3 Preparation of ex vivo human skin

Abdominal human skin was obtained within 24 h after cosmetic surgery. After the fat was removed the skin was dermatomed to a thickness of 600 μm using a Padgett Electro Dermatome Model B. Subsequently, the skin was stretched on Styrofoam covered with parafilm and was washed once with 70% ethanol and twice with PBS.

2.4 Microneedle application

In this study six different microneedle arrays were used, as shown in figure 1. All microneedles in this study had a length of 300 μm. The U-Needle (UN) microneedle arrays contained 17 (8+9), 9 (4+5), 5 (2+3), and 3 (1+2) microneedles per array (figure 1A1-4, respectively) and were applied onto the skin with a hand-held applicator. The Tyndall and Leiden University (LU) microneedle arrays (fig B and C) contained 16 (4x4) microneedles per array and were applied by using an electrically-driven impact-insertion applicator at a velocity of 3 m/s, as described previously [9].

The different microneedles that were used in this study have been previously described. In brief, UN microneedles are *in-plane* microneedles that are wet-etched (KOH) from 380 μm thick $\langle 100 \rangle$ silicon wafers at 70° from a $\langle 100 \rangle$ wafer, yielding a three faced microneedle tip and a three faced shaft with near atomic flat $\langle 111 \rangle$ planes. At the intersection of two non-parallel $\langle 111 \rangle$ planes a near atomic sharp blade is formed, whereas at the intersection of three non-parallel $\langle 111 \rangle$ planes a near atomic sharp tip is formed [10]. Tyndall microneedles are *out-of-plane* microneedles that are wet-etched (KOH) from $\langle 100 \rangle$ silicon wafers. The microneedles have an octagonal shape and a sharp tip that is formed on top of the frustum where the eight high index planes $\langle 312 \rangle$ come together [11]. Finally, LU microneedles are made from commercially available (Becton and Dickinson) stainless steel 30G hypodermic needles that are mounted in a polyether ether ketone (PEEK) mold [3].

2.5 Penetration ability of different microneedles into ex vivo human skin by a trypan blue assay

In order to test the penetration ability of the different microneedle arrays into the skin, a trypan blue assay was performed. This was done by first applying the microneedles onto ex vivo human skin, and subsequently applying a drop of 70 μL 0.4% trypan blue in PBS onto the area of microneedle application at room temperature and at 100% relative humidity to prevent evaporation of the drop. After one hour the trypan blue solution was removed and the skin was washed once with 70% ethanol and twice with PBS. Subsequently, the stratum corneum side of the skin was photographed under a stereo microscope (magnification of 10x). Next, the epidermis was heat separated from the dermis at 60°C for 2 minutes, and the upper dermis side was photographed under a stereo microscope (magnification of 10x).

2.6 Fluorescence microscopy and confocal imaging of ovalbumin delivery into ex vivo human skin

Fluorescence microscopy was used to evaluate whether ovalbumin is able to diffuse into the skin via the formed conduits. Therefore, microneedles were first used to pierce ex vivo human skin, and subsequently a drop of 70 μL PBS, containing 100 μg Alexa-Fluor® 555 labeled ovalbumin, was applied onto the area of microneedle application. The skin was kept at 100% relative humidity to prevent evaporation of the drop. After two hours the drop was removed and the skin was washed as described above. Subsequently, the skin was analyzed by fluorescence microscopy (Nikon Eclipse E600) with a mercury light source, a Cy3 filter set, 400x magnification, and an exposure time of 18 μs .

In order to evaluate the depth of ovalbumin delivery and to visualize the microneedle conduits generated by the microneedles into ex vivo human skin, confocal laser scanning microscopy (CLSM) was used (Bio-Rad Radiance 2100 confocal laser scanning system, equipped with a Nikon Eclipse TE2000-U inverted microscope with a helium neon laser at 543 nm with a 570-nm long-pass emission filter). For controlling the confocal laser scanning system and for image acquisition, the Laser Sharp 2000 software (Bio-Rad, Hercules, USA) was used. Images of the microneedle conduits in ex vivo human skin were taken with a xy scan (2980x2980 μm) from 0-600 μm with depth intervals of 50 μm . Subsequently, these

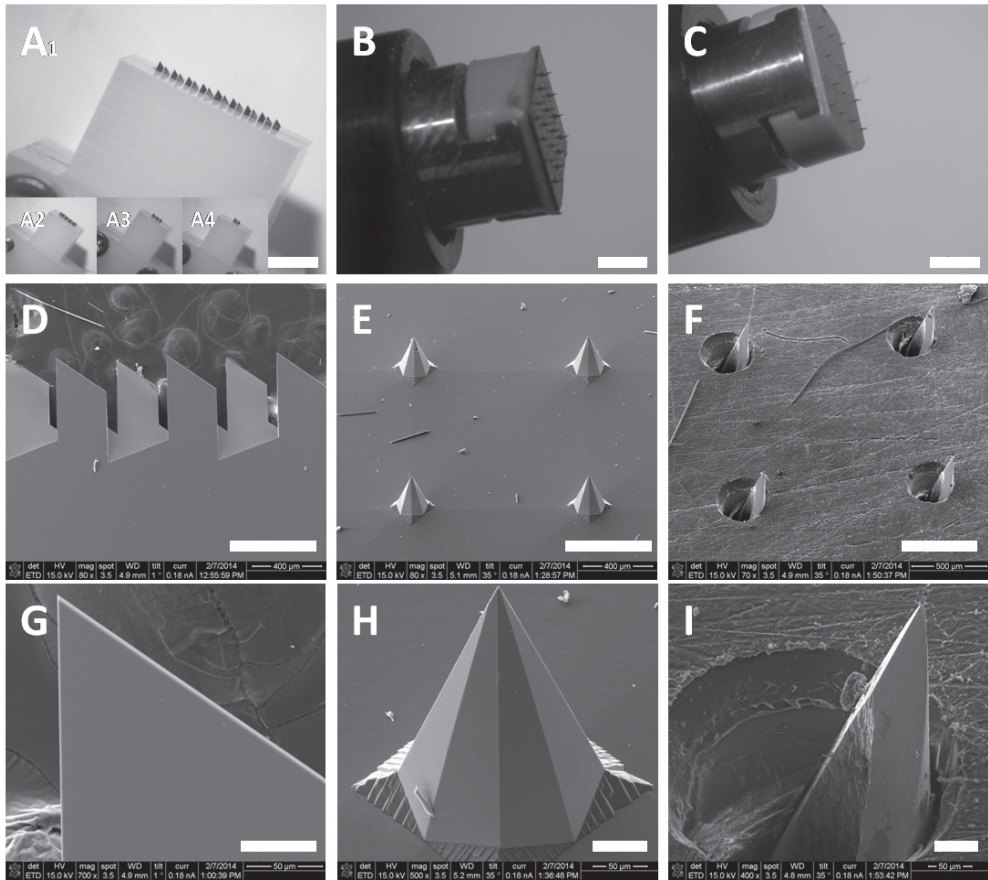


Figure 1: Images of 300 μm long U-Needle (A, D, G), Tyndall National Institute (B, E, H) and Leiden University (C, F, I) microneedle arrays that are mounted on an applicator for manual piercing (A) or on an impact-insertion applicator (B and C), and scanning electron microscopy images of these microneedle arrays (D-F) and zoomed in on the tip of a single microneedle (G-I). Size bars represents 2 mm (A-C), 500 μm (D-F), and 50 μm (G-I).

images were used to calculate the depth of ovalbumin delivery with ImageJ (available from rsbweb.nih.gov/ij/), by loading the image stack into the program and increasing the depth resolution 5x with a bilinear interpolation. Next, the fluorescence intensity as a function of depth was calculated. Subsequently, the intensity was plotted as a function of the depth in Prism 5 for Windows, and by linear regression ($\text{intensity}(\text{depth})=10$, background fluorescence of non-treated skin) the maximum delivery depth was calculated. Furthermore, the confocal images were loaded into ImageSurfer version 1.20 (available from <http://imagesurfer.cs.unc.edu/>) to reconstruct the conduits generated by the microneedles into human skin in a 3 dimensional space.

To visualize the formed conduits and simultaneously visualize the different layers of the skin, fluorescent nanoparticles were visualized in cryo-fixed skin. To this end,

UN 17-microneedle arrays were used to pierce *ex vivo* human skin onto which 70 μL with TMC-Rhodamin B nanoparticles (200-300 nm) were applied as described above. These nanoparticles were prepared as previously described [12]. Subsequently, skin was embedded in Tissue-Tek® O.C.T. compound in a gelatin capsule and was cryo-fixed in liquid nitrogen. Next, cryosections with a thickness of 5 μm were cut on a Leica® CM3050S cryostat, and the skin was fixed with acetone for 10 minutes. Then, the nuclei in the fixed skin were labeled with VectaShield® mounting medium with DAPI, and the skin was photographed under a fluorescence microscope (magnification of 100x, DAPI and Cy3 filter set with an exposure time of 5 s and 1 s, respectively). Finally, the fluorescence images with the two different filter sets were overlaid in ImageJ.

2.7 Quantification of ovalbumin delivery into *ex vivo* human skin

To quantify the amount of protein that was delivered into *ex vivo* human skin, radioactively labeled (^{125}I) ovalbumin, prepared as previously described [13], was used. *Ex vivo* human skin was pierced with the different microneedle arrays and subsequently a drop of 70 μL , containing 100 μg of radioactively labeled ovalbumin, was applied onto the skin as described above. After 2 hours the drop was removed and the skin was washed and dried twice with a cotton swab soaked in PBS. Subsequently, to remove the remaining ovalbumin from the skin surface the skin was tape-stripped twice by using Scotch tape. All the cleaning and tape samples were kept for γ -measurements, as well as the sheets of skin that were treated with microneedles. Next, a calibration curve was prepared (1 ng - 50 μg radioactively labeled ovalbumin) to quantify the dose of ovalbumin that was delivered into the skin. Finally, the γ -counts of the samples were measured for 1 minute on a Perkin Elmer Wallac Wizard 1470 automatic gamma counter.

2.8 Immunizations

In order to test the IgG responses after microneedle-based immunization, mice were immunized thrice with intervals of three weeks. The effect of a large number of parameters on the serum IgG responses was investigated, as described below:

1. The effect of the **number of microneedles** in a microneedle array. For these studies UN microneedle arrays were used that contained 3, 5, 9, or 17 microneedles per array.
2. The effect of using **differently shaped microneedles** with the same length (300 μm). Here, the UN 17-, Tyndall 16- and LU 16-microneedles were compared.
3. The adjuvant effect of using an **impact-insertion applicator**. This was done by first manually applying the UN 3- or 17-microneedle arrays onto the skin, followed (after removal of the microneedles) by no punch or with a punch of 3 m/s by the impact-insertion applicator (with an empty backplate). The UN microneedle arrays pierce *ex vivo* human skin when applied with a manual insertion device [13].

4. The effect of **size of microneedle application area**. For this study the same number of microneedles was applied onto a larger surface area, i.e., a single application by a UN 17-microneedle array was compared to six applications by a UN 3-microneedle array.
5. The effect of **microneedle application site**. For this study mice were immunized by using a UN 17-microneedle array on the ventral abdomen or the ear pinna.

Mice that were immunized to investigate the above described parameters 1-4 were treated with microneedles on the ventral abdomen skin. After microneedle application and removal, 100 µg of ovalbumin in 70 µL PBS was occlusively applied onto the skin, as previously described [14]. After two hours the patch was removed and the skin was washed with hand-warm tap water. All mice were anesthetized with 150 mg/kg ketamine and 10 mg/kg xylazine by intraperitoneal injection, and one day before each immunization the ventral abdomen skin of the mice was shaved. Parameters 1 and 2 were investigated with 11 mice per group and parameters 3-5 with 8 mice per group.

2.9 Serum IgG detection

Ovalbumin specific antibodies were determined by a sandwich ELISA as described previously [14]. In brief, 96-well plates for ELISA were coated overnight with 1 µg/mL ovalbumin in a 0.04 M carbonate buffer at pH 9.6 at 4 °C (100 µL/well). Next, the plates were blocked for 1 h at 37°C with 1% BSA in PBS. Thereafter, two-fold dilutions of the sera of individual mice were prepared in 96-well plates and were incubated for 1.5 h at 37°C. Then, the wells were incubated for 1 h at 37°C with HRP conjugated goat anti-mouse IgG (γ chain specific). Finally, 100 µL TMB was added per well and after 15 minutes the reaction was stopped by adding 100 µL/well 2 M H₂SO₄, after which the optical density was measured at 450 nm. Antibody titers were expressed as the log value of the serum dilution at the mid-point of a complete S-shaped absorbance-dilution curve.

2.10 Statistical analysis

Statistical analysis was performed using Prism 5 for Windows. The statistical significance of the depth of ovalbumin delivery was calculated by using a one-way ANOVA and the statistical significance of ovalbumin-specific IgG titers calculated using a two-way ANOVA with a Bonferroni post test.

3. Results and discussion

3.1 Penetration ability of microneedles

For each microneedle array it is essential that the microneedles penetrate the stratum corneum to enable drug delivery into the viable skin [5, 6]. To evaluate skin penetration by microneedle arrays several dyes have been used [3, 9, 15-17], including trypan blue [3, 9]. In order to examine whether the different microneedle arrays are able to pierce *ex vivo* human

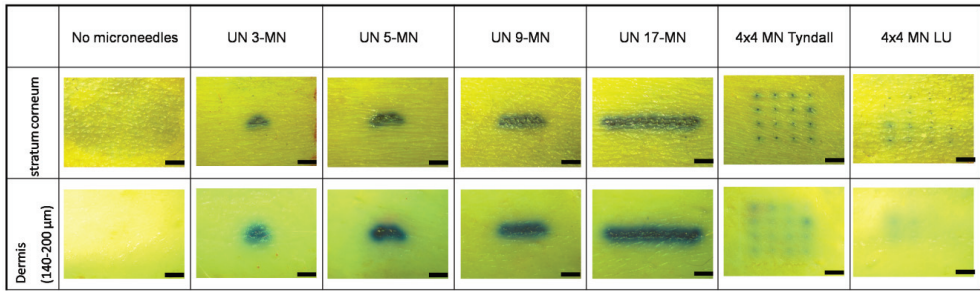


Figure 2: Penetration ability of microneedles assessed by a trypan blue assay. Different microneedles were applied onto dermatomed *ex vivo* human skin and subsequently a drop of trypan blue was applied for 1 hour. Then, the skin was photographed from the stratum corneum (upper images) side. Next, the dermis was heat separated from the epidermis (lower images). Tyndall and LU microneedles were applied by an impact-insertion applicator and UN microneedles by a device for manual insertion. Photographs were made by a stereo microscope with a magnification of 10x; the size bar represents 1 mm.

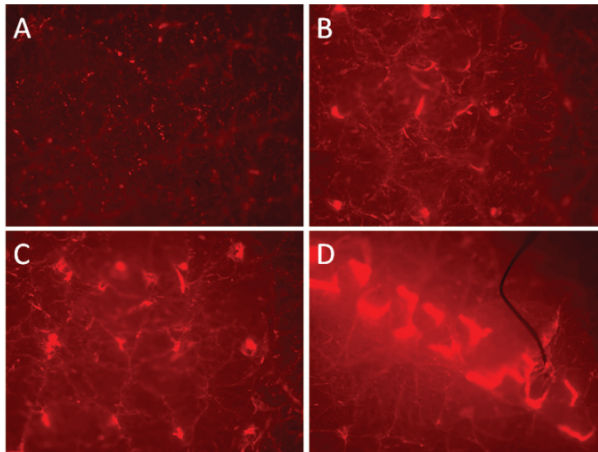


Figure 3: Application of fluorescently labeled ovalbumin (Alexafluor-555) onto *ex vivo* human skin, without microneedle pretreatment (A), or pretreated with LU 16-microneedles (B), Tyndall 16-microneedles (C), and UN 17-microneedles. Tyndall and LU microneedles were applied by an impact-insertion applicator and UN microneedles by a device for manual insertion.

skin a trypan blue assay was performed. As shown in figure 2, after microneedle application dark blue stains were visible on the stratum corneum. However, this does not prove that the microneedles have penetrated the skin. Therefore, the epidermis was separated from the dermis, which revealed that trypan blue had penetrated into the top layer of the dermis (approximately 150-200 μm deep [6]) after microneedles pretreatment. In contrast, when no microneedles were applied, only a weak blue stain was visible on the stratum corneum side and no staining in the dermis was observed. Although all the microneedles had a length of 300 μm, pretreatment with the UN and Tyndall microneedles, both made of silicon, resulted in more intense staining of trypan blue in the dermis compared to pretreatment with the LU microneedles. This difference in staining can be explained by the geometry of the microneedles (figure 1): the LU microneedles were thinner and less sharp than the UN and Tyndall microneedles. Besides, microneedles etched from silicon are generally sharper than microneedles made of stainless steel. Indeed, the LU microneedles had a tip diameter

of 4-5 μm , the Tyndall microneedles 1-1.5 μm , and the UN microneedles had a diameter of less than 50 nm. The extreme sharpness of the UN microneedle arrays resulted in an efficient and reproducible penetration of the skin by applying the microneedles by only hand-force using a device for manual insertion. However, to reproducibly penetrate *ex vivo* skin with either Tyndall or LU microneedle arrays, the use of an impact-insertion applicator was required (data not shown) [9]. In conclusion, the trypan blue assay revealed that all the different microneedle arrays that were used in this study are able to reproducibly penetrate human skin.

3.2 Delivery of fluorescently labeled ovalbumin into *ex vivo* human skin

After it was shown that the different microneedle arrays are able to pierce *ex vivo* human skin by using a low-molecular weight model compound (trypan blue), the delivery of a 45-kDa biomacromolecule, ovalbumin, into the skin was investigated. Therefore, fluorescently labeled ovalbumin was applied onto *ex vivo* human skin that was non-treated or pretreated with the LU Tyndall, or UN microneedle arrays (figure 3). Figure 3A shows that hardly any fluorescence was visible on non-treated *ex vivo* human skin, indicating that no ovalbumin was delivered into the skin. However, when we pretreated the skin with microneedle arrays, fluorescence patterns similar to the trypan blue images (figure 2) were visible (figure 3B-D). This already suggests that microneedle pretreatment with all microneedle arrays resulted in the delivery of biomacromolecules into the skin. To obtain more evidence on the delivery of ovalbumin into *ex vivo* human skin, studies were also performed by using CLSM. The images are shown after application of LU microneedles (figure 4A), Tyndall microneedles (figure 4B), and UN microneedles (figure 4C). Subsequently, from the CLSM the penetration depth of fluorescently labeled ovalbumin into the skin was calculated (figure 4D). This image shows that ovalbumin was delivered to a depth of approximately 75% of the length of the microneedles for the LU and Tyndall microneedles. However, upon piercing of the U-Needle microneedles, fluorescently labeled ovalbumin was delivered to a depth of approximately 95% of the microneedle length. Despite this difference, we expect that the LU and Tyndall microneedles were fully inserted into the skin, because an impact-insertion applicator was used. The difference in depth of ovalbumin delivery might be caused by the shape of the microneedles, i.e., U-Needle microneedles are much broader than the ones of the two other arrays (figure 1), resulting in the formation of larger conduits upon microneedle pretreatment (figure 2), which apparently leads to delivery of ovalbumin deeper into the skin (figure 4).

Next, to visualize the conduits in the skin as well as the skin structure, TMC-rhodamine nanoparticles were used. These large nanoparticles (200-300 nm) are expected to only coat the conduits and the slightly negatively charged stratum corneum, i.e., the top layer of the skin, but are not expected to rapidly diffuse into the epidermis/dermis. Upon application of UN 17-microneedle arrays onto *ex vivo* human skin, it was shown that the microneedles pierce through the stratum corneum, into the skin (figure 4E).

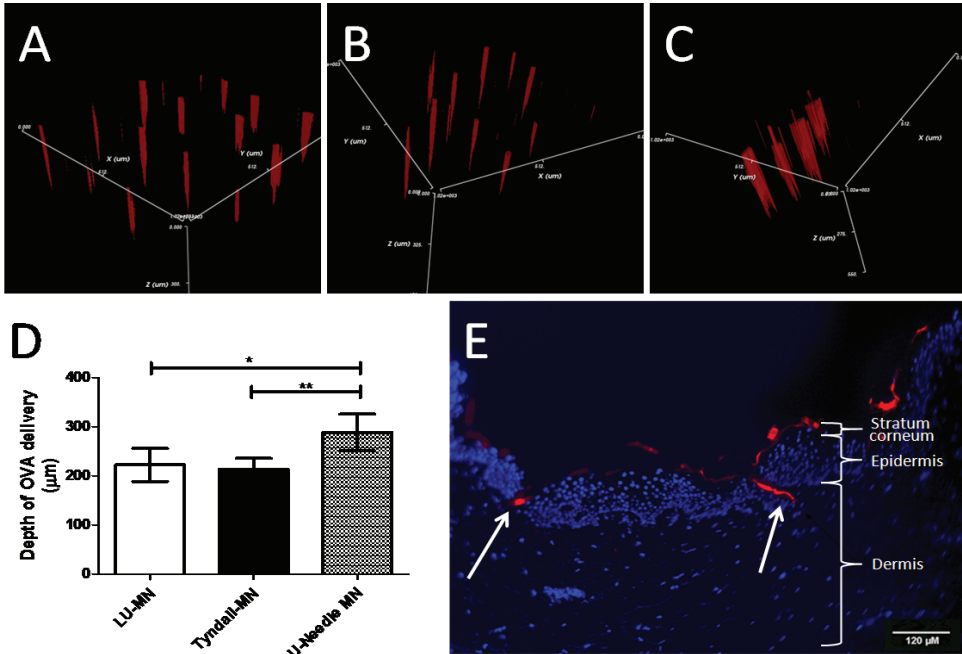


Figure 4: Representative confocal laser scanning microscopy (CLSM) imaging (2980x2980x600 µm (x,y,z)) of fluorescently labeled ovalbumin delivery into *ex vivo* human skin pretreated with LU 16- (A), Tyndall 16- (B), and UN 9-microneedle arrays (C). CLSM images were used to determine the depth of ovalbumin delivery into the skin (mean ± SD, n=10) (D). Cryosection of *ex vivo* human skin to visualize the conduits formed by UN 17-microneedle arrays by using TMC-rhodamine (red) nanoparticles and DAPI (blue) fluorescence (E). Statistical significance: *p<0.05, **p<0.01.

3.3 Quantification of ovalbumin delivery into *ex vivo* human skin

Following common practice [13, 18-20], the amount of ovalbumin delivered into the skin *via* microneedles was quantified by radioactivity. The results are shown in figure 5. After different microneedle arrays were applied onto *ex vivo* human skin, a solution with radioactively labeled ovalbumin was applied. Subsequently, the solution was removed and the skin was washed twice with a cotton swab soaked in PBS, which led to a removal of 300-700 ng (wash 1, data not shown) and 30-100 ng (wash 2, figure 5A) ovalbumin from the skin surface. Subsequently, the skin was tape-stripped twice to remove most of the stratum corneum adsorbed ovalbumin. The tape-stripping led to the removal of 21-43 (first strip) and 4-20 ng (second strip) ovalbumin (figure 5A). Finally, the amount of ovalbumin that was delivered into the skin, after it was washed and tape-stripped, was quantified (figure 5B). As expected, hardly any ovalbumin, 0.16 ± 0.04 µg (mean ± SD, n=3), was delivered into the skin without microneedle pretreatment. Furthermore, upon LU microneedle pretreatment 1.04 ± 0.13 µg ovalbumin (mean ± SD, n=3) was delivered into the skin and pretreatment with Tyndall microneedles led to an intradermal delivery of 2.55 ± 0.08 µg (mean ± SD, n=3)

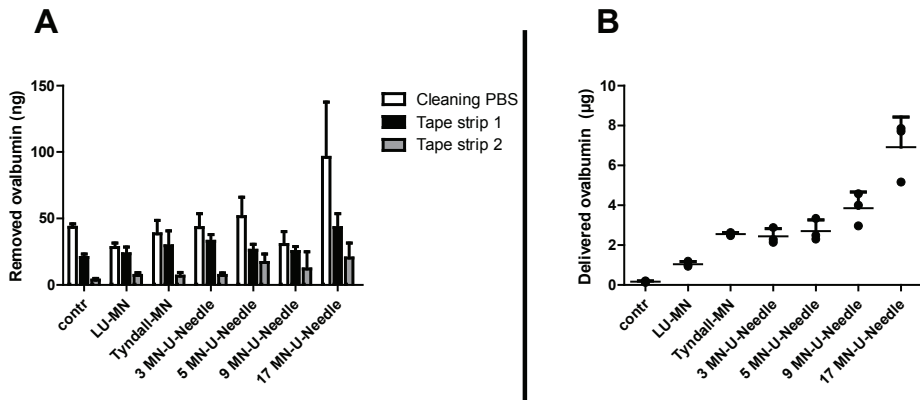


Figure 5: Delivery of radioactively labeled ovalbumin into *ex vivo* human skin. Removal of the excess of ovalbumin (expressed in ng) by cleaning the skin with a cotton swap soaked with PBS and removal of the stratum corneum by tape-stripping (A), and the delivered amount of ovalbumin (expressed in µg) determined after the skin was cleaned and the stratum corneum adsorbed ovalbumin was removed (B). Values are expressed as the mean ± SD of three individual measurements.

ovalbumin. Pretreatment of *ex vivo* human skin with UN 3-, 5-, 9-, or 17-microneedles led to an intradermal delivery of 2.44 ± 0.39 , 2.71 ± 0.55 , 3.84 ± 0.82 , and 6.91 ± 1.52 µg ovalbumin (mean ± SD, $n=3$), respectively. In conclusion, the microneedles that were used in this study led to an up to 43-fold increased ovalbumin delivery compared to no microneedle treatment. Moreover, the delivered dose of ovalbumin into *ex vivo* human skin was dependent on the number of microneedles per microneedle array. The higher levels of radioactively labeled ovalbumin after UN microneedle pretreatment compared to the other microneedle arrays correspond to the higher fluorescence intensity of fluorescently labeled ovalbumin in figure 3D.

3.4 Ovalbumin-specific IgG responses after microneedle pretreatment in mice

3.4.1 Effect of dose by different microneedles

By using the different microneedle arrays a different dose of ovalbumin was delivered into the skin. To investigate whether this difference in dose affects the ovalbumin-specific IgG responses, mice were immunized by using the UN 3-, 5-, 9-, and 17-microneedle arrays as well as the LU 16- and Tyndall 16-microneedles. As shown in figure 6A, the ovalbumin-specific IgG responses upon microneedle-based vaccination were similar, no matter which dose was delivered by the different microneedles (cf. figure 5B). Similar observations were reported by Widera *et al.*, who observed only minimal differences in ovalbumin-specific IgG titers after the booster immunization of hairless guinea pigs with 0.4 µg, 5 µg, or 36 µg ovalbumin by using 225 µm long microneedles [19]. Therefore, we conclude that the maximum ovalbumin-specific IgG response in BALB/c mice is already obtained at a dose as low as 1 µg when using the above described microneedles.

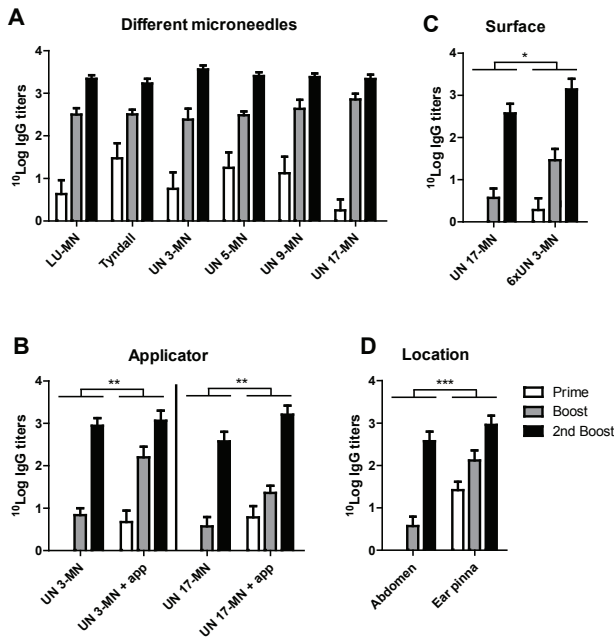


Figure 6: Ovalbumin-specific serum IgG responses upon vaccination with ovalbumin. Only the LU and Tyndall microneedles were applied with an applicator (A). After microneedle application in the UN + App microneedle groups the applicator was used with an empty backplate (B). Values are shown as mean \pm SEM, $n=11$ for panel A, and $n=8$ for panel B-D, and non responding mice were given an arbitrary titer of 1. Statistical analysis: * $p<0.05$, ** $p<0.01$, *** $p<0.001$.

3.4.2 Effect of an impact-insertion applicator

Impact-insertion applicators are often required to pierce microneedles into the skin [4-6, 9, 20]. Therefore, the effect of applying the impact-insertion applicator itself, other than its potentially positive effect on the piercing efficiency, was investigated. To this end, the UN 3- and 17-microneedle arrays were applied manually with and without subsequent treatment with the impact-insertion applicator (with an empty backplate). As shown in figure 6B, the ovalbumin-specific IgG responses were on average 5 (prime), 12 (boost) and 2 fold higher (2^{nd} boost) when the impact-insertion applicator was applied onto the skin after it was pretreated with microneedles. This shows a mechanical adjuvant effect of applying the impact-insertion applicator at the microneedle application site.

3.4.3 Effect of microneedle application area

The effect on the ovalbumin-specific IgG responses of applying a small (UN 3) microneedle array six times on a larger skin surface area was compared to applying one larger microneedle array (UN 17) once, so with a similar number of microneedles (18 versus 17). Figure 6C shows that applying six times a UN 3-microneedle array led to 2 (prime), 8 (boost), and 4 fold higher (2^{nd} boost) IgG responses than applying one UN 17-microneedle array. There might be a minimal difference in the delivered dose of ovalbumin by applying these two approaches (figure 5). However, we do not expect that this influences the immune response as with a dose of 1 μg ovalbumin high IgG levels are already achieved (figure 6A). Rather, this difference in IgG responses might be explained by reaching more antigen presenting cells in the skin when

a UN 3-microneedle array (0.34 mm² backplate surface area) is randomly applied on 2 cm² skin surface compared to the application of one UN 17-microneedle array (2.2 mm² backplate surface area).

3.4.4 Effect of the vaccination site of microneedles

In the literature microneedle-based immunization is not uniformly performed *via* one specific skin site, e.g., there are reports about microneedle-based vaccination *via* the ventral abdomen skin [12, 14, 21], the lateral area of the thorax [15, 19] and the ear pinna [18, 20, 22]. In our group microneedles have been applied *via* the ventral abdomen skin. Several studies have shown that dermal DNA vaccination *via* the ear pinna is very potent in mice and dogs [23-25]. Forg *et al.* showed the superiority of the ear pinna over abdominal skin for DNA vaccination [23]. This is probably caused by a high number of antigen presenting cells, i.e., the ear pinna is very thin resulting in two epidermises close to each other. Furthermore, the ear pinna is closely connected to one major draining lymph node (superfiscia cervicalis) [23]. However, for microneedle-based vaccination a direct comparison between the ear pinna and the abdominal skin has not been reported yet. To study the effect of the location of microneedle application, UN 17-microneedles were applied onto the ventral abdomen or onto the left ear pinna, upon which subsequently a patch with ovalbumin was applied. Figure 6D shows that microneedle-based immunization *via* the ear pinna leads to 26 (prime), 36 (boost), and 2 fold higher (2nd boost) ovalbumin-specific IgG responses than microneedle-based immunization *via* the ventral abdomen. In conclusion, this data shows the importance of the location of microneedle application.

3.4.5 Improvement of microneedle-based vaccination

As discussed above we might have reached the plateau of IgG titers for microneedle-based immunization for unadjuvanted ovalbumin in BALB/c mice. Therefore, it might be feasible to decrease the delivered amount of ovalbumin by microneedles per immunization, but increase the number of immunizations to obtain even higher immune responses. Furthermore, to increase antigen-specific IgG responses different complementary approaches should be pursued, e.g., applying the microneedles over a larger surface and on a location close to lymph nodes, such as the ear pinna, or adjuvanting the vaccine mechanically (e.g., applicator, high density microneedles) and/or chemically (e.g., Quil-A, LPS, CpG).

4. Conclusion

All microneedle arrays that were used in this study successfully penetrated the stratum corneum upon application onto the skin, as determined by a trypan blue assay. The amount of ovalbumin delivered into *ex vivo* human skin *via* the poke and patch approach depended on the geometry and size of the microneedle array, but this did not affect the ovalbumin-specific IgG response. However, antigen-specific IgG responses were found to be dependent

on the usage of an impact-insertion applicator, the microneedle application area, and the location of microneedle application. Finally, these data can be used to optimize the antigen-specific IgG responses upon microneedle-based vaccination not only for the poke and patch, but also for other microneedle-based immunization approaches that are currently used for vaccination.

Acknowledgements

This research was financially supported by the “programma Nano4Vitality” of the Dutch Ministry of Economic Affairs and the province Overijssel. Furthermore, we acknowledge J. Wissink, U-Needle BV and Dr. N. Tas, University of Twente, Transducer Science and Technology Department (TST) for the supply of microneedle arrays. Finally, we acknowledge Dr. Conor O’Mahony, Tyndall National Institute, University College Cork, Ireland, for supplying us with Tyndall microneedle arrays.

References

- [1] M.I. Haq, E. Smith, D.N. John, M. Kalavala, C. Edwards, A. Anstey, A. Morrissey, J.C. Birchall, Clinical administration of microneedles: skin puncture, pain and sensation. *Biomed Microdevices* 11 (2009) 35-47.
- [2] S. Kaushik, A.H. Hord, D.D. Denson, D.V. McAllister, S. Smitra, M.G. Allen, M.R. Prausnitz, Lack of Pain Associated with Microfabricated Microneedles. *Anesth Analg* 92 (2001) 502-504.
- [3] F.J. Verbaan, S.M. Bal, D.J. van den Berg, W.H.H. Groenink, H. Verpoorten, R. Lüttge, J.A. Bouwstra, Assembled microneedle arrays enhance the transport of compounds varying over a large range of molecular weight across human dermatomed skin. *Journal of Controlled Release* 117 (2007) 238-245.
- [4] T.R.R. Singh, N.J. Dunne, E. Cunningham, R.F. Donnelly, Review of Patents on Microneedle Applicators. *Recent Patents on Drug Delivery & Formulation* 5 (2011) 11-23.
- [5] Y.-C. Kim, J.-H. Park, M.R. Prausnitz, Microneedles for drug and vaccine delivery. *Advanced Drug Delivery Reviews* 64 (2012) 1547-1568.
- [6] K. van der Maaden, W. Jiskoot, J. Bouwstra, Microneedle technologies for (trans)dermal drug and vaccine delivery. *Journal of controlled release* 161 (2012) 645-655.
- [7] A. Kumar, X. Li, M.A. Sandoval, B.L. Rodriguez, B.R. Sloat, Z. Cui, Permeation of antigen protein-conjugated nanoparticles and live bacteria through microneedle-treated mouse skin. *International Journal of Nanomedicine* 6 (2011) 1253-1264.
- [8] K. Matsuo, Y. Yokota, Y. Zhai, Y.-S. Quan, F. Kamiyama, Y. Mukai, N. Okada, S. Nakagawa, A low-invasive and effective transcutaneous immunization system using a novel dissolving microneedle array for soluble and particulate antigens. *Journal of Controlled Release* 161 (2012) 10-17.
- [9] F.J. Verbaan, S.M. Bal, D.J. van den Berg, J.A. Dijkman, M. van Hecke, H. Verpoorten, A. van den Berg, R. Luttge, J.A. Bouwstra, Improved piercing of microneedle arrays in dermatomed human skin by an impact insertion method. *Journal of Controlled Release* 128 (2008) 80-88.
- [10] J. Wissink, J.W. Berenschot, N.R. Tas, Atom sharp needles, the missing link in microneedle drug delivery. *Proceedings of Medical Devices Conference*, 6 October 2008, Copenhagen.
- [11] N. Wilke, A. Mulcahy, S.-R. Ye, A. Morrissey, Process optimization and characterization of silicon microneedles fabricated by wet etch technology. *Microelectronics Journal* 36 (2005) 650-656.
- [12] S.M. Bal, Z. Ding, G.F.A. Kersten, W. Jiskoot, J.A. Bouwstra, Microneedle-Based Transcutaneous Immunisation in Mice with N-Trimethyl Chitosan Adjuvanted Diphtheria Toxoid Formulations. *Pharm. Res.* 27 (2010) 1837-1847.
- [13] K. van der Maaden, H. Yu, K. Sliedregt, R. Zwier, R. Lebox, M. Oguri, A. Kros, W. Jiskoot, J.A. Bouwstra, Nanolayered chemical modification of silicon surfaces with ionizable surface groups for pH-triggered protein adsorption and release: application to microneedles. *Journal of Materials Chemistry B* 1 (2013) 4466-4477.
- [14] Z. Ding, E. Van Riet, S. Romeijn, G.F.A. Kersten, W. Jiskoot, J.A. Bouwstra, Immune modulation by adjuvants combined with diphtheria toxoid administered topically in BALB/c mice after microneedle array pretreatment. *Pharmaceutical Research* 26 (2009) 1635-1643.
- [15] J.A. Matriano, M. Cormier, J. Johnson, W.A. Young, M. Buttery, K. Nyam, P.E. Daddona, Macroflux microprojection array patch technology: a new and efficient approach for intracutaneous immunization. *Pharmaceutical Research* 19 (2002) 63-70.
- [16] H. Kalluri, C.S. Kolli, A.K. Banga, Characterization of Microchannels Created by Metal Microneedles: Formation and Closure. *The AAPS Journal* 3 (2011) 473-481.
- [17] D.P. Wermeling, S.L. Banks, D.A. Hudson, H.S. Gill, J. Gupta, M.R. Prausnitz, A.L. Stinchcomb, Microneedles permit transdermal delivery of a skin-impermeant medication to humans. *Proc Natl Acad Sci*

U S A 105 (2008) 2058-2063.

- [18] H.-I. Ng, G.J.P. Fernando, M.A.F. Kendall, Induction of potent CD8+ T cell responses through the delivery of subunit protein vaccines to skin antigen-presenting cells using densely packed microprojection arrays. *Journal of controlled release* 162 (2012) 477-484.
- [19] G. Widera, J. Johnson, L. Kim, L. Libiran, K. Nyam, P.E. Daddona, M. Cormier, Effect of delivery parameters on immunization to ovalbumin following intracutaneous administration by a coated microneedle array patch system. *Vaccine* 24 (2006) 1653-1664.
- [20] A.P. Raphael, T.W. Prow, M.L. Crichton, X. Chen, G.J.P. Fernando, M.A.F. Kendall, Targeted, Needle-Free Vaccinations in Skin using Multilayered, Densely-Packed Dissolving Microprojection Arrays. *Small* 6 (2010) 1785-1793.
- [21] Z. Ding, F.J. Verbaan, M. Bivas-Benita, L. Bungener, A. Huckriede, D.J. van den Berg, G. Kersten, J.A. Bouwstra, Microneedle arrays for the transcutaneous immunization of diphtheria and influenza in BALB/c mice. *Journal of Controlled Release* 136(1) (2009) 71-78.

- [22] M.P. Ruutu, X. Chen, O. Joshi, M.A. Kendall, I.H. Frazer, Increasing mechanical stimulus induces migration of Langerhans cells and impairs the immune response to intracutaneously delivered antigen. *Experimental Dermatology* 20 (2010) 529-536.
- [23] P. Forg, P.v. Hoegen, W. Dalemans, V. Schirmmayer, Superiority of the ear pinna over muscle tissue as site for DNA vaccination. *Gene Therapy* 5 (1998) 789-797.
- [24] D.L. Lodmell, M.J. Parnell, J.T. Weyhrich, L.C. Ewalt, Canine rabies DNA vaccination: a single-dose intradermal injection into ear pinnae elicits elevated and persistent levels of neutralizing antibody. *Vaccine* 21 (2003) 3998-4002.
- [25] D.L. Lodmell, L.C. Ewalt, M.J. Parnell, C.E. Rupperecht, C.A. Hanlon, One-time intradermal DNA vaccination in ear pinnae one year prior to infection protects dogs against rabies virus. *Vaccine* 24 (2006) 412-416.

CHAPTER 4

COATED MICRONEEDLES

FLUORESCENT NANOPARTICLE ADHESION ASSAY: A NOVEL METHOD FOR SURFACE pK_a DETERMINATION OF SELF-ASSEMBLED MONOLAYERS ON SILICON SURFACES

Koen van der Maaden¹
Karen Sliedregt²
Alexander Kros²
Wim Jiskoot¹
Joke Bouwstra¹

[Langmuir, 28 \(2012\)
3403–3411](#)

¹Division of Drug Delivery
Technology, Leiden/
Amsterdam Center for Drug
Research (LACDR), Leiden
University

²Department of Soft Matter
Chemistry, Leiden Institute
of Chemistry (LIC), Leiden
University

Abstract

Since the computer industry enables us to generate smaller and smaller structures, silicon surface chemistry is becoming increasingly important for (bio-) analytical and biological applications. For controlling the binding of charged biomacromolecules such as DNA and proteins on modified silicon surfaces, the surface pK_a is an important factor. Here we present a fluorescent nanoparticle adhesion assay as a novel method to determine the surface pK_a of silicon surfaces modified with weak acids or bases. This method is based upon electrostatic interactions between the modified silicon surface and fluorescent nanoparticles with an opposite charge. Silicon slides were modified with 3-aminopropyltriethoxysilane (APTES) and were further derivatized with succinic anhydride. Layer thickness of these surfaces was determined by ellipsometry. After incubating the surfaces with an amine-reactive fluorescent dye, fluorescence microscopy revealed that the silicon surfaces were successfully modified with amine- and carboxyl-groups. Two surface pK_a values were found for APTES surfaces by the fluorescent nanoparticle adhesion assay. The first surface pK_a (6.55 ± 0.73) was comparable with the surface pK_a obtained by contact angle titration (7.3 ± 0.8), and the second surface pK_a (9.94 ± 0.19) was only found by using the fluorescent nanoparticle adhesion assay. The surface pK_a of the carboxyl-modified surface by the fluorescent nanoparticle adhesion assay (4.37 ± 0.59) did not significantly differ from that found by contact angle titration (5.7 ± 1.4). In conclusion, we have developed a novel method to determine the surface pK_a of modified silicon surfaces: the fluorescent nanoparticle adhesion assay. This method may provide a useful tool for designing pH-dependent electrostatic protein and particle binding/release, and to design surfaces with a pH-dependent surface charge for (bio-) analytical lab-on-a-chip devices or drug delivery purposes.

1. Introduction

Surface modification is used in a broad range of applications. Self-assembling monolayers (SAMs) and functionalized surfaces are used for e.g. DNA and protein biosensors [1, 2], antibody microarrays [3], protein immobilization [4], long range electron transfer [5], and proton transfer reactions [6]. There are multiple strategies for the immobilization of proteins, DNA, or colloidal particles on these surfaces, such as immobilization *via* covalent bonding, physical entrapment, van der Waals interactions, hydrophobic interactions, and electrostatic interactions [1, 3-5, 7]. Furthermore, the surface properties of SAMs and functionalized surfaces are affected by their charged state. Since SAMs and functionalized surfaces are often used in an aqueous environment, and much of these surfaces have a pH-dependent charge, it is very important to know their surface pK_a value [6, 8-10].

Various methods have been described to determine the surface pK_a of SAMs on conductive materials, such as gold electrodes, mercury electrodes, silver surfaces, etc. These methods include electrochemical titration [11, 12], interfacial capacitance measurements [13], surface potential measurements [14, 15], interfacial impedance [16, 17], piezoelectric quartz crystal microbalance [18], indirect laser-induced temperature jump method [19], and optical absorption [20, 21]. However, most of these methods are complicated or lack accuracy because of their invasive character [16, 17]. Moreover, these methods are not suitable for the pK_a determination of (semi-conductive) silicon surfaces. Silicon is of great interest because techniques to generate micro- and nano-structures on silicon are well developed. These structures can be used for biological or analytical applications such as lab-on-a-chip devices, biosensors, and microneedles [22, 23].

For the surface pK_a determination of modified silicon surfaces contact angle titration [6, 10, 11, 20, 24], chemical force titration, which is a form of atomic force microscopy (AFM) whereby the tip of the AFM is chemically modified [10, 25], and infrared (IR) spectroscopy [26, 27] have been described. IR spectroscopy has been used for the surface pK_a determination of carboxyl modified silicon surfaces, whereby the silicon wafer was used as an ATR crystal in a pH regulated liquid cell. IR spectroscopy enables the quantification of COOH and COO⁻ groups and thereby the determination of the pK_a [26, 27]. By chemical force titration the pK_a can be determined very locally on the modified surface. Consequently, to obtain a representative pK_a value of the surface, multiple spots on the surface should be measured. Other drawbacks of AFM are that the method is expensive, labor intensive, and requires special expertise [28]. In addition, a complicated factor is the coating of the tip of the AFM with a molecule which has a pK_a by itself [9, 10, 25, 28].

Contact angle titration is a technique to analyze proton transfer reactions at low-energy surfaces and surface wettability as a function of pH. By this method the contact angles of buffered water drops are measured at various pH values. If the surface has a pK_a , the contact angle will be a function of the pH. Subsequently, in theory the surface pK_a can be extracted from the titration curve where the proton transfer reaction takes place, visible as a change in the contact angle [6, 8, 24]. The major disadvantage of contact angle titrations is that it is

difficult to extract the pK_a values from the titration curves, mainly because the contact angle rarely forms a unique thermodynamic equilibrium with the SAM as described by Young's equation [29].

Silicon surfaces can be modified with molecules with ionizable groups, such as amine-terminated and carboxyl-terminated surface groups. The charge of these groups will depend on their surface pK_a and the surrounding pH value. If the silicon surface is charged, the surface should be able to bind particles with an opposite charge. In this paper, we present a new method to determine the apparent surface pK_a of modified silicon surfaces by an indirect method, which is based upon electrostatic interactions between the modified silicon surface and fluorescently labeled polystyrene nanoparticles with either a stable positive or negative charge over a broad pH range. We compare our new method with the conventional contact angle titration.

2. Experimental

2.1 Chemicals

For the preparation of aqueous solutions and the cleaning of the silicon surfaces deionized water with a resistivity of 18 M Ω -cm, produced by a Millipore water purification system (MQ water), was used. Hydrogen peroxide (30%), (3-aminopropyl)triethoxysilane (APTES), succinic anhydride, (3-carboxypropyl)trimethylammonium chloride (CPTA), ethylenediaminetetraacetic acid (EDTA), (4-(2-hydroxyethyl)-1-piperazineethanesulfonic acid (HEPES), sulfate-modified (5%) polystyrene fluorescent orange (520 nm excitation/540 nm emission) nanoparticles of 100 nm and, amine-modified (5%) polystyrene fluorescent orange nanoparticles of 100 nm were purchased from Sigma Aldrich. Alexa-Fluor® 488 carboxylic acid succinimidyl ester was purchased from Invitrogen. N,N'-dicyclohexylcarbodiimide (DCC) and N-hydroxysuccinimide (NHS) were purchased from Fluka, and 1,4-dioxane was from J.T. Baker Chemicals B.V. Sulfuric acid 96-98% and acetone were obtained from BOOM lab equipment, methanol HPLC grade, tetrahydrofuran (THF) AR, and toluene AR were purchased from BIOSOLVE, and acetonitrile HPLC Far UV was from LAB-SCAN Analytical Sciences. Silicon wafers <110> dsp of 0.38 mm thickness were a kind gift of U-Needle B.V. The wafers were cut in pieces of either 1 by 1 cm or 1 by 2.5 cm. Black 96-well plates were purchased from Greiner Bio-One, polystyrene cuvettes (10x4x45 mm) were from Sarstedt, Slide-A-Lyzer® Dialysis Cassettes 3,500 MWCO were purchased from Thermo Scientific, and molecular sieves 4Å 8 to 12 mesh were from Acros Organics.

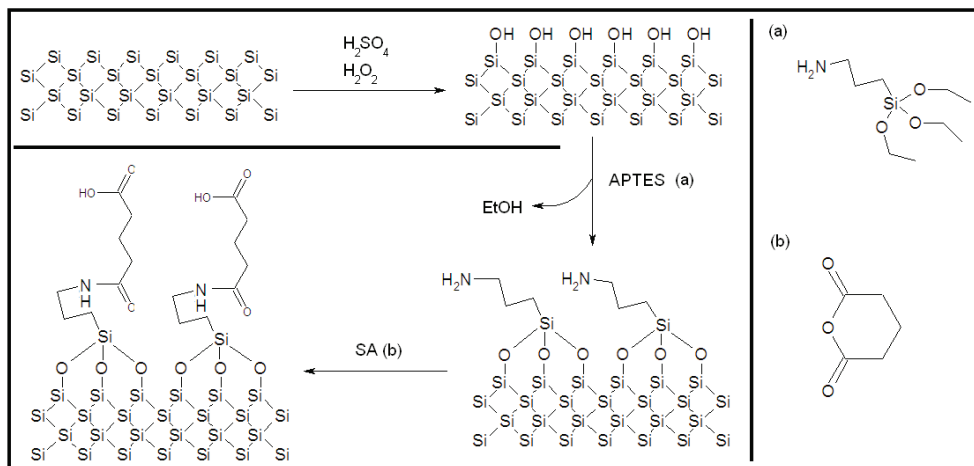


Figure 1: Reaction scheme for the modification of silicon surfaces, showing the generation of SiOH groups, modification of these groups with APTES (a), yielding an amine-modified surface and subsequent reaction with succinic anhydride (SA) (b), yielding a carboxyl-modified surface.

2.2 Surface chemistry of amine and carboxyl-modified silicon slides

The chemical modification of the silicon surfaces, depicted in figure 1, was a multiple step procedure involving (1) cleaning of the surface (i.e. fat removal) and generating SiOH groups [7, 30], (2) silanization and stabilization of the surface (i.e. curing and removal of residual ethoxy groups from APTES as reported by Kim *et al.* 2009 and Howarter *et al.* 2006) [7, 31-33], and (3) converting the amine surface to a carboxylic surface [4].

Each of these steps is described below.

1. Cleaning of the silicon slides. The silicon slides were treated once with acetone and twice with methanol and were subsequently dried in a vacuum oven at 50°C for 30 min. Then, the silicon slides were incubated for 60 min at 80°C in a freshly prepared piranha mixture (a mixture of 30% H_2O_2 and 70% H_2SO_4). **Caution: piranha solution reacts violently with organic compounds, and it should not be stored in closed containers.** Finally, the silicon slides were washed twice in MQ water and five times in methanol and then dried in a vacuum oven at 50°C for 30 min.

2. Generation of an amine-modified surface. The silicon slides were incubated for 24 h at room temperature on a shaking device in 2% (v/v) APTES in toluene. Subsequently, the amine-modified silicon slides were washed once with toluene and three times with methanol. Then, the amine-modified silicon slides were cured under argon for 30 min at 120°C, and were incubated in MQ water for 2 h at 40°C to remove unreacted ethoxy groups. Finally, the slides were flushed once with methanol and dried in a vacuum oven at 50°C for 30 min.

3. Generation of a carboxyl-modified surface. The amine-modified silicon slides were incubated in a 20 mg/mL solution of succinic anhydride in 1,4-dioxane for 30 min at 80°C. Then,

the silicon slides were washed three times with methanol and dried in a vacuum oven for 30 min at 50°C.

All modified silicon slides were stored under argon until use.

2.3 Preparation and characterization of fluorescent quaternary ammonium-modified nanoparticles

In order to determine the surface pK_a of silicon surfaces modified with weak acids and weak bases, stable fluorescent nanoparticles are needed with either a positive or negative charge over a broad pH range. Since amine-modified polystyrene nanoparticles lack stability at $pH > 8$, these nanoparticles were modified with CPTA into quaternary ammonium-modified nanoparticles. This was done in a two-step procedure. First, the carboxylic group of CPTA was activated with NHS. Subsequently, CPTA was coupled onto the amine groups of the amine-modified nanoparticles, shown in figure 2.

Synthesis of CPTA-NHS: CPTA (100 mg, 0.55 mmol) and NHS (108 mg, 0.94 mmol, 1.7 eq.) were dissolved in 12.5 mL acetonitrile with molecular sieves 4A under magnetic stirring for 15 min at room temperature. Then, the solution was cooled on ice under magnetic stirring for 15 min. Subsequently, DCC (216 mg, 1.05 mmol, 1.9 eq.) dissolved in 2.15 mL acetonitrile was added to the reaction mixture, and the solution was stirred for 16 h at room temperature. Subsequently, the stirrer was turned off and the solution was put on ice for 15 min to precipitate the dicyclohexylurea, and the resulting suspension was then filtered on a fritted funnel. The precipitate was washed with 5 mL acetonitrile, and was then discarded (the reaction product is in the acetonitrile). Subsequently, the acetonitrile with the reaction product was vacuum evaporated, leaving a brownish residue. Then, 6.25 mL THF was added to this residue to dissolve non reacted NHS and DCC, and the mixture was put on ice for 2 h. Then, the product was collected on a glass filter and was washed with 5 mL THF [34]. Finally, the product was dried in a vacuum oven for 16 h at 30°C, weighed (46 mg, 0.17 mmol, 31% yield), and was stored at -80°C until use. For the confirmation of the desired reaction product 1H and ^{13}C NMR was used and the following peak shifts were identified: 1H NMR D_2O 300 MHz δ 3.45 (2H, m, $N(CH_3)_3CH_2$), 3.15 (9H, s, $N(CH_3)_3$), 2.95 (4H, s, $CO(CH_2)_2CO$), 2.90 (2H, t, $NHS-CO_2CH_2CH_2$), 2.30 (2H, m, $CH_2CH_2CH_2$). ^{13}C NMR D_2O 75 MHz δ 173.3 (CO of NHS), 169.3 (CO_2-NHS), 64.8 ($CH_2CH_2N(CH_3)_3$), 53.0 ($N(CH_3)_3$), 27.3 (CO_2CH_2), 25.5 (CH_2 of NHS), 17.9 ($CH_2CH_2CH_2$).

Coupling of CPTA to nanoparticles: For the coupling of CPTA to the amine-modified fluorescent polystyrene nanoparticles, 100 μL of these nanoparticles were diluted with 900 μL solution 1, composed of 1:4 THF: 100 mM HEPES buffer (pH 6.0) under magnetic stirring. Then, 10 mg CPTA-NHS dissolved in 100 μL solution 1 was added and the mixture was left to react for 1 h at room temperature. To confirm that the CPTA was coupled and thereby stable nanoparticles had been formed, the particle size and size distribution was determined by dynamic light scattering (DLS) and the zeta potential by laser Doppler electrophoresis on a Zetasizer Nano (Malvern Instruments) at pH values between 2-12. Subsequently, the CPTA-

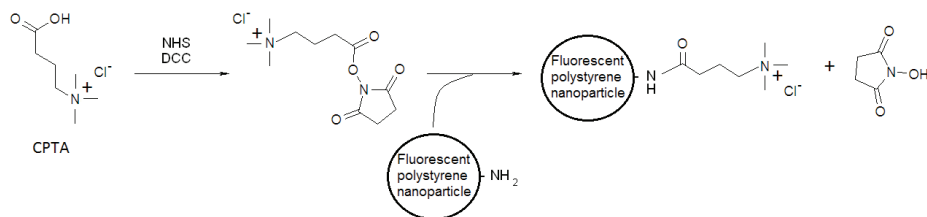


Figure 2: Synthesis of CPTA-modified nanoparticles. CPTA, (3-carboxypropyl)trimethylammonium chloride; NHS, N-hydroxysuccinimide; DCC, dicyclohexylcarbodiimide.

modified polystyrene nanoparticles were dialyzed on a 5 mM HEPES buffer (pH 6.0) for 6 h at room temperature, and were stored in a dark vial at 4°C until use. Finally, a calibration curve was made with the amine-modified nanoparticles, from which the concentration CPTA-modified nanoparticles was determined.

2.4 Reactivity of modified surfaces with a fluorescent dye

To determine whether the silicon surface was successfully modified into an amine-modified surface and subsequently a carboxyl-modified surface, a fluorescent dye which reacts specifically with primary amines was used. Silicon slides of 1 by 2.5 cm were incubated for 1 h in 5 mL acetonitrile with 10 µg Alexa Fluor® 488 carboxylic acid succinimidyl ester at room temperature. Then, the silicon slides were washed twice with acetonitrile and five times with methanol, and were subsequently dried in a vacuum oven at 50°C for 30 min. Finally, the silicon surfaces were photographed under a fluorescence microscope, Nikon Eclipse E600 with a mercury light source, a GFP filter set, a magnification of 400x and an exposure time of 10 seconds. The pictures of the surfaces were analyzed by plotting the pixel intensity against the pixel position on the surface by the ‘interactive 3D surface plot’ plugin in ImageJ (available from rsbweb.nih.gov/ij/), with the following settings: grid size 128, smoothing 3.0, max. 40%, and min. 8%. The efficiency (E) of the derivatization of the amine surface with succinic anhydride was determined by equation 1, where I_0 is the average pixel intensity of the non-modified surface, I_a is the average pixel intensity of the amine-modified surface, and I_c is the average pixel intensity of the carboxyl-modified surface.

$$E = 100 - \left[\frac{(I_c - I_0)}{(I_a - I_0)} \right] * 100 \quad (\text{Equation 1})$$

2.5 Ellipsometry

The layer thickness and the optical properties of the amine coating and the carboxyl coating on the silicon slides, compared to the unmodified surface (after piranha treatment), was determined by spectroscopic ellipsometry. Spectroscopic ellipsometry measures the change in polarization upon reflection, which is represented by Ψ (the amplitude ratio) and

Δ (the phase difference), and derives the layer thickness from it. Ψ and Δ were measured on a Woollam M-2000F rotating compensator spectroscopic ellipsometer at five different angles of incidence (55°, 60°, 65°, 70°, and 75°) and in a range between 246 nm and 1000 nm, and were analyzed by the WVASE32 software version 3.632. The device was calibrated with a standard 25 nm silicon oxide layer on a 0.7 mm silicon wafer. For each type of surface three silicon slides were used, where the layer thickness per silicon slide was determined as the average of 5 different spots. For the determination of the layer thickness of the organic layers the Cauchy fitting model was used with the following settings for the optical constants: $A_n=1.45$ and $B_n=0.01$.

2.6 pKa determination by the fluorescent nanoparticle adhesion assay

For the pK_a determination of modified silicon surfaces negatively charged nanoparticles were used for the titration of the positive (amine) surface, and positively charged nanoparticles were used for the titration of the negative (carboxyl) surface, as depicted in figure 3. As a control, non-modified piranha treated surfaces were titrated with positively and negatively charged nanoparticles.

To determine the surface pK_a a 1 mM EDTA buffer with 1 μ L of 2.5% fluorescent nanoparticles per mL was prepared. Then, the pH was adjusted between 2 and 12 with either 0.1 and 0.01 M NaOH or 0.1 M and 0.01 M HCl to make 20 nanoparticle suspensions, each with a different pH. For each pH value two aliquots of 0.75 mL were transferred into 1.5 mL cuvettes, one with and one without the modified silicon slide. The amine-modified silicon slide (weak base) was incubated with the negatively charged nanoparticles for 4 h, and the carboxyl-modified silicon slide (weak acid) was incubated with the positively charged nanoparticles for 2 h. Incubations were done at room temperature and by using a shaking device. Then, two times 200 μ L from each sample cuvette were transferred to a black 96-well plate and the fluorescence was measured at an excitation wavelength of 520 nm and an emission wavelength of 540 nm with a Tecan Infinite® M1000 plate reader. Subsequently, the relative fluorescence was calculated for the different pH values. Relative fluorescence values (compared to the 100% fluorescence value of the nanoparticle sample from the cuvette without silicon slide) were plotted against the pH. Finally, according to the Henderson-Hasselbalch equation, the S-shaped curve was fitted in Origin version 8.1. From this fitted curve the surface pK_a was calculated as the pH value at the midpoint of the S-shaped curve.

2.7 pKa determination by contact angle titration

The surface pK_a obtained by contact angle titration was used to compare the obtained pK_a value with our new method for the surface pK_a determination of modified silicon surfaces. Therefore, multiple 10 mM HEPES buffers with different pH values in a pH range between 2 and 13 were prepared. Then, contact angle titrations were performed on non-modified silicon surfaces (after piranha treatment), on amine-modified silicon surfaces, and on carboxyl-modified silicon surfaces. To determine the contact angle, a drop of 5 μ L HEPES buffer was

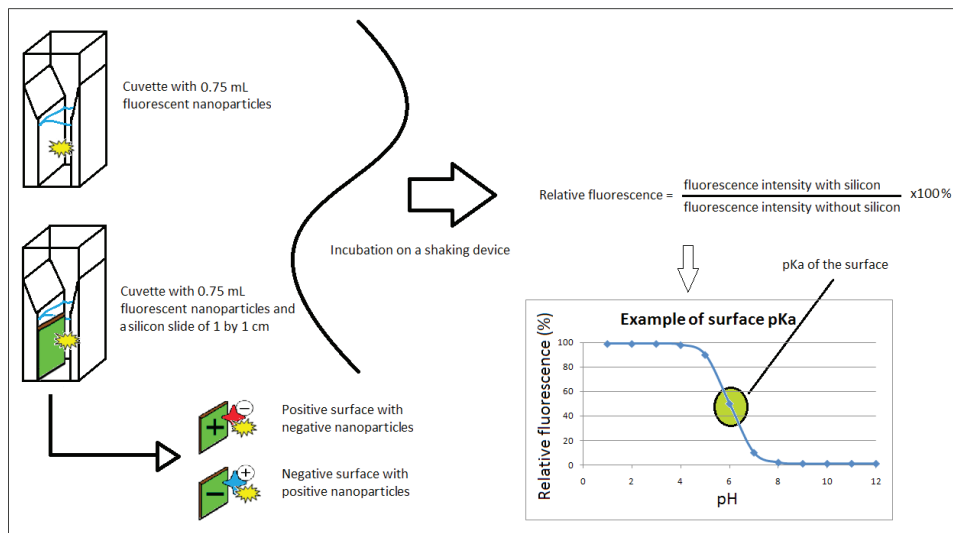


Figure 3: Schematic representation of our newly developed fluorescent nanoparticle adhesion assay for determination of the surface pK_a of modified silicon surfaces.

put on the silicon surface at room temperature and after 15 seconds a picture was taken (Sony Super SteadyShot). Then, the pictures of the contact angles were converted into black-and-white pictures, and were subsequently analyzed in ImageJ (available from rsbweb.nih.gov/ij/) by the plugin LB_ADSA (contact angle measurement) as described by Stalder *et al.* [35]. Finally, the surface pK_a was determined as the pH value where the contact angle changes.

3. Results and discussion

3.1 Characterization of surface modified fluorescent polystyrene nanoparticles

To determine in which pH range the surface-modified fluorescent polystyrene nanoparticles are usable for determining the pK_a of modified silicon surfaces, the pH dependence of the physicochemical stability of these nanoparticles was determined. Figure 4 shows a representative graph of the average size, the PDI, the zeta potential, and the fluorescence of the surface-modified nanoparticles as a function of the pH. The sulfate-modified nanoparticles turned out to be negatively charged and colloidally stable between pH 2-13, indicating that these nanoparticles can be used as such for the pK_a determination over a broad pH range of surfaces with basic groups. The amine-modified polystyrene nanoparticles started to aggregate at $pH \geq 8$, as reflected by an increase in particle size and size distribution (PDI), and a drop in zeta potential. This demonstrates that at alkaline conditions these particles are colloidally unstable and therefore unsuitable for the surface pK_a determination. For this reason the particles were modified with CPTA. The CPTA-modified nanoparticles, carrying a permanent positive charge (see figure 4c), were shown to be stable until $pH > 11$ (figure

4a, 4b). This indicates that the coupling of CPTA was successful and led to particles that are colloiddally stable between pH 2-11. These particles can be used for the titration of surfaces with acidic groups within this range. In figure 4d the fluorescence intensity of the three different nanoparticles is shown as a function of pH. The fluorescence intensity of the sulfate-modified fluorescent nanoparticles was shown to be stable from pH 3-12. It was shown that the fluorescence intensity of amine-modified fluorescent nanoparticles decreased to 50% at pH > 8. However, the fluorescence intensity of the CPTA-modified nanoparticles is stable pH 2-4 and between pH 6-11. The CPTA-modified nanoparticles show a decrease in fluorescence intensity between pH 4-6, which could be due to binding of these particles to the surface of the cuvettes. However, this does not influence the pK_a determination since the relative fluorescence is measured.

3.2 Confirmation of silicon modification by fluorescence microscopy

To determine whether the silicon surface was successfully modified using APTES (amine-modified) and subsequently SA (carboxyl-modified) and to determine the surface coverage, a primary amine reactive dye (Alexa-Fluor® 488 carboxylic acid succinimidyl ester) was used on non-modified, amine-modified, and carboxyl-modified silicon surfaces. It is expected that this dye only binds to the amine-modified surface and not to the non-modified surface and the amine-modified surface derivatized with carboxyl-groups. Thus, only the amine-modified surface is expected to be fluorescent, which is indicated by an increase of the average pixel intensity.

In figure 5 on the left side fluorescence microscopy pictures are shown of the differently modified silicon slides and on the right side their 3D analysis (pixel intensity versus position in the picture). The minimum base value for the pixel intensity of the amine-modified surface was increased compared to the minimum base value of the pixel intensity of the non-modified surface, which indicates that there are amine-groups present on the surface. Besides, in figure 5d it appears that there is a complete surface coverage of amine groups. Furthermore, the ground value of the pixel intensity of the carboxyl-modified surface was about the same as for the non-modified surface, thus the amine-modified surface was successfully converted into a carboxyl-modified surface. The efficiency of modifying the amine-modified surface into a carboxyl-modified surface was calculated according to equation 1, and was estimated to be higher than 95%. This is more than the ca. 40% reported by Kim *et al.* [4] who used NHS-carboxyfluorescein for conjugation with surface amine groups on silicon. This discrepancy could be explained by the differences between the succinic anhydride coupling procedures: 5 mg/mL succinic anhydride in THF with 5% triethylamine for 4 h at room temperature by Kim *et al.*, versus 20 mg/mL succinic anhydride in 1,4-dioxane for 30 min at 80°C by us.

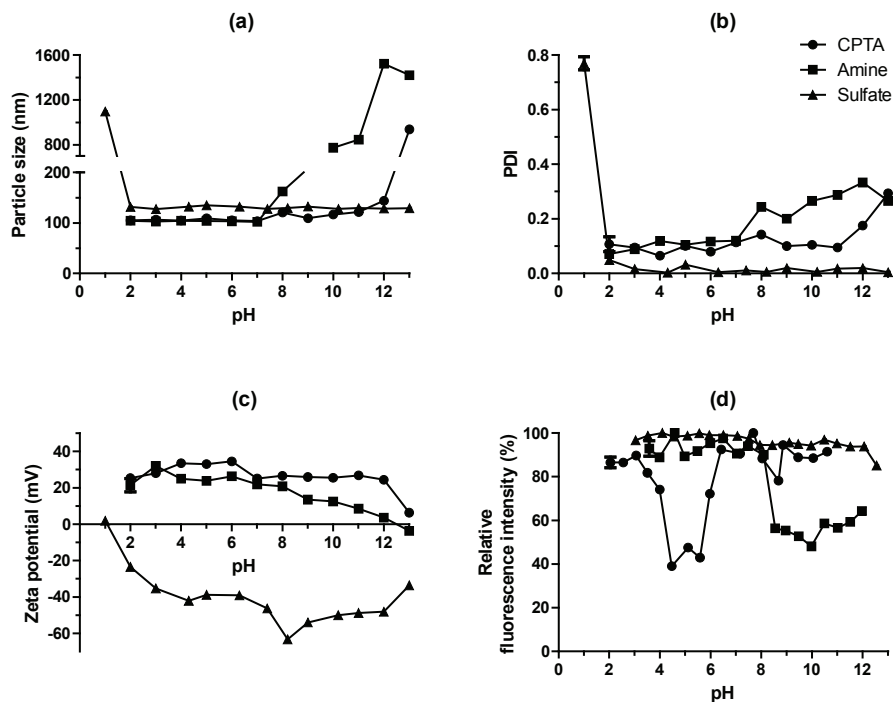


Figure 4: Representative graphs showing the physicochemical properties of surface-modified polystyrene nanoparticles. Average size (a) and size distribution (PDI) (b) measured by dynamic light scattering, zeta potential (c) measured by laser Doppler electrophoresis, and relative fluorescence intensity (d) are shown of CPTA-modified nanoparticles (circles), amine-modified nanoparticles (squares) and sulfate modified nanoparticles (triangles). Representative standard deviations are indicated for each of the measured parameters at the lowest pH values.

3.3 Determination of layer thickness by ellipsometry

Ellipsometry was used to determine the layer thickness of the non-modified surface, the amine-modified surface, and the carboxyl-modified surface. The natural silicon oxide and the SiOH groups after piranha treatment accounted for 1.512 ± 0.240 nm ($n=3$, mean \pm SD). The thickness of this layer was set as a constant for the fitting of the data of the amine-modified surface and the carboxyl-modified surface.

After the silicon slides were modified with APTES ($-\text{SiC}_3\text{H}_8\text{N}$) the layer thickness had increased by 0.639 ± 0.159 nm ($n=3$, mean \pm SD) compared to the silicon slides after piranha treatment. This value is consistent with data found in the literature for a monolayer of APTES [10], however, also values of > 15 nm have been found for the layer thickness of APTES coatings [4, 32, 33], whereby the layer thickness was dependent on the used coating method. These much larger reported thicknesses correspond to interreacted APTES layers [32].

After the modification of amine-modified slides with succinic anhydride ($-\text{SiC}_8\text{H}_{14}\text{NO}_3$), the layer thickness had increased by 1.924 ± 0.462 nm ($n=3$, mean \pm SD) compared to silicon slides after piranha treatment. The increase of layer thickness compared to the amine-modified silicon slides was 1.285 ± 0.462 nm, which is slightly higher than the value of 0.5 ± 0.1 nm reported

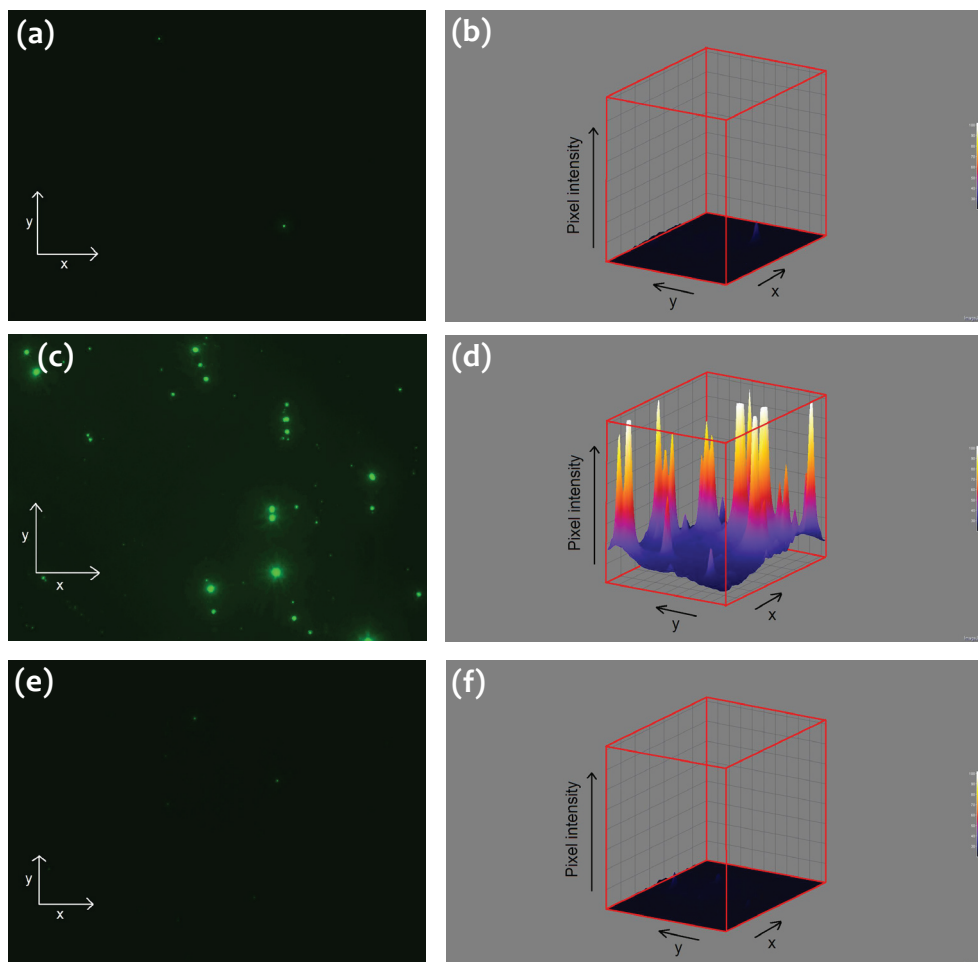


Figure 5: Fluorescent surface modification with a primary amine reactive fluorescent dye (Alexa-Fluor® 488 carboxylic acid succinimidyl ester) for the confirmation of amine-based surface modifications. Left: representative pictures by fluorescence microscopy (magnification of 400x, surface of 0.054 mm², 811x1070 μm) of non-modified (a), amine-modified (c), and carboxyl-modified (e) silicon surfaces after incubation with the fluorescent dye. Right: pixel intensity versus position in the pictures on the left after 3D analysis of non-modified (b), amine-modified (d), and carboxyl-modified (f) silicon surfaces. Note the elevated fluorescence background level of the amine-modified (d) surface.

by Kim *et al.* [4]. This difference can be explained by the different coating efficiency (40% vs. 95%). Furthermore, 1.285 ± 0.462 nm corresponds with the theoretical surface thickness (0.9 nm) of a monolayer of SA.

3.4 Surface pK_a determination by the fluorescent nanoparticle adhesion assay

The apparent surface pK_a of amine-modified surfaces and carboxyl-modified surfaces was determined by our new method after the nanoparticle binding conditions were optimized with respect to buffer, buffer concentration, nanoparticle binding time, and nanoparticle

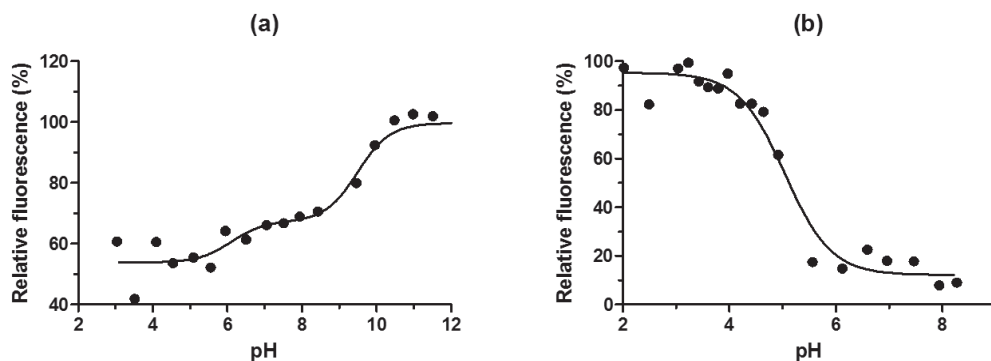


Figure 6: Surface pK_a determination of surface-modified silicon by the fluorescent nanoparticle adhesion assay. A representative example of 3 independent surface pK_a determinations of (a) amine-modified surfaces with sulfate-modified nanoparticles, and (b) carboxyl-modified surfaces with CPTA-modified nanoparticles is shown.

concentration (data not shown). This method is based upon the pH-dependent binding of fluorescent nanoparticles with a positive or negative charge to an oppositely charged surface with (de)protonatable groups. The surface pK_a was defined as the pH value at the midpoint of the S-shaped curve of the relative fluorescence intensity versus pH.

Furthermore, no titratable groups were found for the non-modified surfaces with negatively charged nanoparticles (supporting information). However, a gradually decreasing relative fluorescence curve between pH 6-9 was found for the non-modified surface with positive nanoparticles (supporting information), indicating several degrees of deprotonation of the surface silanol groups [36]. However, this did not interfere with the pK_a determination by the fluorescent nanoparticle adhesion assay, since the CPTA nanoparticle adhesion onto piranha treated surfaces started after the point where the carboxylic surface had the maximum adsorption of these CPTA nanoparticles. Furthermore, when the surface was derivatized with phenolic groups, CPTA nanoparticle adhesion started at pH values above 7 (supporting information).

Figure 6a shows a representative surface pK_a determination of amine-modified silicon slides with sulfate-modified polystyrene fluorescent nanoparticles. Fitting a 2 S-shaped curve according to the Henderson-Hasselbalch equation for two pK_a values revealed two surface pK_a values for the amine-modified silicon slides. The midpoint of the first S-shaped curve revealed a surface pK_a of 6.55 ± 0.73 ($n=3$, mean \pm SD) and a second surface pK_a of 9.94 ± 0.19 ($n=3$, mean \pm SD). The first surface pK_a value is in compliance with the literature, where comparable surface pK_a values (pK_a 3.9-7.6) have been reported for APTES films [9, 25, 37]. Zhang *et al.* reported a surface pK_a of 7.4 for APTES films on silicon surfaces by chemical force titration. However, the same group observed a similarly attractive interaction (similar to the pK_a of 7.4) in the force curves with chemical force titrations of 3-aminopropyl on the surface at pH > 8 when the sample-tip distance was gradually decreased [10]. This may indicate the

presence of a second surface pK_a above 8, which would be in compliance with our results (second surface pK_a of 9.94). Furthermore, our results show that the second surface pK_a had a much higher influence on the binding of fluorescent nanoparticles to the silicon surface.

In figure 6b a representative picture is shown of a surface pK_a determination of the carboxyl-modified silicon surface with CPTA-modified polystyrene fluorescent nanoparticles. The surface pK_a of the carboxyl-modified silicon surfaces was found to be 4.37 ± 0.59 ($n=3$, mean \pm SD). This is in compliance with pK_a values found in the literature where pK_a values of $-COOH$ terminated surfaces between 4.4 and 6.5 have been reported [9, 11, 18, 25]. However, also pK_a values of up to 10.3 have been reported for aliphatic $-COOH$ terminated surfaces, which is dependent on the chain length ($-CH_2-$) between the $-COOH$ group and the surface (substrate): longer chain lengths lead to higher surface pK_a values [12]. Overall, the surface pK_a of our carboxyl-modified surface (short chain length) is within the expected and reported range.

3.5 pK_a determination by contact angle titration

For comparison, the surface pK_a of amine-modified and carboxyl-modified silicon surfaces was also determined by contact angle titration, see table 1 and figure 7. The contact angle titrations revealed a surface pK_a of 7.3 ± 0.8 for the 3-aminopropyl surface ($n=3$, mean \pm SD) and a surface pK_a of 5.7 ± 1.4 for the carboxyl-modified surface, which is in agreement with surface pK_a values obtained by the contact angle titration reported in literature [6, 8, 9, 11, 20]. Furthermore, the surface pK_a of the amine-modified surface by contact angle titration was comparable to the first surface pK_a obtained by the fluorescent nanoparticle adhesion assay of the same surface. However, a second surface pK_a of an APTES SAM as detected by the new method was not observed by contact angle titration. This perhaps could be due to lack of sensitivity of the contact angle titration. The surface pK_a of the carboxyl-modified silicon surface determined by the fluorescent nanoparticle adhesion assay was within the standard deviation of the pK_a value found by the contact angle titration.

The standard deviations of the contact angle titrations were very high, and did not lead to a precise determination of the surface pK_a value. However, the contact angle titrations showed a different profile after the silicon surface was modified with APTES or with APTES derivatized with succinic anhydride. This offers the possibility to use this method to evaluate the surface modification. In conclusion, our new method enabled us to determine the surface

Table 1: Surface pK_a values obtained by the fluorescent nanoparticle adhesion assay and by contact angle titration of amine-modified silicon surfaces and carboxyl-modified silicon surfaces.

	Amine-modified surface	Carboxyl-modified surface
Fluorescent nanoparticle adhesion assay	pK_a 1: 6.55 ± 0.73 pK_a 2: 9.94 ± 0.19	pK_a : 4.37 ± 0.59
Contact angle titration	pK_a : 7.3 ± 0.8	pK_a : 5.7 ± 1.4

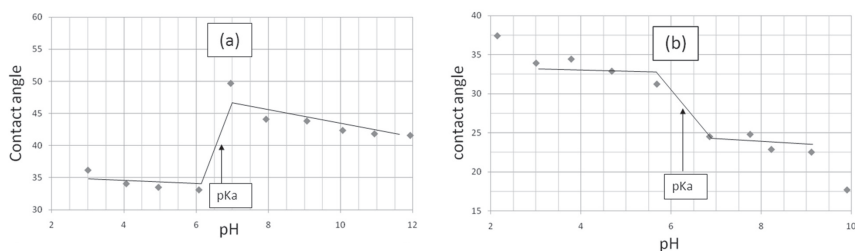


Figure 7: Examples of pK_a determinations of (a) amine-modified and (b) carboxyl-modified silicon surfaces by contact angle titration.

pK_a value of modified silicon surfaces with smaller standard deviations and could reveal surface pK_a values which cannot be determined by contact angle titration.

In summary, we have developed a new method to determine the apparent pK_a of (modified silicon) surfaces, which is based upon electrostatic interactions between charged surface groups and fluorescent polystyrene nanoparticles with a permanent opposite charge. The fluorescence intensity of suspensions of fluorescent nanoparticles is determined after the nanoparticles are incubated in buffer with and without modified silicon slides at various pH values. Subsequently, the binding of nanoparticles to the surface, is calculated by dividing the fluorescence intensity of the nanoparticle suspension with a silicon slide by the fluorescence intensity of the suspension without silicon slides. Then the relative fluorescence values are plotted against the pH, and the surface pK_a is obtained from the S-shaped curve according to the Henderson-Hasselbalch equation, which leads to a reproducible determination of the apparent surface pK_a . We have found two surface pK_a values of 6.55 ± 0.73 and 9.94 ± 0.19 for an amine-modified surface, and a surface pK_a of 4.37 ± 0.59 for a carboxyl-modified surface. This method could be a useful tool to design pH-dependent electrostatic protein and particle binding/release systems, and to design surfaces with a pH-dependent surface charge for (bio-) analytical lab-on-a-chip or drug delivery purposes.

Acknowledgements

Financially supported by programme Nano4Vitality of the Ministry of Economic affairs and the provinces Gelderland and Overijssel, and NanoNextNL. Furthermore, we acknowledge U-Needle B.V. for supplying us with cut silicon wafers. Finally, we thank J.P.M. van der Ploeg for his help with the ellipsometric measurements.

References

- [1] M. Tichoniuk, D. Gwiazdowska, M. Ligaj, M. Filipiak, Electrochemical detection of foodborne pathogen *Aeromonas hydrophila* by DNA hybridization biosensor. *Biosensors and Bioelectronics* 26 (2010) 1618-1623.
- [2] M. Frasconi, C. Tortolini, F. Botre, F. Mazzei, Multifunctional Au Nanoparticle Dendrimer-Based Surface Plasmon Resonance Biosensor and Its Application for Improved Insulin Detection. *Anal. Chem.* 82 (2010) 7335-7342.
- [3] W. Kusnezow, A. Jacob, A. Walijew, F. Diehl, J.D. Hoheisel, Antibody microarrays: an evaluation of production parameters. *Proteomics* 3 (2003) 254-264.
- [4] J. Kim, J. Cho, P.M. Seidler, N.E. Kurland, V.K. Yadavalli, Investigations of Chemical Modifications of Amino-Terminated Organic Films on Silicon Substrates and Controlled Protein Immobilization. *Langmuir* 26 (2010) 2599-2608.
- [5] E. Ruckenstein, Z.F. Li, Surface modification and functionalization through the self-assembled monolayer and graft polymerization. *Advances in Colloid and Interface Science* 113 (2005) 43-63.
- [6] S.E. Creager, J. Clarke, Contact-Angle Titrations of Mixed mMercaptoalkanoic Acid/Alkanethiol Monolayers on Gold. Reactive vs Nonreactive Spreading, and Chain Length Effects on Surface pKa Values. *Langmuir* 10 (1994) 3675-3683.
- [7] N. Graf, E. Yegen, A. Lippitz, D. Treu, T. Wirth, W.E.S. Unger, Optimization of cleaning and aminosilanization protocols for Si wafers to be used as platforms for biochip microarrays by surface analysis (XPS, ToF-SIMS and NEXAFS spectroscopy). *Surf. Interface Anal.* 40 (2008) 180-183.
- [8] T.R. Lee, R.I. Carey, H.A. Biebuyck, G.M. Whitesides, The Wetting of Monolayer Films Exposing Ionizable Acids and Bases. *Langmuir* 10 (1994) 741-749.
- [9] D.V. Vezenov, A. Noy, L.F. Rozsnyai, C.M. Lieber, Force Titrations and Ionization State Sensitive Imaging of Functional Groups in Aqueous Solutions by Chemical Force Microscopy. *J. Am. Chem. Soc.* 119 (1997) 2006-2015.
- [10] H. Zhang, H.-X. He, J. Wang, T. Mu, Z.-F. Liu, Force titration of amino group-terminated self-assembled monolayers using chemical force microscopy. *Appl. Phys. A* 66 (1998) S269-S271.
- [11] J. Zhao, L. Luo, X. Yang, E. Wang, S. Dong, Determination of Surface pKa of SAM Using an Electrochemical Titration Method. *Electroanalysis* 11(15) (1999) 1108-1111.
- [12] Z. Dai, H. Ju, Effect of chain length on the surface properties of x-carboxy alkanethiol self-assembled monolayers. *Phys. Chem. Chem. Phys.* 3 (2001) 3769-3773.
- [13] M.A. Bryant, R.M. Crooks, Determination of Surface pKa Values of Surface-Confined Molecules Derivatized with pH-Sensitive Pendant Groups. *Langmuir* 9 (1993) 385-387.
- [14] J.J. Betts, B.A. Pethica, The ionization characteristics of monolayers of weak acids and bases. *Trans. Faraday Soc.* 52 (1956) 1581-1589.
- [15] J. Caspers, E. Goormaghtigh, J. ferreira, R. BRASSEUR, M. vandenBanden, J.-M. Ruysschaert, Acido-Basic Properties of Lipophilic Substances: A Surface Potential Approach. *Journal of Colloid and Interface Science* 91 (1983) 546-551.
- [16] M. Opallo, J. Dojlido, Dissociation equilibrium of o-phthalic acid on the mercury electrode. *J. Electroanal. Chem* 127 (1981) 211-217.
- [17] J. Dojlido, M. Dmowska-Stańczak, Z. Galus, Adsorption and dissociation equilibrium of benzoic acid on the mercury electrode. *J. Electroanal. Chem.* 94 (1978) 107-122.
- [18] K. Sugihara, K. Shimazu, Electrode Potential Effect on the Surface pKa of a Self-Assembled 15-Mercaptohexadecanoic Acid Monolayer on a Gold/Quartz Crystal Microbalance Electrode. *Langmuir* 16 (2000) 7101-7105.
- [19] J.F. Smalley, K. Chalfant, S.W. Feldberg, T.M. Nahir, E.F. Bowden, An Indirect Laser-Induced Temperature Jump Determination of the Surface pKa of 11-Mercaptoundecanoic Acid Monolayers Self-Assembled on Gold. *J. Phys. Chem. B* 103 (1999) 1676-1685.
- [20] K.S. Mayya, V. Patil, M. Sastry, On the Stability of Carboxylic Acid Derivatized Gold Colloidal Particles: The Role of Colloidal Solution pH Studied by Optical Absorption Spectroscopy. *Langmuir* 13 (1997) 3944-3947.
- [21] J. Bagg, M.D. Haber, H.P. Gregor, Composition of Stearic and Behenic Acid Monolayers From Sodium-Containing Substrates. *Journal of Colloid and Interface Science* 22 (1966) 138-143.
- [22] J.G.E. Gardeniers, A. van den Berg, Lab-on-a-chip systems for biomedical and environmental monitoring. *Anal. Bioanal. Chem.* 378 (2004) 1700-1703.
- [23] C.D. Chin, V. Linder, S.K. Sia, Lab-on-a-chip devices for global health: Past studies and future opportunities. *Lab Chip* 7 (2007) 41-57.
- [24] S. Demirci, T. Caykara, Formation of dicarboxylic acid-terminated monolayers on silicon wafer surface. *Surface Science* 604 (2010) 649-653.
- [25] T.Z. Mengistu, V. Goel, J.H. Horton, S. Morin, Chemical Force Titrations of Functionalized Si(111) Surfaces. *Langmuir* 22 (2006) 5301-5307.
- [26] D. Aureau, F. Ozanam, P. Allongue, J.-N. Chazalviel, The Titration of Carboxyl-Terminated Monolayers Revisited: In Situ Calibrated Fourier Transform Infrared Study of Well-Defined Monolayers on Silicon. *Langmuir* 24 (2008) 9440-9448.
- [27] T. Vallant, J. Kattner, H. Brunner, U. Mayer, H. Hoffmann, Investigation of the Formation and Structure of Self-assembled Alkylsiloxane Monolayers on Silicon Using In Situ Attenuated Total Reflection Infrared Spectroscopy. *Langmuir* 15 (1999) 5339-5346.
- [28] H.X. He, C.Z. Li, J.Q. Song, T. Mu, L. Wang, H.L. Zhang, Z.F. Liu, Force Titration of a Carboxylic Acid Terminated Self-Assembled Monolayer Using Chemical Force Microscopy. *Molecular Crystals and Liquid Crystals* 294 (1997) 99-102.
- [29] C.D. Bain, E.B. Troughton, Y.T. Tao, J. Evall, G.M. Whitesides, R.G. Nuzzo, Formation of Monolayer Films by the Spontaneous Assembly of Organic Thiols from Solution onto Gold. *J. Am. Chem. Soc.* 111 (1989) 321-335.
- [30] J.J. Cras, C.A. Rowe-Taitt, D.A. Nivens, F.S. Ligler, comparison of chemical cleaning methods of glass in preparation for silanization. *Biosensors & Bioelectronics* 14 (1999) 683-688.
- [31] J. Kim, Effects of Curing Conditions on the Structure and Stability of Amino-Functionalized Organic Films on Silicon Substrates. *PIKE technologies*, 2010.
- [32] J.A. Howarter, J.P. Youngblood, Optimization of Silica Silanization by 3-Aminopropyltriethoxysilane. *Langmuir* 22 (2006) 11142-11147.
- [33] J. Kim, P. Seidler, L.S. Wan, C. Fill, Formation, structure, and reactivity of amino-terminated organic

films on silicon substrates. *Journal of Colloid and Interface Science* 329 (2009) 114–119.

[34] C. Morano, X. Zhang, L.D. Fricker, Multiple Isotopic Labels for Quantitative Mass Spectrometry. *Anal. Chem.* 80 (2008) 9298–9309.

[35] A.F. Stalder, T. Melchior, M. Müller, D. Sage, T. Blu, M. Unser, Low-Bond Axisymmetric Drop Shape Analysis for Surface Tension and Contact Angle Measurements of Sessile Drops. *Colloids and Surfaces A: Physicochemical and Engineering Aspects* 364 (2010) 72–81.

[36] P.K. Jal, S. Patel, B.K. Mishra, Chemical modification of silica surface by immobilization of functional groups for extractive concentration of metal ions. *Talanta* 62 (2004) 1005–1028.

[37] P. Abiman, G.G. Wildgoose, A. Crossley, J.H. Jones, R.G. Compton, Contrasting pKa of Protonated Bis(3-aminopropyl)-Terminated Polyethylene Glycol “Jeffamine” and the Associated Thermodynamic Parameters in Solution and Covalently Attached to Graphite Surfaces. *Chem. Eur. J.* 13 (2007) 9663 – 9667.

Supporting Information

We have performed the fluorescent nanoparticle adhesion assay (FNAA) on unmodified, piranha treated surfaces with negatively and positively charged nanoparticles. Figure S1A shows that negatively charged nanoparticles do not adhere to piranha treated surfaces. However, as show in figure S1B, there is a gradually increased adsorption of positively charged nanoparticles to piranha treated surfaces between pH 6-9, which is above the surface pK_a value of the carboxyl-modified surface (pK_a 4.37±0.59) found by the FNAA.

To confirm the general applicability of the FNAA, we have applied it to two additional surfaces, namely a phenol-modified silicon surface and a pyridine-modified silicon surface. We found a pK_a of 8.1 for a phenol modified surface with the positively charged nanoparticles, and a pK_a of 6.8 for a pyridine modified surface (figure S2).

We have performed a contact angle titration of a carboxyl modified surface with a 10 mM phosphate buffer (see figure S3) to check whether the type of buffer would influence the surface pK_a value. The calculated pK_a 6.05±0.64 (n=2) is very similar to that calculated from the contact angle titration with HEPES buffer (5.7±1.4). Finally, fluorescence microscopy photographs of nanoparticle adhesion are shown in figure S4.

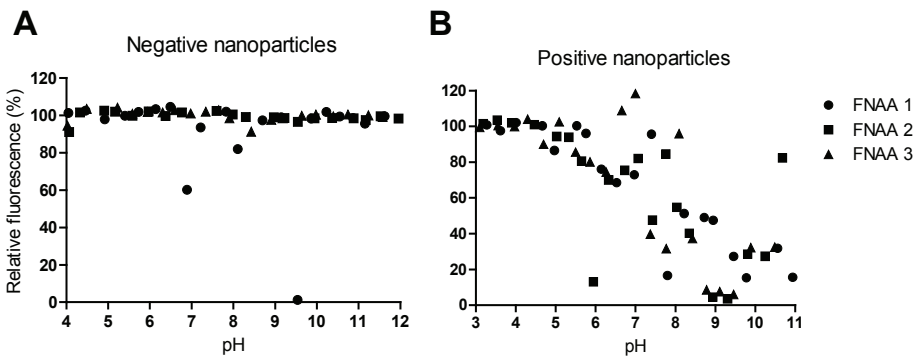


Figure S1: Fluorescent nanoparticle adhesion assay (FNAA) of piranha treated surfaces with (negatively charged) sulfate-modified fluorescent orange nanoparticles (A) and with (positively charged) CPTA-modified fluorescent orange nanoparticles (B).

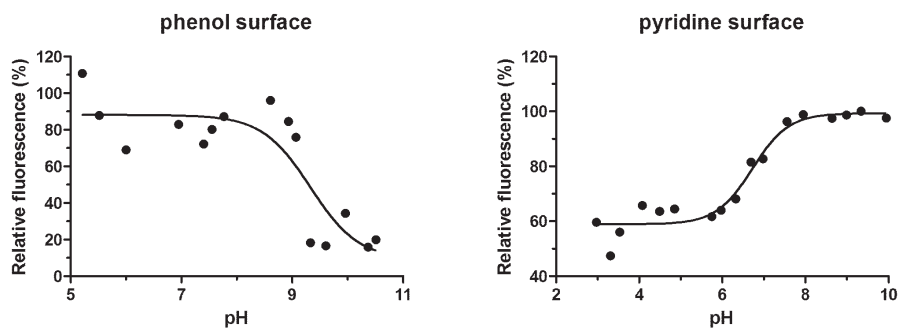


Figure S2: Fluorescent nanoparticle adhesion assay of (left) a phenol-modified surface with positively charged nanoparticles and (right) a pyridine-modified surface with negatively charged nanoparticles.

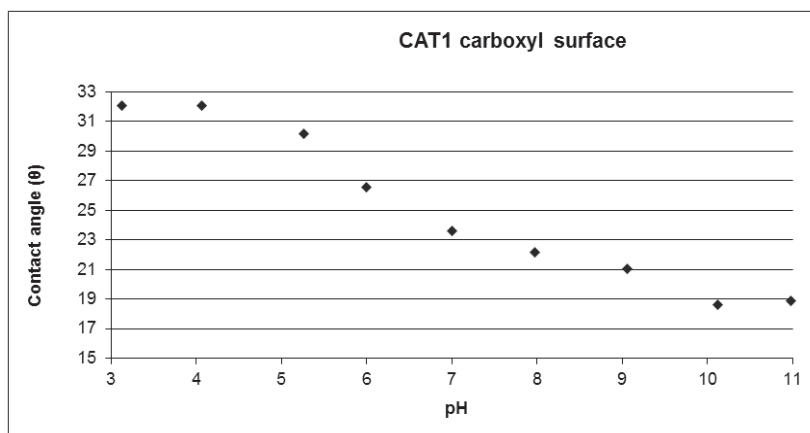


Figure S3: Representative example of a contact angle titration of a carboxyl-modified silicon surface with a 10 mM phosphate buffer.

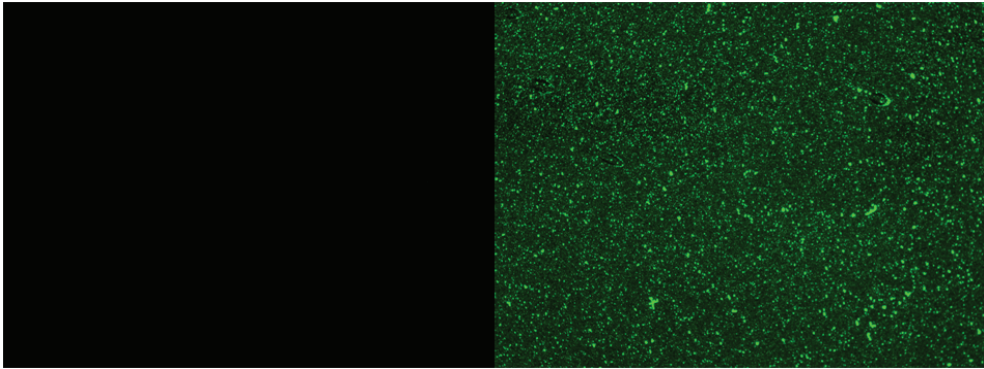


Figure S4: Typical fluorescence microscopy pictures of nanoparticle adhesion to silicon surfaces. Left panel: incubation of an unmodified silicon surface with negatively charged fluorescent nanoparticles (pH 6); right panel: incubation of an APTES-modified silicon surface with negatively charged nanoparticles (pH 6) (10x magnification, 811x1070 μm , GFP filter set).

NANOLAYERED CHEMICAL MODIFICATION OF SILICON SURFACES WITH IONIZABLE SURFACE GROUPS FOR pH-TRIGGERED PROTEIN ADSORPTION AND RELEASE: APPLICATION TO MICRONEEDLES

Koen van der Maaden¹
Huixin Yu¹
Karen Sliedregt²
Raphäel Zwier³
Romain Lebourg¹
Masashi Oguri¹
Alexander Kros²
Wim Jiskoot¹
Joke A. Bouwstra¹

[Journal of Materials
Chemistry B, 1 \(2013\)
4466-4477](#)

¹Division of Drug Delivery
Technology, Leiden
Academic Centre for Drug
Research (LACDR), Leiden
University, Leiden, the
Netherlands

²Department of Soft
Matter Chemistry, Leiden
Institute of Chemistry
(LIC), Leiden University,
Leiden, The Netherlands

³Fine Mechanical
Department, Leiden
institute of Physics (LION),
Leiden University, Leiden,
The Netherlands

Abstract

The aim of this work was to develop a nanolayered pH-sensitive coating method whereby proteins are coated at a suitable pH on the surface of chemically modified biomedical/bioanalytical microdevices and protein release is triggered by a pH-shift upon contact with physiological environment. In this work such a coating was developed and was applied onto microneedles. First, the surface of microneedle arrays was modified with basic groups with a surface pK_a below physiological pH. This modification was a multistep procedure: first the surface was hydroxylated in a piranha mixture, then 3-aminopropyl-triethoxysilane was coupled (yielding a “pH-independent” surface with a positive charge over a broad pH range), next 4-pyridinecarboxaldehyde was coupled to the obtained surface amine groups and finally the imine bond was reduced by sodium cyanoborohydride. The obtained pH-sensitive pyridine-modified microneedles were coated with ovalbumin at surface $pK_a > pH > pI$ of the protein, thus the surface of the microneedles is positively charged and the protein is negatively charged. The coating efficiency of ovalbumin was 95% for the amine-modified (pH-independent) and the pyridine-modified (pH-sensitive) surfaces, whereas a non-modified surface had a coating efficiency of only 2%. After the protein-coated microneedle arrays were pierced into the skin, having a $pH >$ surface pK_a of the microneedle arrays, 70% of the protein was released within 1 minute, whereas the protein release from pH-independent microneedle arrays was only 5%. In conclusion, we developed a procedure to efficiently coat microneedle arrays with proteins that are released upon piercing into human skin.

1. Introduction

Chemical surface modifications by self-assembled layers are applied in a broad range of applications, including biomedical and bioanalytical microdevices for drug delivery and the analysis of biological samples. Here we present a novel coating procedure for microdevices: a nanolayered pH-sensitive coating applied onto microdevices and the subsequent coating thereof with a model protein. The concept of pH-sensitive coating and release is based upon electrostatic interactions between the protein and the surface of the microdevice, whereby a protein is adsorbed to the surface at a suitable pH where the surface of the microdevice is charged. Subsequently, upon contact with physiological environment (pH 7.4) the surface of the microdevice becomes uncharged, causing the electrostatic bond to break and releasing the adsorbed protein.

We apply the pH-sensitive coating technique to microneedles. Microneedles are needle like structures with a size in the micrometer range that are used to deliver drugs *via* the skin. The skin is an attractive organ for drug administration since the skin is an easily accessible organ and drug delivery *via* the skin is potentially pain free. However, the skin barrier located in the uppermost layer of the skin, the stratum corneum, limits drug delivery *via* this route [1, 2]. Therefore, microneedles should be long enough to penetrate the 10-20 μm thick stratum corneum layer, but short enough to avoid pain sensation [1, 3].

Protein delivery into the skin *via* microneedles has been achieved *via* various approaches [1, 3, 4]. Among those microneedles that are used to penetrate the stratum corneum and contain and deliver the drug as a single delivery system are currently of most interest. There are three methods to use microneedles as a single drug delivery system: 1) by using porous microneedles which contain a drug in solution inside the pores, 2) by using dissolving microneedles wherein the drug is encapsulated, and 3) by using drug-coated microneedles [1]. Dissolving microneedles degrade after hydration inside the skin and coated microneedles dissolve their coated layer upon hydration inside the skin. In this paper we focus on the development of coated microneedles.

The major benefit of using coated microneedles is that the coating process can be performed at ambient conditions in an aqueous environment, and that a dry coating may be more stable than a liquid formulation [5-7]. However, most coating procedures require complex coating devices which often do not allow the coating of multiple microneedle arrays simultaneously [6, 8, 9]. Furthermore, coating of microneedles mostly requires a selected set of excipients which 1) reduce the surface tension between the microneedle surface and the coating solution, and 2) increase the viscosity of the coating solution [5, 6, 10]. Another disadvantage of current coating procedures is that there is a relatively high premature drug loss [11]. Finally, most coating procedures require multiple dip-coating steps, often generating thick coatings which negatively influence the sharpness of the needle tip diameter and thereby compromise the penetration ability of these microneedle arrays [8, 9].

Here, a nanolayered pH-sensitive coating was developed and applied onto the surface of microneedle arrays to adsorb a model protein, ovalbumin, which is released into the skin

upon piercing. First, the surface properties of silicon surfaces modified with a weak base, and the isoelectric point of ovalbumin were determined to define the pH range in which ovalbumin can be coated on the surface. Subsequently, the binding and release of ovalbumin from the chemically modified silicon surface and the antigenicity of ovalbumin after release were determined. Finally, after the chemical coating was applied onto the surface of *in-plane* silicon microneedles with a length of 300 μm , which were coated with ovalbumin at optimum pH, the microneedles were assessed for morphology and release of fluorescent- and radioactively labeled ovalbumin in human *in vitro* skin.

2. Experimental

2.1 Materials

Deionized water with a resistivity of 18 $\text{M}\Omega\cdot\text{cm}$, produced by a Millipore water purification system (MQ water), was used for the preparation of solutions and the cleaning of the silicon surfaces. Sulfate-modified polystyrene fluorescent orange (520 nm/540 nm, ex/em) nanoparticles of 100 nm, human serum from human male AB plasma, (3-aminopropyl)triethoxysilane (APTES), ethylenediaminetetraacetic acid (EDTA), NaCl, CaCl_2 , 4-(2-hydroxyethyl)-1-piperazineethanesulfonic acid (HEPES), hydrogen peroxide (30%), 4-pyridinecarboxaldehyde, acetic acid, sodium cyanoborohydride, Triton X-100, Tween-20, and Tween-80 were purchased from Sigma Aldrich. Sulfuric acid 96-98% and acetone were obtained from BOOM lab equipment, and sterile phosphate buffered saline (PBS) was obtained from Braun. Alexa-Fluor® 488 carboxylic acid succinimidyl ester, chicken egg ovalbumin-Alexa-Fluor® 488, and stabilized chromochen 3,3',5,5'-tetramethylbenzidine (TMB) were purchased from Invitrogen, and chicken egg ovalbumin grade VII was purchased from CALBIOCHEM®. Flat bottomed black 96-well plates and MICROLON® ELISA-plates were obtained from Greiner Bio-One, and polystyrene cuvettes (10x4x45 mm) were from Sarstedt. Molecular sieves 4Å 8 to 12 mesh were purchased from Acros Organics, acetonitrile HPLC Far UV was from LAB-SCAN analytical sciences, and methanol HPLC grade, 2-propanol AR, and toluene AR were purchased from BIOSOLVE. Silicon wafers <110> dsp of 0.38 mm thickness, cut in pieces of either 1 by 1 cm or 1 by 2.5 cm, and silicon microneedle arrays with either 9 or 17 microneedles per array with a surface area of 0.3 mm^2 and a length of 300 μm per microneedle were a kind gift of U-needle B.V. Bovine serum albumin (BSA) fraction V was obtained from Roche. Polyclonal mouse anti-ovalbumin antibody was obtained from LifeSpan Biosciences, Inc., Pierce® Iodination beads and Pierce® polyclonal rabbit anti-ovalbumin antibodies conjugated with horseradish peroxidase (HRP) were obtained from Thermo Scientific. Iodine-125 radionuclide, 2 mCi (74 MBq), Specific Activity: ~17 Ci (629 GBq)/mg, 10^{-5} M NaOH (pH 8-11) (Reductant Free), Concentration: 100 mCi/mL was obtained from Perkin-Elmer. Amicon® ultra centrifugal filter units with a molecular weight cut off of 30 kDa were obtained from Millipore™.

2.2 Methods

2.2.1 Generation of a physiologically relevant surface pKa

The modification of silicon surfaces with pyridine is a multistep procedure. The hydroxylation and the generation of amine groups on the surface were performed as previously described [12], in brief: the surface, either of silicon microneedles or silicon slides, was cleaned with acetone and methanol and was subsequently hydroxylated with a freshly prepared piranha mixture (30 v% H₂O₂ and 70 v% H₂SO₄) for 1 h at 80 °C. Then, amine-modified surfaces were formed by incubating the hydroxylated silicon surfaces in 2% (v/v) APTES in toluene for 24 h at room temperature.

The pyridine-modified surfaces were formed in a two-step procedure. First, an imine bond was formed by incubating the amine-modified surface for 16 h in 100 mM 4-pyridinecarboxaldehyde in anhydrous isopropanol with 1% (v/v) acetic acid at room temperature. Subsequently, the pyridine-modified surface was stabilized by reducing the imine bond to a secondary amine in 50 mM NaBH₃CN in isopropanol for 2 h at room temperature. Finally, the modified silicon surfaces were washed with isopropanol (2x) and with methanol (3x), and dried in a vacuum oven at 50°C for 30 minutes. The modified silicon surfaces were stored under argon until used.

2.2.2 Reactivity of modified silicon surfaces with a fluorescent dye

To determine whether pyridine-modified surfaces were successfully synthesized, a fluorescent dye was used which specifically reacts with primary amines. The non-modified, the amine-modified, and the pyridine-modified silicon slides of 1 by 2.5 cm were incubated for 1 h at room temperature in 5 mL 2 µg/mL Alexa Fluor® 488 carboxylic acid succinimidyl ester in acetonitrile. Subsequently, the non-reacted fluorescent dye was removed by washing the silicon slides with acetonitrile (2x) and methanol (5x). Finally, the silicon slides were dried in a vacuum oven at 50°C for 30 minutes and visualized under a fluorescence microscope (Nikon Eclipse E600) with a mercury light source, a magnification of 100x, a GFP filter set, and imaged with a 10 s exposure time.

The pictures were analyzed in ImageJ (available from rsbweb.nih.gov/ij/) with the plugin ‘interactive 3D surface plot’, where the pixel intensity was plotted against the pixel position on the surface. The following settings were used: grid size 128, smoothing 3.0, max. 50%, and min. 4%. The derivatization efficiency of the amine-modified surface into a pyridine-modified surface was determined by equation 1:

$$\text{Derivatization efficiency} = 100 - \left[\frac{(I_m - I_o)}{(I_a - I_o)} \right] * 100 \quad (\text{Equation 1})$$

Here I_m represents the average pixel intensity of the pyridine-modified surface, I_o represents the average pixel intensity of the non-modified surface, and I_a represents the average pixel intensity of the amine-modified surface [12].

2.2.3 Surface analysis by atomic force microscopy

In order to analyze the surface roughness of the coating, non-modified surfaces, pyridine-modified surfaces, and pyridine-modified surfaces coated with ovalbumin were analyzed by atomic force microscopy (AFM) on a Veeco Nanoscope IIIa Multimode AFM in tapping mode with scan size of $1 \mu\text{m}^2$, a scan rate of 1 Hz, and an Si cantilever at 75 kHz. The data was analyzed in Gwyddion software version 2.25 (available from: <http://gwyddion.net/>).

2.2.4 Surface pK_a determination by the fluorescent nanoparticle adhesion assay

The surface pK_a of pyridine-modified silicon surfaces was determined by the fluorescent nanoparticle adhesion assay [12]. This method determines the surface pK_a by using the fraction of nanoparticles that is bound to the surface and the fraction of nanoparticles that is in solution as a function of the pH. Because pyridine is a weak base and gets positively charged when reducing the pH, negatively charged nanoparticles were used.

First, 20 nanoparticle suspensions were prepared, each with a different pH in a range of 2-12, in a 1 mM EDTA buffer with $1 \mu\text{L}$ of 2.5% sulfate-modified fluorescent orange nanoparticles per mL. Subsequently, two aliquots of 0.75 mL nanoparticle suspension were transferred to two 1.5 mL cuvettes for each pH value, wherefrom one cuvette was used as a negative control and the second cuvette was used to be incubated with a 1×1 cm pyridine-modified silicon slide. After the pyridine-modified silicon slides were incubated for 4 hour on a shaking device, two times $200 \mu\text{L}$ of each sample was transferred to a black 96-well plate and the emission at 540 nm was measured with an excitation wavelength of 520 nm on a Tecan Infinite® M1000. Subsequently, the relative fluorescence was calculated for each pH value by dividing the fluorescence of the nanoparticle suspension incubated with a pyridine-modified silicon slide though the fluorescence intensity of a non-incubated sample at the same pH. The binding (100 - relative fluorescence) was plotted as a function of the pH and was fitted in Prism 5 for Windows according to the Henderson-Hasselbalch equation, from which the surface pK_a was determined [12].

2.2.5 Determination of the isoelectric point of ovalbumin

The net charge of a protein plays an important role in its binding to the pyridine-modified silicon surface. Therefore, the isoelectric point (pI) of ovalbumin was determined by measuring the ζ -potential as a function of the pH by laser Doppler electrophoresis on a Zetasizer Nano (Malvern Instruments). The ζ -potential of ovalbumin was determined in a 10 mM phosphate buffer with a pH in the range between 3-6 and an ovalbumin concentration of 1 mg/mL.

2.2.6 Ovalbumin binding to pyridine-modified surfaces

To determine whether proteins are able to bind to the pyridine-modified silicon surfaces, the binding was investigated by using ovalbumin. Therefore, pyridine-modified silicon slides of 1 by 2.5 cm were incubated in 1.5 mL 1 mM EDTA buffer, pH 5.8, with different doses of

ovalbumin (6.25 μg , 12.5 μg , 25 μg , 50 μg , 100 μg , or 250 μg) in 2 mL cuvettes. For all ovalbumin doses the same amount of ovalbumin conjugated with Alexa Fluor® 488 (12.5 μg) was mixed with non-fluorescent ovalbumin, except the 6.25 μg and 12.5 μg dose which were solely fluorescent ovalbumin. As a negative control 25 μg (12.5 μg fluorescently labeled + 12.5 μg native) ovalbumin was incubated with a piranha treated surface in 1.5 mL 1 mM EDTA buffer. The binding of ovalbumin to the pyridine-modified silicon surface was determined by measuring the concentration of non-bound ovalbumin in solution at different time points (1-480 minutes, $n=3$, each dose on a different day) by fluorescence on a Tecan Infinite® M1000 plate reader with an excitation wavelength of 488 nm and an emission wavelength of 522 nm.

2.2.7 Ovalbumin release from pyridine-modified surfaces

In order to examine whether ovalbumin is able to detach from the chemically modified silicon slides different release media were used. Therefore, APTES and pyridine-modified silicon slides of 1 by 2.5 cm were first coated with 25 μg fluorescently labeled ovalbumin and were quantified for ovalbumin adsorption as described above. Then, the silicon slides were transferred into 1.5 mL release media and the released amount ovalbumin was determined by fluorescence at time points between 1 and 60 minutes. The amount of released ovalbumin was divided by the adsorbed ovalbumin to calculate the release percentage. The release from the pyridine-modified silicon slides was assessed in the following release media: 1 mM EDTA pH 5.5 with 1 M NaCl; 5 mM EDTA pH 7.4; 5 mM EDTA pH 9; 1 mM EDTA pH 10; PBS; human serum; 1 mM HEPES pH 5.5 with 1.3 mM CaCl_2 ; 0.1 M HCl; 1 mM EDTA pH 5.5 with 1% Triton X-100. The release of ovalbumin from an amine-modified surface was assessed in 5 mM EDTA buffer at pH 7.4 and 9.0 as a control for a “pH-independent” surface.

2.2.8 Antigenicity of released ovalbumin

The antigenicity of the released ovalbumin from the pyridine-modified surface was investigated by enzyme-linked immunosorbent assay (ELISA). Polyclonal mouse antibody against chicken ovalbumin was 2000x diluted in 0.05 M carbonate buffer at pH 9.6 and coated overnight at 4°C on a 96-well plate for ELISA (100 μL /well). Subsequently, the plate was washed 4 times with washing buffer (0.1x PBS with 0.05% (v/v) Tween 20) and blocked with 100 μL /well 1% (w/v) BSA in PBS for 1 h at 37°C. Then, 100 μL /well of solution with released ovalbumin and a calibration curve of ovalbumin (0.01-50 $\mu\text{g}/\text{mL}$) were prepared in 0.05% Tween 80, 0.5% BSA, 0.5x PBS and were incubated for 1.5 h at 37°. Next, the plate was washed and incubated with 100 μL /well 1000x diluted polyclonal anti-ovalbumin rabbit antibody HRP conjugate for 1 h at 37°C. Subsequently, the plate was washed, 100 μL TMB was added to each well, and after 15 minutes the reaction was stopped by adding 100 μL 2 M H_2SO_4 to each well and the absorbance was measured at 450 nm on a Tecan Infinite® M1000 plate reader. The released amount of ovalbumin (R_{ELISA}) was determined from the ovalbumin ELISA calibration curve. Furthermore, the released amount of ovalbumin of the same samples was determined by the intrinsic fluorescence of ovalbumin ($R_{\text{intr. fluo}}$) at an excitation wavelength of 280 nm and

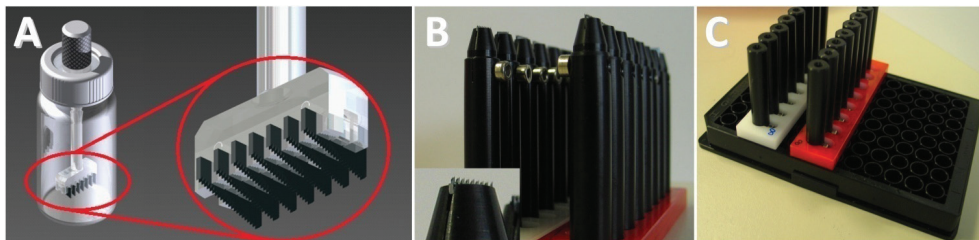


Figure 1: Microneedle coating devices: (A) PCTFE holder loaded with microneedle arrays for applying a chemical coating on the microneedle surface, (B) microneedle arrays mounted in a POM holder, which is also the applicator used to apply the microneedles onto the skin, and (C) microneedle arrays being coated with a protein in a commercially available 96-well plate.

an emission wavelength of 320 nm. Finally, the antigenicity of the released ovalbumin was determined by equation 2:

$$\text{Antigenicity} = [R_{\text{ELISA}}/R_{\text{intr. fluo}}]*100\% \quad (\text{Equation 2})$$

2.2.9 Coating of microneedles

For the assessment of the applicability of microneedles with pH-sensitive surface modifications, the surface of silicon microneedle arrays were modified with APTES or pyridine groups as described above. The *in-plane* microneedle arrays consist of either 9 or 17 microneedles per array with a surface of 0.3 mm² per microneedle, resulting in a total available surface area of respectively 2.7 mm² and 5.1 mm² per array. For chemical modification of the microneedles surface a highly chemical resistant coating device (figure 1A), made of polychlorotrifluoroethylene (PCTFE), was developed by the Fine Mechanical Department, Faculty of Science of Leiden University. After the chemical coating was applied, the microneedles were transferred to a polyoxymethylene (POM) holder (figure 1B), which were also used as an applicator for applying the microneedles onto the skin. The chemically modified microneedle arrays were coated with either 0.5 µg (9 microneedle array) or 1.0 µg (17 microneedle array) ovalbumin in 145 µL 1 mM EDTA at pH 5.8 for 1 h in a commercially available 96-well plate (figure 1C).

The ability to modify the surface of the silicon microneedle arrays with amine groups was assessed by using 10 µg Alexa Fluor® 488 carboxylic acid succinimidyl ester in 2 mL acetonitrile, to modify the amine groups of APTES-coated microneedle arrays. These microneedles were then photographed under a fluorescence microscope with a magnification of 100x, a GFP filter set, and an exposure time of 400 ms.

2.2.10 SEM of microneedles

To analyze the microneedle sharpness and the coating-thickness before and after the different coating procedures, a thin layer of carbon was coated on the microneedles and subsequently analyzed by scanning electron microscopy (SEM) on a FEI NOVA nanoSEM 200.

2.2.11 Fluorescence microscopy and confocal imaging of ovalbumin delivery into *in vitro* human skin

The dermal delivery of ovalbumin by the coated microneedle arrays was assessed on *in vitro* abdominal or mammary human skin, which was obtained from a local hospital within 24 h after cosmetic surgery, and was dermatomed to a thickness of 600 μm using a Padgett Electro Dermatome Model B (Kansas City, MO, USA) after the fat was removed. Pyridine pre-coated microneedle arrays (9 microneedles/array) coated with fluorescently labeled ovalbumin were three times applied on *in vitro* human skin for either 15, 60, or 300 seconds each time, and subsequently the skin was cleaned with MQ water. The ovalbumin-coated microneedle arrays were photographed by fluorescence microscopy (GFP filter set, 100x magnification, exposure time of 5 s) before and after they had pierced the human skin, and the *in vitro* human skin was analyzed by fluorescence microscopy (GFP filter set, 40x magnification, exposure time of 500 μs). Besides, to assess the deepness of the ovalbumin delivery inside *in vitro* human skin confocal laser scanning microscopy (CLSM) was performed with a Bio-Rad Radiance 2100 confocal laser scanning system, equipped with a Nikon Eclipse TE2000-U inverted microscope with either a 4x or 20x Plan Apo lens with an argon laser at 488 nm with a 500 nm long pass emission filter. For controlling the confocal laser scanning system and for image acquisition the Laser Sharp 2000 software (Bio-Rad, Hercules, USA) was used. Images of the conduits created by the microneedles in *in vitro* skin were taken with an xz scan from 0-600 μm , with a depth resolution of 1.05 μm . Furthermore, xyz-images were taken every 10 μm until a depth of 400 μm was reached.

2.2.12 Delivery of radioactively labeled ovalbumin into *in vitro* human skin

To quantify the amount of protein that was delivered into *in vitro* human skin from a “pH-sensitive” and a “pH-independent” surface, we used radioactively labeled ovalbumin to bind to the surface of pyridine-modified and amine-modified microneedles. Therefore, 1 mg ovalbumin in 1 mL PBS was labeled with ^{125}I by incubating it with 4.6 MBq Iodine-125 in the presence of 4 iodination beads, according to the manufacturer’s protocol. Radio-labeled ovalbumin was purified by washing it three times with PBS in a 30 kDa centrifugal filter unit. Subsequently, microneedle arrays with 17 microneedles were coated for 1 h with 1 μg radio-labeled ovalbumin (dissolved in 1 mM EDTA, pH 5.8), which were subsequently air-dried, and were applied on *in vitro* human skin for one minute. The γ -counts of the microneedle arrays before and after penetration, and of the microneedle-pierced skin were measured for 5 minutes on a Perkin Elmer Wallac Wizard 1470 Automatic Gamma Counter.

3. Results

3.1 Surface modification and analysis of flat silicon surfaces and ovalbumin charge

To test whether the silicon surface was successfully modified, we used Alexa Fluor® 488 carboxylic acid succinimidyl ester, a fluorescent dye that only reacts with primary amines. The dye was incubated with a non-modified surface, an amine-modified surface, and an

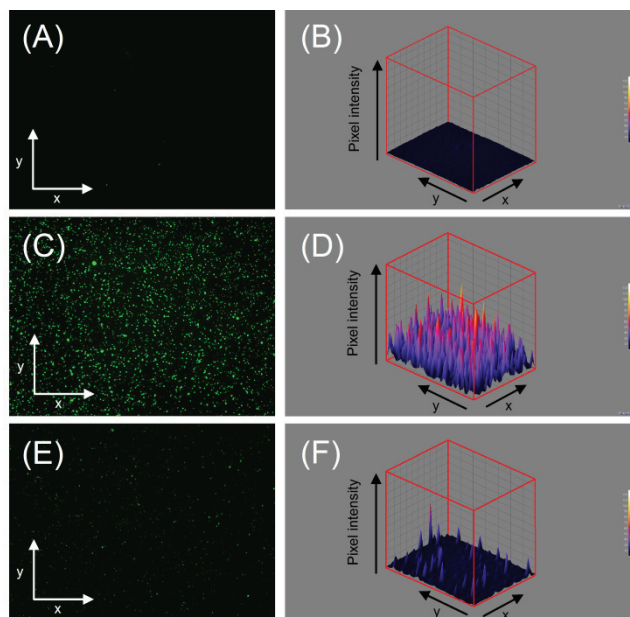


Figure 2: Representative fluorescence microscopy images (0.868 mm²) of (A) a non-modified, (C) an amine-modified, and (E) a pyridine-modified silicon surface incubated with a primary amine reactive fluorescent dye. The corresponding 3D plots of the pixel intensity as a function of the position of the surface are shown on the right side of the image (B, D, F).

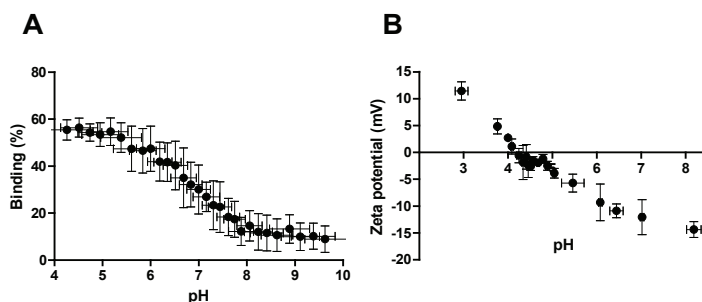


Figure 3: (A) Determination of the surface pK_a of pyridine-modified silicon surfaces by the fluorescent nanoparticle adhesion assay, (B) determination of the isoelectric point of ovalbumin by laser Doppler electrophoresis.

amine-modified surface that was derivatized into a pyridine-modified surface. Subsequently, fluorescence microscopy images of these surfaces were 3D-analyzed by plotting the pixel intensity as a function of the position on the surface, as shown in figure 2. This figure shows that the silicon surfaces were successfully modified with amine groups (2C and 2D vs 2A and 2B) and that these surfaces were subsequently successfully derivatized into pyridine groups (2E and 2F vs 2C and 2D) with an efficiency of $78.5 \pm 4.8\%$ ($n=3$, mean \pm SD) as calculated by equation 1.

Subsequently, the surface pK_a of the pyridine-modified silicon surface and the pI of ovalbumin were determined since both the surface charge of the silicon surface and the charge of the protein as a function of the pH are very important for a protein to bind to a chemically modified ionizable silicon surface. Figure 3A shows the results of a surface pK_a determination of a pyridine-modified silicon surface by the fluorescent nanoparticle adhesion assay, and figure 3B shows the pH-dependent zeta potential of ovalbumin determined by

laser Doppler electrophoresis. The surface pK_a of pyridine-modified surfaces determined by the Henderson-Hasselbalch equation was 6.91 ± 0.30 ($n=3$, mean \pm SD), thus at a $pH < 5.9$ more than 90% of the pyridine-modified surface is positively charged. The zeta potential of ovalbumin was gradually decreasing between pH 3 and 7, and had a pI of 4.36 ± 0.21 ($n=3$, mean \pm SD), thus having a negative charge above that pH value [13, 14]. As protein solubility and stability is minimal at $pH \approx pI$ [15], an optimal adsorption of ovalbumin to pyridine-modified surfaces is expected in a pH range of 5.5 to 6.5.

To determine the surface properties of the non-modified and chemically modified surfaces before and after ovalbumin binding, the surfaces were analyzed by atomic force microscopy [13]. Non-modified surfaces were very flat with an arithmetic average of the 3D roughness of 0.332 ± 0.063 nm. Furthermore, when the surfaces were modified with pyridine groups and subsequently coated with $5 \mu\text{g}/\text{cm}^2$ ovalbumin in 1 mM EDTA at pH 5.8 the arithmetic average of the 3D roughness was 0.925 ± 0.049 nm ($n=3$, mean \pm SD) and 0.627 ± 0.147 nm ($n=3$, mean \pm SD) respectively. This indicates that after chemical modification and after coating with ovalbumin the surface was still very flat and comparable to the 3D roughness of surfaces with similar modifications with APTES described in the literature [12, 13, 16, 17].

3.2 Coating of flat silicon surfaces with ovalbumin

Pyridine-modified surfaces (5 cm^2) were coated with ovalbumin at pH 5.8, a pH value that assures a high positive charge on the pyridine-modified surface (pyridine groups 93% protonated, as calculated by the Henderson-Hasselbalch equation) and is well above ovalbumin's pI resulting in a negative charge for ovalbumin. Different doses of ovalbumin, corresponding to surface densities up to $20 \mu\text{g}/\text{cm}^2$, were coated on the pyridine-modified surfaces, as shown in figure 4A. For each dose of ovalbumin the maximum coating was reached within 2 hours with an average coating efficiency of 95%, which was comparable to ovalbumin coating efficiencies on plain amine-modified silicon surfaces. However, when we incubated a non-modified surface with ovalbumin ($25 \mu\text{g}/5 \text{ cm}^2$) at pH 5.8 for 2 hours, the coating efficiency was only $1.85 \pm 0.93\%$ (mean \pm SD, $n=3$). This shows that chemical modification of the flat silicon surfaces drastically increases protein adsorption.

3.3 Release of ovalbumin from flat silicon surfaces

The release of ovalbumin from a “ pH -sensitive” pyridine-modified surface was assessed under various conditions and was compared to that from a “ pH -independent” amine-modified surface, as shown in figure 4B and 4C. These images show that at pH 5.8, as expected, no ovalbumin was released from a “ pH -sensitive” pyridine-modified surface. However, when the pH was increased to 7.4 or higher, more than 45% of the ovalbumin was released from the pyridine-modified surface. This was 2-3 times as much compared to the release from a “ pH -independent” amine-modified surface at the same pH value, indicating that a “ pH -sensitive” surface promotes the release of ovalbumin. Despite the partial release, we found that ovalbumin did not lose its antigenicity after it was released from the chemically modified

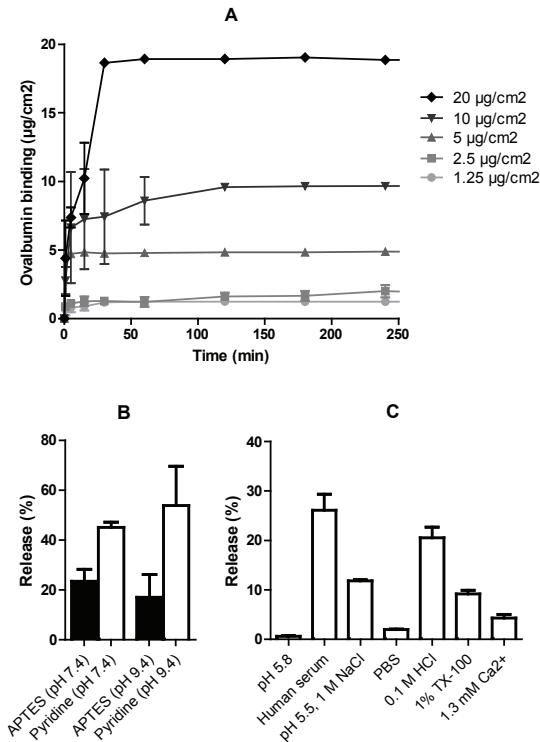


Figure 4: (A) Binding of different amounts of ovalbumin to pyridine-modified surfaces in time at pH 5.8 and (B) comparison between the release of ovalbumin from a 5 µg/cm² ovalbumin-coated “pH-independent” surface (APTES, black bars) and from a “pH-sensitive” surface (pyridine, white bars) at physiological pH (7.4) and at a pH where pyridine groups should be completely uncharged (9.4). Furthermore, (C) the release of ovalbumin from a 5 µg/cm² ovalbumin-coated pH-sensitive surface in physiological relevant release media, human serum and PBS, is shown as well as the release of ovalbumin with different skin components at a pH where no release is expected (pH 5.8). Also the release is shown at a pH value where both ovalbumin and the pH-sensitive surface are positively charged (0.1 M HCl).

surface in 5 mM EDTA at pH 7.4, being 103.0±29.8% (mean ± SD, n=3).

Other components in the skin such as lipids, surfactants, salts and calcium ions could induce the release of ovalbumin from pyridine-modified surfaces. Therefore, the effect of these components was assessed at pH 5.8 where the pH-induced release is minimal. In figure 4C it is shown that a high salt concentration (1 M NaCl), a surfactant (Triton X-100), and Ca²⁺ induced partial release of ovalbumin from the silicon surface (albeit substantially less than at neutral or alkaline pH), indicating that for skin delivery factors other than pH could also play a role. In contradiction to the release of ovalbumin from pyridine-modified surfaces in a 5 mM EDTA buffer at pH 7.4 hardly any ovalbumin was released in PBS at the same pH (2.01±0.07%), which is probably due to crystal formation on the pyridine-modified surfaces when PBS is used (data not shown). Furthermore, when an acidic solution (0.1 M HCl), which has a pH below the pI of ovalbumin, was used to make the pyridine surface as well as ovalbumin positively charged, 20% ovalbumin was released, likely due to repulsive electrostatic forces.

3.4 Application of the chemical modification and coating technology to silicon microneedle arrays

In the previous sections we demonstrated the successful modification and subsequent coating with ovalbumin of flat silicon surfaces. The next step was to apply the pH-sensitive coating on the surface of silicon microneedle arrays. Therefore, we used a specially designed coating device, as shown in figure 1A. To assess the chemical modification of the microneedle

surface, microneedles were first modified with amine groups and subsequently a fluorescent dye was covalently bound (figure 5C). This image shows that the whole surface of the microneedles was fluorescent, indicating that the microneedle surface was successfully modified with amine groups. For generating the pH-sensitive coating on the surface of the microneedles, the amine groups on the microneedles were modified with pyridine in the chemical coating device (figure 1A). Then, for achieving the subsequent protein coating onto the pyridine-modified microneedle surface, the microneedle arrays were mounted in a holder (figure 1B, 1C) to coat them with ovalbumin in a 96-well plate (one array per well). The binding of ovalbumin to the APTES and pyridine-modified microneedles was $18.5 \mu\text{g}/\text{cm}^2$ (comparable to flat chemically modified silicon surfaces), corresponding to $0.50 \mu\text{g}$ and $0.94 \mu\text{g}$ ovalbumin on an array of 9 and 17 microneedles, respectively.

3.5 Release of ovalbumin from microneedles into *in vitro* human skin

To examine the applicability of the coating technology on microneedles *in vitro*, we first investigated the effect of wear time (the time that a microneedle array stays inside the skin) and number of applications of one coated pH-sensitive microneedle array on the release of ovalbumin from the microneedles into the skin. Therefore, pH-sensitive microneedle arrays coated with fluorescently labeled ovalbumin (Alexa Fluor® 488) were applied three times with different wear times between 15 and 300 s on *in vitro* human skin, as shown in figure 5A. We observed that, independent of the wear time, most of the ovalbumin was released after the first application (representative fluorescence microscopy images of a 3×15 s application into *in vitro* human skin, figure 5B). Furthermore, based on the fluorescence of the microneedles before and after skin application we conclude that most of the fluorescently labeled ovalbumin disappeared from the microneedles after a single application into the skin (figure 5D). However, when pH-independent amine-modified microneedle arrays coated with fluorescently labeled ovalbumin were pierced into the skin, hardly any fluorescence was visible in the skin samples (data not shown). Furthermore, these ovalbumin-coated microneedle arrays had about the same fluorescence intensity by fluorescence microscopy before and after they had penetrated the skin (data not shown). These results were confirmed by doing a similar study with radioactively labeled ovalbumin: with our pH-sensitive coating (single application of 60 seconds) we found that $71.2 \pm 10.0\%$ (mean \pm SD, $n=3$) of the ovalbumin was released from the microneedles into *in vitro* human skin. Regarding the coating and release efficiency of ovalbumin from the pH-sensitive coated microneedle arrays, for dermal vaccination a sufficient dose of coated ovalbumin can be delivered by microneedles. However, when we used a “pH-independent” amine-modified surface coating only $4.73 \pm 2.87\%$ (mean \pm SD, $n=3$) of the radioactive ovalbumin was released from the microneedles. These data, combined with the release of ovalbumin from flat silicon chemically modified surfaces, show that pH-triggered release is crucial for effective delivery of ovalbumin into human skin.

Microneedles often require the use of an applicator since microneedles regularly do not penetrate the skin completely upon manual application onto skin [1, 18-20]. Therefore,

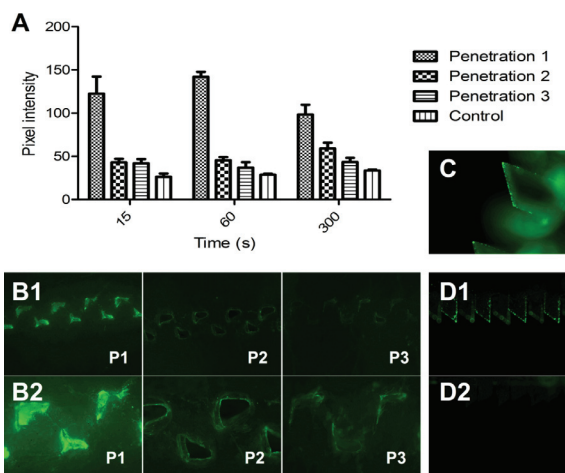


Figure 5: (A) Pyridine-modified microneedles coated with 1 μg fluorescently labeled (Alexa Fluor[®] 488) ovalbumin were applied three times on *in vitro* human skin with three different wear times (15, 60, and 300 seconds). The bars represent the pixel intensity (mean \pm SD, $n=3$) of the fluorescence of the microneedle holes filled with fluorescent ovalbumin and the control represents the background fluorescence of the skin. (B) Representative example of three successive microneedle piercings (P1, P2, P3) with one coated microneedle array in human skin *in vitro*, with a magnification of 40x (B1) and 100x (B2). (C) Microneedles to which a fluorescent dye (Alexa Fluor[®] 488) is covalently coupled to its surface. (D) Ovalbumin-coated microneedle array before skin penetration (D1) and after 3x application for 15 seconds (D2).

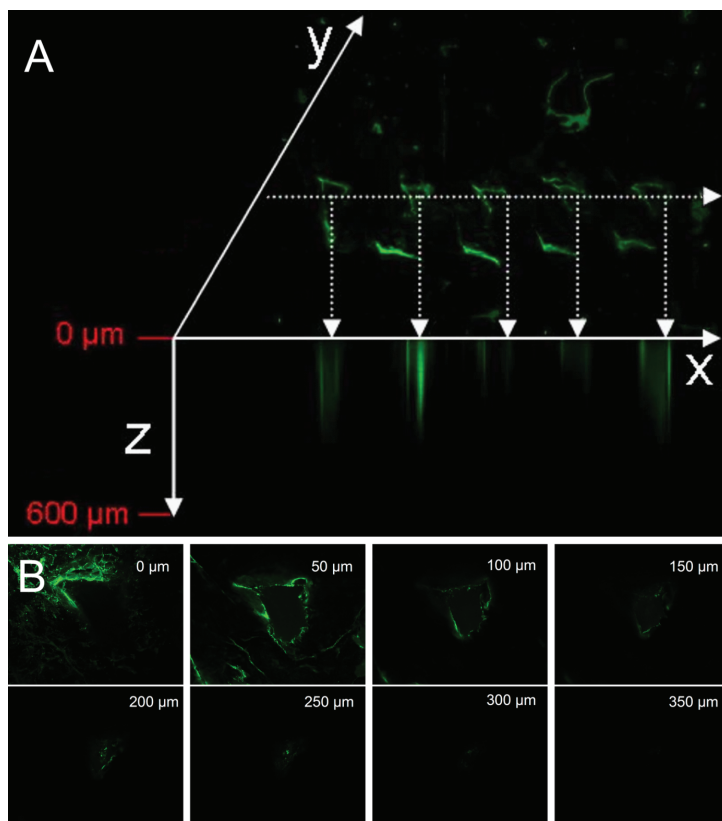


Figure 6: A) Visualization by confocal laser scanning microscopy of ovalbumin delivery by ovalbumin-coated pyridine-modified microneedle arrays. Ovalbumin was fluorescently labeled with Alexa Fluor[®] 488. On the xy-plane the surface of *in vitro* human skin is shown after microneedle penetration (40x magnification, 2980x2384 μm), and on the xz plane an in-depth scan of ovalbumin delivery in the upper row of microneedle penetrations is shown. B) xyz visualization of ovalbumin delivery into a single microchannel in *in vitro* human skin (200x magnification, 596x477 μm).

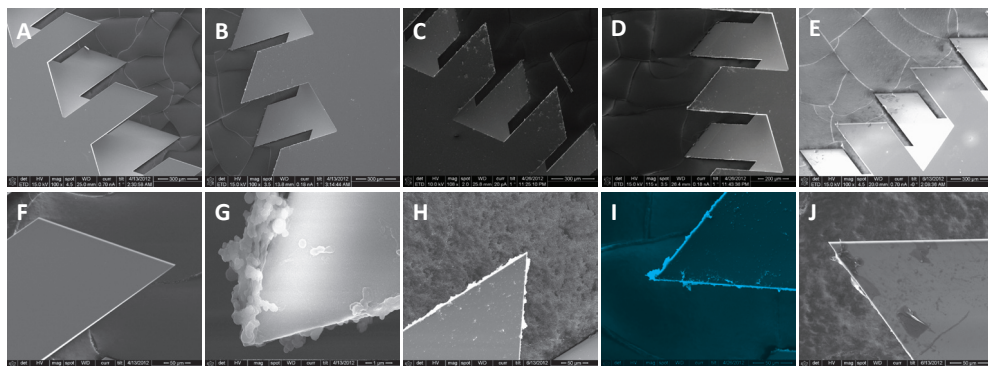


Figure 7: SEM images of (A) a non-modified microneedle array, (B) an amine-modified microneedle array, (C) a pyridine-modified microneedle array, and (D) a pyridine-modified microneedle array coated with ovalbumin before skin penetration and (E) after skin penetration, and (F-J) zoomed in on one of the tips of the microneedle arrays, respectively.

the depth of ovalbumin delivery into *in vitro* human skin was determined by CLSM after the application of ovalbumin-coated pH-sensitive microneedle arrays on human *in vitro* skin using the manual applicator. Furthermore, CLSM was used to visualize the microchannels generated by the pH-sensitive pyridine-modified microneedle arrays coated with ovalbumin. Figure 6A shows an xy-image of the surface of the skin and at the position of the microchannels an in-depth scan was made from the surface of the skin to a depth of 600 μm . Furthermore, xyz-images were made with a magnification of 200x to visualize the ovalbumin delivery into a single microchannel (figure 6B). Of the confocal microscopy images 3D reconstructions of the ovalbumin delivery into the skin were made (movie available online, <http://pubs.rsc.org/en/Content/ArticleLanding/2013/TB/c3tb20786b#!divAbstract>). These images show that there was almost no ovalbumin present on the surface of the skin, but that it was rather delivered into the epidermis and dermis. Furthermore, these images show that ovalbumin was delivered up to 300 μm in depth, indicating that the whole microneedle had pierced the skin.

To determine to what extent the coating changed the structure of the microneedles, the microneedles were visualized by SEM before and after the different coating procedures (shown in figure 7). The tip of non-modified microneedles was very sharp (diameter < 10 nm), and therefore the application of these microneedles by using an applicator for manual piercing was sufficient to penetrate the skin. Also, after the surface of the microneedles was chemically modified with amine groups, pyridine groups, and subsequently coated with ovalbumin, the microneedle tip was still very sharp (diameter < 100 nm). After the coated microneedles were pierced into the skin, the tips of the microneedles were still very sharp (diameter < 100 nm), indicating that the needles stay intact after they had pierced the skin.

4. Discussion

Coated microneedle arrays have great potential for pain free administration of potent biologicals, such as therapeutic proteins and vaccines, *via* the skin [1, 3]. In the design of such devices, it is important to have a high coating efficiency as well as a high release efficiency of the coated drug into the skin in order to minimize the loss of expensive drug. We successfully developed a novel coating procedure which is based upon pH-dependent electrostatic interactions, whereby proteins are efficiently coated onto microneedles and efficiently released from microneedles into the skin.

For initial experiments plain silicon slides were used instead of microneedle arrays, because it is easier and more accurate to measure derivatization and coating efficiencies on a large flat surface than on the small tip of a microneedle.

The coating efficiency of flat silicon surfaces was very high (95%) for coating densities up to 20 $\mu\text{g}/\text{cm}^2$ (figure 4A). Moreover, ovalbumin was successfully released from the pH-sensitive surface in a pH-dependent manner. However, under none of the incubation conditions (figure 4B) ovalbumin release from flat pyridine modified silicon surfaces was complete. One of the reasons is the presence of residual surface charge on the modified surfaces at physiological pH. Although 79% of the surface amine groups were derivatized into pyridine groups (figure 2), still 21% of the primary amine groups are unmodified. About 97% of these primary amine groups will be protonated at physiological pH [12]. Furthermore, pyridine-modified surfaces have a pK_a of 6.91 (figure 3B), meaning that 39.4% of the pyridine groups are charged at physiological pH. Combining these two effects one can calculate that at physiological pH 51% of the ionizable (pyridine and APTES) groups will be protonated and thus can still electrostatically interact with the negatively charged ovalbumin (especially because the negative charge of ovalbumin will be higher at pH 7.4 than at the coating pH of 5.8). Furthermore, these data combined with the low release with 1 M NaCl at pH 5.8 indicates that the release mechanism of ovalbumin from pyridine-modified silicon surfaces was predominantly pH-dependent, rather than ionic strength dependent. Besides, this technology is promising for vaccination since the released ovalbumin from pyridine-modified silicon surfaces did not lose its antigenicity as shown by ELISA. This indicates that the native epitopes of ovalbumin, which are recognized by the ovalbumin specific antibodies, are still intact.

The little release of ovalbumin from “pH-independent” amine-modified flat silicon surfaces (figure 4B) can be explained by the fact that APTES surfaces have two pK_a values (6.55 and 9.94), where the first pK_a accounts for about 25% of the surface charge [12]. This implies that at pH 7.4, only 22% of the APTES surface is deionized. However, a high pH (9.4) of the release medium did not lead to a higher release of ovalbumin from an amine-modified and a pyridine-modified surface, even though at that pH value respectively 42% and 83% of the ionizable surface groups should be uncharged. This may be caused by an increased negative charge of ovalbumin at elevated pH (figure 3A), conformational changes of ovalbumin in the adsorbed state and/or non-electrostatic (e.g., hydrophobic) interactions contributing to adsorption.

Similar to plain silicon surfaces, the surface of microneedle arrays was successfully chemically modified (figure 5C) and coated with ovalbumin (figure 5D1). As determined by SEM, the coating thickness on flat silicon surfaces, including the cutting planes of the microneedles, was very small (< 20 nm) after chemical modification and after ovalbumin coating (figure 7). In addition, coated silicon surfaces retained a very flat surface, as determined by AFM. These results were similar to comparable modifications reported in the literature [12, 13, 16, 17]. Furthermore, the coating thickness at the cutting edges of the microneedles was larger (100-1000 nm) after APTES coupling, indicating that APTES tends to aggregate at the edges of surfaces. However, ovalbumin coating on the pH-sensitive microneedles was much thinner than most coatings reported in the literature, which are generally 3-15 μm thick [8, 10, 11, 18]. Therefore, this nanolayered pH-sensitive coating retains the geometry of the microneedles without compromising their sharpness.

Ovalbumin-coated pH-sensitive microneedles penetrated human skin successfully and delivered the fluorescently labeled ovalbumin up to a depth of 300 μm (figure 6). The major fraction of the fluorescently labeled ovalbumin dose was released from the pH-sensitive coating after a single application for 15 s into human skin (figure 5). This was confirmed by a radioactivity assay demonstrating that the release of ovalbumin from a pH-sensitive microneedle array into *in vitro* human skin was 71% after a single application of 60 s. This delivery efficiency was high compared to that of other coatings described in the literature, which show a release of the active compound varying between 1-91% mostly within 15 minutes, depending on the coating procedure [5, 7, 10, 11, 21-24]. Moreover, a relative high amount of active compound is lost during these coating procedures, in sharp contrast with our novel coating method.

In contrast to the pH-sensitive coating, the pH-independent coating resulted in only 5% release of the ovalbumin from a microneedle array, which shows the necessity of the pH-sensitive coating for the delivery of ovalbumin. Furthermore, the release efficiency of ovalbumin from the microneedle arrays into *in vitro* human skin differed from that of flat silicon surfaces into a buffered solution: the release from a pH-independent microneedle was lower than that from a pH-independent flat surface, and the release from a pH-sensitive microneedle was higher than that from a pH-sensitive flat surface. These differences may be caused to some extent by the analytical method (fluorescence vs. radioactivity) but more importantly to the differences in release medium (the complex environment in human skin, containing lipids, calcium, and proteins, vs. a simple buffered solution), suggesting that pH is not the only factor contributing to the release of ovalbumin into human skin.

Despite the protein ovalbumin showed an excellent binding onto and an excellent release from pyridine-modified silicon microneedles, this approach will not be suitable for each protein. In the case of ovalbumin, the protein bound reversibly onto the surface, but proteins may undergo conformational changes in the adsorbed state, aggregate and/or bind irreversibly onto surfaces, as reviewed by Rabe *et al.* [25]. Furthermore, the packing, loading and the reversibility of protein adsorption is dependent on many factors, including the buffer

composition, ionic strength, pH, temperature, type of protein (e.g. hard/soft), shape of the protein, and the distribution of charge and isoelectric point of the protein [25-27]. Therefore, for some proteins it might be beneficial to encapsulate them into micro/nano-particles prior to microneedle adhesion.

Drug delivery into the skin *via* microneedles is minimally-invasive and potentially pain free and can be achieved *via* several approaches. However, for each approach it is important to minimize the amount of drug loss and to deliver the drug in a reproducible manner and fast (especially for patient compliance in vaccination). Therefore, this novel approach of coating microneedles in a pH-dependent manner has great advantages: the coating and release efficiencies are high, and the major part of the drug is released within 15 s. Furthermore, the pH-sensitive microneedle coating can be combined with a Layer-by-Layer coating, whereby multiple nanolayers are formed by alternate coating of positive and negatively charged polyelectrolytes [28, 29]. Besides, drugs that are encapsulated into micro- or nanoparticles can be coated on the surface of microneedles, thus this pH-sensitive coating procedure has a broad application ability to deliver drugs into the skin by microneedles. Furthermore, the developed microneedle holders for 96-well plates render the coating procedure amenable for high throughput screening of different coating excipients/compounds (figure 1) and the coating procedure can be fully automated.

5. Summary and conclusion

Silicon surfaces were successfully modified with pyridine groups with a high derivatization efficiency of 79%. Because ovalbumin has a *pI* of 4.4 and the pyridine-modified surfaces were shown to have a surface pK_a of 6.9, there is a coating window between pH 5.4-6.8. Pyridine-modified silicon surfaces were coated with ovalbumin at pH 5.8 in a 1 mM EDTA buffer without using further excipients. This led to a high coating efficiency of ovalbumin (> 95%) with a dose up to 20 $\mu\text{g}/\text{cm}^2$ within 2 h coating time. The *in vitro* release of ovalbumin at physiological pH was 45% within the first minute whereby the released protein retained its antigenicity.

Microneedles modified with the pH-sensitive surface modification and subsequently coated with ovalbumin, released the major fraction of ovalbumin after a single application of 15 s into *in vitro* human skin. Furthermore, the microneedle coating minimally affected the microneedle's geometry and sharpness, since the coating on the cutting planes was < 20 nm thick and the tip diameter of the microneedles was < 100 nm after coating.

In conclusion, this nanolayered pH-sensitive coating for microdevices may provide a useful tool for the delivery of potent therapeutic proteins and vaccines.

Acknowledgements

This work was financially supported by program Nano4Vitality of the Ministry of economic affairs and the provinces Gelderland and Overijssel. Furthermore, we acknowledge Jeroen Wissink, U-Needle BV and Niels Tas, University of Twente, Transducer Science and Technology

Department (TST) for the supply of microneedle arrays and slides cut from silicon wafers. K. S. and A. K. acknowledge the financial support of NanonextNL. Also, we acknowledge Dr. Federica Galli for the help with the AFM. Finally, we acknowledge Prof. Dr. J. Kuiper and R. J. v.d. Sluis of the Division of Biopharmaceutics, LACDR, Leiden University, for their help with the radioactive assays.

References

- [1] K. van der Maaden, W. Jiskoot, J. Bouwstra, Microneedle technologies for (trans)dermal drug and vaccine delivery. *Journal of controlled release* 161 (2012) 645–655.
- [2] M.R. Prausnitz, R. Langer, Transdermal drug delivery. *Nature Biotechnology* 26 (2008) 1261–1268
- [3] S.M. Bal, Z. Ding, E. van Riet, W. Jiskoot, J. Bouwstra, Advances in transcutaneous vaccine delivery: do all ways lead to Rome? *Journal of Controlled Release* 148 (2010) 266–282.
- [4] M.R. Prausnitz, H.S. Gill, J.-H. Park, *Modified Release Drug Delivery*, Vol. 2nd ed New York: Healthcare, 2008, pp. 295–309.
- [5] H.S. Gill, M.R. Prausnitz, Coating formulations for microneedles. *Pharmaceutical Research* 24 (2007) 1369–1380.
- [6] H.S. Gill, M.R. Prausnitz, Coated microneedles for transdermal delivery. *Journal of Controlled Release* 117 (2007) 227–237.
- [7] X. Chen, G.J.P. Fernando, M.L. Crichton, C. Flaim, S.R. Yukiko, E.J. Fairmaid, H.J. Corbett, C.A. Primiero, A.B. Ansaldo, I.H. Frazer, L.E. Brown, M.A.F. Kendall, Improving the reach of vaccines to low-resource regions, with a needle-free vaccine delivery device and long-term thermostabilization. *Journal of Controlled Release* 152 (2011) 349–355.
- [8] X. Chen, T.W. Prow, M.L. Crichton, D.W.K. Jenkins, M.S. Roberts, I.H. Frazer, G.J.P. Fernando, M.A.F. Kendall, Dry-coated microprojection array patches for targeted delivery of immunotherapeutics to the skin. *Journal of Controlled Release* 139 (2009) 212–220.
- [9] M. Ameri, P.E. Daddona, Y.-F. Maa, Demonstrated Solid-State Stability of Parathyroid Hormone PTH(1–34) Coated on a Novel Transdermal Microprojection Delivery System. *Pharmaceutical Research* 26 (2009) 2454–2463.
- [10] M. Cormier, B. Johnson, M. Ameri, K. Nyam, L. Libiran, D.D. Zhang, P. Daddona, Transdermal delivery of desmopressin using a coated microneedle array patch system. *Journal of Controlled Release* 97 (2004) 503–511.
- [11] J.A. Matriano, M. Cormier, J. Johnson, W.A. Young, M. Buttery, K. Nyam, P.E. Daddona, Macroflux microprojection array patch technology: a new and efficient approach for intracutaneous immunization. *Pharmaceutical Research* 19 (2002) 63–70.
- [12] K. van der Maaden, K. Sliedregt, A. Kros, W. Jiskoot, J. Bouwstra, Fluorescent Nanoparticle Adhesion Assay: a Novel Method for Surface pKa Determination of Self-Assembled Monolayers on Silicon Surfaces. *Langmuir* 28 (2012) 3403–3411.
- [13] J. Chesko, J. Kazzaz, M. Ugozzoli, D.T. O’Hagan, M. Singh, An investigation of the factors controlling the adsorption of protein antigens to anionic PLG microparticles. *Journal of Pharmaceutical Sciences* 94 (2005) 2510–2519.
- [14] G.L. Morefield, D. Jiang, I.Z. Romero-Mendez, R.L. Geahlen, H. HogenEsch, S.L. Hem, Effect of phosphorylation of ovalbumin on adsorption by aluminum-containing adjuvants and elution upon exposure to interstitial fluid. *Vaccine* 23 (2005) 1502–1506.
- [15] M.R.H. Krebs, G.L. Devlin, A.M. Donald, Protein Particulates: Another Generic Form of Protein Aggregation? *Biophysical Journal* 92 (2007) 1336–1342.
- [16] J. Kim, J. Cho, P.M. Seidler, N.E. Kurland, V.K. Yadavalli, Investigations of Chemical Modifications of Amino-Terminated Organic Films on Silicon Substrates and Controlled Protein Immobilization. *Langmuir* 26 (2010) 2599–2608.
- [17] J.A. Howarter, J.P. Youngblood, Optimization of Silica Silanization by 3-Aminopropyltriethoxysilane. *Langmuir* 22 (2006) 11142–11147.
- [18] M. Pearton, V. Saller, S.A. Coulman, C. Gateley, A.V. Anstey, V. Zarnitsyn, J.C. Birchall, Microneedle delivery of plasmid DNA to living human skin: Formulation coating, skin insertion and gene expression. *Journal of controlled release* 160 (2012) 561–569.
- [19] F.J. Verbaan, S.M. Bal, D.J. van den Berg, J.A. Dijkman, M.v. Hecke, H. Verpoorten, A. van den Berg, R. Lutttge, J.A. Bouwstra, Improved piercing of microneedle arrays in dermatomed human skin by an impact insertion method. *Journal of Controlled Release* 128 (2008) 80–88.
- [20] R.F. Donnelly, R. Majithiya, T.R.R. Singh, D.I.J. Morrow, M.J. Garland, Y.K. Demir, K. Migalska, E. Ryan, D. Gillen, C.J. Scott, A.D. Woolfson, Design, optimization and characterisation of polymeric microneedle arrays prepared by a novel laser-based micromoulding technique. *Pharmaceutical Research* 28 (2011) 41–57.
- [21] M.L. Crichton, A. Ansaldo, X. Chen, T.W. Prow, G.J.P. Fernando, M.A.F. Kendall, The effect of strain rate on the precision of penetration of short densely packed microprojection array patches coated with vaccine. *Biomaterials* 31 (2010) 4562–4572.
- [22] G. Widera, J. Johnson, L. Kim, L. Libiran, K. Nyam, P.E. Daddona, M. Cormier, Effect of delivery

parameters on immunization to ovalbumin following intracutaneous administration by a coated microneedle array patch systemaa. *Vaccine* 24 (2006) 1653-1664.

[23] A.K. Andrianov, D.P. DeCollibus, H.A. Gillis, H.H. Kha, A. Marin, M.R. Prausnitz, L.A. Babiuk, H. Townsend, G. Mutwiri, Poly[di(carboxylatophenoxy) phosphazene] is a potent adjuvant for intradermal immunization. *Proc Natl Acad Sci U S A* 106 (2009) 18936–18941.

[24] A.K. Andrianov, A. Marin, D.P. DeCollibus, Microneedles with Intrinsic Immunoadjuvant Properties: Microfabrication, Protein Stability, and Modulated Release. *Pharmaceutical Research* 28 (2011) 58–65.

[25] M. Rabe, D. Verdes, S. Seeger, Understanding protein adsorption phenomena at solid surfaces. *advances in Colloid and Interface Science* 162 (2011) 87-106.

[26] W. Norde, J. Lyklema, Interfacial behaviour of proteins, with special reference to immunoglobulins. A physicochemical study. *Advances in Colloid and Interface Science* 179-182 (2012) 5-13.

[27] C. Pinholt, R.A. Hartvig, N.J. Medlicott, L. Jorgensen, The importance of interfaces in protein drug delivery -- why is protein adsorption of interest in pharmaceutical formulations? *Expert Opinion Drug Delivery* 8 (2011) 949-964.

[28] P.C. DeMuth, X. Su, R.E. Samuel, P.T. Hammond, D.J. Irvine, Nano-Layered Microneedles for Transcutaneous Delivery of Polymer Nanoparticles and Plasmid DNA. *Adv Mater* 22 (2010) 4851-4856.

[29] E.M. Saurer, R.M. Flessner, S.P. Sullivan, M.R. Prausnitz, D.M. Lynn, Layer-by-Layer Assembly of DNA- and Protein-Containing Films on Microneedles for Drug Delivery to the Skin. *Biomacromolecules* 11 (2010) 3136-3143.

OVALBUMIN-COATED pH-SENSITIVE MICRONEEDLE ARRAYS EFFECTIVELY INDUCE OVALBUMIN-SPECIFIC ANTIBODY AND T-CELL RESPONSES IN MICE

Koen van der Maaden¹
Eleni Maria Varypataki^{1,2}
Stefan Romeijn¹
Ferry Ossendorp²
Wim Jiskoot¹
Joke Bouwstra¹

[European Journal of
Pharmaceutics and
Biopharmaceutics, in press
\(2014\)](#)

¹Division of Drug Delivery
Technology, Leiden
Academic Centre for Drug
Research (LACDR), Leiden
University

²Department of
Immunohematology and
Blood Transfusion, Leiden
University Medical Center,
Leiden, the Netherlands

Abstract

The aim of this work was to study the applicability of antigen-coated pH-sensitive microneedle arrays for effective vaccination strategies. Therefore, a model antigen (ovalbumin) was coated onto pH-sensitive (pyridine-modified) microneedle arrays to test pH-triggered antigen release by applying the coated arrays onto *ex vivo* human skin, and by conducting a dermal immunization study in mice.

The release of antigen into *ex vivo* human skin from the coated microneedles was determined by using radioactively labeled ovalbumin. To investigate the induction of antigen-specific IgG, and CD4⁺ and CD8⁺ T-cell responses, BALB/c mice were immunized with antigen-coated pH-sensitive microneedles by the ‘coat and poke’ approach. These responses were compared to responses induced by the ‘poke and patch’ approach, and subcutaneous and intradermal vaccination with classic hypodermic needles.

The pH-sensitive microneedle arrays were efficiently coated with ovalbumin (95% coating efficiency) and upon application of six microneedle arrays 4.27 of 7 µg ovalbumin was delivered into the skin, showing a release efficiency of 70%. In contrast, the ‘poke and patch’ approach led to a delivery of only 6.91 of 100 µg ovalbumin (7% delivery efficiency). Immunization by means of ovalbumin-coated microneedles resulted in robust CD4⁺ and CD8⁺ T-cell responses comparable to those obtained after subcutaneous or intradermal immunization with conventional needles. Moreover, it effectively induced IgG responses, however, it required prime-boost immunizations before antibodies were produced.

In conclusion, antigen delivery into *ex vivo* human skin by antigen-coated pH-sensitive microneedle arrays is more efficient than the ‘poke-and-patch’ approach and *in vivo* vaccination studies show the applicability of pH-sensitive microneedles for the induction of both T cell and B cell responses.

1. Introduction

Vaccination is one of the most cost-effective and successful approaches to prevent infectious diseases by preventing approximately 6 million deaths per year [1]. Besides vaccination against infectious diseases, therapeutic vaccines, such as anti-cancer vaccines, are being developed [2-4]. Despite the benefits of vaccination campaigns, however, vaccination does not always induce adequate immune responses [3-5]. Furthermore, subcutaneous or intramuscular vaccination requires medical personnel and causes pain, fear and stress in children and their parents [6-8]. To overcome these disadvantages, the use of microneedles for dermal vaccine delivery has been proposed [6, 8-10]. Moreover, dermal vaccine delivery has dose-sparing potential because the skin is a potent immune organ [6, 8].

Microneedles are micron-sized structures with a length of < 1 mm, which are used to deliver a drug or vaccine into the skin in a minimally-invasive manner. In general, microneedles can be used by four different approaches to deliver a drug into the skin, as reviewed elsewhere [6, 8]. In this study we compare two microneedle approaches for effective vaccine delivery. In the ‘poke and patch’ approach, microneedles are used to pierce the stratum corneum to create micropores. Subsequently, a patch with a vaccine formulation is applied onto the micropores for the vaccine to diffuse into the skin. By the ‘coat and poke’ approach, the microneedle surface is first coated with a vaccine that is subsequently released upon piercing of the skin.

Vaccine delivery by the ‘poke and patch’ approach is technically simpler than by using coated microneedles, since microneedle pretreatment does not require the development of a coating wherein the antigen’s integrity is retained. However, the ‘poke and patch’ approach involves a two-step delivery, i.e., first the skin is pierced and then a patch is applied on the site of microneedle application. In contrast, coated microneedles are a single-unit drug delivery system [6]. By the ‘poke and patch’ approach a relatively high dose of vaccine can be applied, but the patch must to be worn for a relatively long time (> 2 h) to deliver a generally low percentage of the vaccine into the skin [11-14]. In contrast, coated microneedles can be developed in such a way that the vaccine is delivered within minutes with a high delivery efficiency up to 30-70% [15-17], but microneedles can only be coated with a limited amount of vaccine [6, 15]. However, coated microneedles have the potential of dose sparing compared to the ‘poke and patch’ approach provided that the coating and the release are very effective [6, 11, 15].

As previously reported, pH-sensitive microneedles offer an easy and effective way to coat a microneedle array with a protein that is released into the skin upon application [15]. In this work the surface of microneedles is modified with a weak base to obtain its pH-sensitivity. Subsequently, microneedles are coated at a pH value where the vaccine is negatively charged, thus above its isoelectric point, and the microneedle surface is positively charged, thus below the surface pK_a . In this study we investigate the applicability of pH-sensitive microneedles for vaccination purposes by using ovalbumin as a model antigen. We compare the ‘coat and poke’ approach with the ‘poke and patch’ approach, subcutaneous and intradermal injections for the induction of IgG, and CD4⁺ and CD8⁺ T-cell responses.

2. Materials and methods

2.1 Mice

Female BALB/c mice (H2^d) were obtained from Charles River (Maastricht, the Netherlands), which were maintained under standardized conditions in the animal facility of the Leiden Academic Centre for Drug Research, Leiden University. The mice were 8 weeks old at the start of the vaccination study and the study was carried out under the guidelines complied by the animal ethic committee of the Netherlands, and was approved by the 'Dierexperimentencommissie Universiteit Leiden (UDEEC)' under number 13065.

2.2 Generation of pH-sensitive microneedles and the coating thereof with ovalbumin

In this study *in-plane* silicon microneedle arrays, each containing 17 microneedles per array with a microneedle length of 300 μm , as shown in figure 1, were used. The arrays, which were kindly provided by U-Needle B.V. (Enschede, the Netherlands), had a configuration of 8 microneedles on the front and 9 on the back. In order to generate pH-sensitive microneedles, their surface was first modified with amine groups that were subsequently derivatized into pyridine groups, a weak base with a surface $\text{p}K_{\text{a}} \approx 6.9$, as reported previously [15, 18]. Finally, pH-sensitive microneedles were coated with ovalbumin grade VII (CALBIOCHEM®) in a 96-well plate by incubating the arrays for 2 hours in a 1 mM EDTA buffer at pH 5.8 with 10 $\mu\text{g}/\text{mL}$ ovalbumin; this resulted in the coating of the surface of the 17 microneedles with in total 1 μg ovalbumin [15].

2.3 Human skin

Abdomen *ex vivo* human skin was obtained from local hospitals within 24 hours after cosmetic surgery and was dermatomed to a thickness of 600 μm .

2.4 Microneedle application

Microneedle arrays in this study were applied by two different approaches: the 'coat and poke' and the 'poke and patch' approach. For the 'coat and poke' approach, each pH-sensitive microneedle array was coated with 1 μg ovalbumin and was subsequently pierced into the skin. After one minute the microneedle array was removed from the skin. For the 'poke and patch' approach, one uncoated microneedle array was used to pierce the skin and subsequently a patch with 70 μL phosphate buffered saline (PBS) (163.9 mM Na⁺, 140.3 mM Cl⁻, 8.7 mM HPO₄²⁻, and H₂PO₄⁻; pH 7.4) containing 100 μg ovalbumin was applied on the site of microneedle application for two hours. After dermal ovalbumin delivery by microneedles, the skin was extensively washed: *ex vivo* human skin was washed twice with a cotton swap soaked in PBS and tape-stripped (Scotch tape) twice; *in vivo* mouse skin was washed with lukewarm tap water.

2.5 Delivery of ovalbumin into *ex vivo* human skin

To determine the amount ovalbumin that was delivered into dermatomed (600 μm) *ex*

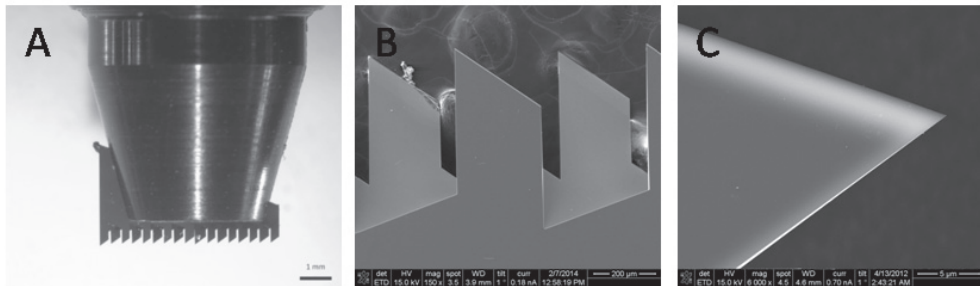


Figure 1: *In-plane* silicon microneedle array mounted in a specially designed holder and photographed under a stereo microscope (0.8x magnification) (A), electron micrograph of a microneedle array (150x magnification) (B) and zoomed in on the tip of a single microneedle (6000x magnification) (C).

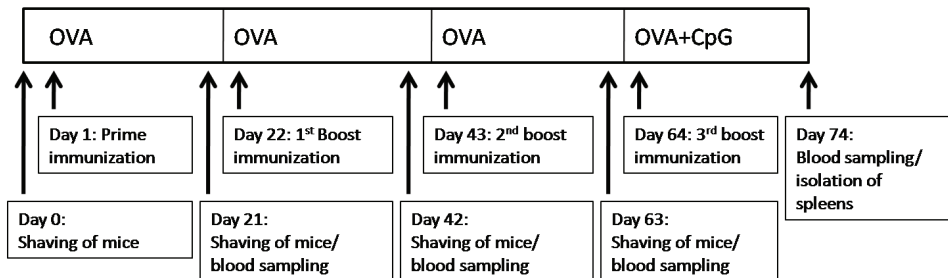


Figure 2: Immunization scheme of mice

vivo human skin by the ‘coat and poke’ and the ‘poke and patch’ approach, a calibration curve (1 ng - 50 µg) was prepared of radioactively labeled ovalbumin (¹²⁵I) [15]. The γ-counts of the samples were measured for 1 minute on a Perkin Elmer Wallac Wizard 1470 Automatic Gamma Counter.

2.6 Immunizations

Mice were immunized according to figure 2. One day prior to each immunization, the abdominal ventral skin of the mice was shaved. Prior to microneedle treatment mice were anesthetized with 150 mg/kg ketamine and 10 mg/kg xylazine. Mice were immunized thrice with ovalbumin (day 1, 22, and 43) and once with ovalbumin adjuvanted with CpG (ODN1826) (day 64). To determine the ovalbumin-specific IgG responses the sera of immunized mice were collected on day 21, 42, 63, and 74. Besides, spleens were collected on day 74 to assess the induction of ovalbumin-specific CD4⁺ and CD8⁺ T-cell responses.

For the ‘coat and poke’ approach mice were immunized with 6 microneedle arrays/mouse and for the ‘poke and patch’ approach mice received a patch with ovalbumin or PBS after the skin was poked with one microneedle array (8 mice/group). Mice that were immunized by subcutaneous or intradermal injection (5 mice/group) received 5 µg ovalbumin in 100 µL and 30 µL PBS, respectively.

At the fourth immunization (day 64), mice received ovalbumin adjuvanted with CpG (5 mice/group) to induce antigen-specific T-cells. Prior to application of an ovalbumin-coated microneedle array, a drop of 5 μ L containing 5 μ g CpG was applied onto the mouse skin through which one coated microneedle array was applied. Each mouse in the coated microneedle group was treated with six microneedle arrays per immunization. Furthermore, 200 μ g CpG was added to the patch formulation of mice that were immunized by the 'poke and patch' approach. Finally, 10 μ g CpG was added to the formulations that were injected subcutaneously or intradermally.

2.7 Analysis of the sera for ovalbumin-specific IgG responses

Ovalbumin specific antibodies were determined by a sandwich ELISA, as described previously [19]. Antibody titers were expressed as the log value of the serum dilution at the mid-point of a complete S-shaped absorbance-dilution curve. Non responders were given an arbitrary titer of 1.

2.8 Analysis of splenocytes for ovalbumin specific CD4⁺ responses

Antigen-specific CD4⁺ and CD8⁺ T-cell activation was determined by measuring endogenous splenic CD4⁺/CD8⁺ CD69⁺ T-cells 10 days after the last immunization. In brief, splenocyte suspensions were prepared from spleens that were aseptically removed. To remove the erythrocytes, 2 mL of lysis buffer (150 mM NH₄Cl, 10 mM KHCO₃, 1 mM EDTA-2Na, pH 7.2) was added to the splenocyte suspensions. After 2 minutes the cells were washed and resuspended in Iscove's modified Dulbecco's medium (IMDM) (Invitrogen Life Technologies) supplemented with 8% (v/v) fetal calf serum (Greiner Bioscience), 50 μ M 2-mercaptoethanol, 2 mM glutamine, 100 IU/ml penicillin, to a concentration of 25*10⁶ cells/mL. Next, of each splenocyte suspension two times 2.5*10⁶ cells were transferred to a round bottom 96-well plate in a volume of 200 μ L, one of which was incubated with 10 μ g/mL ovalbumin [20]. After both splenocyte suspensions were incubated overnight at 37°C with 5% CO₂, the cells were labeled for flow cytometric analysis in PBS/ 0.1% bovine serum albumin. The following antibodies were used: 7-AAD (1:500) (Life Technologies); CD3_{V500} (1:100) (BD Biosciences); CD4_{Qdot605} (1:1000), CD8 α _{Alexafluor700} (1:200), and CD69_{FITC} (1:100) (eBiosciences). For the compensation of CD69_{FITC}, CD3_{FITC} was used. Of each splenocyte suspension 1*10⁶ cells were analyzed by flow cytometry on a LSR-II (BD™). Prior to the flow cytometric measurements, the different colors were auto-compensated in the BD FACSDiva™ software. The gating/analysis was performed in FowJo v10 (Supplemental Information). Finally, the percentage ovalbumin-specific endogenous CD4⁺/CD8⁺ T-cells was calculated from the difference in percentage CD4⁺/CD8⁺ CD69⁺ T-cells incubated with and without ovalbumin.

2.9 Statistical analysis

Statistical analysis was performed by using Prism 5 for Windows. For the ovalbumin-specific IgG titers and endogenous ovalbumin-specific CD4⁺ and CD8⁺ T-cell responses the

mean \pm SEM were calculated, and the statistical significance was determined by a two-way ANOVA for the IgG titers and a one-way ANOVA for the CD4⁺ and CD8⁺ T-cell responses, both with a Bonferroni post test.

3. Results and discussion

3.1 Delivery of protein antigen

As reported previously, silicon microneedle arrays of which the surface is modified with pH-sensitive groups offer a fast, easy and effective approach to deliver protein drugs, such as antigens, into the skin. In our previous study we have shown that positively charged pH-sensitive microneedle arrays are coated with 1 μ g ovalbumin with a coating efficiency of 95% [15]. The amount of ovalbumin that is delivered with syringes by using conventional hypodermic needles is very controlled. However, the amount of ovalbumin that is delivered into the skin by using the ‘coat and poke’ approach or the ‘poke and patch’ approach is not known. Therefore, radioactively labeled ovalbumin was used to quantify the dermal delivery of ovalbumin by microneedles, and the results are summarized in table 1. This table shows that the delivery efficiency of ovalbumin by pH-sensitive microneedles is about 10-fold higher compared to ovalbumin delivery by the ‘poke and patch’ approach. However, the delivery efficiency of ovalbumin *via* the ‘poke and patch’ approach can be enhanced by increasing the microneedle length and the time that the patch is applied. It has been reported that delivering plain ovalbumin by the ‘poke and patch’ approach with 200, 500, and 1000 μ m long microneedles lead to a delivery of 5%, 12%, and 23% after 24 hours, respectively [14]. In conclusion, in our settings using antigen-coated pH-sensitive microneedle arrays requires a 10 fold lower amount of antigen to deliver the same dose into the skin as compared to the ‘poke and patch’.

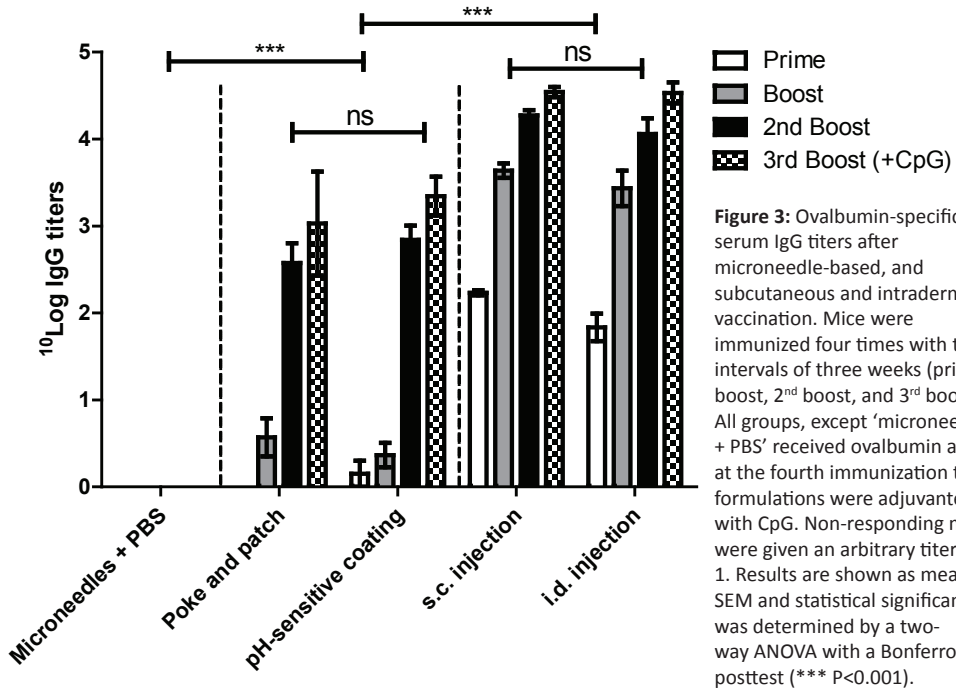
3.2 Ovalbumin-specific antibody responses in mice

In order to test the applicability of the pH-sensitive coating for vaccination purposes, immunization by using ovalbumin-coated pH-sensitive microneedles was compared to immunization by ovalbumin delivered *via* the ‘poke and patch’ approach, and *via* subcutaneous and intradermal injection by using conventional needles. The ovalbumin-specific serum IgG responses are shown in figure 3. The estimated dose of ovalbumin that is delivered by

Table 1: The delivery of radioactively labeled ovalbumin into *ex vivo* human skin by the ‘coat and poke’ and the ‘poke and patch’ approach.

	Ovalbumin used (μ g)	Ovalbumin coated (μ g)	Ovalbumin delivery (μ g)	Delivery efficiency (%)
‘Coat and poke’ (pH-sensitive)	6	5.7 [15]	4.27 \pm 0.60	70
‘Poke and patch’	100	Not applicable	6.91 \pm 1.52	7

Ovalbumin-specific IgG responses



microneedles into mice was based upon the delivery into *ex vivo* human skin.

As expected, mice mock-treated with PBS did not show detectable ovalbumin-specific IgG antibody levels. Comparing the microneedle groups that received ovalbumin, after the prime 1 out of 8 mice induced ovalbumin-specific antibody responses upon microneedle treatment in the pH-sensitive microneedle group and none in the 'poke and patch' group. After the first boost immunization all groups that received ovalbumin showed comparable ovalbumin-specific IgG responses, however, the number of responders was different: in the 'poke and patch' group 5 out of 8 and in the pH-sensitive microneedle group 4 out of 8 mice responded. Finally, all mice that received ovalbumin showed ovalbumin-specific IgG responses after the 2nd and 3rd boost immunization. The ovalbumin-specific IgG titers of the mice that received similar amounts (ca 4-7 µg) of ovalbumin by the 'poke and patch' approach or by ovalbumin-coated pH-sensitive microneedles were comparable.

In contrast to ovalbumin delivery by microneedles, all mice that were subcutaneously or intradermally injected with ovalbumin already produced ovalbumin-specific IgG antibodies after the prime immunization. Furthermore, the IgG titers of the mice that were immunized by using hypodermic needles were 10 times higher. However, immunization with microneedles can lead to antibody responses with titers comparable to conventional injections, although

the induction time is longer and requires more successive immunizations with the 17 microneedle arrays with a length of 300 μm .

There have been several studies reported using microneedle-based immunization of ovalbumin with contradicting results. For example, Chen *et al.* (2013) showed that rats immunized with 1 mg ovalbumin by using dissolving microneedles with a length of 600 μm gave higher ovalbumin-specific IgG levels compared to intramuscular immunization [21]. Raphael *et al.* showed that immunizing mice with 7.6 μg ovalbumin adjuvanted with Quil-A by using 92 μm long dissolving microneedles led to comparable ovalbumin-specific IgG titers as intramuscular immunization with 15 μg ovalbumin adjuvanted with Quil-A 28 days after immunization. However, 102 days after immunization the ovalbumin-specific IgG responses were higher after microneedle-based immunization than after intramuscular immunization [22]. Guo *et al.* showed that mice immunized with 2 μg ovalbumin by using dissolving microneedles with a length of 550 μm led to comparable ovalbumin-specific IgG titers compared to intramuscular immunization [23]. Importantly, it has been shown that the microneedle length greatly influences the ovalbumin-specific IgG responses in rats and mice, e.g., 800-1000 μm long microneedles induced stronger IgG responses than 200-500 μm long microneedles [14, 24], but the former ones are more likely to induce pain [8]. Finally, Kumar *et al.* showed that by applying the 'poke and patch' approach immunization with 10.5 μg ovalbumin nanoparticles resulted in slightly, but not significantly, lower IgG responses compared to subcutaneous immunization with the same dose. However, a dose of 70 μg ovalbumin led to significantly lower ovalbumin-specific IgG responses compared to subcutaneous immunization [14]. In conclusion, microneedle-based vaccination with ovalbumin by using 300 μm long microneedles resulted in robust antibody responses, although lower than conventional injection, with 100% seroconversion and is likely pain-free upon application [8].

3.3 Ovalbumin-specific T-cell responses in mice

After the 3rd boost immunization endogenous ovalbumin-specific CD4⁺ and CD8⁺ T-cell responses were evaluated by determining the upregulated expression of the activation marker CD69 on splenic CD4⁺ and CD8⁺ T-cells [20, 25, 26]. The percentage ovalbumin-specific CD4⁺ and CD8⁺ T-cells was calculated by subtracting the background signal from the percentage ovalbumin-incubated CD69⁺ cells (as shown in supplemental information S12). Figure 4 shows that the percentages of ovalbumin-specific CD4⁺ (4A) and CD8⁺ (4B) T-cells in mice that received ovalbumin were significantly higher ($p < 0.01$) than those in PBS treated (naive) mice. Furthermore, a trend was observed towards higher percentages of ovalbumin-specific CD4⁺ and CD8⁺ T-cells upon ovalbumin delivery by pH-sensitive microneedles compared to ovalbumin delivery by the 'poke and patch' approach, but the differences were not statistically significant. Moreover, immunization by using microneedles and by subcutaneous or intradermal immunization led to comparable percentages of ovalbumin-specific CD4⁺ and

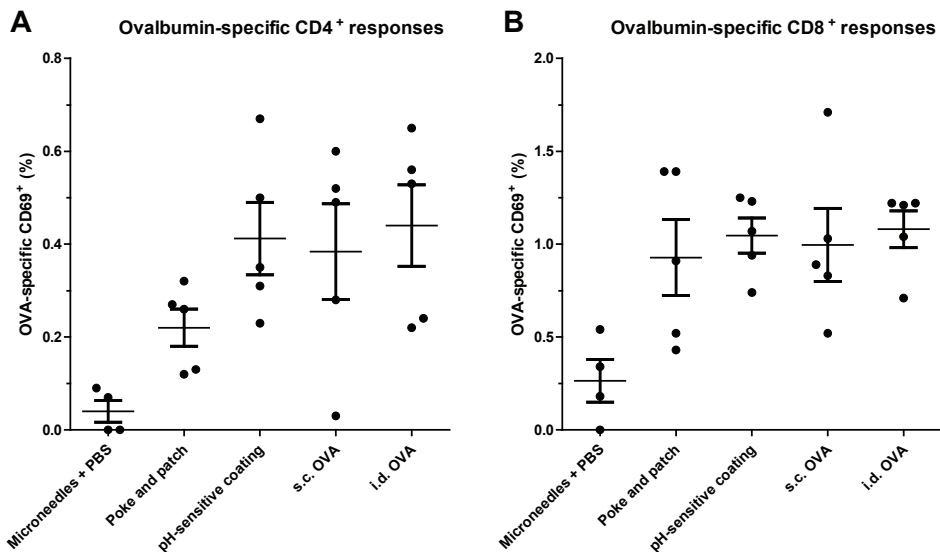


Figure 4: Endogenous ovalbumin-specific CD4⁺ (A) and CD8⁺ (B) T-cells calculated by the difference between CD69 expression of non-stimulated and ovalbumin restimulated splenocytes (mean ± SEM). Each dot represents an individual immunized mouse.

CD8⁺ T-cells. In the literature it was shown that vaccination with 10 µg ovalbumin by using 600 µm long dissolving microneedles leads to efficient anti-tumor and antiviral immune responses by the induction of ovalbumin-specific CD8⁺ and CD4⁺ Th₁ responses [27]. Furthermore, it has been reported that using 110 µm long ovalbumin-coated ultra-high-density microneedle arrays lead to superior CD8⁺ T-cell responses in mice compared to intramuscular immunization [28]. In conclusion, these and our present results show that microneedle-based immunization is highly suited for inducing T-cell responses even more pronounced than IgG responses.

5. Conclusion

In conclusion, ovalbumin delivery into *ex vivo* human skin by ovalbumin-coated pH-sensitive microneedle arrays is very efficient compared to that by the ‘poke and patch’ approach. Immunization by microneedles can lead to comparable IgG responses as by conventional subcutaneous or intradermal immunization, although requires more immunizations before antigen-specific antibodies are produced. To further improve the antigen-specific antibody responses several strategies could be explored, such as adding an adjuvant, changing the microneedle length, density, number, or vaccinating *via* a different skin site. Furthermore, ovalbumin-specific CD4⁺ and CD8⁺ T-cell responses are effectively induced after microneedle-based immunization, similar to subcutaneous and intradermal immunization by conventional hypodermic needles. Therefore, these results show the applicability of pH-sensitive microneedles for controlled intradermal vaccination.

Acknowledgements

This research was financially supported by the programma Nano4Vitality of the Dutch Ministry of Economic Affairs and the province Overijssel. Furthermore, we acknowledge J. Wissink, U-Needle BV and Dr. N. Tas, University of Twente, Transducer Science and Technology Department (TST) for the supply of microneedle arrays.

References

- [1] F. Andre, R. Booy, H. Bock, J. Clemens, S. Datta, T. John, B. Lee, S. Lolekha, H. Peltola, T. Ruff, M. Santosham, H. Schmitt, Vaccination greatly reduces disease, disability, death and inequity worldwide. *Bulletin of the World Health Organization* 86 (2008) 140-146.
- [2] W.R. Gerritsen, The evolving role of immunotherapy in prostate cancer. *Annals of Oncology* 23 (2012) VIII22–VIII27.
- [3] J. Chen, G. Ni, X.S. Liu, Papillomavirus virus like particle-based therapeutic vaccine against human papillomavirus infection related diseases: Immunological problems and future directions. *Cellular Immunology* 269 (2011) 5-9.
- [4] G. Gonzalez, T. Crombet, A. Lage, Chronic vaccination with a therapeutic EGF-based cancer vaccine: a review of patients receiving long lasting treatment. *Current Cancer Drug Targets* 11 (2011) 103-110.
- [5] Y. Kang, J. Guo, Z. Chen, Closing the door to human immunodeficiency virus. *Protein Cell* 4 (2013) 86-102.
- [6] K. van der Maaden, W. Jiskoot, J. Bouwstra, Microneedle technologies for (trans)dermal drug and vaccine delivery. *Journal of controlled release* 161 (2012) 645–655.
- [7] T. Warger, H. Schild, G. Rechtsteiner, Initiation of adaptive immune responses by transcutaneous immunization. *Immunology Letters* 109 (2007) 13-20.
- [8] Y.-C. Kim, J.-H. Park, M.R. Prausnitz, Microneedles for drug and vaccine delivery. *Advanced Drug Delivery Reviews* 64 (2012) 1547-1568.
- [9] M.I. Haq, E. Smith, D.N. John, M. Kalavala, C. Edwards, A. Anstey, A. Morrissey, J.C. Birchall, Clinical administration of microneedles: skin puncture, pain and sensation. *Biomed Microdevices* 11 (2009) 35-47.
- [10] S. Kaushik, A.H. Hord, D.D. Denson, D.V. McAllister, S. Smitra, M.G. Allen, M.R. Prausnitz, Lack of Pain Associated with Microfabricated Microneedles. *Anesth Analg* 92 (2001) 502-504.
- [11] S.L. Banks, K.S. Paudel, N.K. Brogden, C.D. Loftin, A.L. Stinchcomb, Diclofenac Enables Prolonged Delivery of Naltrexone Through Microneedle-Treated Skin. *Pharmaceutical Research* 28 (2011) 1211-1219.
- [12] H. Chen, H. Zhu, J. Zheng, D. Mou, J. Wan, J. Zhang, T. Shi, Y. Zhao, H. Xu, D. Yang, Iontophoresis-driven penetration of nanovesicles through microneedle-induced skin microchannels for enhancing transdermal delivery of insulin. *Journal of Controlled Release* 139 (2009) 63-72.
- [13] A.V. Badkar, A.M. Smith, J.A. Eppstein, A.K. Banga, Transdermal delivery of interferon alpha-2B using microporation and iontophoresis in hairless rats. *Pharmaceutical Research* 24 (2007) 1389-1395.
- [14] A. Kumar, X. Li, M.A. Sandoval, B.L. Rodriguez, B.R. Sloat, Z. Cui, Permeation of antigen protein-conjugated nanoparticles and live bacteria through microneedle-treated mouse skin. *International Journal of Nanomedicine* 6 (2011) 1253-1264.
- [15] K. van der Maaden, H. Yu, K. Sliedregt, R. Zwier, R. Lebox, M. Oguri, A. Kros, W. Jiskoot, J.A. Bouwstra, Nanolayered chemical modification of silicon surfaces with ionizable surface groups for pH-triggered protein adsorption and release: application to microneedles. *Journal of Materials Chemistry B* 1 (2013) 4466-4477.
- [16] X. Chen, T.W. Prow, M.L. Crichton, D.W.K. Jenkins, M.S. Roberts, I.H. Frazer, G.J.P. Fernando, M.A.F. Kendall, Dry-coated microprojection array patches for targeted delivery of immunotherapeutics to the skin. *Journal of Controlled Release* 139 (2009) 212-220.
- [17] G. Widera, J. Johnson, L. Kim, L. Libiran, K. Nyam, P.E. Daddona, M. Cormier, Effect of delivery parameters on immunization to ovalbumin following intracutaneous administration by a coated microneedle array patch system. *Vaccine* 24 (2006) 1653-1664.
- [18] K. van der Maaden, K. Sliedregt, A. Kros, W. Jiskoot, J. Bouwstra, Fluorescent Nanoparticle Adhesion Assay: a Novel Method for Surface pKa Determination of Self-Assembled Monolayers on Silicon Surfaces. *Langmuir* 28 (2012) 3403–3411.
- [19] Z. Ding, E. van Riet, S. Romeijn, G.F.A. Kersten, W. Jiskoot, J.A. Bouwstra, Immune modulation by adjuvants combined with diphtheria toxoid administered topically in BALB/c mice after microneedle array pretreatment. *Pharmaceutical Research* 26 (2009) 1635-1643.
- [20] L. Cui, Y. Sun, H. Xu, H. Xu, H. Cong, J. Liu, A polysaccharide isolated from *Agaricus blazei* Murill (ABP-AW1) as a potential Th1 immunity-stimulating adjuvant. *Oncology Letters* 6 (2013) 1039-1044.
- [21] M.-C. Chen, S.-F. Huang, K.-Y. Lai, M.-H. Ling, Fully embeddable chitosan microneedles as a sustained release depot for intradermal vaccination. *Biomaterials* 34 (2013) 3077-3086.
- [22] A.P. Raphael, T.W. Prow, M.L. Crichton, X. Chen, G.J.P. Fernando, M.A.F. Kendall, Targeted, Needle-Free Vaccinations in Skin using Multilayered, Densely-Packed Dissolving Microprojection Arrays. *Small* 6 (2010) 1785-1793.
- [23] L. Guo, J. Chen, Y. Qiu, S. Zhang, B. Xu, Y. Gao, Enhanced transcutaneous immunization via dissolving microneedle array loaded with liposome encapsulated antigen and adjuvant. *International Journal of Pharmaceutics* 447 (2013) 22-30.
- [24] K. Matsuo, Y. Yokota, Y. Zhai, Y.-S. Quan, F. Kamiyama, Y. Mukai, N. Okada, S. Nakagawa, A low-invasive and effective transcutaneous immunization system using a novel dissolving microneedle array for soluble and particulate antigens. *Journal of Controlled Release* 161 (2012) 10-17.
- [25] H. Beacock-Sharp, A.M. Donachie, N.C. Robson, A.M. Mowat, A role for dendritic cells in the priming of antigen-specific CD4+ and CD8+ T lymphocytes by

immune-stimulating complexes in vivo. *International Immunology* 15 (2003) 711-720.

[26] B. Avgustin, V. Kotnik, M. Škoberne, T. Malovrh, A. Skralovnik-Stern, M. Tercelj, CD69 Expression on CD4+ T Lymphocytes after In Vitro Stimulation with Tuberculin Is an Indicator of Immune Sensitization against *Mycobacterium tuberculosis* Antigens. *Clinical and Diagnostic Laboratory Immunology* 12 (2005) 101-106.

[27] M. Zaric, O. Lyubomska, O. Touzelet, C. Poux, S. Al-Zahrani, F. Fay, L. Wallace, D. Terhorst, B.

Malissen, S. Henri, U.F. Power, C.J. Scott, R.F. Donnelly, A. Kissenpfennig, Skin Dendritic Cell Targeting via Microneedle Arrays Laden with Antigen-Encapsulated Poly-D,L-lactide-co-Glycolide Nanoparticles Induces Efficient Antitumor and Antiviral Immune Responses. *ACS Nano* 7 (2013) 2042-2055.

[28] H.-I. Ng, G.J.P. Fernando, M.A.F. Kendall, Induction of potent CD8+ T cell responses through the delivery of subunit protein vaccines to skin antigen-presenting cells using densely packed microprojection arrays. *Journal of controlled release* 162 (2012) 477-484.

Supplemental information

Analysis of splenocytes in FowJo v10 as follows. The lymphocytes were gated from the forward (FSC)-sideward scattering (SSC) dotplot (figure S11A). From this population the living T-cells, 7-AAD negative and CD3 (AmCyan) positive, were selected (figure S11B). Subsequently, the percentage of CD4⁺ (Qdot605) CD8⁻ (AlexaFluor700) T-cells (figure S11C) that was positive for CD69 (FITC) (figure S11D) and the percentage of CD4⁺ (Qdot605) CD8⁺ (AlexaFluor700) T-cells (figure S11C) that was positive for CD69 (FITC) was determined.

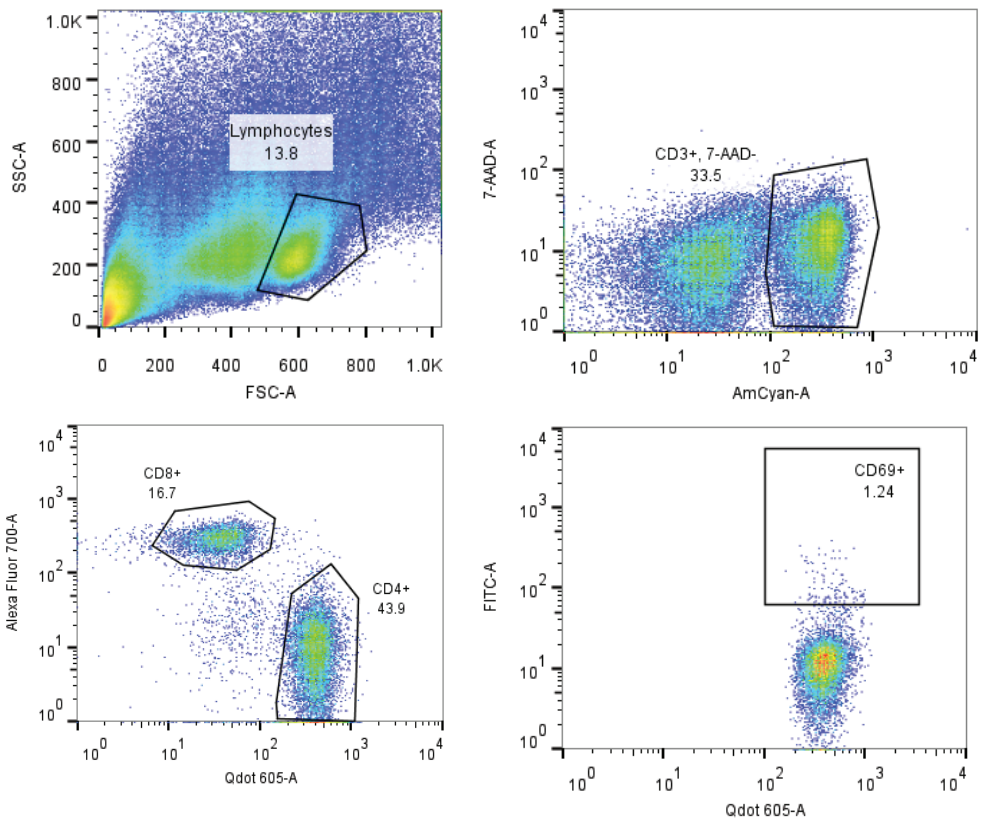


Figure S11: Gating strategy for the analysis of splenocytes by flow cytometry. Dot plots of the forward scattering (FSC) versus sideward scattering (SSC) (A), 7-AAD versus CD3 (AmCyan) (B), CD8 (AlexaFluor700) versus CD4 (Qdot605) (C), and CD4 versus CD69 (FITC).

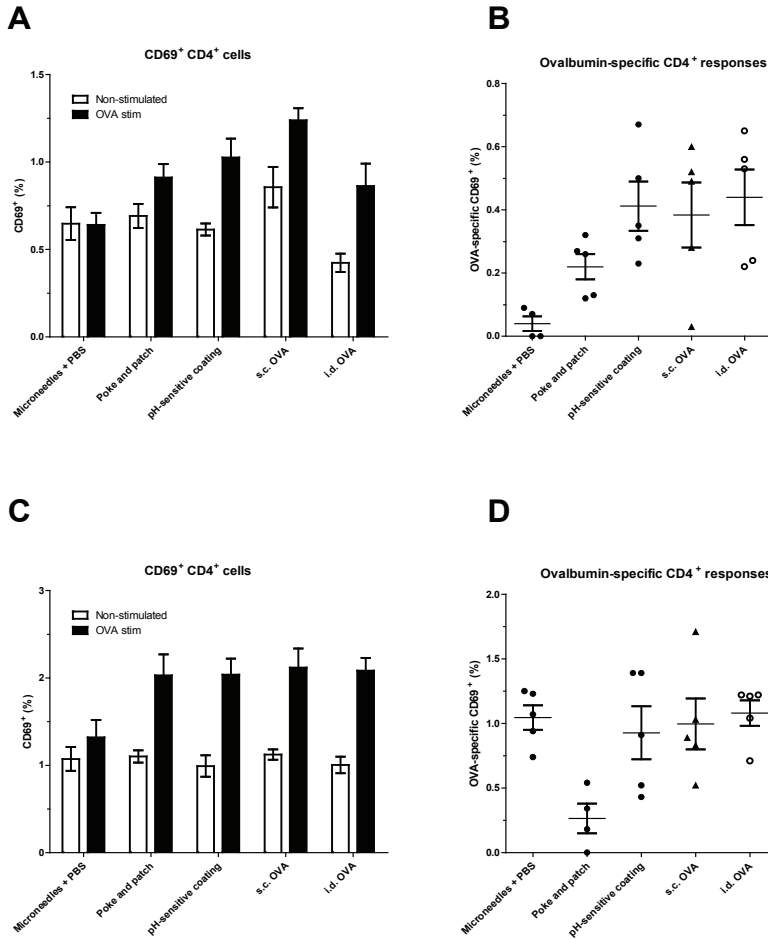


Figure S12: Expression of the surface marker CD69 on CD4⁺ (A and B) and CD8⁺ (C and D) T-cells upon restimulation of splenocytes with ovalbumin (black bars) compared to non-stimulated splenocytes (white bars) (A and C). Ovalbumin-specific CD4⁺ T-cells calculated by the difference between the non-stimulated and ovalbumin restimulated splenocytes (B and D).

CHEMICAL MODIFICATIONS OF SILICON SURFACES FOR THE GENERATION OF A TUNABLE ISOELECTRIC POINT

Koen van der Maaden
Jasmine Tomar
Wim Jiskoot
Joke Bouwstra

[Langmuir, 30 \(2014\)
1812–1819](#)

Abstract

The aim of this work was to generate a tunable surface isoelectric point (sIEP), where the surface is modified with two molecules: a weak base (pyridine), carrying a pH-dependent positive charge, and a derivative of a strong acid (sulfate), carrying a permanent negative charge in a physiologically relevant pH range. To this end, silicon surfaces were modified with 3-aminopropyltriethoxysilane. These amine-modified surfaces were subsequently derivatized into pyridine- or sulfate-modified surfaces. Then, the surface pK_a of pyridine-modified surfaces was determined by a fluorescent nanoparticle adhesion assay (FNAA). Next, these values were used to calculate in which ratio the chemicals must be present in the reaction mixture to generate a mixed pyridine/sulfate-modified surface with a target sIEP. After preparing surfaces with a target sIEP, a FNAA with positively and negatively charged nanoparticles was used to verify the sIEP of the generated surfaces. The FNAA revealed that pyridine-modified surfaces had a pK_a of 6.69 ± 0.18 . When an sIEP was generated, negative nanoparticles bound to surfaces at pH values below the sIEP and positive nanoparticles bound at pH values above the sIEP. Furthermore, we found sIEP values of 5.97 ± 0.88 when we aimed for an sIEP of 6.2, and 7.12 ± 0.21 when we aimed for an sIEP of 7.1. Finally, the pH-dependent binding and release of a negatively and positively charged (bio)polymer was investigated for a target sIEP of 7. A negatively charged polymer (*poly(I:C)*) was bound at a $pH < sIEP$ and released at a $pH > sIEP$ with a release efficiency of $85 \pm 9\%$ and a positively charged polymer (*trimethyl chitosan*) bound at a $pH > sIEP$ and released at a $pH < sIEP$ with a release efficiency of $72 \pm 9\%$. In conclusion, we established a method for preparing modified silicon surfaces with a tunable sIEP, which can be used for pH-dependent binding and release of biomacromolecules.

1. Introduction

The modification of surfaces with self-assembling monolayers is used for numerous applications, such as bio-analytical applications, including chromatography [1], antibody microarrays [2], DNA and protein biosensors [3, 4], and biomedical applications, including nanoparticles [5, 6], and implants [7, 8]. In many of these applications biomacromolecules such as DNA, RNA, peptides and proteins, or drugs and (drug-containing) nanoparticles are immobilized by a variety of methods. These methods employ physical entrapment, hydrophobic interactions, covalent bonding, van der Waals interactions, and electrostatic interactions [2, 3, 9-11]. However, in many cases of drug delivery the compound must be desorbed from the surface in order to become active or to be taken up by target cells. Immobilization of biomacromolecules *via* electrostatic interactions has great potential, since most of these compounds are either positively or negatively charged. Furthermore, detachment of these compounds when adsorbed by electrostatic interactions can be achieved by ion competition [12] or by removing/changing the charge of the compounds and/or the surface by a pH shift [13].

In order to change the charged state of the surface, it needs to possess groups having at least one pK_a , whereby the charged state of the surface is dependent on the surface pK_a of the (acidic or basic) groups and the surrounding pH. However, according to the Henderson-Hasselbalch equation a pH difference of 4 pH units ($pK_a \pm 2$) is required to have either a high (99% of the maximum) or a low (1%) surface charge. To bind oppositely charged compounds a high surface charge could be beneficial. For the release however, especially for large molecules such as biomacromolecules or polymers, even at a low surface charge of < 1%, the release from the surface might be hampered. Furthermore, many biomacromolecules such as proteins are susceptible to deformation, aggregation, and hydrolysis at pH values deviating substantially from physiological pH [14-16]. Therefore, a surface pK_a does not always lead to the optimal surface properties for selective adsorption/release of biomacromolecules or polymers. A more sophisticated way of using electrostatic interactions for selective adsorption and desorption of biologically relevant compounds, is by generating a surface isoelectric point (sIEP). The benefit of having an sIEP, is that the surface can either be positively ($pH < sIEP$) or negatively ($pH > sIEP$) charged and that this change in surface charge takes place over a small pH range. For instance, a negatively charged compound can bind to a surface at $pH < sIEP$ and is repelled at $pH > sIEP$.

Recently, Lin *et al.* synthesized surfaces with a tunable sIEP by changing the ratio of amine and carboxylic groups on gold surfaces [17], and Kuo *et al.* synthesized surfaces with a tunable sIEP on silicon surfaces by varying the ratio between amine and thiol groups on the surface [18]. However, surface amine groups on gold, e.g., aminothiols, are unstable because these molecules can undergo chemical transformation, e.g., photoassisted oxidation of amine groups into nitroso groups and oxidation of thiol groups into sulfonate groups [19-21]. Furthermore, these surfaces are only stable up to 100°C [19]. Also amine groups on silicon substrates have stability issues, e.g., amino alkoxysilanes, can react with carbon dioxide and

form imines [22, 23] thereby losing their charge.

In this work we generated a model to generate a tunable sIEP by using two different surface groups, as shown in figure 1, of which one group has a pH-independent charge over a broad pH range and the other group has a pH-dependent charge. Therefore, a layer of 3-aminopropyltriethoxysilane (APTES) was coated on silicon surfaces by self-assembly. These surfaces were then modified with pyridine groups of which the surface pK_a was determined. The reactivity ratios of amine-modified surfaces into pyridine- and sulfate-modified surfaces was determined to calculate and generate surfaces with an sIEP of 6 and 7, as confirmed by a fluorescent nanoparticle adhesion assay (FNAA) by using positively and negatively charged nanoparticles.

2. Materials and methods

2.1 Materials

Succinic anhydride, APTES, amine-modified fluorescent orange nanoparticles of 100 nm, sulfate-modified fluorescent orange nanoparticles of 100 nm, 4-pyridinecarboxaldehyde (4-PCA), sodium cyanoborohydride, acetic acid, 4-formyl-1,3-benzenedisulfonic acid disodium salt (4-FBDA), H_2O_2 , EDTA, rhodamine B isothiocyanate, and HPLC grade methanol were purchased from Sigma Aldrich. 96-98% H_2SO_4 was obtained from Boom lab equipment, 1,4-dioxane was from Baker Chemicals B.V., 2-propanol Mallinckrodt analytical grade reagent (AR) and toluene AR were from Biosolve, and Acetonitrile HPLC Far UV was from LAB-SCAN Analytical Sciences. 1.5 mL polystyrene cuvettes were purchased from Sarstedt, black 96 well plates were from Greiner, and molecular sieves 4Å and 8 to 12 mesh were from Acros Organics. Chitosan (Mw 120 kDa) with a degree of deacetylation of 92% was purchased from Primex, *poly(I:C)* (LMW) rhodamine was obtained from InvivoGen, and Alexa-Fluor® 488 carboxylic acid succinimidyl ester was purchased from InvitroGen. Deionized water with a resistivity of 18 MΩ·cm, produced by a Millipore water purification system (MQ water), was used for the preparation of solutions and the cleaning of the silicon surfaces. Silicon wafers <110> with a thickness of 0.38 mm, cut in pieces of 1x1 cm and of 1x2.5 cm, were a kind gift of U-Needle B.V.

2.2 Methods

2.2.1 Synthesis of rhodamine B labeled trimethyl chitosan (TMC)

N-trimethyl chitosan chloride (TMC), with a degree of quaternization of 18%, was synthesized by methylating chitosan by iodomethane in the presence of NaOH as described by Hamman and Kotzé [24]. In brief, a mixture of 2 g of chitosan, 12 mL 3.75 M NaOH, 12 mL iodomethane, and 4.8 g sodium iodine in 80 mL N-methylpyrrolidone was refluxed for 1 hour at 60°C. Subsequently, the obtained polymer (TMC) was precipitated by ethanol and was washed on a fritted funnel by ethanol and diethyl ether. Next, TMC was purified by dialysis

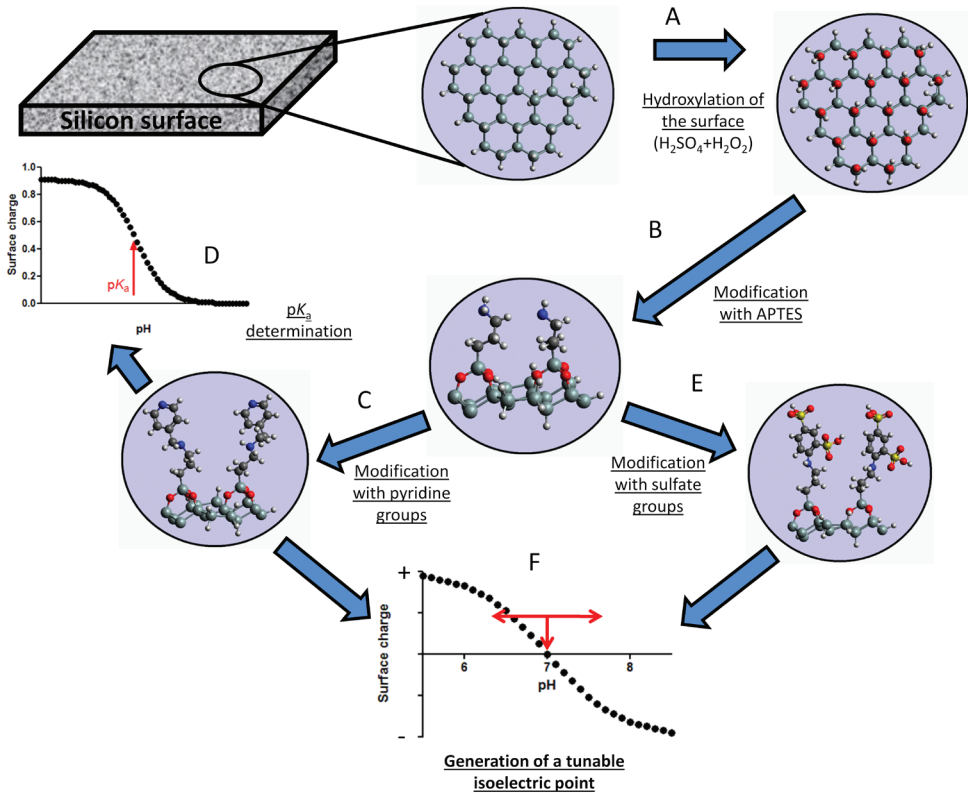


Figure 1: Schematic scheme of the principle of the generation of a tunable surface isoelectric point (sIEP) by modifying surfaces with positively charged groups with a pK_a in a physiologically relevant pH range and with groups that have a permanent negative charge in the same range. After the silicon surface is oxidized with a piranha mixture (A), the surface is modified with APTES (B). Subsequently, this surface is derivatized into a pyridine-modified surface (C) of which the surface pK_a is determined (D). The surface pK_a and the apparent derivatization efficiencies to generate pyridine- (C) and sulfate-modified (E) surfaces are used to generate a tunable sIEP (F). Index of molecules: large gray balls (Si), black balls (C), red balls (O), blue balls (N), white balls (H), and yellow balls (S).

against 0.17 M NaCl for 4 days and against MQ water for 2 days, and was subsequently freeze dried.

In order to quantify the polymer, TMC was dissolved in 0.1 M carbonate buffer at pH of 9 and was fluorescently labeled with rhodamine B isothiocyanate in a weight ratio of respectively 15:1 for 1 hour [25]. Next, rhodamine B labeled TMC was dialyzed against MQ water until rhodamin B was undetectable by fluorescence, and was finally freeze dried.

2.2.2 Surface modification

Chemically modified surfaces were prepared as schematically illustrated in figure 2 and described in detail below. In order to modify surfaces with pyridine groups for a positive charge and sulfate groups for a negative charge, silicon surfaces were first modified with APTES. This was done in a two-step procedure, as described previously [26]. Briefly: first, flat silicon surfaces of 1x1 cm were incubated for 30 min in a freshly prepared piranha solution (7 H₂SO₄ : 3 H₂O₂) at 120°C, and were then incubated in a 2% APTES solution in toluene for 24 h to obtain amine-modified surfaces. Then, these surfaces were cured for 30 minutes at 120°C and were subsequently incubated for 2 hours in MQ water at 40°C to remove non-reacted ethoxy groups. Next, the surface amine groups were derivatized into either carboxyl-modified surfaces, pyridine-modified surfaces, or sulfate-modified surfaces. To obtain a carboxyl-modified surface, amine-modified surfaces were incubated for 30 min in a 20 mg/mL succinic anhydride solution in 1,4-dioxane at 80°C. Both pyridine-modified surfaces and sulfate-modified surfaces were prepared by a two-step procedure. First, amine-modified surfaces were incubated with 15 mM of either 4-pyridinecarboxaldehyde (4-PCA) to generate a pyridine-modified surface, or 4-formyl-1,3-benzenedisulfonic acid disodium salt (4-FBDA) to generate a sulfate-modified surface, in a 1:8 isopropanol:methanol mixture with 1% acetic acid to which molecular sieves (0.15 g/mL) were added, for 16 h at room temperature. Finally, the imine bond was reduced to a secondary amine by incubating the silicon surfaces in a freshly prepared 50 mM sodium cyanoborohydride solution in isopropanol for 2 h at room temperature. The modified surfaces were stored under argon until use.

2.2.3 Fluorescent nanoparticle adhesion assay

In order to determine the binding of nanoparticles to the chemically modified silicon surfaces, the unbound fraction of nanoparticles was determined as described previously [26]. First, a nanoparticle suspension (1 μL of 2.5% solids per mL) of either positive (amine-modified) or negative nanoparticles (sulfate-modified) were prepared in a 1 mM EDTA buffer at a certain pH value. The fluorescence intensity of these nanoparticles is linearly dependent on a nanoparticle concentration between 0.03-2 μL nanoparticle suspension (2.5% solids)/mL buffer. Subsequently, two aliquots of 0.75 mL were transferred to two 1.5 mL cuvettes, to one of which a silicon slide was added. The cuvettes were incubated for 2 h at room temperature on a shaking device at 500 rpm. Next, two times 200 μL of the incubated nanoparticle suspensions with a silicon slide (FI_{silicon}) and without a silicon slide (FI_{control}) were transferred to a black 96 well plate and the emission at 540 nm was measured with an excitation wavelength of 520 nm on a Tecan Infinite® M1000. These fluorescence values were used to calculate the binding percentage (B), according to equation 1.

$$B = (1 - [FI_{\text{silicon}}] / [FI_{\text{control}}]) * 100\% \quad (\text{Equation 1})$$

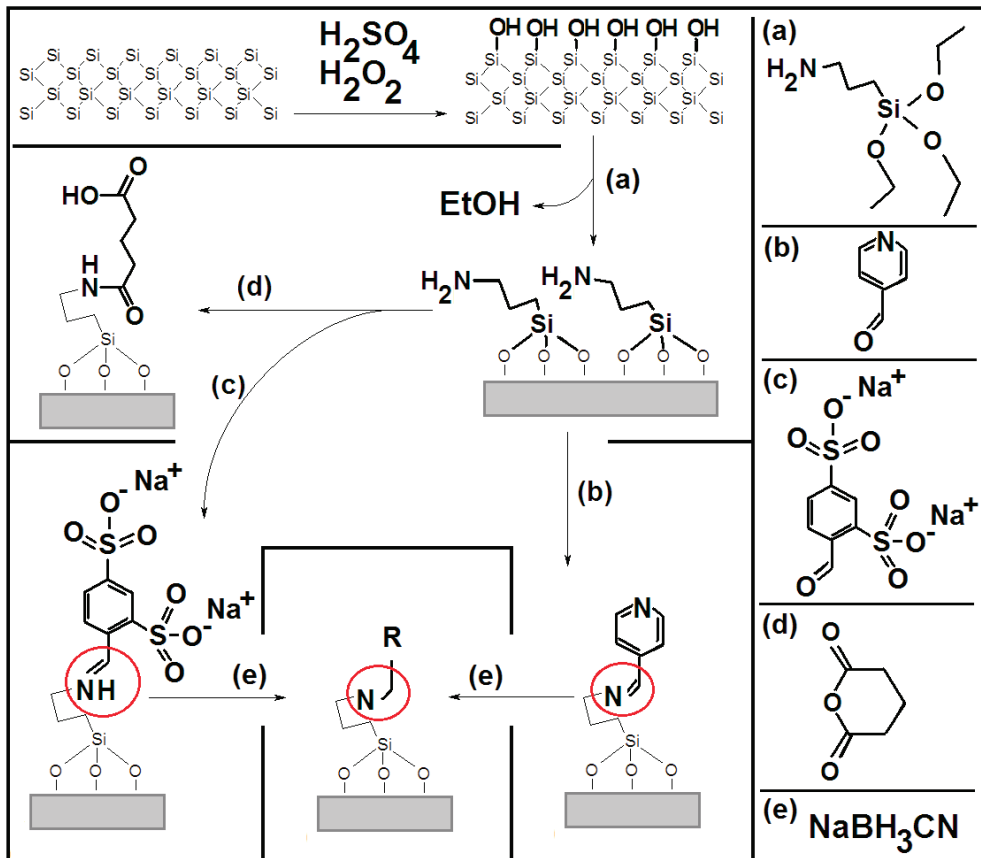


Figure 2: Preparation of chemically modified surfaces. First, silicon surfaces were hydroxylated by a piranha mixture ($\text{H}_2\text{SO}_4\text{:H}_2\text{O}_2$). Subsequently, the hydroxylated surfaces were reacted with APTES (a), yielding an amine-modified surface. Next, the amine-modified surfaces were modified into either carboxyl-modified surfaces by reaction with succinic anhydride (d), or into pyridine- and sulfate-modified surfaces by reaction with 4-PCA (b) and 4-FBDA (c), respectively. The latter two were incubated with sodium cyanoborohydride (e) to form a stable secondary amine.

2.2.4 pKa determination of pyridine-modified surfaces

In order to develop a model to predict and generate an sIEP, the surface charge as a function of the pH of each molecule that is present on the surface needs to be known. Therefore, the surface pK_a of pyridine-modified surfaces was determined by the FNAA [26]. Since pyridine is a weak base and gets positively charged when reducing the pH, negatively charged nanoparticles were used to determine its pK_a value. Therefore, the binding percentage of negatively charged fluorescent nanoparticles to 1x1 cm pyridine-modified silicon surfaces was determined as a function of the pH of the nanoparticle suspension. For each titration 20 different pH values were used. Subsequently, the binding percentage was plotted as a function of the pH and was fitted in Prism 5 for Windows according to the Henderson-Hasselbalch equation. The pH at the midpoint of the S-shaped curve was determined as the surface pK_a .

2.2.5 Reactivity ratio

In order to generate an sIEP by mixing two chemicals, it is important to know in which ratio these chemicals react with amine-modified surfaces, since the ratio of the two chemicals on the surface determines the charge and thereby the sIEP. Therefore, 4-PCA (pyridine) and 4-FBDA (sulfate) modified silicon slides were incubated with a fluorescent dye that only reacts with primary amines, i.e., only the non-derivatized amine groups on the surface are fluorescently labeled. This was done by incubating the chemically modified surfaces with 2 $\mu\text{g}/\text{mL}$ Alexa-Fluor® 488 carboxylic acid succinimidyl ester in acetonitrile in the dark for 1 hour at room temperature [26, 27]. Subsequently, the chemically modified surfaces were photographed by fluorescence microscopy (Nikon Eclipse E600 with a mercury light source, a magnification of 100x, a GFP filter set, and imaged with a 10 s exposure time). The pixel intensity of the fluorescence microscopy images of 4-FBDA, 4-PCA, APTES, and piranha treated surfaces was calculated in ImageJ (available from rsbweb.nih.gov/ij/). Subsequently, these pixel intensities were used to calculate the derivatization efficiency (DE) of amine-modified surfaces into 4-PCA (pyridine) or into 4-FBDA (sulfate) according to equation 2.

$$\text{Derivatization efficiency} = 100 - \left(\frac{I_m - I_o}{I_a - I_o} \right) * 100 \quad (\text{Equation 2})$$

Here I_m represents the average pixel intensity of 4-PCA (pyridine) or 4-FBDA (sulfate) modified surfaces, I_o represents the average pixel intensity of the non-modified (piranha treated) surfaces, and I_a represents the average pixel intensity of the amine-modified surfaces [26, 27]. The reactivity ratio (RR) was calculated as follows:

$$\text{RR} = \text{DE}_{4\text{-PCA (pyridine)}} / \text{DE}_{4\text{-FBDA (sulfate)}} \quad (\text{Equation 3})$$

2.2.6 Comparative nanoparticle adhesion

The adhesion of both positively and negatively charged nanoparticles was determined as a function of time to ensure that both nanoparticles adsorb to an oppositely charged surface in a comparable manner. In order to compare the binding properties, such as binding percentage and binding time, to an oppositely charged surface, silicon surfaces modified with a compound with one positively charged group (APTES, charge +1) and with one negatively charged group (carboxyl, charge -1, derivatization efficiency > 95% [26]) were prepared. Next, positively charged nanoparticles were incubated with a 1x2.5 cm (5 cm²) carboxyl-modified silicon surface (pKa=4.37 [26]) at pH 10, to ensure a complete deprotonation of the surface carboxylic groups. Conversely, negatively charged nanoparticles were incubated with a 1x2.5 cm (5 cm²) amine-modified silicon surface (pKa=6.55 and 9.94 [26]) at pH 3, to ensure a complete protonation of the surface amine groups. Both chemically modified silicon surfaces were incubated with 1.5 mL nanoparticle dispersions in a concentration of 1 μL nanoparticles (2.5% solids) per mL. Finally, the binding percentage of the positively charged nanoparticles to the carboxyl-modified surface and the binding percentage of the negatively charged

nanoparticles to the amine-modified surface were determined in a time frame of 2 hours.

2.2.7 Preparation of modified silicon surfaces with a tunable surface isoelectric point

In order to generate an sIEP of choice (target sIEP), the predetermined surface pK_a of pyridine-modified surfaces and the reactivity ratio were used to calculate the required relative amounts of 4-PCA (pyridine) and 4-FBDA (sulfate) in the reaction mixture, as explained below. First, according to the Henderson-Hasselbalch equation, the fraction of protonated pyridine (α_{BH^+}) is calculated for the pH equal to the target sIEP (pH (target sIEP)) according to equation 4:

$$\alpha_{BH^+} = 1 / (1 + 10^{pH(\text{target sIEP}) - pK_a}) \quad (\text{Equation 4})$$

At the target sIEP, the number of positively charged groups ($BH^+_{\text{target sIEP}}$) should equal the number of negatively charged groups (A). Taking into account the differences in derivatization efficiencies of 4-PCA and 4-FBDA and assuming a net charge of -2 for 4-FBDA (which has two sulfonyl groups ($pK_a < 1$)), we calculated the required ratio of the 4-FBDA and 4-PCA concentration in the reaction mixture according to equation 5:

$$[4\text{-FBDA}] / [4\text{-PCA}] = \alpha_{BH^+} * RR / 2 \quad (\text{Equation 5})$$

Finally, the concentrations [4-PCA] and [4-FBDA] for a target sIEP were calculated in such a way that [4-PCA] + [4-FBDA] = 50 mM.

According to the procedure described above, surfaces were prepared with a target sIEP of 6.2 and 7.1. To determine the sIEP, a FNAAs was performed at 14 different pH values with either positively or negatively charged nanoparticles and the relative fluorescence was determined as a function of the pH. This assay was performed trice for each target sIEP. Subsequently, the sIEP was determined as described below:

The binding of positive and negative nanoparticles was calculated in Prism 5 for Windows from the binding “log vs response-variable slope” curves, by subtracting the top asymptote from the relative fluorescence values to correct for non-specific binding. Subsequently, the sIEP was determined as the intersection of the “log vs response-variable slope” curves of the binding.

Next, the binding of fluorescently labeled nanoparticles onto the surface was sorted for every 0.3 pH units. Then, the binding of the positively charged nanoparticles was subtracted from the binding of the negatively charged particles for every sorted pH value and was normalized to have values between -1 and 1. This value was defined as the arbitrary surface charge, which was plotted as a function of the pH.

To visualize the fluorescent nanoparticle adhesion onto the sIEP surfaces fluorescence microscopy was used (Nikon Eclipse E600 with a mercury light source, a magnification of 100x, a GFP filter set, and imaged with a 5 s exposure time).

2.2.8 pH-dependent binding and release of a positively and negatively charged polymer

In order to test the applicability of the pH-sensitive coating/release system for e.g. pharmaceutical applications, a surface was prepared with a target sIEP of 7.1 as described above. Subsequently, a negatively or positively charged polymer was coated onto the sIEP=7 surface in 0.75 mL of a 1 mM EDTA solution for 1 hour at room temperature at a pH of 5.7 and 8.6, respectively. The negatively charged polymer *poly(I:C)* (a synthetic analog of dsRNA) was coated onto the sIEP=7 surface in concentrations of 10 $\mu\text{g/mL}$ or 1 $\mu\text{g/mL}$ ($\text{pH} < \text{sIEP}$), and the positively charged polymer *TMC* was coated onto the sIEP=7 surface in concentrations of 100 $\mu\text{g/mL}$ or 10 $\mu\text{g/mL}$ ($\text{pH} > \text{sIEP}$). Both polymers were fluorescently labeled with rhodamine B, the fluorescence of which was measured at an excitation wavelength of 550 nm and an emission wavelength of 580 nm. The amount of bound polymer was determined by measuring the unbound fraction of polymer and applying equation 1. Next, *poly(I:C)* and *TMC* coated sIEP=7 surfaces were incubated in 0.75 mL of a 5 mM EDTA solution for 30 minutes at room temperature at a pH of 8.6 and 5.5, respectively. Subsequently, the released amount of polymer was determined in the release solution by fluorescence as described above. The percentage of released polymer was calculated by dividing the released amount of polymer by the amount of bound polymer.

3. Results and discussion

3.1 pK_a and reactivity ratio determination

In order to develop a tunable sIEP, whereby one molecule with a permanent charge over a biological relevant pH range and one molecule with a pK_a within that range is used, the surface pK_a of that molecule needs to be known. Therefore, a FNAAs was performed on pyridine-modified silicon surfaces at different pH values between pH 4-9. Figure 3 shows the data of all individual pK_a determinations combined, whereby each point is the average binding at five subsequent pH values. According to the Henderson-Hasselbalch equation a curve was fitted to each individual titration ($n=3$), and a surface pK_a of 6.69 ± 0.18 (mean \pm SD, $n=3$) was found for pyridine-modified surfaces. This surface pK_a did not differ from the value that we have reported previously (6.91 ± 0.30 (mean \pm SD, $n=3$)) [27], which shows the reproducibility of this surface modification, even when 4-PCA is reacted with APTES surfaces in a different solvent mixture; 1:8 isopropanol:methanol versus isopropanol only.

After the pK_a of pyridine-modified surfaces was determined, the derivatization efficiencies of 4-PCA (pyridine) and 4-FBDA (sulfate) were determined. Surfaces were incubated with a fluorescent dye that only reacts with primary amines, thus only the non-derivatized amine groups are fluorescently labeled. After the surfaces were imaged by fluorescence microscopy, the average pixel intensity was used to calculate the derivatization efficiencies according to equation 2. For 4-FBDA (sulfate) modified surfaces a derivatization efficiency of $86.7 \pm 3.2\%$ and for 4-PCA (pyridine) a derivatization efficiency of $75.2 \pm 6.5\%$ (mean \pm SD, $n=3$) was found, which was comparable to the value that was reported previously for 4-PCA (78.5%) [27]. From

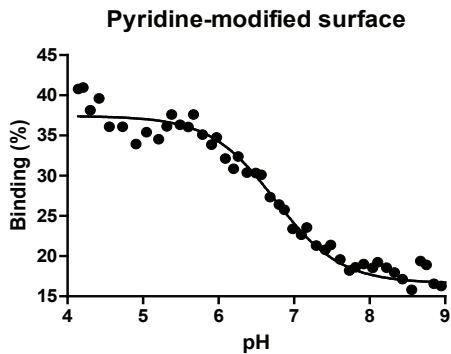


Figure 3: pK_a determination of pyridine-modified surfaces by a fluorescent nanoparticle adhesion assay with negatively charged nanoparticles. The binding of nanoparticles is plotted against the pH and the pK_a corresponds to the pH value at the mid-point of the S-shaped curve that was fitted according to the Henderson-Hasselbalch equation.

the derivatization efficiencies the reactivity ratio (4-PCA:4-FBDA) was calculated to be 0.87 by applying equation 3.

3.2 Nanoparticle adhesion to a positively or negatively charged surface

In order to test whether the intersection of positively charged nanoparticles and negatively charged nanoparticles can be used to determine the sIEP, both types of particles need to bind in a comparable way. Therefore, silicon surfaces with a charge (Q) of +1 (amine-modified surface) and with a charge of -1 (carboxyl-modified surface) were synthesized, rather than a 4-FBDA (sulfate-modified) surface which has two negatively charged groups. Subsequently, the positive and negative nanoparticles were incubated with the carboxyl- and pyridine-modified surfaces, respectively, as shown in figure 4. This figure shows that both positively and negatively charged nanoparticles bind to a comparable extent, and therefore these particles can be used to determine the sIEP.

3.3 Preparation and determination of the surface isoelectric point of modified silicon surfaces

After the required unknown parameters were determined ($pK_a=6.69$, $RR=0.87$), two reaction mixtures with different ratios of 4-PCA and 4-FBDA were calculated according to equation 5. For a surface with a target sIEP of 6.2 and 7.1 a $[4-FBDA]/[4-PCA]$ ratio of 0.320 and 0.127 were calculated, respectively. Subsequently, for the preparation of modified silicon surfaces with a target sIEP of 6.2, a reaction mixture with 37.88 mM 4-PCA and 12.12 mM 4-FBDA was used, and for the ones with a target sIEP of 7.1 a mixture of 44.38 mM 4-PCA and 5.62 mM 4-FBDA was used. Next, a FNAA was performed, showing sIEP values that were very close to the ones we aimed for (figure 5). The sIEP was calculated by the intersection of the nanoparticle binding curves. This led to a calculated sIEP of 5.97 ± 0.88 and 7.12 ± 0.21 (mean \pm SD, $n=3$) for a target sIEP of 6.2 and 7.1, respectively (representative examples figure 5A and 5B for a target sIEP of 6 and 7). Subsequently, from the binding of the positively and negatively charged nanoparticles the arbitrary surface charge was calculated, as described above (2.2.7) which is shown in figure 5C and 5D, for a target sIEP of 6.2 and 7.1, respectively. These images

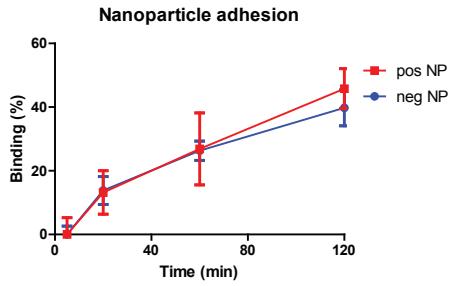


Figure 4: The adhesion of negatively charged nanoparticles (neg NP) at pH 3 onto a positively charged (amine) surface and the adhesion of positively charged nanoparticles (pos NP) at pH 10 onto a negatively charged (carboxyl) surface as a function of time.

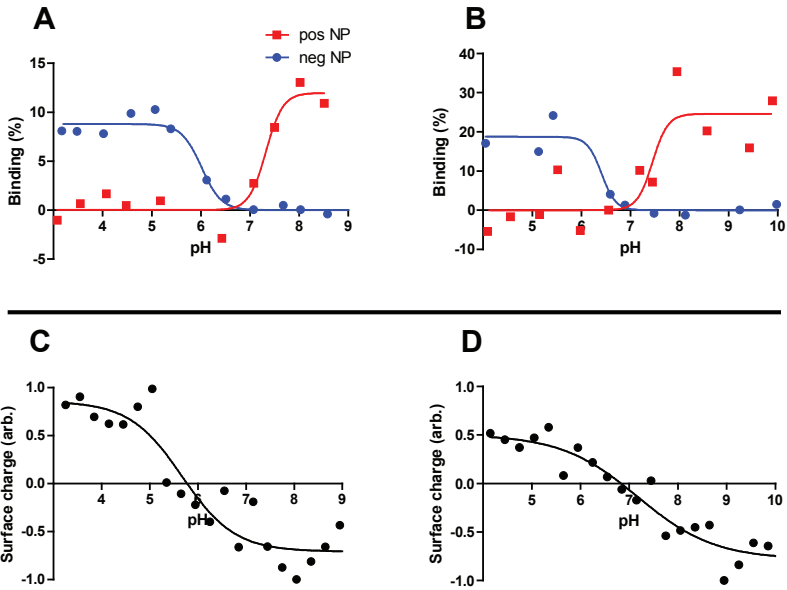


Figure 5: Fluorescent nanoparticle adhesion with positively (pos NP) and negatively (neg NP) charged nanoparticles on surfaces with a surface isoelectric point (sIEP) of 6 (A, C) or 7 (B, D), a representative titration showing the binding (A, B), and the arbitrary surface charge calculated from the positively and negatively charged nanoparticles for a chosen target sIEP (C, D).

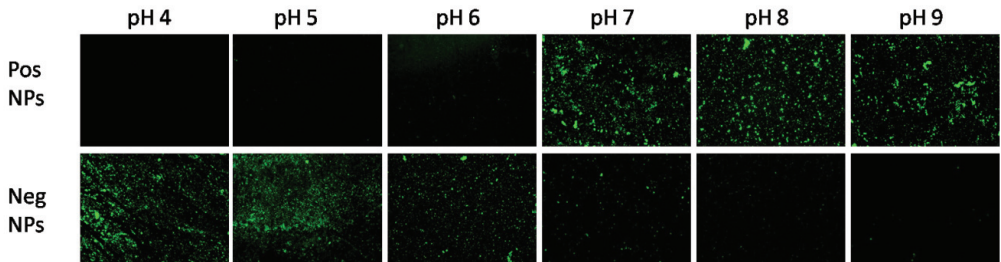
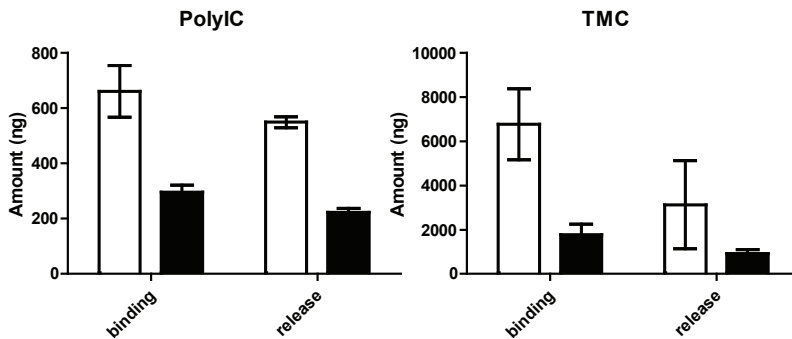


Figure 6: Fluorescence microscopy imaging of silicon surfaces with an isoelectric point of 7 after incubation with positively charged fluorescent nanoparticles (Pos NPs) or with negatively charged fluorescent nanoparticles (Neg NPs) at different pH values.

A



B

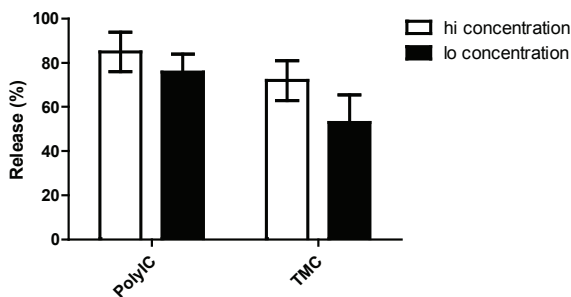


Figure 7: *Poly(I:C)* and *TMC* binding onto surfaces with an isoelectric point of 7 at a pH value of respectively 5.7 and 8.6. *poly(I:C)* was coated in a concentration of 10 or 1 $\mu\text{g}/\text{mL}$ and *TMC* in 100 or 10 $\mu\text{g}/\text{mL}$ (hi and lo concentration, respectively). Subsequently, *poly(I:C)* and *TMC* were released at a pH of 8.6 and 5.5, respectively (A). The release of *poly(I:C)* and *TMC* calculated in percentages (B).

clearly show the transition between a positively charged and a negatively charged surface, and further emphasize that the sIEP value was successfully tuned to an aimed value.

After surfaces with a target sIEP of 7.1 were incubated with either positively or negatively charged nanoparticles at different pH values, the surfaces were photographed under a fluorescence microscope, as shown in figure 6. These images show that there is a turning point of negatively charged nanoparticle adhesion towards positively charged nanoparticle adhesion between pH 6 and 7. In conclusion, figure 5 and 6 show that by generating an sIEP, dependent on the pH either positive or negative nanoparticles bind to the surface, and that the surface sIEP can be tuned to a value of choice, provided that the pK_a and the sIEP are sufficiently close to each other, i.e., less than one pH unit.

3.4 Proof of concept: pH-dependent binding and release of a positively and negatively charged polymer

In order to test the applicability of surfaces with an sIEP for pH-dependent capture and release of charged molecules, we chose to prepare a surface with an sIEP of 7. A negatively (*poly(I:C)*) and positively (*TMC*) charged polymer were selected to bind to these surfaces. As shown in figure 7A, *poly(I:C)* was coated onto sIEP=7 surfaces (2 cm^2) at a pH < sIEP (pH=5.7) in a concentration of 10 and 1 $\mu\text{g}/\text{mL}$, which led to a coated dose of 661 ± 94 ng and 295 ± 26 ng

(mean \pm SD, $n=3$), respectively. Subsequently, these surfaces were incubated for 30 minutes in a release solution with $\text{pH} > \text{sIEP}$ ($\text{pH}=8.6$), which led to a release of 549 ± 20 ng and 222 ± 15 ng (mean \pm SD, $n=3$), respectively. Furthermore, figure 7A shows that the binding of TMC at a $\text{pH} > \text{sIEP}$ ($\text{pH}=8.6$) was 6.77 ± 1.61 μg and 1.78 ± 0.48 μg (mean \pm SD, $n=3$) at a coating concentration of 100 and 10 $\mu\text{g}/\text{mL}$, respectively. Subsequently, these TMC coated surfaces were incubated for 30 minutes at a $\text{pH} < \text{sIEP}$ ($\text{pH}=5.5$), which led to a release of 3.13 ± 1.99 μg and 0.920 ± 0.187 μg (mean \pm SD, $n=3$), respectively. Figure 7B shows the release of *poly(I:C)* and TMC in percentages of the coated dose, which were respectively $85\pm 9\%$ and $76\pm 8\%$ (mean \pm SD, $n=3$) for *poly(I:C)*, and $72\pm 9\%$ and $53\pm 12\%$ (mean \pm SD, $n=3$) for TMC for a high and low dose of coated polymer. The generation of tunable sIEP surfaces can be applied onto biomedical microdevices, such as microneedles, for pH-sensitive coating of microneedles with a drug and subsequently releasing the drug into the skin by a pH-shift [27]. In conclusion, these data show the applicability of an sIEP coating in a physiological relevant pH range for controlled binding and subsequent release of charged (bio)macromolecules.

4. Conclusion

In this work we have shown to be able to generate surfaces with a predefined sIEP. For the generation of an sIEP it is important to choose two oppositely charged compounds, one of which should have a pK_a in the range of the desired sIEP. After choosing the compounds, the surface pK_a of the molecules that are coupled to the surface and the derivatization efficiencies of the different molecules need to be determined. Furthermore, we have shown to be able to bind positively and negatively charged (bio)macromolecules and subsequently release them in a pH-dependent manner. In conclusion, this data shows the tunability of silicon surfaces towards a chosen sIEP by using a specific ratio of two different molecules, which may have bio-analytical and bio-medical applications, such as drug delivery.

References

- [1] D.A. Barrett, G. Power, M.A. Hussain, I.D. Pitfield, P.N. Shaw, M.C. Davies, Protein interactions with model chromatographic stationary phases constructed using self-assembled monolayers. *J. Sep. Sci.* 28 (2005) 483-491.
- [2] W. Kusnezow, A. Jacob, A. Walijew, F. Diehl, J.D. Hoheisel, Antibody microarrays: an evaluation of production parameters. *Proteomics* 3 (2003) 254-264.
- [3] M. Tichoniuk, D. Gwiazdowska, M. Ligaj, M. Filipiak, Electrochemical detection of foodborne pathogen *Aeromonas hydrophila* by DNA hybridization biosensor. *Biosens. Bioelectron.* 26 (2010) 1618-1623.
- [4] M. Frasconi, C. Tortolini, F. Botre, F. Mazzei, Multifunctional Au Nanoparticle Dendrimer-Based Surface Plasmon Resonance Biosensor and Its Application for Improved Insulin Detection. *Anal. Chem.* 82 (2010) 7335-7342.
- [5] M.-A. Neouze, U. Schubert, Surface Modification and Functionalization of Metal and Metal Oxide Nanoparticles by Organic Ligands. *Monatsh. Chem.* 139 (2008) 183-195.
- [6] G. Pieters, L.J. Prins, Catalytic self-assembled monolayers on gold nanoparticles. *New J. Chem.* 36 (2012) 1931-1939.
- [7] K. Cai, A. Rechtenbach, J. Hao, J. Bossert, K.D. Jandt, Polysaccharide-protein surface modification of titanium via a layer-by-layer technique: Characterization and cell behaviour aspects. *Biomaterials* 26 (2005) 5960-5971.

- [8] K. Cai, Y. Hu, K.D. Jandt, Y. Wang, Surface modification of titanium thin film with chitosan via electrostatic self-assembly technique and its influence on osteoblast growth behavior. *J. Mater. Sci.* 19 (2008) 499-506.
- [9] E. Ruckenstein, Z.F. Li, Surface modification and functionalization through the self-assembled monolayer and graft polymerization. *Adv. Colloid Interface Sci.* 113 (2005) 43-63.
- [10] J. Kim, J. Cho, P.M. Seidler, N.E. Kurland, V.K. Yadavalli, Investigations of Chemical Modifications of Amino-Terminated Organic Films on Silicon Substrates and Controlled Protein Immobilization. *Langmuir* 26(4) (2010) 2599-2608.
- [11] N. Graf, E. Yegen, A. Lippitz, D. Treu, T. Wirth, W.E.S. Unger, Optimization of cleaning and aminosilanization protocols for Si wafers to be used as platforms for biochip microarrays by surface analysis (XPS, ToF-SIMS and NEXAFS spectroscopy). *Surf. Interface Anal.* 40 (2008) 180-183.
- [12] C. Friedsam, A.D.C. Bécares, U. Jonas, M. Seitz, H.E. Gaub, Adsorption of polyacrylic acid on self-assembled monolayers investigated by single-molecule force spectroscopy. *New J. Phys.* 6 (2004).
- [13] R.A. Shimkunas, E. Robinson, R. Lam, S. Lu, X. Xu, X.-Q. Zhang, H. Huang, E. Osawa, D. Ho, Nanodiamond-insulin complexes as pH-dependent protein delivery vehicles. *Biomaterials* 30 (2009) 5720-5728.
- [14] M.R.H. Krebs, G.L. Devlin, A.M. Donald, Protein Particulates: Another Generic Form of Protein Aggregation? *Biophys. J.* 92 (2007) 1336-1342.
- [15] E.Y. Chi, S. Krishnan, T.W. Randolph, J.F. Carpenter, Physical Stability of Proteins in Aqueous Solution: Mechanism and Driving Forces in Nonnative Protein Aggregation. *Pharm. Res.* 20 (2003) 1325-1336.
- [16] A. Hawe, M. Wiggenhorn, M. van de Weert, J.H.O. Garbe, H.-c. Mahler, W. Jiskoot, Forced Degradation of Therapeutic Proteins. *J. Pharm. Sci.* 101 (2012) 895-913.
- [17] W.-C. Lin, S.-H. Lee, M. Karakachian, B.-Y. Yu, Y.-Y. Chen, Y.-C. Lin, C.-H. Kuo, J.-J. Shyue, Tuning the surface potential of gold substrates arbitrarily with self-assembled monolayers with mixed functional groups. *Phys. Chem. Chem. Phys.* 11 (2009) 6199-6204.
- [18] C.-H. Kuo, H.-Y. Chang, C.-P. Liu, S.-H. Lee, Y.-W. You, J.-J. Shyue, Effect of surface chemical composition on the surface potential and iso-electric point of silicon substrates modified with self-assembled monolayers. *Phys. Chem. Chem. Phys.* 13 (2011) 3649-3653.
- [19] C. Vericat, M.E. Vela, G. Benitez, P. Carro, R.C. Salvarezza, Self-assembled monolayers of thiols and dithiols on gold: new challenges for a well-known system. *Chem. Soc. Rev.* 39 (2009) 1805-1834.
- [20] J. Maciel, C.L. Martins, M.A. Barbosa, The stability of self-assembled monolayers with time and under biological conditions. *J. Biomed. Mater. Res.* 94A (2010) 833-843.
- [21] S.-H. Lee, W.-C. Lin, C.-H. Kuo, M. Karakachian, Y.-C. Lin, B.-Y. Yu, J.-J. Shyue, Photooxidation of Amine-Terminated Self-Assembled Monolayers on Gold. *J. Phys. Chem.* 114 (2010) 10512-10519.
- [22] J. Kim, P. Seidler, C. Fill, L.S. Wan, Investigations of the Effect of Curing Conditions on the Structure and Stability of Amino-Functionalized Organic Films on Silicon Substrates by Fourier-Transform Infrared Spectroscopy. *Surf. Sci.* 602 (2008) 3323-3330.
- [23] E.T. Vandenberg, L. Bertilsson, B. Liedberg, K. Uvdal, R. Erlandsson, H. Elwing, I. Lundström, Structure of 3-Aminopropyl Triethoxy Silane on Silicon Oxide. *J. Colloid Interface Sci.* 147 (1991) 103-118.
- [24] J.H. Hamman, A.F. Kotzé, Effect of the type of base and number of reaction steps on the degree of quaternization and molecular weight of N-trimethyl chitosan chloride. *Drug Dev. Ind. Pharm.* 27 (2011) 373-380.
- [25] S.M. Bal, Z. Ding, G.F.A. Kersten, W. Jiskoot, J.A. Bouwstra, Microneedle-Based Transcutaneous Immunisation in Mice with N-Trimethyl Chitosan Adjuvanted Diphtheria Toxoid Formulations. *Pharm. Res.* 27 (2010) 1837-1847.
- [26] K. van der Maaden, K. Sliedregt, A. Kros, W. Jiskoot, J. Bouwstra, Fluorescent Nanoparticle Adhesion Assay: a Novel Method for Surface pKa Determination of Self-Assembled Monolayers on Silicon Surfaces. *Langmuir* 28 (2012) 3403-3411.
- [27] K. van der Maaden, H. Yu, K. Sliedregt, R. Zwier, R. Lebourg, M. Oguri, A. Kros, W. Jiskoot, J.A. Bouwstra, Nanolayered chemical modification of silicon surfaces with ionizable surface groups for pH-triggered protein adsorption and release: application to microneedles. *J. Mater. Chem. B* 1 (2013) 4466-4477.

LAYER-BY-LAYER ASSEMBLY OF INACTIVATED POLIOVIRUS AND N-TRIMETHYL CHITOSAN ON PH-SENSITIVE MICRONEEDLES FOR DERMAL VACCINATION

Koen van der Maaden¹
Emine Sekerdag¹
Pim Schipper¹
Gideon Kersten^{1,2}
Wim Jiskoot¹
Joke Bouwstra¹

¹ Division of Drug Delivery
Technology, Leiden Academic
Centre for Drug Research
(LACDR), Leiden University

² Institute for Translational
Vaccinology (Intravacc)

Abstract

Purpose The aim of this work was to coat pH-sensitive microneedle arrays with inactivated polio vaccine (IPV) particles and N-trimethyl chitosan chloride (TMC) via electrostatic interactions, and assess the immunogenicity of the polyelectrolyte multi-nanolayer coating after topical application of the coated microneedles in rats.

Methods The surface of 200 µm long microneedles was first chemically modified with pH-sensitive (pyridine) groups and then coated with negatively charged IPV and a positively charged polymeric adjuvant (TMC). To obtain a sufficient high antigen dose, ten layers of IPV were alternately coated with TMC. The binding of IPV and TMC onto pH-sensitive microneedles was quantified and visualized by using fluorescently labeled TMC and IPV. The release of IPV and TMC from the microneedles was evaluated in *ex vivo* human skin by fluorescence and the immunogenicity was assessed after topical application of the coated microneedles in rats.

Results pH-sensitive microneedles were homogeneously coated with ten alternated layers of IPV and TMC, resulting in 45 DU IPV and 700 ng TMC per microneedle array. Fluorescence microscopy imaging revealed that both IPV and TMC were released into *ex vivo* human skin upon application of the coated microneedles. Finally, the *in vivo* application of IPV-TMC coated pH-sensitive microneedles in rats led to the induction of IPV specific antibody responses, showing the release and immunogenicity of the coating *in vivo*.

Conclusion Topical administration of pH-sensitive microneedles coated with polyelectrolyte multi-nanolayers of antigens and oppositely charged polymeric adjuvants may be a useful approach for microneedle-based vaccination.

1. Introduction

The skin is an attractive site for drug administration because the skin is easily accessible and dermal drug delivery is potentially pain free [1-3]. However, the top layer of the skin, the stratum corneum, is an impermeable barrier that keeps foreign entities, including drugs, from entering the skin. Therefore, several drug delivery systems and devices have been developed to overcome the stratum corneum barrier [4-7]. One of the promising systems are microneedles. Microneedles are needle-like structures that are no longer than 1 mm and are used to pierce the stratum corneum to facilitate the delivery of a drug into the skin. Microneedles should be long enough to pierce the stratum corneum, but preferably short enough to avoid bleeding and pain sensation. Microneedles have been under development for the past two decades for minimally-invasive dermal drug delivery [8-11].

Microneedles have been used by different approaches to deliver a drug into the skin, as reviewed elsewhere [8, 9]. One of these approaches is the ‘coat and poke’ approach. By this approach microneedles are first coated with a drug. These drug coated microneedles are subsequently used to pierce the skin. After piercing the coating is hydrated, leading to the release of the drug from the microneedles into the skin. An advantage of using coated microneedles is that they are a single-unit drug delivery system. Another benefit of using the ‘coat and poke’ approach is that after coating the strength of the microneedles is retained [8-10]. However, one major disadvantage of using coated microneedles is that only small amounts of drugs can be coated onto the microneedles. Therefore, this approach is only applicable to very potent drugs such as vaccines. Besides, to coat sufficient amounts of drugs, often thick layers are required as often surfactants and polymers are included in the coating formulation, which may result in a decrease in microneedle tip sharpness. This impairs the penetration ability of the microneedles into the skin [9, 12, 13].

During the past few years two different approaches have been developed to obtain ultrathin drug coatings in the nanometer range onto microneedles. The first approach is based on a nanolayered (< 20 nm) pH-sensitive surface modification that only minimally impairs the sharpness of atom sharp microneedles [14]. These pH-sensitive (pyridine-modified) microneedles were coated with ovalbumin at a pH value (5.8) that is below the pK_a (6.9) of pyridine surfaces and above the isoelectric point of ovalbumin (4.4). Upon application of these coated microneedles ovalbumin was efficiently released (70%) by a pH shift into *ex vivo* human skin (physiological pH of 7.4) [14]. The second approach is by using a layer-by-layer assembly to generate polyelectrolyte multi-nanolayers [15-17]. Polyelectrolyte multi-nanolayers are formed by alternately coating a negatively and positively charged compound onto microneedles. This approach has been used for the dermal delivery of DNA [16, 17], nanoparticles [15, 16], and proteins [17]. Combining these approaches can lead to ultrathin coatings to coat sufficient amounts of drugs onto the microneedle surface that are efficient release upon topical application while retaining the microneedle sharpness.

In this study we combined a layer-by-layer assembly with the previously reported pH-sensitive surface modification to coat silicon microneedle arrays. The surface of 200 μm long microneedles was first chemically modified with pH-sensitive (pyridine) groups that were subsequently coated with negatively charged inactivated polio vaccine (IPV) particles and a positively charged polymeric adjuvant, N-trimethyl chitosan chloride (TMC), by a layer-by-

layer approach. The release of IPV and TMC from the microneedles was evaluated in *ex vivo* human skin and the immunogenicity was assessed after topical application of the coated microneedles in rats.

2. Materials and methods

2.1 Preparation, characterization and quantification of TMC and IPV

TMC with a degree of quaternization of 18% and fluorescently labeled with rhodamine B ($TMC_{\text{rhod.B}}$) was synthesized as previously described [18]. In brief, 120 kDa chitosan (Primex) was methylated by iodomethane in the presence of NaOH and was labeled with rhodamine B isothiocyanate. Subsequently, $TMC_{\text{rhod.B}}$ was purified by dialysis and freeze dried. Plain IPV (serotype 1) and fluorescently labeled (Alexa Fluor® 488) IPV ($IPV_{\text{AF-488}}$), obtained from Intravacc, were used for immunization and visualization, respectively. Plain IPV, $IPV_{\text{AF-488}}$ and $TMC_{\text{rhod.B}}$ were quantified by measuring the fluorescence on a Tecan Infinite® M1000 plate reader. $TMC_{\text{rhod.B}}$ was excited at 550 nm and detected at 580 nm. Plain IPV was quantified by ELISA or intrinsic fluorescence (emission of 330 nm at an excitation wavelength of 280 nm) and $IPV_{\text{AF-488}}$ was excited at 488 nm and its emission detected at 522 nm. Plain IPV, $IPV_{\text{AF-488}}$ and $TMC_{\text{rhod.B}}$ were quantified by fluorescence by using a calibration curve that was linear between 100 ng/mL and 10 µg/mL for each of the compounds. To determine the antigenicity of IPV, the D-antigen (representing native polio particles) was analyzed by an enzyme-linked immunosorbent assay (ELISA) as previously described [19]. The samples were compared to a reference suspension (non-treated plain IPV) that was diluted to the same concentration as the samples. 1 DU IPV contains ~13 ng viral protein [20]. Finally, the zeta potential of plain IPV (0.5 mg/mL) in a 10 mM phosphate buffer at pH 5.8 was measured by laser Doppler electrophoresis on a Zetasizer Nano (Malvern Instruments).

2.2 Chemical modification of microneedles

The surface of microneedles (576 microneedles on a backplate of 5x5 mm, Robert Bosch GmbH) was chemically modified to obtain pH-sensitive microneedles (pyridine-modified) that have a surface pK_a of 6.9 [14]. First, the microneedle surface was hydroxylated by incubation with a freshly prepared piranha solution ($H_2SO_4:H_2O_2$ 7:3 (v/v)) for one hour at 120°C. Next, the microneedle surface was modified with amine groups by incubating the top side of the microneedle arrays with 15 µL of a 2% (v/v) APTES (Sigma Aldrich) solution in toluene at room temperature. To introduce surface roughness on the microneedles 0.1% (v/v) H_2O was added to the APTES solution. Furthermore, to prevent evaporation of the APTES solution, the microneedles were kept in a chamber wherein the air was saturated with toluene. After 24 hours the microneedles were cured for 30 minutes at 120°C and were incubated for two hours at 40°C in Milli-Q water to remove unreacted ethoxy groups, obtaining amine-modified microneedles. Subsequently, these amine-modified microneedles were incubated overnight in 100 mM 4-pyridinecarboxaldehyde (Sigma Aldrich) in anhydrous isopropanol at room temperature. Finally, to form a stable secondary amine, the microneedles were incubated in 50 mM sodium cyanoborohydride (Sigma Aldrich) in isopropanol for two hours. The obtained pH-sensitive, pyridine-modified microneedles were stored under vacuum until use.

2.3 Location of pH-sensitive groups on the microneedle surface

To assess whether the chemical (amine) modification was successful, a fluorescent dye was used that only reacts with primary amines. Therefore, 15 μL of 10 $\mu\text{g}/\text{mL}$ Alexa Fluor® 488 carboxylic acid succinimidyl ester (Invitrogen) in anhydrous acetonitrile was reacted to amine-modified microneedles in the dark for one hour at room temperature. Finally, the microneedles were washed twice with acetonitrile and five times with methanol to obtain fluorescent-modified microneedles.

To visualize the location of pH-sensitive (pyridine) surface groups, fluorescently labeled negatively charged nanoparticles (Sigma Aldrich) were coated onto the positively charged microneedle surface. To this end, pH-sensitive microneedles were incubated with 50 μL of a 1 $\mu\text{L}/\text{mL}$ sulfate-modified fluorescent red nanoparticle dispersion (2.5% solids) (Sigma Aldrich) in a 1 mM EDTA buffer at pH 5.8. At this pH value the pyridine groups are positively charged [14]. After one hour the microneedles were washed in 1 mL 1 mM EDTA buffer at pH 5.8, obtaining nanoparticle-coated pH-sensitive microneedles.

The fluorescent-modified microneedles and the nanoparticle-coated pH-sensitive microneedles were visualized by using fluorescence microscopy (Nikon Eclipse E600) and confocal laser scanning microscopy (CLSM) with a depth resolution of 1.05 μm on a Nikon Eclipse TE2000-U with a Bio-Rad Radiance 2100 confocal laser scanning system [14]. An argon laser (488 nm) was used for the visualization of fluorescent-modified microneedles with a 500 nm long pass emission filter and a helium neon laser (543 nm) was used to visualize nanoparticle-coated pH-sensitive microneedles with a 570 nm long pass emission filter. Non-modified microneedle arrays were imaged as a negative control.

2.4 Layer-by-layer coating of IPV and TMC onto microneedles

pH-sensitive microneedles were coated with either plain IPV or IPV_{AF-488} and TMC_{rhod.B} by a layer-by-layer approach. The layer-by-layer approach is based on electrostatic interactions between oppositely charged polyelectrolytes and was performed as schematically presented in figure 1. pH-sensitive (pyridine-modified) microneedle arrays were used (1). To obtain a positive surface charge onto the pH-sensitive microneedles, the coating was performed at pH 5.8 in a 1 mM EDTA buffer. The top side of the surface-modified microneedle arrays was coated

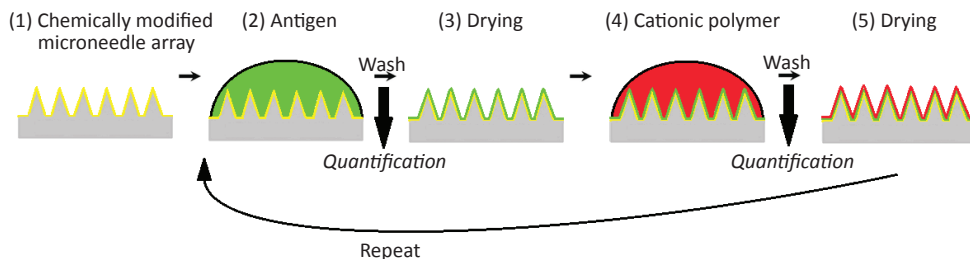


Figure 1: Schematic presentation of the layer-by-layer coating procedure of microneedles. The procedure starts by modifying the surface of microneedle arrays with pH-sensitive groups (1). Next, the microneedles are coated with a layer of plain IPV or IPV_{AF-488} (2) and are subsequently washed and dried (3). Then, the microneedles are coated with a layer of TMC_{rhod.B} (4), washed and dried (5). Steps 2-5 are performed ten times.

with a layer of IPV by incubating the microneedles with either 50 μ L of a 10 μ g/mL plain IPV or IPV_{AF-488} suspension (2). After one hour the microneedles were washed with 500 μ L 1 mM EDTA at pH 5.8. After the microneedles were dried under a stream of pressurized air (3), they were incubated for one hour with 50 μ L of a 10 μ g/mL TMC_{rhod.B} solution (4). Subsequently, the microneedles were washed and dried as described above (5). Steps 2-5 were performed ten times to obtain pH-sensitive microneedles coated with ten alternating layers of IPV (plain or fluorescently labeled) and TMC_{rhod.B}. The amount of IPV and TMC_{rhod.B} that bound onto the microneedle surface was quantified by measuring the unbound fraction of IPV and TMC_{rhod.B} in the wash samples.

2.5 Visualization of IPV-TMC layer-by-layer coated microneedles

To visualize the pH-sensitive TMC-IPV coated microneedle arrays CLSM was performed with a depth resolution of 5 μ m/step on a Nikon TE 2000-e with a 20x Plan APO objective. An argon laser (488 nm) was used for the visualization of IPV_{AF-488} with a 530/50 emission filter and a diode-pumped solid-state laser (561 nm) with a 590/50 emission filter was used for the visualization of TMC_{rhod.B}. Image acquisition and processing was performed by using NIS elements. Besides, the structure, geometry, and the surface morphology of the microneedle arrays were analyzed by using scanning electron microscopy (SEM) on a FEI NOVA nanoSEM 200.

2.6 Microneedle application onto ex vivo human skin

Ex vivo human skin was supplied by local hospitals within 24 hours after cosmetic surgery and was dermatomed to a thickness of 600 μ m [14]. Next, the skin was stretched on Styrofoam that was covered with parafilm. After the pH-sensitive IPV_{AF-488} - TMC_{rhod.B} coated microneedle arrays were attached onto the skin by using dermal tape (Leukosilk), an impact-insertion applicator [21] was used to pierce the microneedles into the skin at 3 m/s. After five minutes the microneedles were removed and the skin surface was visualized by fluorescence microscopy by using a GFP and Cy3 filter set for the visualization of IPV_{AF-488} and TMC_{rhod.B}, respectively. The IPV-TMC coating on the microneedles was examined by fluorescence microscopy before and after skin application. Besides, 10 μ m thick cryosections (Leica Cryostat) of the microneedle treated skin were made of which the nuclei were stained with VectaShield® mounting medium with DAPI (Vector Lab). Finally, the cross sections were visualized by fluorescence microscopy using a DAPI, GFP, and Cy3 filter set.

2.7 Immunization study

Female Wistar Han rats (10 per group, 175-250 g, Charles River) were immunized twice with intervals of three weeks by intramuscular injection with 5 DU plain IPV (corresponding with 65 ng viral protein) or PBS (100 μ L/hind leg), or by applying three plain IPV-TMC_{rhod.B} coated microneedle arrays (containing 45 DU IPV on the microneedles and backplate per array) for one minute on the ear pinna. Sera were collected 3 weeks after the boost immunization. Animals were maintained under standardized conditions in the animal facility of the Leiden Academic Centre for Drug Research, Leiden University. The study was carried out under the guidelines complied by the animal ethic committee of the Netherlands and was approved by

the “Dierexperimentencommissie Universiteit Leiden (UDEEC)” under number 12084.

2.8 IgG ELISA

To determine the D-antigen (representing native polio particles) and C-antigen (representing precursor or partially denatured polio particles) IPV-type-1 specific serum IgG responses, the sera of immunized rats were analyzed by ELISA as previously described [22]. Endpoint titers were determined by 4-parameter analysis using the Gen5™ 2.0 data analysis software (BioTek Instruments, Inc., Winooski, VT) and defined as the reciprocal of the serum dilution producing a signal identical to that of antibody-negative serum samples at the same dilution plus three times the standard deviation [20, 23].

3. Results and discussion

3.1 Charge of IPV at coating pH

In our previous study we have shown that coating of a model antigen (ovalbumin) onto pH-sensitive (pyridine-modified) microneedles was efficiently performed above its isoelectric point, at pH 5.8 [14]. The ζ -potential of plain IPV at the same pH value in 1 mM EDTA buffer was measured to verify whether these conditions may also be suitable for the coating of IPV onto pH-sensitive microneedles. The isoelectric point of IPV is unknown but likely lower than that of live poliovirus type 1 (6.2 [24]) since formaldehyde (used to inactivate the virus) reacts with amine groups. This is expected to result in a decrease of the isoelectric point of proteins by several pH units [25]. Indeed, laser Doppler electrophoresis performed at pH 5.8 revealed a ζ -potential of -7.75 ± 0.88 mV (mean \pm SD, $n=3$), demonstrating that the isoelectric point of IPV is below 5.8.

3.2 pH-dependent stability of IPV

Another requirement of pH-sensitive coatings is that the antigen's antigenicity should be retained at coating pH. Therefore, the pH-dependent stability of IPV was investigated, as reported in figure 2. Figure 2 shows that IPV was stable between pH 4 and 11 in a 1 mM EDTA buffer for at least one hour, indicating that IPV can be coated onto microneedles at a broad pH range. Only at pH 12, the highest pH tested, IPV completely lost its antigenicity.

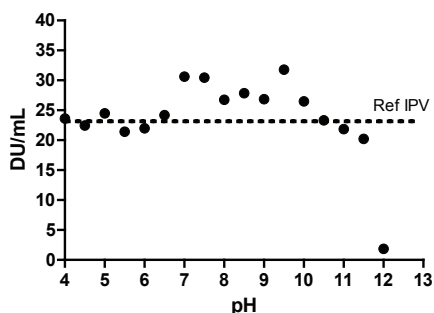


Figure 2: Stability of a 300 ng/mL IPV suspension (expressed as DU/ml) after it was incubated for one hour at different pH values in a 1 mL 1 mM EDTA buffer. The dotted line is the D-antigen concentration that was measured in the reference suspension.

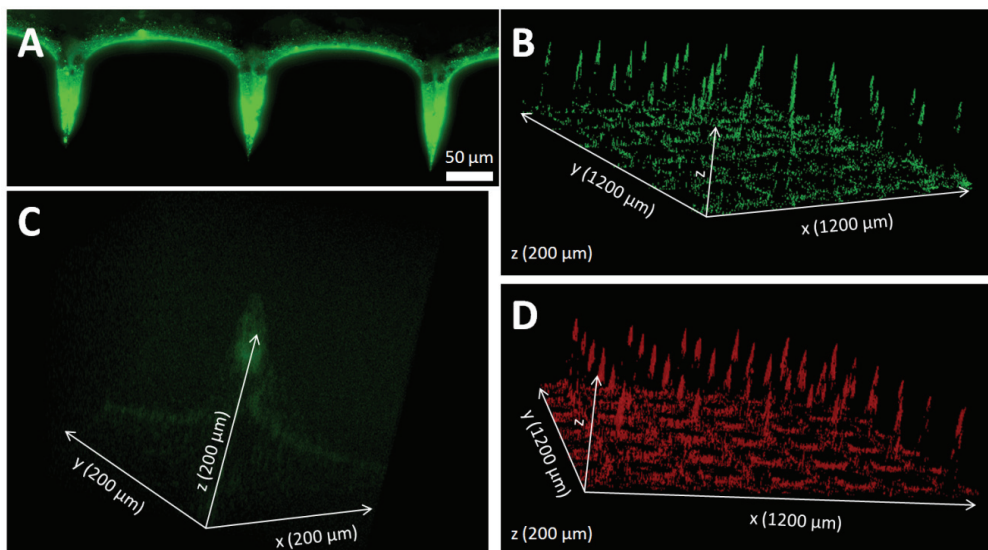


Figure 3: Representative fluorescence images of chemically modified microneedle arrays that contain 24x24 microneedles per array. An amine-modified microneedle array that was incubated with an amine-reactive fluorescent dye photographed by fluorescence microscopy from the side (A), confocal laser scanning microscopy (CLSM) of 6x6 microneedles (B) and zoomed in on the tip of a single microneedle (C). CLSM of a 100 nm nanoparticle-coated pH-sensitive microneedle array (D).

3.3 Location of pH-sensitive groups on the microneedle surface

Fluorescence imaging showed that the surface of amine-modified microneedle arrays (by APTES coupling), incubated with a fluorescent dye that only reacts with primary amines, was successfully modified with amine groups (figure 3A). Besides, CLSM revealed that the amine groups are mostly present on the tip of the microneedles (figure 3B and 3C), which could be explained because APTES tends to aggregate at the edges of surfaces [14]. No fluorescence was observed when non-modified microneedles were incubated with the amine-reactive fluorescent dye (data not shown).

To visualize whether the next step in the surface modification was successful, which is the introduction of pH-sensitive (pyridine) groups, fluorescently labeled negatively charged sulfate-modified fluorescent nanoparticles were coated onto the pH-sensitive microneedles at pH 5.8, a pH at which the surface pyridine groups are positively charged [14, 18]. The coated microneedles were visualized by CLSM (figure 3D). This figure shows that the pH-sensitive surface groups were mainly present on the tip of the microneedles. These results are in line with a previous study in which the surface of silicon microneedles with a different geometry were successfully modified with amine and pyridine groups [14]. This indicates that this modification procedure is a generic method for modifying the surface of silicon microneedle arrays.

3.4 Layer-by-layer coating of IPV and TMC onto microneedles

In order to coat pH-sensitive microneedles with a high dose of IPV, the microneedles were coated by a layer-by-layer approach. Since pH-sensitive microneedles are positively charged

at the coating pH (5.8), the first coating was performed with IPV (plain IPV or IPV_{AF-488}), which is negatively charged at this pH (see section 3.1). Subsequently, the IPV covered surface was coated with positively charged TMC_{rhod.B}. This alternated coating of IPV and TMC_{rhod.B} was performed ten times and between each coating step the amount of IPV and TMC_{rhod.B} was quantified, as shown in figure 4. There was a linear relationship between the number of layers and the amount of IPV (IPV_{AF-488}: R²=0.98; plain IPV (intrinsic fluorescence): R²=0.92; and plain IPV (ELISA): R²=0.98) and TMC_{rhod.B} (R²=0.97) that are coated onto the microneedle surface. Furthermore, figure 4 shows that IPV (as determined by intrinsic fluorescence and ELISA) and IPV_{AF-488} (as determined by the fluorescence of Alexa Fluor® 488) bound in a comparable manner onto the microneedle surface. However, the amount of plain IPV that was coated onto the microneedles as determined by ELISA was 25% lower compared to the amount as determined by the intrinsic fluorescence of IPV. This could indicate that 75% of the microneedle-coated IPV is the D-antigenic form. Finally, this figure shows that comparable amounts of IPV and TMC_{rhod.B} were coated onto the microneedles.

3.5 Visualization of IPV-TMC coated microneedles

The CLSM results shown in figure 5 demonstrate that both IPV (5A) and TMC (5B) were homogeneously coated (5C) onto the surface of pH-sensitive microneedle arrays by a layer-by-layer approach. Besides, SEM was used to visualize the microneedle geometry and the morphology of the coating, as shown in figure 6. This figure shows an overview of a part of a microneedle array that contains 576 microneedles on a backplate of 5x5 mm (6A) and increasingly zoomed-in pictures on the surface of a microneedle before (figure 6B1-6B3, respectively) and after coating (figure 6C1-6C3, respectively). The surface morphology was clearly changed from a smooth into a rougher one after it was coated with 10 layers of IPV alternated with TMC (figure 6C3) compared to non-modified microneedles (figure 6B3). Finally, this figure reveals that modification of microneedles with pH-sensitive groups and the subsequent coating thereof with ten layers of IPV alternated with TMC does not visibly impair microneedle sharpness. In contrast, coatings based on different procedures (e.g., multiple dip coating steps with highly viscous solvents) generally lead to thick coatings/reduced microneedle sharpness and thereby might compromise the penetration ability of microneedle arrays [12, 13]. Therefore, these results illustrate the advantage of coating procedures that are based on polyelectrolyte nanolayers and pH-sensitive electrostatic interactions.

3.6 Microneedle application onto *ex vivo* human skin

To determine whether the IPV-TMC multilayers can be released from the surface of pH-sensitive microneedles into the skin, the coated microneedle arrays were applied onto *ex vivo* human skin. As shown in figure 7, both IPV_{AF-488} (7A) and TMC_{rhod.B} (7B) were delivered into the skin in the conduits (C). Besides, hardly any fluorescence was visible on the tips of the microneedles after topical application (data not shown). However, we were unable to quantify the amount of IPV and TMC that was released from the microneedles into the skin (because of the auto fluorescence of the *ex vivo* human skin). To quantify the released amount of IPV and TMC into the skin, radioactively labeled analogues should be used [26]. To confirm that IPV_{AF-488} and TMC_{rhod.B} were indeed delivered into the skin rather than onto the stratum

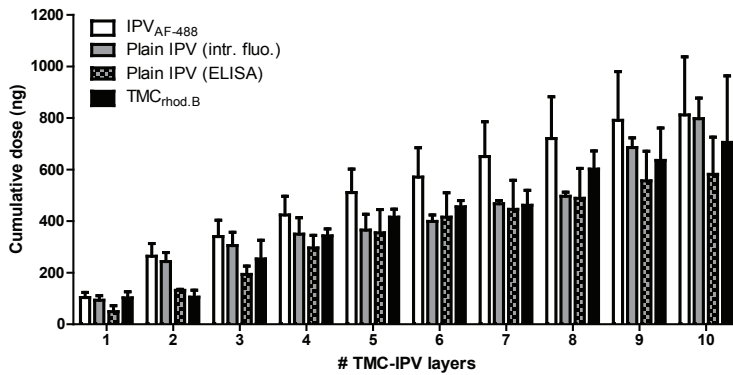


Figure 4: Cumulative dose of IPV and TMC during the coating of pH-sensitive microneedle arrays with IPV alternated with TMC. Each layer # consisted of one coating with either plain IPV or IPV_{AF-488} (negatively charged) and one coating with TMC_{rhod.B} (positively charged). Bars are represented as mean \pm SD, n=3.

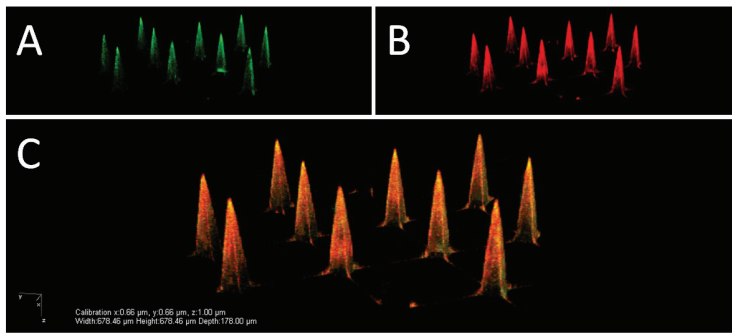


Figure 5: Representative CLSM images of pH-sensitive microneedles that were coated by a layer-by-layer approach with 10 layers of IPV alternated with TMC: IPV_{AF-488} (A), TMC_{rhod.B} (B), and an overlay of these images (C).

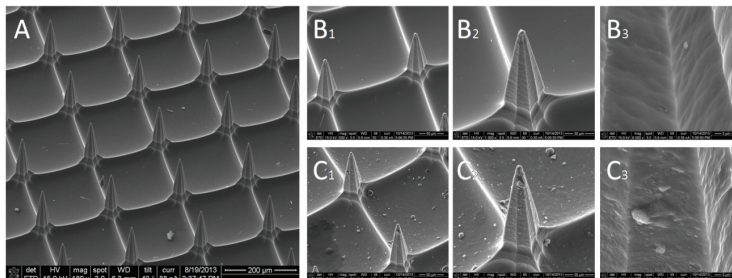


Figure 6: Representative SEM images of non-modified microneedles (A and B) and pH-sensitive microneedles coated with ten layers of IPV alternated with TMC (C) at a magnification of 500 (1), 1000 (2), and 8000 times (3).

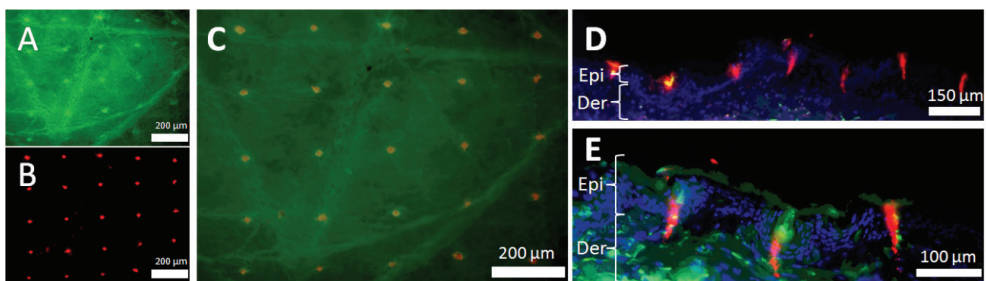


Figure 7: Representative fluorescence microscopy images of IPV-TMC-coated pH-sensitive microneedles that have been applied for 5 minutes onto *ex vivo* human skin. Images from the stratum corneum side of the skin with a GFP filter for IPV_{AF-488} (A) and a Cy3 filter for TMC_{rhod.B} (B) that are overlaid (C), and cross sections of the microneedle penetrated skin (D and E), showing IPV_{AF-488} (green), TMC_{rhod.B} (red) and DAPI stained nuclei (blue) in the epidermis (Epi) and dermis (Der).

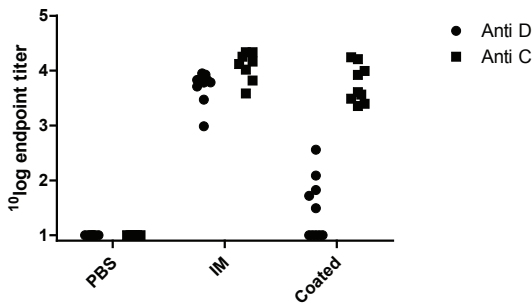


Figure 8: Inactivated poliovirus (IPV) type-1 specific serum IgG titers against C- and D-antigen upon immunization *via* coated microneedles or intramuscular (IM) injection. Non responders were given an arbitrary titer of 10.

corneum, cryosections of the pierced skin were made (7D and 7E). This figure shows that IPV and TMC were indeed successfully delivered into the skin, and that the delivery was both in the viable epidermis and in the top layer of the dermis. In conclusion, TMC-IPV multilayers are successfully released into *ex vivo* human skin within five minutes of microneedle application.

3.7 Immunization of rats with IPV-TMC coated microneedles

Two distinct antigenic forms of IPV exist: the C-antigen, which is expressed on non-infectious polio particles like some viral precursor forms as well as stressed virus or vaccine, and the D-antigen, which is expressed on native infectious polio virus [27]. The D-antigen of IPV is the immunorelevant structure, which is responsible for the induction of virus neutralizing antibodies upon immunization [19, 20]. To assess whether IPV-TMC coated pH-sensitive microneedles can be used for vaccination, an immunization study in rats was performed. Figure 8 shows that immunization of rats with plain IPV-TMC_{rhod.B} coated microneedles successfully led to the induction of IPV-specific antibody responses. Despite the low anti-D-antigen responses, this figure shows that using antigen-TMC coated microneedles can be used for vaccination because high and robust anti-C-antigen antibodies, similarly as compared to intramuscular immunization, were induced upon vaccination. However, the D-antigen antibodies upon immunization with coated microneedles were lower compared to intramuscular immunization, which could indicate that the D-antigen was partly converted into C-antigen during its coating onto the microneedle surface. This highlights the importance of choosing the proper antigen/stabilizing the antigen for coating pH-sensitive microneedles, e.g., IPV is very sensitive to surface induced degradation (if IPV is directly coated onto ELISA plates, it immediately converts into C-antigen). To retain the D-antigen during coating, IPV should be stabilized, e.g., by encapsulation into nanoparticles. Besides, our IPV stock also contained C-antigen, as indicated by the anti-C-antigen responses upon intramuscular immunization. This is atypical since C-antigen is being removed during the purification. Therefore, it is likely formed during longtime storage (the batch was expired for human use) and/or the coating process. D- to C-antigen conversion as a result of the coating procedure may occur easier in aged material. In addition, as coating of plain IPV determined by D-antigenicity was high, another explanation could be that the C-antigen is better released than the D-antigen (e.g., has a different charge). However, this coating method could be a suitable approach for microneedle-based vaccination when using a more stable antigen/stabilized antigen for antigen-TMC coated pH-sensitive microneedles.

4. Conclusion

Microneedles were successfully chemically modified with pyridine groups, which are mainly present on the tips of the microneedles. These pH-sensitive microneedles were coated at a pH value where IPV is negatively charged and the surface of microneedles is highly positively charged, enabling a good binding of IPV onto the surface. Furthermore, we have shown that ten layers of IPV alternated with TMC were successfully and homogeneously coated onto the surface of pH-sensitive microneedles and that this coating only minimally impairs microneedle sharpness. Besides, we have shown that IPV and TMC were released into the conduits formed after application of IPV-TMC coated pH-sensitive microneedles onto *ex vivo* human skin. Finally, the *in vivo* application of IPV-TMC coated pH-sensitive microneedles in rats led to the induction of both C- and D-antibody responses, the former non-inferior to intramuscular immunization, showing the release and immunogenicity of the coating *in vivo*.

Acknowledgements

We thank Dr. Michael Stumber (Robert Bosch GmbH) for the supply of microneedle arrays.

References

- [1] M.I. Haq, E. Smith, D.N. John, M. Kalavala, C. Edwards, A. Anstey, A. Morrissey, J.C. Birchall, Clinical administration of microneedles: skin puncture, pain and sensation. *Biomedical Microdevices* 11 (2009) 35-47.
- [2] S. Kaushik, A.H. Hord, D.D. Denson, D.V. McAllister, S. Smitra, M.G. Allen, M.R. Prausnitz, Lack of Pain Associated with Microfabricated Microneedles. *Anesthesia & Analgesia* 92 (2001) 502-504.
- [3] N. Roxhed, B. Samel, L. Nordquist, P. Griss, G. Stemme, Painless drug delivery through microneedle-based transdermal patches featuring active infusion. *IEEE transactions on bio-medical engineering* 55 (2008) 1063 - 1071.
- [4] A. Arora, M.R. Prausnitz, S. Mitragotri, micro-scale devices for transdermal drug delivery. *International Journal of Pharmaceutics* 364 (2008) 227-236.
- [5] A.K. Banga, Microporation applications for enhancing drug delivery. *Expert Opinion on Drug Delivery* 6 (2009) 343-354.
- [6] R.K. Subedi, S.Y. Oh, M.-K. Chun, H.-K. Choi, Recent Advances in Transdermal Drug Delivery. *Archives of Pharmacol Research* 33 (2010) 339-351.
- [7] A.M. Ball, K.M. Smith, Optimizing transdermal drug therapy. *American Journal of Health-System Pharmacy* 65 (2008) 1337-1346.
- [8] Y.-C. Kim, J.-H. Park, M.R. Prausnitz, Microneedles for drug and vaccine delivery. *Advanced Drug Delivery Reviews* 64 (2012) 1547-1568.
- [9] K. van der Maaden, W. Jiskoot, J. Bouwstra, Microneedle technologies for (trans)dermal drug and vaccine delivery. *Journal of Controlled Release* 161 (2012) 645-655.
- [10] M.R. Prausnitz, R. Langer, Transdermal drug delivery. *Nature Biotechnology* 26 (2008) 1261 - 1268
- [11] S. Henry, D.V. McAllister, M.G. Allen, M.R. Prausnitz, Microfabricated microneedles: a novel approach to transdermal drug delivery. *Journal of Pharmaceutical Sciences* 87 (1998) 922-925.
- [12] M. Ameri, P.E. Daddona, Y.-F. Maa, Demonstrated Solid-State Stability of Parathyroid Hormone PTH(1-34) Coated on a Novel Transdermal Microprojection Delivery System. *Pharmaceutical Research* 26 (2009) 2454-2463.
- [13] X. Chen, T.W. Prow, M.L. Crichton, D.W.K. Jenkins, M.S. Roberts, I.H. Frazer, G.J.P. Fernando, M.A.F. Kendall, Dry-coated microprojection array patches for targeted delivery of immunotherapeutics to the skin. *Journal of Controlled Release* 139 (2009) 212-220.
- [14] K. van der Maaden, H. Yu, K. Sliedregt, R. Zwier, R. Lebox, M. Oguri, A. Kros, W. Jiskoot, J.A. Bouwstra, Nanolayered chemical modification of silicon surfaces with ionizable surface groups for pH-triggered protein adsorption and release: application to microneedles. *Journal of Materials Chemistry B* 1 (2013) 4466-4477.
- [15] P.C. DeMuth, J.J. Moon, H. Suh, P.T. Hammond, D.J. Irvine, Releasable layer-by-layer assembly of stabilized lipid nanocapsules on microneedles for enhanced transcutaneous vaccine delivery. *ACS Nano* 6 (2012) 8041-8051.
- [16] P.C. DeMuth, X. Su, R.E. Samuel, P.T. Hammond, D.J. Irvine, Nano-Layered Microneedles for Transcutaneous Delivery of Polymer Nanoparticles and Plasmid DNA. *Advanced Materials* 22 (2010) 4851-4856.
- [17] E.M. Saurer, R.M. Flessner, S.P. Sullivan, M.R. Prausnitz, D.M. Lynn, Layer-by-Layer Assembly of DNA- and Protein-Containing Films on Microneedles for Drug Delivery to the Skin. *Biomacromolecules* 11 (2010) 3136-3143.
- [18] K. van der Maaden, J. Tomar, W. Jiskoot, J.

- Bouwstra, Chemical Modifications of Silicon Surfaces for the Generation of a Tunable Surface Isoelectric Point. *Langmuir* 30 (2014) 1812-1819.
- [19] G. Kersten, T. Hazendonk, C. Beuvery, Antigenic and immunogenic properties of inactivated polio vaccine made from Sabin strains. *Vaccine* 17 (1999) 2059-2066.
- [20] J. Westdijk, D. Brugmans, J. Martin, A. van't Oever, W.A.M. Bakker, L. Levels, G. Kersten, Characterization and standardization of Sabin based inactivated polio vaccine: Proposal for a new antigen unit for inactivated polio vaccines. *Vaccine* 29 (2011) 3390-3397.
- [21] F.J. Verbaan, S.M. Bal, D.J. van den Berg, J.A. Dijkman, M. van Hecke, H. Verpoorten, A. van den Berg, R. Luttge, J.A. Bouwstra, Improved piercing of microneedle arrays in dermatomed human skin by an impact insertion method. *Journal of Controlled Release* 128 (2008) 80-88.
- [22] K. van der Maaden, B. Trietsch, H. Kraan, E.M. Varypataki, S. Romeijn, R. Zwier, H. van der Linden, G. Kersten, T. Hankemeier, W. Jiskoot, J. Bouwstra, Novel hollow microneedle technology for depth controlled microinjection-mediated dermal vaccination: a study with polio vaccine in rats. *Pharmaceutical Research* 31 (2014) 1846-1854.
- [23] J. Westdijk, P. Koedam, M. Barro, B.P. Steil, N. Collin, T.S. Vedvick, W.A.M. Bakker, P. van der Ley, G. Kersten, Antigen sparing with adjuvanted inactivated polio vaccine based on Sabin strains. *Vaccine* 31 (2013) 1298-1304.
- [24] Y.E. Thomassen, G. van Eikenhorst, L.A. van der Pol, W.A.M. Bakker, Isoelectric point determination of live polioviruses by capillary isoelectric focusing with whole column imaging detection. *Analytical Chemistry* 85 (2013) 6089-6094.
- [25] V.K. Rait, T.J. O'Leary, J.T. Mason, Modeling formalin fixation and antigen retrieval with bovine pancreatic ribonuclease A: I-structural and functional alterations. *Laboratory Investigation* 84 (2004) 292-299.
- [26] K. van der Maaden, E.M. Varypataki, S. Romeijn, F. Ossendorp, W. Jiskoot, J. Bouwstra, Ovalbumin-coated pH-sensitive microneedle arrays effectively induce ovalbumin-specific antibody and T-cell responses in mice. *European Journal of Pharmaceutics and Biopharmaceutics* <http://dx.doi.org/10.1016/j.ejpb.2014.05.003> (2014).
- [27] M. Ferguson, D.J. Wood, P.D. Minor, Antigenic structure of poliovirus in inactivated vaccines. *Journal of General Virology* 74 (1993) 685-690.

CHAPTER 5

HOLLOW MICRONEEDLES

NOVEL HOLLOW MICRONEEDLE TECHNOLOGY FOR DEPTH CONTROLLED MICROINJECTION-MEDIATED DERMAL VACCINATION: A STUDY WITH POLIO VACCINE IN RATS

Koen van der Maaden^{1*}
Bas Trietsch^{2*}
Heleen Kraan³
Eleni Maria Varypataki¹
Stefan Romeijn¹
Raphäel Zwier⁴
Heiko van der Linden²
Gideon Kersten^{1,3}
Thomas Hankemeier²
Wim Jiskoot¹
Joke Bouwstra¹

Pharmaceutical Research, 31
(2014) 1846–1854

¹ Division of Drug Delivery
Technology, Leiden Academic
Centre for Drug Research
(LACDR), Leiden University

² Division of Analytical
Biosciences, Leiden Academic
Centre for Drug Research
(LACDR), Leiden University

³ Institute for Translational
Vaccinology (Intravacc)

⁴ Fine Mechanical
Department, Leiden Institute
of Physics (LION), Leiden
University

* Authors contributed equally

Abstract

Purpose The aim of the study was to develop a cheap and fast method to produce hollow microneedles and an applicator for injecting vaccines into the skin at a pre-defined depth and test the applicability of the system for dermal polio vaccination.

Methods Hollow microneedles were produced by hydrofluoric acid etching of fused silica capillaries. An electromagnetic applicator was developed to control the insertion speed (1–3 m/s), depth (0–1000 μm), and angle (10° – 90°). Hollow microneedles with an inner diameter of 20 μm were evaluated in *ex vivo* human skin and subsequently used to immunize rats with an inactivated poliovirus vaccine (IPV) by an intradermal microinjection of 9 μL at a depth of 300 μm and an insertion speed of 1 m/s. Rat sera were tested for IPV-specific IgG and virus-neutralizing antibodies.

Results Microneedles produced from fused silica capillaries were successfully inserted into the skin to a chosen depth, without clogging or breakage of the needles. Intradermal microinjection of IPV induced immune responses comparable to those elicited by conventional intramuscular immunization.

Conclusions We successfully developed a hollow microneedle technology for dermal vaccination that enables fundamental research on factors, such as volume, insertion depth, and insertion angle, on the immune response.

1. Introduction

Conventional vaccinations are performed by intramuscular or subcutaneous injections, causing pain and stress especially in toddlers and children. In addition, needlestick injuries and re-use of needles in developing countries carry the risk of transmitting biohazardous pathogens like hepatitis B and HIV. Because of the natural function of the skin, it is a highly immunologically active site. Therefore, it is not surprising that intradermal injections result in potent immune responses, but they are relatively difficult to perform and very painful [1]. Advances in microfabrication techniques are making intradermal injections using microneedles a feasible alternative to traditional injections. Microneedles can be used to only penetrate a shallow part of the skin (i.e. $< 300 \mu\text{m}$), thereby offering the possibility to deliver a vaccine into the epidermis or dermis, which is expected to yield a potent immune response. The minimally-invasive, potentially pain free nature and ease of the injections can reduce the risk of infections and alleviate the need for trained personnel [2-4].

One of the vaccines for which microneedle-based delivery would be advantageous is inactivated polio vaccine (IPV), as outlined below. Poliomyelitis, or polio, is a crippling and life-threatening disease that has been very effectively combated by widespread vaccination [5]. The majority of the vaccinations that helped to largely eradicate this disease have been performed using the oral polio vaccine (OPV) [6]. While very effective and easy to administer, this live attenuated vaccine can in rare cases revert to a pathogenic form and cause vaccine-associated paralytic poliomyelitis [7]. With reduced incidence of wild poliomyelitis and the associated change in risk/benefit considerations, the use of IPV has become the vaccination method of choice [8, 9]. While being a safer vaccine, IPV cannot be administered orally but is usually delivered using intramuscular or subcutaneous injection. Because of the widespread use of injected polio vaccines, switching to microneedles for less-invasive injections could benefit a large population by reducing infection risk and pain. Additionally, alleviating the need for trained personnel and dose sparing injections could reduce the costs of large vaccination programs [10, 11].

Among the available microneedles, hollow microneedles are especially attractive because the dose and the rate of drug delivery is controlled and there is no or limited need to reformulate the vaccine [2]. Hollow microneedles are commonly produced by pulling heated glass capillaries, using micromachining, or using microfabrication technologies on silicon wafers [12-15]. Pulled capillaries, however, may suffer from a low reproducibility in tip shape, low throughput production process and clogging problems because of a narrowing inner diameter towards the tip. While silicon needles can alleviate many of these problems, their production is complex and prohibitively expensive for routine use.

In this paper we present a novel microneedle fabrication method based on wet etching of capillaries that is cheap and easy to scale up. Batchwise fabrication of 100 microneedles can be performed in a lab without specialized equipment and the process can easily be adapted to the production of larger batches or even to a continuous process. The microneedles have a constant inner diameter, preventing clogging, and a tip shape that can be tuned with the

etch time. To ensure controlled and reproducible injection, we present a novel microneedle applicator. The penetration depth can be adjusted as well as the angle of insertion, the injection speed and time. We demonstrate reproducible injections in human skin *in vitro* and successful intradermal vaccination of rats with IPV using these hollow microneedles in combination with the applicator. This minimally-invasive, potentially pain free vaccination method resulted in a similar immune response as conventional intramuscular vaccination, showing the potential of etched microneedles for intradermal vaccination.

2. Materials and methods

2.1 Production of microneedles

Polyimide coated fused silica capillaries (Polymicro, Phoenix AZ, USA, 375 μm outer diameter, 20 μm inner diameter) were wet etched into microneedles. First, the lumen of the capillaries was filled with silicone oil AK350 (Boom Chemicals, Meppel, the Netherlands) to protect the inside of the capillary from the etchant. Subsequently, to etch the capillaries into microneedles, batches of up to 81 capillaries were mounted in a holder with one end suspended in 49% (w/w) HF, as shown in figure 1. The length of the capillary that is immersed in HF could be adjusted by the level of HF in the container as well as by the position of the screws of the holder during mounting. The shape of the microneedle tip was investigated as a function of etching time up to 30 hours. The microneedles chosen for the intradermal injections were etched for 4 hours. In order to connect the microneedles to the applicator, the sharp capillaries were glued into Luer adapters using medical grade glue (Loctite M-31 CL, Henkel, Düsseldorf, Germany). Luer adapters were acquired by removing the needle from Microlance® 26G hypodermic needles (BD, Franklin Lakes, NJ, USA). Finally, the polyimide coating was removed from the microneedles by submersion of the etched capillaries into hot sulfuric acid (96-98%, Boom chemicals, Meppel, the Netherlands) for 5 min at 200°C, and the silicone oil was removed by flushing the microneedles with acetone.

To assess the reproducibility of the tip shape, the tip angle of 55 microneedles with 20 μm inner diameter was measured after 4 hours etching. Image analysis was performed using ImageJ (available from rsbweb.nih.gov/ij/).

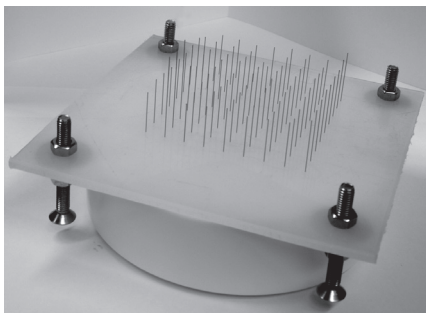


Figure 1: A batch of 81 fused silica capillaries mounted in a polyethylene holder and placed over a Teflon container with 49% HF. All needles are etched simultaneously by immersion in 49% HF. Immersion depth can be adjusted by the HF level in the container and the screw positions of the holder during mounting.

2.2 Microneedle applicator

In order to enable insertion of the microneedles into the skin to a controlled depth in a reproducible way, an applicator for hollow microneedles was developed. The flexibility of the skin can hamper skin penetration and reduce the depth accuracy of injections. The insertion speed, insertion depth, and angle of insertion are important factors to overcome this and achieve successful depth controlled penetration and drug delivery. As shown in figure 2, the applicator uses an electromagnet (a) to insert the microneedle mounted on the Luer connection (c) into the skin. The electromagnet is actuated using a controllable power source. Application of a variable current through the electromagnet allows for a tuned insertion speed from 1-3 m/s [16]. Furthermore, the controlled power supply regulates the wear time, to accurately and reproducibly control the time the microneedle is kept inside the skin. For injection, the skin is placed on a platform positioned below the injector (g). The penetration depth is controlled by a guide-plate (d) that can be adjusted with a micrometer actuator (b). The position of the guide-plate is adjusted so that the microneedle protrudes the desired distance through the hole in the plateau when the electromagnet is actuated. Before injection the injector is lowered so the guide-plate rests on top of the skin. Upon actuation the needle is inserted into the skin at the desired speed and depth, as controlled by the current and plateau position. Additionally the entire applicator can be tilted along a graduated rail (e) for angled insertion (10° - 90° relative to the skin). Insertion at a shallow angle can be used to insert a greater length of the needle into the skin, without penetration into deeper skin layers. The hollow microneedles were attached to a syringe pump that was equipped with a gas tight Luer lock 100 μ L syringe and connected to a fused silica capillary with a diameter of 100 μ m (f) to allow tuning of the liquid delivery rate.

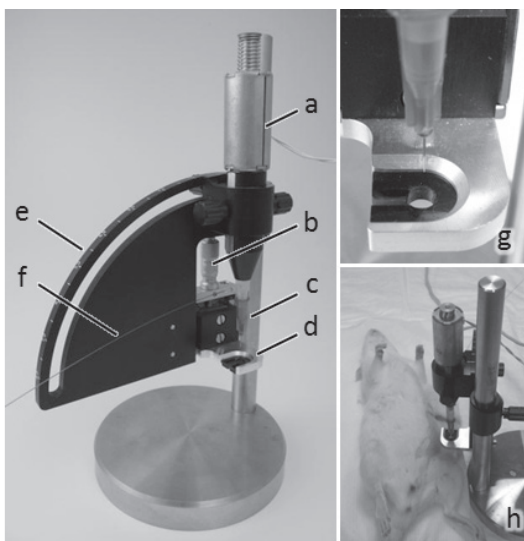


Figure 2: A microneedle applicator was developed using an electromagnet (a) to insert a microneedle (c) into the skin at controlled speed. A micrometer actuator (b) is used to adjust the level of a guide-plate (d) to ensure proper positioning and penetration depth of the microneedle. A graduated rail (e) can be used to tilt the entire applicator for angled insertion. The microneedle is connected to a syringe pump with a capillary (f) for vaccine delivery. Close-up of the guide-plate with a through hole for the needle (g). Microneedle applicator injecting a vaccine into the skin of an anesthetized rat (h).

2.3 Determination of microneedle insertion depth

To determine the microneedle insertion depth, fluorescently labeled human skin was used. *Ex vivo* abdominal or mammary human skin, which was obtained within 24 h after cosmetic surgery, was dermatomed to a thickness of 1200 μm using a Padgett Electro Dermatome Model B (Kansas City, MO, USA) after the fat was removed. The dermatomed skin was incubated overnight on filter paper soaked with 10 $\mu\text{g}/\text{mL}$ fluorescein (Fluka®, Sigma-Aldrich, Steinheim, Germany) with the stratum corneum side to the surface in a Petri dish at 4°C. Before the skin was used for experiments, it was stretched on a piece of expanded polystyrene covered with parafilm, and thereafter the surface of the skin was cleaned 3 times with phosphate buffered saline (PBS) (Braun, Melsungen, Germany, pH 7.4, 163.9 mM Na⁺, 140.3 mM Cl⁻, 8.7 mM HPO₄²⁻, and H₂PO₄⁻). Subsequently, a microneedle was connected to the Luer connection on the microneedle applicator (figure 2c) and the micrometer actuator (figure 2d) was adjusted to a chosen depth up to 400 μm . In order to accurately set the insertion depth, the microneedle position was calibrated. First, the electromagnet was actuated and the microneedle was positioned to be flush with the plateau using the micrometer actuator (figure 2a). This was done by laser alignment, by which a laser was put perpendicular to the guide-plate of the applicator (figure 2d). When a microneedle protrudes past the guide-plate the laser light is scattered at the tip of the microneedle, therefore the needle was determined to be flush with the guide-plate at the point where no light scattering was observed at the microneedle tip. After this calibration of the microneedle position, the microneedle actuator was adjusted to a depth of 100, 200, 300, or 400 μm , and was subsequently pierced into the fluorescently labeled human skin. For each chosen depth 3 microneedles were used to pierce the skin and each microneedle stayed in the skin for 5 s. After the microneedles had pierced the fluorescently labeled skin, the microneedles were analyzed by bright-field microscopy and by fluorescence microscopy (Nikon Eclipse E600, mercury light source, GFP filter set) at 100x magnification and imaged with a 1 s exposure time. Subsequently, the bright-field and fluorescence microscopy images were overlaid in ImageJ, and the insertion depth was expressed as the measured length between the tip of the microneedle and the part up to where the fluorescence was visible.

2.4 Microinjection into skin

To visualize the intradermal injections, a 10 $\mu\text{g}/\text{mL}$ fluorescein solution in PBS was injected into human *ex vivo* skin at different depths (100-400 μm). The skin was stretched on Styrofoam covered with parafilm, and the injection depth was adjusted as described above. The microneedle was connected to a syringe pump with a flow rate of 2 $\mu\text{L}/\text{min}$ to deliver 3 μL of the fluorescein solution. As a negative control 3 μL of the fluorescein solution was dispensed on top of the skin. Furthermore, diffusion of the injected compound into surrounding tissue was assessed by imaging the fluorescence in the skin at several time points after injection. The fluorescence was imaged using a Microsoft Lifecam HD with a 480±5 nm light source

(LED, Conrad) and a 520-540 nm band pass interference filter.

To confirm that microneedle insertion leads to dermal delivery of the injectable, microinjections of 0.4% trypan blue (Sigma) into *ex vivo* skin were performed at a protrusion depth of 300 μm . Microneedles were inserted into either human or rat skin and subsequently a microinjection of respectively 0.5 μL or 3 μL was performed. Next, 10 μm thick cryosections (Leica Cryostat) of the injected human skin and 5 μm thick cryosections of rat skin were made. Subsequently, the cryosections were stained by hematoxylin and eosin (H&E). Finally, the skin was photographed under a stereo microscope (Zeiss Stemi 2000-c) at a magnification of 5x.

2.5 Immunization

To examine the applicability of the hollow microneedles for vaccination purposes, a comparison was made between vaccination of rats by intradermal injection with microneedles, and intradermal and intramuscular injection with a conventional needle.

Female Wistar Han rats (175-250 g) were obtained from Charles River (Maastricht, the Netherlands) and were maintained under standardized conditions in the animal facility of the Leiden Academic Centre for Drug Research, Leiden University. The study was carried out under the guidelines compiled by the animal ethic committee of the Netherlands and was approved by the “Dierexperimentencommissie Universiteit Leiden (UDEEC)” under number 12084. Rats (10 per group) were immunized with either 5 or 15 DU (1/8th and 3/8th human dose, respectively) IPV-type-1 (1 DU \approx 13 ng virus protein) [17] intradermally by hollow microneedles at an protrusion depth of 300 μm and a flow speed of 2 $\mu\text{L}/\text{min}$ for 4.5 minutes. For comparison, rats were immunized with 5 DU IPV/50 μL intradermally on the ventral abdominal skin with a 30G needle and with 5 DU IPV/200 μL intramuscularly with a 26G needle (100 $\mu\text{L}/\text{hind leg}$). As a negative control rats were injected intramuscularly with 200 μL PBS (100 $\mu\text{L}/\text{leg}$). All rats were anesthetized during the immunization with 50 mg/kg ketamine (Nimatek® (100 mg/mL ketamine, Eurovet Animal Health B.V., Bladel, the Netherlands)) and 5 mg/kg xylazine (Rompun® (20 mg/mL xylazine, Bayer B.V., Mijdrecht, the Netherlands)) by intraperitoneal injection. Three weeks after immunization blood samples were collected and the rats were sacrificed. This immunization scheme is identical to the regular IPV potency assay [18].

2.6 IgG ELISA

Polystyrene 96 wells microtiter plates (Greiner Bio-One, Alphen a/d Rijn, the Netherlands) were coated overnight at 4°C with bovine anti-poliovirus type 1 serum (RIVM, Bilthoven, The Netherlands) in PBS pH 7.2 (Gibco from Invitrogen, Paisley, UK). After washing with 0.05% Tween 80 (Merck, Darmstadt, Germany) in tap water, 100 $\mu\text{L}/\text{well}$ monovalent IPV vaccine type 1 (4.5 DU/well) diluted in assay buffer, PBS containing 0.5% (w/v) Protifar (Nutricia, Zoetermeer, the Netherlands) and 0.05% (v/v) Tween 80 (Merck, Darmstadt, Germany), was added. After incubation at 37°C for 2 hours, threefold dilutions of sera samples in assay buffer were added

(100 $\mu\text{L}/\text{well}$) and incubated at 37°C for 2 hours. After washing, plates were subsequently incubated at 37°C for 1 hour with horseradish peroxidase (HRP)-conjugated goat-anti-rat IgG (Southern Biotech, Birmingham, AL) as detection antibody (4000 fold dilution, 100 $\mu\text{L}/\text{well}$). Plates were extensively washed and 100 $\mu\text{L}/\text{well}$ TMB substrate solution, containing 1.1 M sodium acetate (NVI, Bilthoven, the Netherlands), 100 mg/mL 3,3',5,5'-tetramethylbenzidine (Sigma-Aldrich, St. Louis, MO), and 0.006% (v/v) hydrogen peroxide (Merck, Darmstadt, Germany), was added. After 10-15 minutes, the reaction was stopped with 100 $\mu\text{L}/\text{well}$ 2 M H_2SO_4 (NVI, Bilthoven, the Netherlands) and absorbance was measured at 450 nm by using a Biotek L808 plate reader.

Endpoint titers were determined by 4-parameter analysis using the Gen5™ 2.0 data analysis software (BioTek Instruments, Inc., Winooski, VT) and defined as the reciprocal of the serum dilution producing a signal identical to that of antibody-negative serum samples at the same dilution plus three times the standard deviation [17, 19].

2.7 Virus neutralizing antibodies

Virus neutralizing (VN) antibodies against poliovirus type 1 were measured as described elsewhere [19]. In brief, the sera were inactivated at 56°C for 30 min prior to testing, of which 2 fold serial dilutions were made (2^1 to 2^{24}). These dilutions were incubated with 100 cell culture infectious dose 50% (CCID50) of wild type poliovirus type 1 (Mahoney) for 3 hours at 36°C and 5% CO_2 , and the resulting mixtures were subsequently used to inoculate $1 \cdot 10^4$ Vero cells. Virus-neutralizing antibody titers were determined after 7 days by staining the cells with crystal violet and expressed as the last serial dilution with an intact monolayer.

2.8 Statistical analysis

The statistical analysis was performed using Prism 5 for Windows, where the mean \pm SEM ($n=10$) of the IgG and VN titers were calculated. As our data was not-normally distributed, Kruskal-Wallis tests with a Dunns post-hoc test were performed to calculate the statistical significance.

3. Results and discussion

3.1 Production of microneedles: Influence of etch time

The microneedle geometry was observed to be dependent on etch time. The representative different tip shapes that were obtained after 1, 2, 4, 9, 22 and 29 hours of etching ($n=3$) are depicted in figure 3. Less than four hours of etching resulted in blunt needles with strong etching of the lumen of the capillary. Etch times between 4 and 22 hours resulted in increasingly long, thin needles of up to 4 cm. Longer etching resulted in fully dissolving extended portions of the capillary, leaving a short microneedle with an irreproducible tip shape.

When using a constant etch time reproducibly shaped microneedles were obtained.

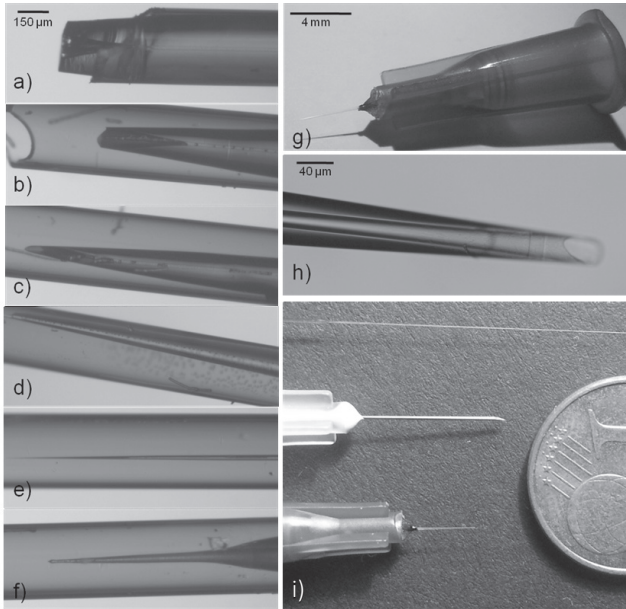


Figure 3: Representative images of the influence of etch time on the tip shape of hollow microneedles etched from capillaries after 1, 2, 4, 9, 22, 29 hours all taken at the same magnification (a-f, respectively); a capillary etched for 4 hours mounted into a Luer hub after removal of the polyimide sleeve, used for dermal drug delivery (g); a typical needle tip opening of microneedles after 4 hours of etching (h); a typical hollow microneedle etched for 22 hours next to a standard 30G needle, a microneedle etched for 4 hours, and a 1 eurocent coin (i).

After 4 hours of etching, microneedles with a tip angle of $15.0^{\circ} \pm 2.8^{\circ}$ were obtained (mean \pm SD of 55 microneedles, see supplementary information, figure S1, for angle distribution).

The observed lumen shapes are caused by displacement of the silicone oil. At the start of etching a small amount of HF is sucked into the lumen by capillary force, etching a short length from the inside. After 4 hours this portion is fully etched away, leaving only the part of the capillary that was protected from inside etching (figure 3c, h).

The outer shape of the needle can be explained by the interaction between the HF and the polyimide coating. The coating is slightly permeable to HF. When HF permeates through the coating it slowly etches the fused silica and delaminates the coating and the fused silica. When the coating is separated from the capillary, HF is sucked in between by capillary force. This HF results in the strong etching that determines the final tip shape. As HF supply through the coating is small, mass transport by diffusion from the tip is limiting the etch rate, resulting in slower etching further away from the tip. This gradient in etch rate results in the sharp tip of the microneedle.

Gluing the microneedles into Luer adapters resulted in needles that can be used and connected with the ease of conventional needles (figure 3g).

The relatively short needles obtained by 4 hours of etching were most suitable for injection into the skin because of their rigidity and robustness. While not suitable for injections into the skin, the extremely long needles can be useful for other applications. The ultra-high aspect ratio of these needles (4 cm long, 20 μ m tip diameter, figure 3i) could be very useful for deep penetration into soft fragile tissue, e.g., for intracerebral injections.

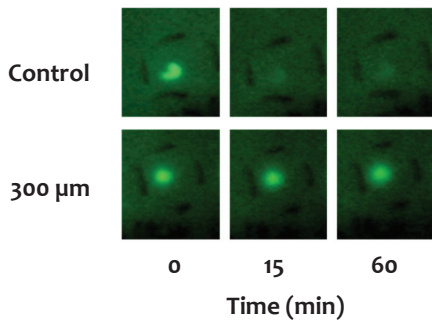
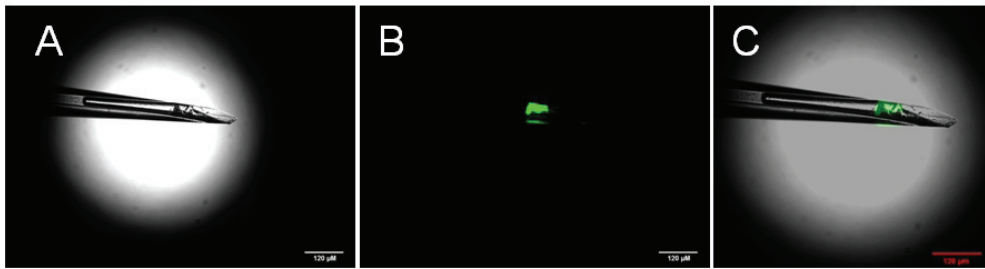


Figure 5: Fluorescence visualization of fluorescein microinjections into *ex vivo* human skin. Control injections (fluorescein dispensed on top of the skin) result in solvent evaporation over time and, consequently, loss of fluorescence, while 300 μm deep injections show no leakage and loss off fluorescence, but prolonged fluorescence inside the skin.

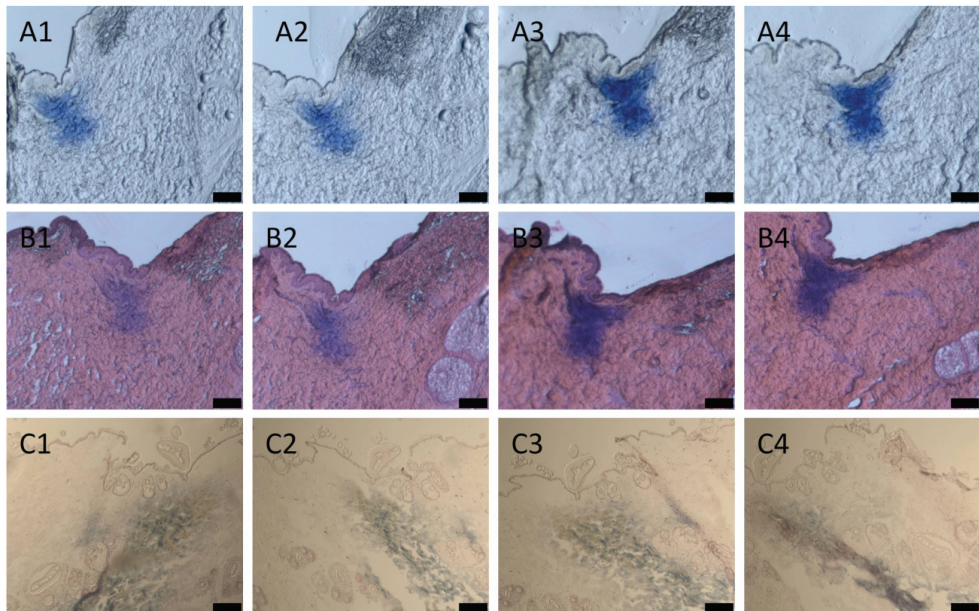


Figure 6: Representative microinjections of trypan blue solution into *ex vivo* skin. Four subsequent 10 μm thick cryosections following a 0.5 μL microinjection into *ex vivo* human skin before (A) and after hematoxylin and eosin (H&E) staining (B). Four subsequent 5 μm thick H&E stained cryosections following a 3 μL microinjection into *ex vivo* rat skin (C). The scale bar is 0.2 mm.

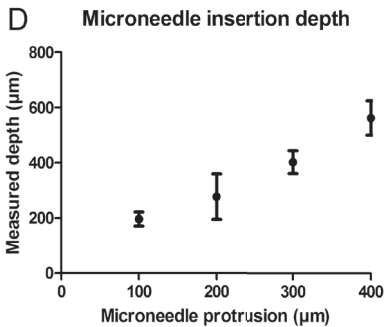


Figure 4: Determination of the depth of microneedle insertion. After hollow microneedles were pierced into fluorescein labeled human skin, one picture of the hollow microneedle was taken by using bright-field microscopy (A), and another picture on the same position was taken by fluorescence microscopy (B). Subsequently, the bright-field and fluorescence microscopy pictures were overlaid (C) from which the depth of microneedle insertion was measured and plotted against the length of the microneedle protruding below the guide-plate (D). Each point in panel D represents the average (\pm SD) of three individual microneedle insertions.

3.2 Applicator

Microneedle applicators are needed for controlled and reproducible microneedle application and reduce the required insertion forces to pierce the stratum corneum for both solid and hollow microneedles [1, 2, 16, 20-24]. The microneedle applicator used in this work was designed for *in-* and *ex vivo* microinjections with easily adjustable insertion speed, depth, angle, and flow rate. Robust performance was observed, i.e., at an insertion speed of 1 m/s no damage of the needles was observed.

In order to construct the system to be completely air free, gas tight syringes and Luer lock connections combined with pressure resistant fused silica tubing were used. This enables constant flow generation at high pressures. As such, the system could be used at relatively high flow rates without using hyaluronidase (2 μ L/min, as compared to literature values of single microneedle injections of 50-300 nL/min) [21, 25, 26]. Flow rates of other systems described in the literature might have been limited by the maximum applicable pressure in systems using common flexible tubing and different pump types [12, 15, 21, 25, 27, 28].

The full tunability of the device is very valuable in a research setting, where varying injections into different skin types and layers are required, e.g., to examine the immune responses as a function of the microneedle insertion depth or injection volume. Whilst completely compatible with use for intradermal microinjections in *in vivo* arms of humans, the freestanding setup of the device is particularly suitable for use in animal studies, as it allows for easy handling of the animals. When used for vaccination of humans, a much simpler applicator with a fixed insertion speed and angle could easily be envisioned. Using a spring loaded, fixed angle applicator would result in a hand held device suitable for a clinical setting.

3.3 Determination of microneedle insertion depth

It is important to control the depth of hollow microneedle insertion into the skin, since this defines whether or not the microneedle injection causes pain and/or bleedings. Fig. 4a-c depicts micrographs of microneedles after insertion into fluorescently labeled *ex vivo* human skin with a velocity of 1 m/s. The distance between the fluorescent dye transferred from the skin and the tip of the needle was used to measure penetration depth. Figure 4d shows that the measured microneedle insertion depth was on average 110 ± 36 μ m (mean \pm SD,

n=4) deeper than the length of the microneedle protruding past the guide-plate. This offset towards a deeper microneedle insertion than the aimed depth could be due to the pressure that is applied by the microneedle applicator guide-plate onto the skin, causing the skin to bulge into the opening in the plateau (figure 2G). However, when corrected for this offset, this applicator for hollow microneedles enables us to accurately and reproducibly insert a microneedle into the skin at a predetermined depth. A linear correlation ($R^2=0.979$) between the protrusion length and insertion depth was observed with an average RSD of 16%. The shown depth accuracy is sufficient to selectively inject into the dermis in rats and would allow for even more control in the relatively thick human skin. In addition to the presented results, strain measurements during insertion could be considered for subsequent research to judge the penetration into the different layers of the skin.

3.4 Microinjection into skin

Intradermal injections were visualized by injection of 3 μL fluorescein at a flow speed of 2 $\mu\text{L}/\text{min}$ into *ex vivo* human skin. Successful injections were observed at all the injection depths that were tested (100-400 μm). As depicted in figure 5, fluorescence from the injected fluorescein was observed below the surface of the skin. No leakage was observed and fluorescence was maintained for prolonged periods of time. The negative control of fluorescein dispensed on top of the skin showed fast evaporation of the solvent, causing rapid loss of fluorescence intensity. No significant difference in fluorescence intensity between penetration depths from 100-400 μm was observed in the skin (data not shown). Furthermore, no clogging of the microneedles was observed even when the microneedles were used for multiple injections.

To determine whether microneedle insertion leads to dermal delivery of the injectable, microinjections into *ex vivo* skin were performed and the injected site was visualized as shown in figure 6. After a microneedle was inserted into *ex vivo* human skin at a protrusion depth of 300 μm , a microinjection of 0.5 μL 0.4% trypan blue was performed. Four subsequent 10 μm thick cryosections of the injected skin before (6A) and after (6B) H&E staining show that the microinjections are indeed inside the dermis. Furthermore, a microinjection into *ex vivo* rat skin of 3 μL at a protrusion depth of 300 μm also led to the delivery of the injectable into the dermis (6C). Figure 6C shows that trypan blue diffused deep inside the dermis when a volume as large as 3 μL was injected.

3.5 Immunization study

In order to test the applicability of the hollow microneedles for dermal vaccination, rats were immunized with IPV serotype 1. The resulting antibody titers are shown in figure 7. This figure shows that the serum IgG responses after the (intradermal) microinjections with hollow microneedles at a protrusion depth of 300 μm are comparable with those after conventional intramuscular immunization and intradermal immunization, and were comparable to IgG responses found in the literature after a single intramuscular immunization with 5 DU IPV

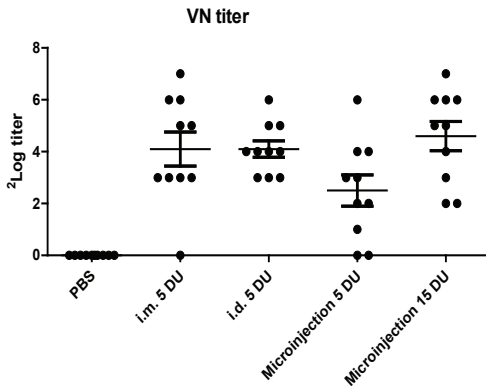


Figure 8: Serum polio-virus neutralizing (VN) antibodies responses after immunization with PBS or 5 DU inactivated poliovirus serotype 1 intramuscularly (i.m.), intradermally (i.d.), or intradermally *via* hollow microneedles with a microinjection of 9 μ L containing either 5 or 15 DU IPV.

type 1 [17]. Furthermore, a higher dose IPV (15 DU) delivered by a microinjection of 9 μ L appeared to slightly increase the IgG response as compared to a 5 DU microinjection, but the difference was not statistically significant. Furthermore, no significant differences were observed between the IgG titers of the microneedle injection groups and the intramuscular and intradermal groups.

Besides the serum IgG responses, the rat sera were analyzed for VN antibodies, as shown in figure 8. Despite the slightly lower VN titers of rats intradermally immunized with a microinjection of 5 DU, compared to conventional intramuscular or intradermal immunization, this difference was not significant. The lower VN titer of the microinjection might be caused by reduced damage of the skin compared to intradermal injection, where the needle is much thicker, is injected at a greater depth, and a larger volume is injected. This intrinsic effect of less invasive injections might be overcome by adding an adjuvant to the IPV suspension [1, 19]. Furthermore, the immune responses by intradermal injection might be higher than by intramuscular injection after booster immunizations, since intradermal immunization can lead to accelerated booster responses [11]. Therefore, in future experiments the insertion depth (50-1000 μ m), the volume effect (3-50 μ L), and the booster effect (up to 3 immunizations) should be evaluated. However, a higher dose of IPV by microinjections led to VN titers comparable to intradermal and intramuscular immunization. Therefore, these data show the applicability of microneedles to successfully induce VN antibodies against polio-virus.

4. Conclusion

Microneedles were fabricated by using a novel cheap and scalable wet etching method that can be employed in a laboratory setting or modified for commercial fabrication. The microneedles were used with a custom-made microneedle applicator for successful depth-controlled intradermal microinjections into human and rat skin. Intradermal microinjection of IPV in rats showed comparable IgG responses to conventional intramuscular injections or intradermal injections. Furthermore, immunization with IPV by microinjection led to the

induction of VN antibodies. Therefore, etched hollow microneedles can offer potentially pain free, minimally-invasive intradermal injections for vaccine delivery. Finally, this hollow microneedle technology enables fundamental research on factors, such as insertion depth, angle of insertion, and volume, on the immune responses after dermal immunization.

Acknowledgements

We thank the Electronics Department at Leiden University for their help in the development of the microneedle applicator. Furthermore, we thank Aat Mulder for preparing the cryosections of rat skin and Pim Schipper for performing the microinjections into *ex vivo* human skin and the subsequent cryosections. This work was (co)financed by the Netherlands Metabolomics Centre (NMC), which is a part of The Netherlands Genomics Initiative/Netherlands Organization for Scientific Research.

References

- [1] S.M. Bal, Z. Ding, E. van Riet, W. Jiskoot, J. Bouwstra, Advances in transcutaneous vaccine delivery: do all ways lead to Rome? *Journal of Controlled Release* 148(3) (2010) 266-282.
- [2] K. van der Maaden, W. Jiskoot, J. Bouwstra, Microneedle technologies for (trans)dermal drug and vaccine delivery. *Journal of controlled release* 161(2) (2012) 645–655.
- [3] M.R. Prausnitz, H.S. Gill, J.-H. Park, Modified Release Drug Delivery, Vol. 2nd ed New York: Healthcare, 2008, pp. 295-309.
- [4] M.R. Prausnitz, Microneedles for transdermal drug delivery. *Adv Drug Deliv Rev* 56(5) (2004) 581-587.
- [5] O.M. Kew, R.W. Sutter, E.M. de Gourville, W.R. Dowdle, M.A. Pallansch, Vaccine-derived poliovirus and the endgame strategy for global polio eradication. *Annual Review of Microbiology* 59(1) (2005) 587-635.
- [6] J. E.Salk, UlrichKrech, J. S.Youngner, B. L.Bennett, L. J.Lewis, P. L.Bazeley, Formaldehyde Treatment and Safety Testing of Experimental Poliomyelitis Vaccines. (2011).
- [7] P.E.M. Fine, I.A.M. Carneiro, Transmissibility and Persistence of Oral Polio Vaccine Viruses: Implications for the Global Poliomyelitis Eradication Initiative. *American Journal of Epidemiology* 150 (1999) 1001-1021.
- [8] J.F. Modlin, Poliomyelitis in the United States: the final chapter? *JAMA: the journal of the American Medical Association* 292 (2004) 1749-1751.
- [9] N. Nathanson, O.M. Kew, From emergence to eradication: the epidemiology of poliomyelitis deconstructed. *American journal of epidemiology* 172 (2010) 1213-1229.
- [10] K.S. Nelson, J.M. Janssen, S.B. Troy, Y. Maldonado, Intradermal fractional dose inactivated polio vaccine: A review of the literature. *Vaccine* 30 (2012) 121-125.
- [11] J.-F. Nicolas, B. Guy, Intradermal, epidermal and transcutaneous vaccination: from immunology to clinical practice. *Expert Review Vaccines* 7 (2008) 1201-1214.
- [12] S. Chandrasekaran, A.B. Frazier, Mechanical characterization of surface micromachined hollow metallic microneedles. *IEEE The Sixteenth Annual International Conference on Micro Electro Mechanical Systems, 2003. MEMS-03 Kyoto (2002)* 363 - 366.
- [13] S.P. Davis, W. Martanto, M.G. Allen, M.R. Prausnitz, Hollow metal microneedles for insulin delivery to diabetic rats. *IEEE Trans. Biomed. Eng* 52 (2005) 909-915.
- [14] H.J.G.E. Gardeniers, R. Luttge, E.J.W. Berenschot, M.J. de Boer, S.Y. Yeshurun, M. Hefetz, R. van't Oever, A. van den Berg, Silicon micromachined hollow microneedles for Transdermal Liquid Transport. *Journal of Microelectromechanical Systems* 12 (2003) 855-862.
- [15] D.V. McAllister, P.M. Wang, S.P. Davis, J.-H. Park, P.J. Canatella, M.G. Allen, M.R. Prausnitz, Microfabricated needles for transdermal delivery of macromolecules and nanoparticles: Fabrication methods and transport studies. *Proc Natl Acad Sci U S A* 100 (2003) 13755-13760.
- [16] F.J. Verbaan, S.M. Bal, D.J. van den Berg, J.A. Dijkman, M. van Hecke, H. Verpoorten, A. van den Berg, R. Luttge, J.A. Bouwstra, Improved piercing of microneedle arrays in dermatomed human skin by an impact insertion method. *Journal of Controlled Release* 128 (2008) 80-88.
- [17] J. Westdijk, D. Brugmans, J. Martin, A. van't Oever, W.A.M. Bakker, L. Levels, G. Kersten, Characterization and standardization of Sabin based inactivated polio vaccine: Proposal for a new antigen unit for inactivated polio vaccines. *Vaccine* 29 (2011) 3390-3397.

- [18] G. van Steenis, A. van Wezel, V. Sekhuis, Potency testing of killed polio vaccine in rats. *Developments in biological standardization* 47 (1981) 119-128.
- [19] J. Westdijk, P. Koedam, M. Barro, B.P. Steil, N. Collin, T.S. Vedvick, W.A.M. Bakker, P. van der Ley, G. Kersten, Antigen sparing with adjuvanted inactivated polio vaccine based on Sabin strains. *Vaccine* 31 (2013) 1298-1304.
- [20] M. Cormier, B. Johnson, M. Ameri, K. Nyam, L. Libiran, D.D. Zhang, P. Daddona, Transdermal delivery of desmopressin using a coated microneedle array patch system. *Journal of Controlled Release* 97 (2004) 503-511.
- [21] P.M. Wang, M. Cornwell, J. Hill, M.R. Prausnitz, Precise microinjection into skin using hollow microneedles. *Journal of Investigative Dermatology* 126 (2006) 1080-1087.
- [22] M.I. Haq, E. Smith, D.N. John, M. Kalavala, C. Edwards, A. Anstey, A. Morrissey, J.C. Birchall, Clinical administration of microneedles: skin puncture, pain and sensation. *Biomed Microdevices* 11 (2009) 35-47.
- [23] M. Yang, J.D. Zahn, Microneedle insertion force reduction using vibratory actuation. *Biomed Microdevices* 6 (2004) 177-182.
- [24] M.L. Crichton, A. Ansaldo, X. Chen, T.W. Prow, G.J.P. Fernando, M.A.F. Kendall, The effect of strain rate on the precision of penetration of short densely-packed microprojection array patches coated with vaccine. *Biomaterials* 31 (2010) 4562-4572.
- [25] W. Martanto, J.S. Moore, O. Kashlan, R. Kamath, P.M. Wang, J.M. O'Neal, M.R. Prausnitz, Microinfusion using hollow microneedles. *Pharmaceutical Research* 23 (2006) 104-113.
- [26] N. Roxhed, B. Samel, L. Nordquist, P. Griss, G. Stemme, Painless drug delivery through microneedle-based transdermal patches featuring active infusion. *IEEE transactions on bio-medical engineering* 55 (2008) 1063 - 1071.
- [27] S.-J. Paik, S. Byun, J.-M. Lim, Y. Park, A. Lee, S. Chung, J. Chang, K. Chun, D.D. Cho, In-plane single-crystal-silicon microneedles for minimally-invasive microfluid systems. *Sensors and Actuators A: Physical* 2004 (2004) 276-284.
- [28] Q. Cui, C. Liu, X.F. Zha, Study on a piezoelectric micropump for the controlled drug delivery system. *Microfluid Nanofluid* 3 (2007) 377-390.

Supplementary information

To assess the variation in the dimensions of the tip angle, a batch of 55 microneedles etched from 20 μm ID capillaries, etched for four hours, was measured as shown in figure S1. The batch of 55 needles had an average tip angle of $15.0^\circ \pm 2.8^\circ$ (mean \pm SD).

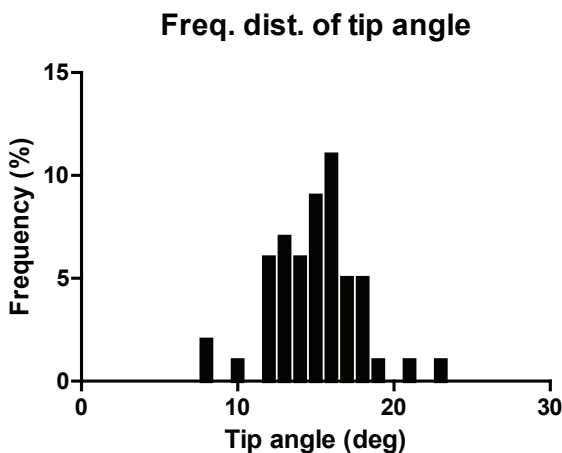


Figure S1: Distribution of the tip angle of 55 microneedles etched for four hours from 20 μm ID capillaries.

CHAPTER 6

SUMMARY, GENERAL
DISCUSSION AND CONCLUSION

SUMMARY, GENERAL DISCUSSION AND CONCLUSION

Summary

Microneedles are a promising tool for vaccination, because they enable minimally-invasive and potentially pain free delivery of vaccines into the skin (*Chapter 2*). Microneedles are needle like structures with a size of less than 1 mm that are used for dermal drug delivery *via* four different approaches. By the ‘poke and release’ approach a drug embedded in dissolving or porous microneedles is released upon application into the skin. In the ‘poke and patch’ approach, microneedles are used to pierce the stratum corneum to create conduits. Subsequently, a patch with a drug formulation is applied onto the conduits enabling the drug to diffuse into the skin. By the ‘coat and poke’ approach, microneedles are coated with a drug that is subsequently released into the skin upon application. By the ‘poke and flow’ approach hollow microneedles are pierced into the skin after which a drug formulation is passed through the bores of the microneedles. The latter three microneedle-based drug delivery approaches were used in this thesis to deliver vaccines into the skin in *Chapter 3, 4 and 5*, respectively.

Chapter 2 provides a detailed overview of methods to produce microneedles from several materials and approaches for microneedle-based vaccine delivery, and contains a section that is dedicated to possible unwanted immunogenicity when delivering biomacromolecules (other than antigens) *via* microneedles. Furthermore, this chapter contains a detailed description of the four described microneedle-based dermal drug delivery approaches with their advantages and disadvantages. The ‘poke and patch’ approach is technically the simplest form of microneedle-based drug delivery, because it does not require a pump or encapsulation/coating process. However, drug delivery *via* this approach is a two-step administration process that requires reformulation of the drug. In contrast, hollow microneedles that are used in the ‘poke and flow’ approach lead to precise dosing without the requirement of reformulating the drug. However, this approach requires sophisticated systems to deliver the drug into the skin. The ‘coat and poke’ and ‘poke and release’ approach are both single-unit

drug delivery systems that require encapsulation, absorption, or adsorption into/onto the microneedles. On the one hand this could lead to degradation of the drug. On the other hand, if degradation is prevented during manufacture, these solid dosage forms may be advantageous with respect to drug stability during storage. The main difference between the ‘coat and poke’ and ‘poke and release’ approach is that porous/polymeric microneedles may have a decreased strength, whereas coating of microneedles may lead to impaired microneedle sharpness. As discussed in this chapter, one common factor for all microneedle approaches is that the microneedles should pierce the stratum corneum in order to deliver a drug into the skin.

The research described in *Chapter 3* focuses on microneedles-based drug delivery by the ‘poke and patch’ approach. The penetration ability of high-density microneedle arrays by microneedle users as well as the applicability of the high-density microneedles/applicator combination in mice *in vivo* was investigated in *Chapter 3.1*. The penetration ability of *ex vivo* human skin by manually applied high-density microneedles was mainly dependent on the force (up to 7.4 N) that was applied onto the microneedle arrays. Further increase of the force or prolonging the application time of the microneedles at a constant force only minimally affected the penetration efficiency. Microneedle application onto human skin by microneedle users using a manual application device led to low penetration efficiencies with low reproducibility. However, using an impact-insertion applicator improved the efficiency and reproducibility of microneedle insertion by microneedle users, enabling self-application of microneedle arrays into the skin. Moreover, the impact-insertion applicator was used for microneedle-mediated antigen delivery, which yielded robust antigen-specific IgG responses in mice. In *Chapter 3.2* factors that influence microneedle-based vaccine delivery and immune responses were investigated, by using ovalbumin as a model antigen. The amount of ovalbumin delivered into *ex vivo* human skin via the ‘poke and patch’ approach depended on the geometry and size of the microneedle array, but this did not affect the ovalbumin-specific IgG response. However, antigen-specific IgG responses were found to be dependent on the usage of an impact-insertion applicator, the microneedle application area, and the location of microneedle application. The knowledge of the influence of these factors on the immune responses could be useful to improve microneedle-based immunization in general.

In *Chapter 4* a novel method is described to coat solid microneedle arrays for dermal vaccine delivery via the ‘coat and poke’ approach. The basic concept is to aid vaccine delivery by modifying the microneedle surface with pH-sensitive groups. In *Chapter 4.1* the development of a novel surface characterization tool is reported: the fluorescent nanoparticle adhesion assay (FNAA). This FNAA was successfully used to determine the surface pK_a of amine- and carboxyl-modified silicon surfaces by using oppositely charged fluorescently labeled nanoparticles. This method provides a useful tool for determining pH-dependent electrostatic protein and particle binding/release and to design solid microneedle surfaces with a pH-sensitive surface charge. In the research described in *Chapter 4.2* pyridine-modified silicon surfaces were synthesized of which the surface pK_a was determined by using

the FNAA. This revealed that pyridine-modified surfaces had a pH-sensitive surface charge with a pK_a of 6.9. Subsequently, the pyridine modification was successfully applied on the surface of silicon microneedles, thereby obtaining pH-sensitive microneedles. These pH-sensitive microneedles were efficiently coated with ovalbumin (coating efficiency > 95%) at a pH below the surface pK_a . Upon application of these microneedles onto *ex vivo* human skin 70% of the coated ovalbumin was released by a pH-shift ($pH > \text{surface } pK_a$) into the skin. Next, in the studies reported in Chapter 4.3 it was shown that antigen delivery from the ovalbumin-coated pH-sensitive microneedles into *ex vivo* human skin is more efficient than *via* the ‘poke-and-patch’ approach. Moreover, *in vivo* vaccination studies showed the applicability of ovalbumin-coated pH-sensitive microneedles for the induction of both B cell and T cell responses in mice. Besides pH-sensitive pyridine-modified silicon surfaces, in Chapter 4.4 surfaces with a tunable isoelectric point (sIEP) were also developed. In this chapter a model was generated to predict and prepare surfaces with a target sIEP. This model was successfully applied to synthesize surfaces with an sIEP of 6 and 7, as confirmed by the FNAA, by simultaneously modifying these surfaces with pyridine and sulfate groups. These modified surfaces are positively charged at $pH < \text{sIEP}$ and negatively charged at $pH > \text{sIEP}$. Besides, the applicability of surfaces with an sIEP was illustrated by using surfaces with an sIEP of 7 to bind positively and negatively charged (bio)macromolecules (trimethyl chitosan (TMC) and poly(I:C), respectively) and subsequently release them in a pH-dependent manner. Finally, in Chapter 4.5 high-density microneedle arrays, which have been shown to penetrate *ex vivo* human skin when using an impact-insertion applicator (Chapter 3.1), were coated with a polio vaccine. Besides, in Chapter 4.5 studies are described in which pH-sensitive (pyridine-modified) microneedles were homogeneously coated *via* a layer-by-layer approach by coating ten layers of negatively charged inactivated poliovaccine (IPV) alternated with positively charged TMC. After the IPV-TMC coated pH-sensitive microneedles were inserted into *ex vivo* human skin, both IPV and TMC were delivered into the skin. Finally, the *in vivo* application of IPV-TMC coated pH-sensitive microneedles in rats led to the induction of antibody responses, showing the release and immunogenicity of the coating *in vivo*.

The research described in Chapter 5 comprises a novel procedure to produce hollow microneedles by hydrofluoric acid etching of fused silica capillaries and presents a novel impact-insertion applicator to accurately insert these microneedles in a controllable manner into the skin at a predefined protrusion depth. Besides, using these hollow microneedles by the ‘poke and flow’ approach resulted in a depth controlled delivery of trypan blue into *ex vivo* rat skin and *ex vivo* human skin. During insertion of the microneedles no clogging or breakage of the microneedles was observed. Finally, an IPV immunization study in rats by using the hollow microneedle/applicator combination showed functional antibody responses comparable to those obtained by conventional immunization.

General discussion

Insertion of solid microneedles

In order to enable vaccine delivery *via* microneedles into the skin, the microneedles should be inserted in a reproducible manner [1, 2]. However, there are several factors that influence the penetration ability of microneedles, e.g., insertion force, microneedle density, length, geometry and sharpness [1]. Therefore, the first aim of this thesis was to investigate the penetration ability of microneedles with and without using an impact-insertion applicator. The different microneedles that were used in this thesis are shown in figure 1. The ‘atom sharp’ U-Needle microneedle arrays (tip diameter < 50 nm) with a length of 300 μm efficiently and reproducibly penetrated *ex vivo* human skin by using a simple device for manual insertion, showing that the microneedle sharpness is of great importance for the penetration ability of microneedles. In contrast, microneedles with a tip diameter of more than 1 μm with a comparable length (Tyndall (300 μm), Leiden University (LU) (300 μm) [3], and Bosch (200 μm) microneedles) required an impact-insertion applicator to reproducibly penetrate human skin. First results showed that the insertion of high-density microneedle arrays into *ex vivo* human skin can be efficiently and reproducibly performed by microneedle users, indicating that microneedles can be self-administered. However, to confirm the self-applicability of these microneedles a comparable penetration study should be performed in humans *in vivo*. Furthermore, the impact-insertion applicator that was used in this thesis would be too large, complex, and expensive for single use. Therefore, a small, cheap and disposable applicator should be developed that is designed for single-use for the insertion of microneedles into the skin.

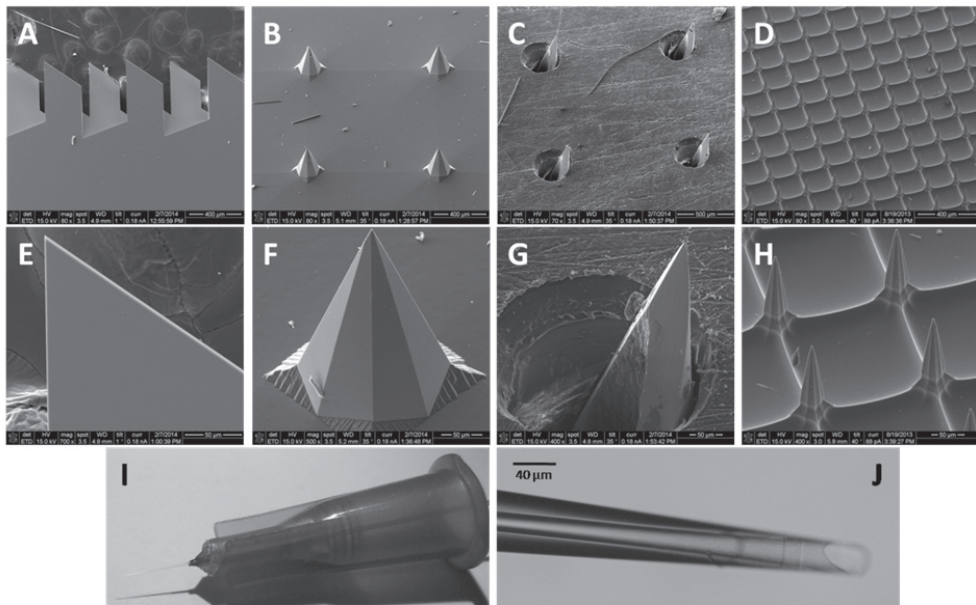


Figure 1: The different microneedles that were used for the research described in this thesis: U-Needle (UN) (A and E), Tyndall National Institute (B, F), Leiden University (LU) (C and G), Bosch (D and H), and fused silica hollow microneedles (I and J).

Antigen-coated microneedles

Antigen-coated microneedles could be especially advantageous for developing countries, because dry formulations may be more stable than liquid formulations. For example, Chen *et al.* (2011) have shown that an influenza vaccine that was coated onto microneedles was stable for at least 6 months at 23°C, whereas the shelf life of the vaccine in liquid form at 25°C is only 14-20 weeks [4]. Moreover, Andrianov *et al.* (2011) have shown that horseradish peroxidase (HRP) that was coated onto microneedles retained 50% of its activity after incubation at 70°C for 24 days in a thermal inactivation study, whereas the half life of HRP in an aqueous solution at 70°C was less than one hour [5]. Because of this increased stability, coated microneedle-based vaccines could circumvent the cold chain and thereby significantly reduce costs and increase vaccination coverage. Furthermore, antigen-coated microneedles are a single-unit drug delivery system that could be self-administered or administered by minimally-trained personnel, which could contribute to cost reduction and increased vaccination coverage.

Coated microneedles also have the advantage that they retain their strength after coating. However, increasing the coating thickness will lead to an increased tip diameter and thereby a reduced microneedle sharpness, which in turn could result in a decreased penetration ability. Besides, only limited amounts of drugs can be coated onto microneedles. Therefore, coating is only suitable for very potent drugs, such as vaccines. Besides, it is important to have a very efficient and reproducible release of the drug from the microneedles into the skin. Therefore, the second aim of this thesis was to develop nanolayered pH-sensitive surfaces to improve the coating and delivery efficiency of microneedles with vaccines without impairing microneedle sharpness and penetration ability.

One important aspect for microneedle-based vaccination *via* coated microneedles is the possibility for upscaling the coating process. The modification of microneedles with pH-sensitive surface groups can easily be included in the manufacturing procedure of microneedles, i.e., a complete wafer with multiple microneedle arrays can be chemically modified. Subsequently, the microneedles should be mounted into an applicator/device that is suitable for high-throughput coating of microneedle arrays with antigens. In this thesis such a device is presented wherein pH-sensitive U-Needle microneedles were mounted. This enabled us to simultaneously coat 96 microneedle arrays in one 96-well plate. Moreover, this coating process could be adapted to coat alternately oppositely charged polyelectrolyte nanolayers onto the surface of microneedles to increase the amount of coated antigen onto pH-sensitive microneedles in a fully automated manner.

Another important aspect of vaccine coated microneedles is that the antigenicity of the vaccine should be retained during coating, storage, and after release to keep its functionality [6]. There are several approaches to retain the antigenicity of vaccines during coating. For example, Kim *et al.* (2010) showed that carboxymethyl cellulose (CMC) was required in the coating formulation to coat a sufficient dose of influenza vaccine onto microneedles. However, the addition of CMC resulted in a reduced antigenicity of the vaccine, which was overcome by adding trehalose to the coating formulation [7]. However, the addition of trehalose is

less suitable for coatings that are based on electrostatic interactions, because trehalose is a non-ionogenic molecule. To retain the antigenicity of antigens in coatings that are based on electrostatic interactions other approaches could be pursued, e.g., by encapsulating the antigen into micro-/nanoparticles before they are coated onto the microneedle surface [8, 9].

Hollow microneedles

Although several different hollow microneedles have been developed by other groups [10-15], they are often produced by expensive processes, e.g., micromachining and cleanroom processing. Also pulling techniques have been used to produce single hollow microneedles. However, such microneedles have an increased risk of clogging since they have a contracting inner diameter towards the tip of the microneedle. Therefore, the third aim of this thesis was to fabricate and characterize hollow microneedles for depth controlled microinjections into skin. Hollow microneedles have been produced from fused silica capillaries by a wet-etching method. This fabrication method is a scalable process that enables the production of large numbers of microneedles. Moreover, this fabrication process does not require expensive equipment and uses cheap materials to produce these microneedles.

An applicator was developed for the application of hollow microneedles into mouse and rat skin *in vivo* and human skin *ex vivo*. This applicator allows the investigation of various parameters, such as the depth of vaccine delivery, injection volume, and injection speed, on the quality of the microinjection. Besides, this applicator allows the investigation of the above described parameters on the immune responses upon vaccination *via* hollow microneedles. In this thesis the hollow microneedles/applicator combination was only used at a protrusion depth of 300 μm with 9 μL vaccine formulation at a flow speed of 2 $\mu\text{L}/\text{min}$ to immunize rats. To optimize vaccination *via* hollow microneedles, subsequent studies should be performed whereby the immune responses and the quality of the microinjection are investigated as a function of delivery parameters, such as protrusion depth, injection volume and antigen dose.

Although this thesis shows the usability of the developed hollow microneedles/applicator combination for vaccination, there are still some major limitations that should be tackled before human application. The major limitation of the developed system is the relatively low flow speed of 2 $\mu\text{L}/\text{min}$. As most vaccines in the Netherlands are formulated in 0.5-1.5 mL [16], this implies that it would require four to twelve hours to vaccinate one person. Therefore, the hollow microneedle/applicator system should be adapted to increase the flow speed and reduce the injection time. Furthermore, as high volume injections (> 0.8 mL) into the skin are painful [17], and to decrease the injection time, the vaccine could be delivered in a small volume, requiring a relatively high concentration. Another approach to decrease the injection time is by increasing the number of microneedles that are simultaneously inserted into the skin. However, if one microneedle is not properly inserted into the skin, the whole formulation will leak through the non-inserted microneedle (path of the least resistance). Therefore, a system that contains multiple hollow microneedles preferably contains a

separate reservoir for each microneedle. Finally, to enable self-administration of vaccines *via* hollow microneedles, a simplified applicator should be developed with a fixed angle of insertion, penetration depth, insertion speed, injection volume and flow speed.

Microneedle-based vaccination

All microneedles studied in this thesis were successfully used to deliver antigens into the skin. The final aim of this thesis was to evaluate the application of the ‘poke and patch’, the ‘coat and poke’, and the ‘poke and flow’ approach for vaccination in animal studies. The ‘poke and patch’ approach is an excellent method to investigate immune responses upon microneedle-based vaccination because it is the most simple approach for microneedle-based drug delivery. Besides, this approach enables a fast investigation of the immune responses upon microneedle-based immunizations with different vaccine formulations. However, this approach would be the least appropriate general method for microneedle-based vaccination of humans, because the delivery is a two-step procedure (i.e., first the microneedles need to pierce the skin, and then the vaccine containing patch needs to be applied) and the delivery efficiencies *via* this approach are generally low (if worn for 2-4 hours) [18, 19]. However, the delivery efficiency could be increased by prolonging the wear time of the patch, but it would require several days to deliver the major dose of antigens from the patch into the skin [19], which is, especially for children, not appropriate.

Numerous geometries of microneedles have been developed with differences in length, sharpness, density, etc. These differences can influence the immune responses. For example, ultra-high-density microneedles that are used in the group of Kendall result in high immune responses in animal models [20-22], which is also true for long microneedles (e.g., 800-1000 μm) that have been used in other groups [23, 24]. However, microneedles with a length of more than 400 μm are more likely to induce pain [1]. In order to obtain optimal immune responses in mice by using short microneedles (< 400 μm), vaccination should be performed *via* the ear, either *via* high-density microneedles or applying microneedle arrays multiple times over a large skin area. Although several clinical studies have been successfully performed in humans [1], the effect of microneedle application site, microneedle density, microneedle length, and the area of microneedle application on the immune responses are unknown. In order to obtain optimal immune responses in humans, clinical studies should be performed whereby the above described factors are investigated. Finally, to direct the immune reaction towards a $T_{\text{H}}1$ or $T_{\text{H}}2$ response and to increase the immune responses upon microneedle-based immunization, either mechanical (impact-insertion applicator) or chemical adjuvants (encapsulation of the antigen in micro-/nanoparticles and/or addition of CpG, LPS, *poly(I:C)*) to the vaccine (coating) formulation) could be included [6].

Conclusion

The different microneedles that were employed in this thesis were successfully used to pierce skin. However, microneedles with a tip in the nanometer range (UN) efficiently and reproducibly pierce skin, whereas microneedles with a tip diameter of more than $1\ \mu\text{m}$ (Tyndall, LU, and Bosch) require an impact-insertion applicator for efficient and reproducible insertion. Besides, an impact-insertion applicator is required to insert fused silica hollow microneedles to a controlled depth into the skin. Therefore, to ensure efficient and reproducible *skin penetration* for self administration of microneedles (either solid or hollow), is by using an applicator that inserts the microneedles by a controlled force or by a controlled velocity, such as an impact-insertion applicator. A suitable approach to investigate the immune response upon microneedle-based vaccination is by using *solid microneedles via* the ‘poke and patch’ approach. However, because the delivery efficiency of this approach is low, it would be too expensive for general immunization. In order to achieve a sufficient amount of vaccine coated on the microneedles while retaining their sharpness, the coating and release process should be efficient, which can be achieved by applying *ultrathin pH-sensitive coatings* for microneedle-based vaccination. *Hollow microneedles* that are produced from fused silica together with the applicator enable a precise dosing to a predetermined depth and do not or only minimally require reformulation of the vaccine. Because they are easily produced in large numbers with low production costs these hollow microneedles could be used for mass immunization. Finally, *microneedle-based vaccination* offers a minimally-invasive and potentially pain free vaccination strategy to successfully induce antigen-specific immune responses.

References

- [1] Y.-C. Kim, J.-H. Park, M.R. Prausnitz, Microneedles for drug and vaccine delivery. *Advanced Drug Delivery Reviews* 64 (2012) 1547-1568.
- [2] T.R.R. Singh, N.J. Dunne, E. Cunningham, R.F. Donnelly, Review of Patents on Microneedle Applicators. *Recent Patents on Drug Delivery & Formulation* 5 (2011) 11-23.
- [3] F.J. Verbaan, S.M. Bal, D.J. van den Berg, J.A. Dijkman, M. van Hecke, H. Verpoorten, A. van den Berg, R. Luttge, J.A. Bouwstra, Improved piercing of microneedle arrays in dermatomed human skin by an impact insertion method. *Journal of Controlled Release* 128 (2008) 80-88.
- [4] X. Chen, G.J.P. Fernando, M.L. Crichton, C. Flaim, S.R. Yukiko, E.J. Fairmaid, H.J. Corbett, C.A. Primiero, A.B. Ansaldo, I.H. Frazer, L.E. Brown, M.A.F. Kendall, Improving the reach of vaccines to low-resource regions, with a needle-free vaccine delivery device and long-term thermostabilization. *Journal of Controlled Release* 152 (2011) 349-355.
- [5] A.K. Andrianov, A. Marin, D.P. DeCollibus, Microneedles with intrinsic immunoadjuvant properties: microfabrication, protein stability, and modulated release. *Pharmaceutical Research* 28 (2011) 58-65.
- [6] S.M. Bal, Z. Ding, E. van Riet, W. Jiskoot, J. Bouwstra, Advances in transcutaneous vaccine delivery: do all ways lead to Rome? *Journal of Controlled Release* 148 (2010) 266-282.
- [7] Y.-C. Kim, F.-S. Quan, R.W. Compans, S.-M. Kang, M.R. Prausnitz, Formulation and coating of microneedles with inactivated influenza virus to improve vaccine stability and immunogenicity. *Journal of Controlled Release* 142 (2010) 187-195.
- [8] P.C. DeMuth, J.J. Moon, H. Suh, P.T. Hammond, D.J. Irvine, Releasable layer-by-layer assembly of stabilized lipid nanocapsules on microneedles for enhanced transcutaneous vaccine delivery. *ACS Nano* 6 (2012) 8041-8051.
- [9] P.C. DeMuth, X. Su, R.E. Samuel, P.T. Hammond, D.J. Irvine, Nano-Layered Microneedles for Transcutaneous Delivery of Polymer Nanoparticles and Plasmid DNA. *Advanced Materials* 22 (2010) 4851-4856.
- [10] D.W. Bodhale, A. Nisar, N. Afzulpurkar, Structural and microfluidic analysis of hollow side-open polymeric microneedles for transdermal drug delivery applications *Microfluidics and Nanofluidics* 8 (2010) 373-392.

- [11] S.P. Davis, W. Martanto, M.G. Allen, M.R. Prausnitz, Hollow metal microneedles for insulin delivery to diabetic rats. *IEEE Transactions on Biomedical Engineering* 52 (2005) 909-915.
- [12] H.J.G.E. Gardeniers, R. Lutttge, E.J.W. Berenschot, M.J. de Boer, S.Y. Yeshurun, M. Hefetz, R. van't Oever, A. van den Berg, Silicon Micromachined Hollow Microneedles for Transdermal Liquid Transport. *Journal of Microelectromechanical Systems* 12 (2003) 855-862.
- [13] J. Gupta, E.I. Felner, M.R. Prausnitz, Minimally-invasive insulin delivery in subjects with type 1 diabetes using hollow microneedles. *Diabetes Technology & Therapeutics* 11 (2009) 329-337.
- [14] W. Martanto, J.S. Moore, O. Kashlan, R. Kamath, P.M. Wang, J.M. O'Neal, M.R. Prausnitz, Microinfusion using hollow microneedles. *Pharmaceutical Research* 23 (2006) 104-113.
- [15] P.M. Wang, M. Cornwell, J. Hill, M.R. Prausnitz, Precise microinjection into skin using hollow microneedles. *Journal of Investigative Dermatology* 126 (2006) 1080-1087.
- [16] RIVM, Bijsluiters Rijksvaccinatieprogramma, available from http://www.rivm.nl/Onderwerpen/V/Vaccins/Bijsluiters_vaccins/Bijsluiters_Rijksvaccinatieprogramma. accessed on: 21-06-2014.
- [17] J. Gupta, S. Park, B. Bondy, E.I. Felner, M.R. Prausnitz, Infusion pressure and pain during microneedle injection into skin of human subjects. *Biomaterials* 32 (2011) 6823-6831.
- [18] A.V. Badkar, A.M. Smith, J.A. Eppstein, A.K. Banga, Transdermal delivery of interferon alpha-2B using microporation and iontophoresis in hairless rats. *Pharmaceutical Research* 24 (2007) 1389-1395.
- [19] S.L. Banks, K.S. Paudel, N.K. Brogden, C.D. Loftin, A.L. Stinchcomb, Diclofenac Enables Prolonged Delivery of Naltrexone Through Microneedle-Treated Skin. *Pharmaceutical Research* 28 (2011) 1211-1219.
- [20] H.-I. Ng, G.J.P. Fernando, M.A.F. Kendall, Induction of potent CD8+ T cell responses through the delivery of subunit protein vaccines to skin antigen-presenting cells using densely packed microprojection arrays. *Journal of Controlled Release* 162 (2012) 477-484.
- [21] A.P. Raphael, T.W. Prow, M.L. Crichton, X. Chen, G.J.P. Fernando, M.A.F. Kendall, Targeted, Needle-Free Vaccinations in Skin using Multilayered, Densely-Packed Dissolving Microprojection Arrays. *Small* 6 (2010) 1785-1793.
- [22] X. Chen, T.W. Prow, M.L. Crichton, D.W.K. Jenkins, M.S. Roberts, I.H. Frazer, G.J.P. Fernando, M.A.F. Kendall, Dry-coated microprojection array patches for targeted delivery of immunotherapeutics to the skin. *Journal of Controlled Release* 139 (2009) 212-220.
- [23] A. Kumar, X. Li, M.A. Sandoval, B.L. Rodriguez, B.R. Sloat, Z. Cui, Permeation of antigen protein-conjugated nanoparticles and live bacteria through microneedle-treated mouse skin. *International Journal of Nanomedicine* 6 (2011) 1253-1264.
- [24] K. Matsuo, Y. Yokota, Y. Zhai, Y.-S. Quan, F. Kamiyama, Y. Mukai, N. Okada, S. Nakagawa, A low-invasive and effective transcutaneous immunization system using a novel dissolving microneedle array for soluble and particulate antigens. *Journal of Controlled Release* 161 (2012) 10-17.

APPENDIX

NEDERLANDSE SAMENVATTING
CURRICULUM VITAE
LIST OF PUBLICATIONS
ABBREVIATIONS
DANKWOORD

Roodgedrukte woorden zijn opgenomen in een verklarende woordenlijst.

Deel I: Inleiding

Vaccinatie

Vaccinatie is één van de grootste successen in de geneeskunde om ziekte en sterfte te voorkomen. Volgens schattingen van de Wereld Gezondheid Organisatie (Engels: World Health Organization, WHO) voorkomt vaccinatie jaarlijks zo'n 6 miljoen doden. Hierdoor zijn **infectieziekten** in westerse landen niet meer de primaire doodsoorzaak. Edward Jenner (1749-1823) en Louis Pasteur (1822-1895) zijn belangrijke pioniers op het gebied van vaccinatie. Zij hebben veel bijgedragen aan het concept vaccinatie en de introductie daarvan om mensen te beschermen tegen infectieziekten. In 1796 isoleerde Jenner de inhoud van puisten van een melkmeisje dat geïnfecteerd was met de koepokken. De geïsoleerde pus injecteerde hij in een 8-jarig jongetje, waarna hij het jongetje besmette met het gevaarlijke pokkenvirus. Jenner observeerde dat het jongetje geen symptomen van de ziekte kreeg. Vervolgens introduceerde Pasteur het gebruik van levende verzwakte ziekteverwekkers voor vaccinatie. Hij ontdekte dat ziekteverwekkende bacteriën die enkele maanden in laboratoriumbuisjes gekweekt waren niet meer in staat zijn om de ziekte te veroorzaken, maar wel hun **immunogeniteit** behouden. Hierdoor kunnen deze levende verzwakte bacteriën gebruikt worden als vaccin om beschermende **immuunreacties** op te wekken. Sindsdien is vaccinatie sterk verbeterd en beschikbaar geworden tegen vele infectieziekten, zoals hepatitis B, difterie, kinkhoest en poliomyelitis. Bovendien zijn er therapeutische vaccins tegen onder andere kanker en hart- en vaatziekten in ontwikkeling.

Ondanks de inspanningen en dusver behaalde successen van wereldwijde vaccinatieprogramma's zijn infectieziekten nog steeds de belangrijkste doodsoorzaak in ontwikkelingslanden. Bovendien is vaccineren erg duur, wat onder andere door de productiekosten van vaccins komt. Daarnaast zijn er minder zichtbare factoren die eveneens bijdragen aan de hoge kosten voor vaccinatie, zoals opslag, transport, verpakking, koelketen (**cold-chain**) en het benodigde medisch personeel om de vaccins toe te dienen. Ook leidt vaccinatie niet altijd tot beschermende immuunreacties. Zo zijn er, ondanks alle inspanningen en onderzoeken die er de afgelopen decennia zijn gedaan, nog steeds geen effectieve vaccins tegen

infectieziekten zoals HIV, malaria, tuberculose en ebola, die momenteel veel slachtoffers eist. Ten slotte worden de meeste vaccins **subcutaan** of **intramusculair** toegediend door middel van klassieke injectienaalden. Hierdoor veroorzaakt vaccinatie pijn, angst en stress in kinderen en hun ouders, wat kan leiden tot een verminderde **vaccinatiegraad**. Om deze obstakels te overwinnen worden nieuwe niet- of **minimaal-invasieve** alternatieve vaccinatiestrategieën overwogen en onderzocht. Voorbeelden hiervan zijn onder andere inhalatiepreparaten en neussprays. Een andere alternatieve vaccinatiestrategie is gebruikmaking van de huid als **toedieningsroute**.

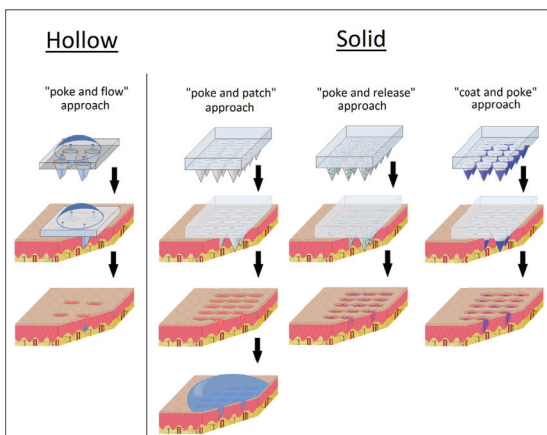
Dermale vaccinatie

De huid wordt constant blootgesteld aan lichaamsvreemde stoffen zoals ziekteverwekkers die het lichaam proberen binnen te dringen. Daarom heeft de huid zich geëvolueerd tot een uitstekende barrière. De eerste barrière van de huid is het stratum corneum (de hoornlaag), dat een fysieke barrière is die vrijwel ondoordringbaar is voor de meeste stoffen. Bovendien bevat de huid gespecialiseerde cellen van het immuunsysteem (de zogenoemde **antigeen-presenterende cellen**) die voorkomen dat binnendringende ziekteverwekkers **systemische infecties** veroorzaken. Aan de andere kant bemoeilijkt deze barrière (voornamelijk de hoornlaag) de toediening van medicijnen *via* de huid. Dit wordt geïllustreerd door het beperkte aantal medicijnen dat beschikbaar is voor toediening *via* de huid (ook wel dermale toediening genoemd): er zijn maar ongeveer 20 farmaceutisch actieve ingrediënten op de markt beschikbaar die *via* de huid met behulp van pleisters worden toegediend, waarvan alle deze ingrediënten bovendien kleine moleculen (grootte ongeveer 1 **nanometer**) zijn. Dit laat zien dat het nog moeilijker is om vaccins en andere **(bio)macromoleculen**, heel veel grotere moleculen of deeltjes (tientallen nanometers tot enkele **micrometers**), *via* de huid toe te dienen. Het heeft daarom ook tot midden jaren '90 geduurd voordat minimaal-invasieve **(trans)dermale** vaccinatie voor het eerst preklinisch met succes werd toegepast. Hierbij werden hoge **antigeen**-specifieke **antistoffen** in muizen verkregen door modelantigenen die verpakt waren in lipide deeltjes aan te brengen op de huid. Later werd de huid als toedieningsroute voor vaccinatie bevestigd in muizen (1998) en in mensen (2000) door vaccin**formuleringen** met cholera toxine op de huid aan te brengen. Echter, daaropvolgende klinische studies hebben uitgewezen dat deze methode niet effectief was. Een veel belovende methode voor minimaal-invasieve dermale vaccinatie is door middel van micronaalden, die voor het eerst beschreven werden in 1998.

Micronaalden

Micronaalden zijn structuren in de orde grootte van micrometers met een lengte van minder dan 1 millimeter die gebruikt worden om medicijnen, inclusief vaccins, in of door de huid af te geven. Micronaalden moeten lang genoeg zijn om door de hoornlaag te prikken en tegelijkertijd kort genoeg zijn om de bloedvaten en zenuwbanen niet te raken. Op deze manier kunnen medicijnen en vaccins op een minimaal-invasieve en een pijnloze manier worden toegediend *via* de huid. Ook zouden micronaald-gemedieerde vaccinaties door patiënten zelf uitgevoerd kunnen worden. Het gebruik van micronaalden zou hierdoor kunnen leiden tot een verbeterde vaccinatiegraad. Daarnaast zou een droge vaccin formulering in of op micronaalden de cold-chain kunnen omzeilen, omdat droge formuleringen thermostabieler kunnen zijn. Ook heeft dermale vaccinatie potentie om de hoeveelheid antigeen te verminderen omdat de huid een immunologisch actief orgaan is. Hierdoor kan het gebruik van micronaalden bijdragen aan een significante vermindering van de kosten voor vaccinatie. Over het algemeen kunnen micronaalden op vier verschillende manieren gebruikt worden om medicijnen, waaronder vaccins, *via* de huid toe te dienen, zie hieronder en figuur 1:

1. 'Poke and flow'. Holle micronaalden worden eerst in de huid geprikt, waarna een medicijn formulering *via* de holle kanalen van de micronaalden de huid in stroomt of wordt gepompt.
2. 'Poke and patch'. De huid wordt voorbehandeld met massieve micronaalden waardoor microporiën in de huid gevormd worden. Vervolgens wordt een reservoir met daarin een medicijnformulering aangebracht op de microporiën, waardoor het medicijn *via* vooral de microporiën de huid in kan **diffunderen**.
3. 'Poke and release'. Een medicijn is ingesloten in oplosbare, bioafbreekbare of poreuze massieve micronaalden. Nadat de micronaalden in de huid gestoken worden, wordt het medicijn afgegeven in de huid.
4. 'Coat and poke'. Het oppervlak van massieve micronaalden wordt eerst gecoat met een medicijn, dat wordt afgegeven nadat de micronaalden in de huid zijn gestoken.



Figuur 1: De verschillende manieren om medicijnen *via* de huid toe te dienen met behulp van holle (hollow) en massieve (solid) micronaalden.

Hoewel micronaalden veel potentie hebben voor dermale vaccinatie, zijn micronaalden alleen vaak niet voldoende om de huid goed en/of reproduceerbaar te penetreren. Daarom zijn er vaak insertie-apparaten (micronaald-applicatoren) nodig die de krachten reduceren die de micronaalden nodig hebben om door de hoornlaag heen te prikken.

Deel II: Doelstellingen van het in dit proefschrift beschreven onderzoek

De hoofddoelen van het onderzoek in dit proefschrift zijn:

1. Het bestuderen van de huidpenetratie door middel van micronaalden, al dan niet in combinatie met een applicator;
2. Het bereiden en karakteriseren van ultradunne, pH-afhankelijke oppervlaklagen om de efficiëntie van de vaccincoating en -afgifte *via* micronaalden te verbeteren zonder de scherpheid van de micronaalden aan te tasten;
3. Het fabriceren en karakteriseren van holle micronaalden voor micro-injecties in de huid op een gedefinieerde diepte;
4. Het in proefdierstudies evalueren van de ‘poke and patch’, de ‘coat and poke’, en de ‘poke and flow’ methoden voor dermale vaccinatie.

Deel III: Samenvatting

Micronaalden zijn een veelbelovend hulpmiddel voor vaccinatie, omdat ze het mogelijk maken om vaccins toe te dienen *via* de huid op een minimaal-invasieve en pijnloze manier (**hoofdstuk 1**). Zoals hierboven beschreven kunnen micronaalden over het algemeen op vier verschillende manieren gebruikt worden om medicijnen *via* de huid af te geven. In dit proefschrift zijn de ‘poke and patch’, de ‘coat and poke’ en de ‘poke and flow’ methoden gebruikt om vaccins *via* de huid toe te dienen in respectievelijk **hoofdstuk 3, 4 en 5**.

Micronaaldtechnologieën voor (trans)dermale toediening

In **hoofdstuk 2** wordt een gedetailleerd overzicht gegeven van de methoden om micronaalden te produceren van verschillende materialen. Daarnaast zijn de verschillende strategieën om vaccins af te geven in de huid met behulp van micronaalden beschreven. Ook is er een sectie gewijd aan mogelijke ongewenste immunogeniciteit als micronaalden gebruikt worden voor de toediening van biomacromoleculen (anders dan antigenen). Bovendien bevat dit hoofdstuk een gedetailleerde beschrijving van de vier hierboven beschreven methoden om medicijnen met behulp van micronaalden af te geven in de huid met hun voor- en nadelen. Holle micronaalden die gebruikt worden in de ‘poke and flow’ methode leiden tot een nauwkeurige dosering van het medicijn in de huid zonder dat het nodig is om het medicijn te **herformuleren**. Desalniettemin vereist deze methode geavanceerde systemen om een medicijn in de huid af te geven. De ‘poke and patch’ methode is technisch de meest eenvoudige vorm van medicijnafgifte met behulp van micronaalden, omdat geen

pomp of insluitings- of coatingsproces vereist is. Echter, medicijnafgifte op basis van deze methode is een tweestaps toedieningsproces die herformulering van het medicijn vereist. Daartegenover zijn de ‘coat and poke’ en de ‘poke and patch’ methode beide een single-unit medicijnafgiftesysteem (éénstaps toedieningsproces), maar deze vereisen insluiting, **absorptie** of **adsorptie** van het medicijn in of aan het oppervlak van de micronaalden. Dit zou enerzijds kunnen leiden tot degradatie van het medicijn. Maar als degradatie voorkomen kan worden tijdens het productieproces, dan zouden deze massieve doseringsvormen anderzijds gunstig kunnen zijn met betrekking tot stabiliteit van het medicijn tijdens opslag en transport. Een belangrijk verschil tussen de ‘coat and poke’ en de ‘poke and release’ methode is dat poreuze/polymere micronaalden minder robuust kunnen zijn, terwijl het coaten kan leiden tot een verminderde scherpte van de tip van de micronaalden. Zoals besproken in dit hoofdstuk is er één gemeenschappelijke factor voor alle medicijnafgiftemethoden met behulp van micronaalden, namelijk dat micronaalden door de hoornlaag moeten prikken om een medicijn in de huid af te geven.

‘Poke and patch’ methode

Het onderzoek dat beschreven is in **hoofdstuk 3** is gefocust op medicijnafgifte door middel van micronaalden die gebruikt worden met de ‘poke and patch’ methode.

In **hoofdstuk 3.1** wordt bestudeerd of hoge-dichtheid **micronaalden arrays** (HD-micronaalden, 2304 micronaalden/cm²) in staat zijn om de hoornlaag te penetreren. Bovendien wordt onderzocht of deze micronaalden in combinatie met een **impact-insertie-applicator** tot een immuunresponse leidt in muizen. Uit deze studie blijkt dat de penetratie van de hoornlaag van **ex vivo** humane huid door handmatig aangebrachte HD-micronaalden voornamelijk afhankelijk is van de gebruikte kracht (tot 7.4 N). Bij een verdere toename van de kracht of het verlengen van de applicatietijd bij een constante kracht wordt de penetratie-efficiëntie nagenoeg niet beïnvloed. Vervolgens is de penetratie-efficiëntie onderzocht. Het handmatig aanbrengen van HD-micronaalden op **ex vivo** humane huid door micronaaldgebruikers leidt tot lage penetratie-efficiënties met een lage reproduceerbaarheid. Daarentegen is de penetratie-efficiëntie en reproduceerbaarheid van micronaaldinsertie sterk verbeterd als een impact-insertie-applicator gebruikt wordt door micronaaldgebruikers. Dit laat dus zien dat het mogelijk is om patiënten zelf micronaalden te laten aanbrengen indien ze een impact-insertie-applicator gebruiken. Ten slotte, als HD-micronaalden worden aangebracht op muizenhuid **in vivo** met behulp van een impact-insertie-applicator voor micronaald-gemedieerde antigeenafgifte, resulteert dit in robuuste antigeen-specifieke antistofresponsen.

In **hoofdstuk 3.2** is onderzocht welke factoren van invloed zijn op de vaccinafgifte en immuunresponsen na toepassing van de ‘poke and patch’ methode, waarbij **ovalbumine** als modelantigeen wordt gebruikt. Hoewel de hoeveelheid afgegeven ovalbumine in **ex vivo** humane huid afhankelijk is van de **geometrie** van de micronaalden alsmede van het aantal micronaalden per micronaald array, heeft de dosis geen invloed op de ovalbumine-specifieke **Immunoglobuline G (IgG)** responsen. Daarentegen zijn de antigeen-specifieke IgG responsen

afhankelijk van het gebruik van een impact-insertie-applicator, het huidoppervlakte waarop de micronaalden geapliceerd zijn en de plaats waar de micronaalden geapliceerd worden. De in deze studie opgedane kennis van de bovenstaande factoren kunnen gebruikt worden om niet alleen de ‘poke and patch’ maar ook de andere micronaald-gemedieerde vaccinatiemethoden te verbeteren.

‘Coat and poke’ methode

In **hoofdstuk 4** wordt een nieuwe methode gepresenteerd om massieve micronaalden te coaten voor dermale vaccinatie middels de ‘coat and poke’ methode. Het basisprincipe van deze methode is om vaccincoating en -afgifte te bevorderen door het oppervlak van micronaalden chemisch te modificeren met moleculen die een pH-afhankelijke lading hebben. De chemische oppervlakmodificaties die in dit hoofdstuk beschreven staan zijn enkele nanometers dik.

In **hoofdstuk 4.1** wordt de ontwikkeling beschreven van een nieuwe methode om oppervlakken te karakteriseren: de **fluorescente** nanodeeltjes adhesie assay (FNAA). Vervolgens wordt deze FNAA toegepast om de oppervlak pK_a -waarde van amine- en carboxyl gemodificeerde siliciumoppervlakken te bepalen, waarbij fluorescent gelabelde nanodeeltjes met een tegenovergestelde lading gebruikt worden. Deze methode is een nuttig gereedschap om pH-afhankelijke elektrostatistische bindingen en afgifte van eiwitten en deeltjes aan oppervlakken te bepalen. Bovendien kan deze methode gebruikt worden om micronaalden met een pH-gevoelig oppervlak te ontwerpen.

De studies in **hoofdstuk 4.2** beschrijven de synthese van pyridine-gemodificeerde oppervlakken waarvan de oppervlak pK_a -waarde is bepaald door middel van de FNAA. Deze studies tonen aan dat pyridine-gemodificeerde oppervlakken een pH-afhankelijke oppervlaklading hebben met een pK_a -waarde van 6,9. Vervolgens is het oppervlak van siliciummicronaalden met succes gemodificeerd met pyridinegroepen, resulterende in pH-gevoelige micronaalden. De verkregen pH-gevoelige micronaalden worden efficiënt gecoat met ovalbumine (coatingefficiëntie > 95%) bij een pH-waarde die lager is dan de oppervlak pK_a -waarde. Als ovalbumine-gecoate pH-gevoelige micronaalden in *ex vivo* humane huid geprikt worden, wordt 70% van de gecoate ovalbumine afgegeven in de huid door een pH-verandering ($pH > \text{oppervlak } pK_a$).

Vervolgstudies (**hoofdstuk 4.3**) tonen aan dat de ovalbumine-afgifte in *ex vivo* humane huid door middel van ovalbumine-gecoate pH-gevoelige micronaalden veel efficiënter is dan *via* de ‘poke and patch’ methode. Bovendien laten vaccinatiestudies in muizen de toepasbaarheid van de antigeen-gecoate pH-gevoelige micronaalden voor het opwekken van antigeen-specifieke **B en T-cellen** *in vivo* zien.

Naast de pH-gevoelige pyridine-gemodificeerde siliciumoppervlakken zijn er ook oppervlakken ontwikkeld met een af te stemmen **iso-elektrisch punt** (IEP), zoals beschreven in **hoofdstuk 4.4**. In dit hoofdstuk is een model gegenereerd om oppervlakken met een vooraf gekozen IEP te voorspellen en te genereren. Dit model wordt vervolgens toegepast om

oppervlakken met een IEP van 6 en 7 te synthetiseren door oppervlakken tegelijkertijd met pyridine- (pH-afhankelijke positieve lading) en sulfaatgroepen (pH-onafhankelijke negatieve lading) te modificeren. Het succes van de synthese van de IEP oppervlakken kon worden aangetoond met behulp van de FNAA. De IEP oppervlakken hebben een positieve lading bij $\text{pH} < \text{IEP}$ en een negatieve lading bij $\text{pH} > \text{IEP}$. Bovendien illustreert de binding van positief en negatief geladen (bio)macromoleculen (respectievelijk trimethyl chitosan (TMC) en *poly(I:C)*) aan oppervlakken met een IEP van 7 de toepasbaarheid van oppervlakken met een IEP. Deze (bio)macromoleculen laten vervolgens weer los van het oppervlak door een pH-verandering. Ten slotte worden HD-micronaalden in **hoofdstuk 4.5** gecoat met een polio vaccin. In **hoofdstuk 3.1** is beschreven dat deze micronaalden *ex vivo* humane huid kunnen penetreren als ze in combinatie met een impact-insertie-applicator gebruikt worden. In het onderzoek dat beschreven is in **hoofdstuk 4.5** worden pH-gevoelige (gemodificeerd met pyridine) micronaalden homogeen gecoat door tien lagen negatief geladen geïnactiveerd polio virus (IPV) af te wisselen met positief geladen TMC. Zowel IPV als TMC worden in de huid afgegeven nadat de IPV-TMC gecoate pH-gevoelige micronaalden in *ex vivo* humane huid gestoken worden. Ten slotte zijn de IPV-TMC gecoate micronaalden gebruikt om ratten dermaal te vaccineren. Uit de polio-specifieke antistoffen blijkt dat de coating is afgegeven in de huid en nog immunogeen is.

‘Poke and flow’ methode

Het onderzoek in **hoofdstuk 5** beschrijft een nieuwe methode om holle micronaalden te produceren door samengesmolten siliciumdioxide (kwarts) **capillairen** te etsen met fluorzuur. Ook beschrijft dit hoofdstuk een nieuwe impact-insertie-applicator om holle micronaalden op een gecontroleerde manier de huid in te steken, waarbij de lengte die de microneaald uitsteekt accuraat kan worden ingesteld. Het gebruiken van deze holle micronaalden/applicatorcombinatie *via* de ‘poke and flow’ methode resulteert in een dieptegecontroleerde afgifte van trypaanblauw in *ex vivo* rattenhuid en *ex vivo* humane huid. Het appliceren van holle micronaalden in huid is uitgevoerd zonder dat er verstoppingen en breuken in de micronaalden optraden. Ten slotte zijn ratten geïmmuniseerd met IPV door gebruik te maken van de combinatie holle micronaalden en de speciaal hiervoor ontwikkelde applicator. Hieruit blijkt dat er na vaccinatie met micronaalden functionele antistof responsen opgewekt worden die vergelijkbaar zijn met de responsen na conventionele intramusculaire vaccinatie.

Deel IV: Conclusies van dit proefschrift

De verschillende micronaalden die in dit proefschrift beschreven staan zijn met succes gebruikt om in de huid te prikken. De micronaalden met een tipdiameter in het nanometergebied blijken in staat om humane huid efficiënt en reproduceerbaar te prikken met een applicator voor handmatige insertie, terwijl micronaalden met een tipdiameter

van meer dan één micrometer een impact-insertie-applicator nodig hebben voor efficiënte en reproduceerbare insertie. Een impact-insertie-applicator is ook een vereiste om holle kwartsmicronaalden met een gecontroleerde diepte in de huid te steken. Om er zeker van te zijn dat de *huidpenetratie* door micronaalden (zowel massieve als holle) voor zelfmedicatie reproduceerbaar en efficiënt is, is het nodig om een applicator te gebruiken die micronaalden in de huid steekt met een gecontroleerde kracht of met een gecontroleerde snelheid, zoals een impact-insertie-applicator. Een geschikte methode om immuunresponsen *via* micronaald-gemedieerde vaccinatie te onderzoeken is door *massieve micronaalden* te gebruiken met de ‘poke and patch’ methode. Deze methode zou echter wellicht te duur zijn voor algemene vaccinatie, omdat de geneesmiddel afgifte-efficiëntie met deze methode laag is. Een andere methode om medicijnen af te geven met behulp van massieve micronaalden is *via* de ‘coat and poke’ methode. Om zowel een toereikende hoeveelheid vaccin op de micronaalden te coaten alsmede de scherpte van de micronaalden te behouden, moet het coatings- en afgifteproces efficiënt zijn. Voor micronaald-gemedieerde vaccinatie kan dit bereikt worden door *ultradunne pH-gevoelige coatings* op het oppervlak van micronaalden toe te passen. *Holle micronaalden* geproduceerd van kwartscapillair, die aangebracht worden met behulp van een applicator, maken het mogelijk om een precieze dosis af te geven op een vooraf bepaalde diepte in de huid. Bovendien is het niet nodig om het vaccin te herformuleren. Omdat deze holle micronaalden makkelijk in groten getale geproduceerd kunnen worden met lage productiekosten, zouden deze holle micronaalden gebruikt kunnen worden voor massa-immunisatie. Ten slotte biedt *micronaald-gemedieerde vaccinatie* een alternatieve strategie om minimaal-invasief en pijnloos te vaccineren en daarmee antigeen-specifieke immuunresponsen op te wekken.

Verklarende woordenlijst

De termen zijn op alfabetische wijze vermeld en dienen in de context van de samenvatting van dit proefschrift gelezen te worden.

Absorptie	Het proces waarbij een stof wordt opgenomen door een poreus materiaal (bijvoorbeeld de opname van water door een spons).
Adsorptie	Het proces waarbij een stof hecht aan het oppervlak van een vaste stof (bijvoorbeeld het zuiveren van water met actieve kool).
Antigeen	Lichaamsvreemde stof (meestal eiwit van een ziekteverwekker), waartegen een immuunreactie opgewekt kan worden.
Antigeen-presenterende cellen	Cellen die antigenen opnemen om deze vervolgens te presenteren aan T-cellen van het immuunsysteem.
Antistof	Ook wel antilichaam of immunoglobuline genoemd; een eiwit geproduceerd door B-cellen dat bindt aan antigenen, van bijvoorbeeld ziekteverwekkers, om deze onschadelijk te maken.
B-cel (Bio)macromoleculen	Cel van het immuunsysteem die antistoffen produceert. Grote moleculen zoals eiwitten of polymeren. Het voorvoegsel 'bio' wordt gebruikt wanneer de moleculen een biologische oorsprong hebben.
Capillair	Een dun buisje.
Cold-chain	Het proces waarbij vaccins bij een optimale temperatuur (meestal +2°C tot +8°C) gekoeld, vervoerd, bewaard en gehanteerd worden van bereiding door de producent tot toediening aan de patiënt.
Diffunderen	Het proces waarbij stoffen zich verplaatsen van een gebied met een hogere concentratie naar een gebied met een lagere concentratie.
Ex vivo	In of op vers geïsoleerd levend weefsel van een organisme.
Fluorescentie	Een natuurkundig verschijnsel waarbij licht vrij komt uit aangeslagen moleculen. Eerst wordt een hoog-energetisch foton geabsorbeerd door een elcetron, waarna het in een aangeslagen toestand verkeert. Als het elektron terug valt in de grondtoestand wordt er een foton met lagere energie (dus met een andere kleur) uitgezonden. Fluorescentie wordt in de wetenschap onder andere gebruikt om stoffen (zoals vaccins) te visualiseren en te kwantificeren.

Formulering	De samenstelling van hulpstoffen van een medicijnpreparaat (bijvoorbeeld een tablet, drankje of injectievloeistof), waarin de werkzame stof stabiel is, een bepaald afgifteprofiel heeft (bijvoorbeeld directe afgifte of vertraagde afgifte) en geschikt is voor toediening.
Geometrie	De vorm; d.w.z. afmeting, lengte en verhouding van hoeken en vlakken van ruimtelijke figuren.
Immunoglobuline G	IgG; antistof die aan antigenen van ziekteverwekkers bindt om de afbraak daarvan te bevorderen.
In vivo	Op of in een levend organisme.
Infectieziekte	Een ziekte die veroorzaakt wordt door een bacterie, schimmel, virus of een parasiet.
Immunogeniciteit	Het vermogen van een antigeen om een immuunreactie op te wekken, bijvoorbeeld de aanmaak van antistoffen te stimuleren.
Immuunreactie	De afweerreactie van het lichaam tegen lichaamsvreemde antigenen.
Impact-insertie-applicator	Een applicator die micronaalden in de huid schiet met een gecontroleerde snelheid.
Intramusculair	In de spieren.
Iso-elektrisch punt	De pH-waarde waarbij een stof een netto lading van nul heeft.
Micrometer	Een tienduizendste ($1/10.000$) van een centimeter.
Micronaalden array	Een oppervlakte waarop zich meerdere micronaalden bevinden.
Millimeter	Een tiende van een centimeter.
Minimaal-invasieve toediening	Een methode om geneesmiddelen toe te dienen en daarbij zo min mogelijk weefselschade aan te richten. Een injectienaald gaat bijvoorbeeld door alle lagen van de huid heen, dus ook door de bloedbanen en pijnreceptoren (invasief), terwijl micronaalden alleen in de bovenste laag van de huid prikken (minimaal-invasief).
Nanometer	Een tienmiljoenste ($1/10.000.000$) van een centimeter.
Ovalbumine	Een kippenei-eiwit dat in de wetenschap vaak als model antigeen gebruikt wordt om nieuwe vaccinatiestrategieën te testen.
pH	De zuurgraad.

pK_a	De zuurconstante; een kwantitatieve maat voor de sterkte van basen en zuren, waarmee de lading van het molecuul bij een bepaalde pH-waarde berekend kan worden.
Subcutaan	Onder de huid.
Systemische infectie	Een infectie waarbij de ziekteverwekker zich door het hele lichaam verspreidt.
T-cel	Cel van het immuunsysteem dat voor een cellulaire immuunreactie zorgt.
Toedieningsroute	De plaats in het lichaam waar het medicijn gegeven/toegediend wordt; hoe het medicijn het lichaam binnen komt.
(Trans)dermaal	Het afgeven van medicijnen in de huid (dermaal) of door de huid heen naar andere delen van het lichaam (transdermaal).
Herformuleren	Het veranderen van de samenstelling van de hulpstoffen van een medicijn formulering.
Vaccinatie	Algemene beschrijving voor het onvatbaar maken tegen (infectie)ziekten.
Vaccinatiegraad	Het percentage van een populatie dat gevaccineerd is tegen een bepaalde ziekte. Als meer dan 90% van de bevolking gevaccineerd is, dan wordt de verspreiding van een ziekteverwekker door de overige 10% geneutraliseerd.

CURRICULUM VITAE

Koen van der Maaden was born on the 23rd of January 1985 in Bergen op Zoom. After graduating from the Titus Brandsma Lyceum in Oss in 2004, he started his study Pharmacy at Utrecht University where he obtained his Bachelor's degree in 2008. From 2008 to 2010 he studied Bio Pharmaceutical Sciences at Leiden University. During his study he did two internships. The first one, entitled "Development of small pDNA-containing liposomes for DNA vaccination", he performed at the Division of Drug Delivery Technology at the Leiden/Amsterdam Center for Drug Research (LACDR). Subsequently, he went to the University Medical Center Hamburg-Eppendorf (UKE) at the Division of Internal Medicine I and the Division of Experimental Immunology and Hepatology for his second internship, entitled "Immunoinformatics-based generation of high-affinity MHC class II peptide epitopes for hepatic auto-antigen expression in mice". In 2010 he obtained his Master's degree with honors (Cum Laude). In February 2010 he started his PhD project at the Division of Drug Delivery Technology under the supervision of Prof. Dr. Joke Bouwstra and Prof. Dr. Wim Jiskoot, which resulted in this thesis. In March 2014 he started as a postdoc at MyLife Technologies, performing his research at Intravacc, working on microneedle-based vaccination *via* porous microneedle arrays.

List of publications

1. **K. van der Maaden**, E. Sekerdag, P. Schipper, G. Kersten, W. Jiskoot, J. Bouwstra, Layer-by-layer assembly of inactivated poliovirus and N-trimethyl chitosan on pH-sensitive microneedles for dermal vaccination, submitted.
2. E.M. Varypataki, **K. van der Maaden**, F. Ossendorp, J. Bouwstra, W. Jiskoot, Cationic liposomes loaded with a synthetic long peptide and poly(I:C): a defined adjuvanted vaccine for induction of antigen specific T-cell cytotoxicity, *The AAPS Journal*, in press.
3. **K. van der Maaden**, E.M. Varypataki, S. Romeijn, F. Ossendorp, W. Jiskoot, J. Bouwstra, Ovalbumin-coated pH-sensitive microneedle arrays effectively induce ovalbumin-specific antibody and T-cell responses in mice, *European Journal of Pharmaceutics and Biopharmaceutics*, in press.
4. **K. van der Maaden**, E.M. Varypataki, H. Yu, S. Romeijn, W. Jiskoot, J. Bouwstra, Parameter optimization toward an optimal efficiency of the ‘poke and patch’ microneedle application method for dermal vaccination, *European Journal of Pharmaceutical Sciences*, 64 (2014) 18-25.
5. **K. van der Maaden**, E. Sekerdag, W. Jiskoot, J. Bouwstra, Impact-insertion applicator improves reliability of skin penetration by solid microneedle arrays, *The AAPS Journal*, 16 (2014) 681-684.
6. **K. van der Maaden**, J. Tomar, W. Jiskoot, J. Bouwstra, Chemical modifications of silicon surfaces for the generation of a tunable surface isoelectric point, *Langmuir*, 30 (2014) 1812-1819.
7. **K. van der Maaden***, S.J. Trietsch*, H. Kraan, E.M. Varypataki, S. Romeijn, R. Zwier, H.J. van der Linden, G. Kersten, T. Hankemeier, W. Jiskoot, J. Bouwstra, Novel hollow microneedle technology for depth-controlled microinjection-mediated dermal vaccination: a study with polio vaccine in rats, *Pharmaceutical Research*, 31 (2014) 1846-1854.
8. **K. van der Maaden**, S.J. Trietsch, H.J. van der Linden, J. Bouwstra, T. Hankemeier, Process and Device for Minimally Invasive Deep Tissue Probing, patent number WO/2014/092566 (2014).
9. **K. van der Maaden**, N.R. Tas, W. Jiskoot, J. Bouwstra, Process to coat an active agent to a surface, patent number WO/2013/036115 A1 (2013).
10. **K. van der Maaden**, H. Yu, K. Sliedregt, R. Zwier, R. Leboux, M. Oguri, A. Kros, W. Jiskoot, J. Bouwstra, Nanolayered chemical modification of silicon surfaces with ionizable surface groups for pH-triggered protein adsorption and release: application to microneedles, *Journal of Materials Chemistry B*, 1 (2013) 4466-4477.
11. **K. van der Maaden**, K. Sliedregt, A. Kros, W. Jiskoot, J. Bouwstra, Fluorescent nanoparticle adhesion assay: a novel method for surface pKa determination of self-assembled monolayers on silicon surfaces, *Langmuir*, 28 (2012) 3403-3411.
12. **K. van der Maaden**, W. Jiskoot, J. Bouwstra, Microneedle technologies for (trans)dermal drug and vaccine delivery, *Journal of Controlled Release*, 161 (2012) 645-655.
13. M.G. Carstens, **K. van der Maaden**, D. van der Velden, T.H.M. Ottenhoff, C.J. Melief, F. Ossendorp, J.A. Bouwstra, W. Jiskoot, Evaluation of the high-pressure extrusion technique as a method for sizing plasmid DNA-containing cationic liposomes, *Journal of Liposome Research*, 21 (2011) 286-295.

*Authors contributed equally

DANKWOORD

Ik kan me nog goed herinneren toen ik zes en half jaar geleden bij DDT in Leiden begon. Ik ging samen met Jonathan, een studiegenoot Farmacie (Universiteit Utrecht), naar Wim om te vragen wat voor onderzoeksprojecten hij had. Eén van de onderzoeksprojecten sprak mij erg aan, het formuleren van DNA in lipide nanodeeltjes, onder begeleiding van Myrra. Tijdens dit project heb ik heel veel van haar geleerd en werd ik zeer geënthousiasmeerd voor het onderzoek. Nadat ik een jaar weg was geweest voor een stage in het buitenland ben ik terug naar Leiden gekomen voor mijn promotieonderzoek. Hier heb ik vier jaar lang erg veel leuke en interessante experimenten kunnen doen in een gezellige omgeving. Tijdens een promotietraject sta je er gelukkig niet volledig alleen voor. Er zijn vele mensen geweest die mij geholpen hebben en/of waar ik goede discussies mee gevoerd heb. Ook al wil ik iedereen bedanken die mij heeft bijgestaan tijdens deze vier jaar (vrienden, naaste familie, bandleden, etc.), beperk ik mij hier tot de mensen die direct wetenschappelijk hebben bijgedragen aan dit proefschrift en hoop dat ik daarbij niemand vergeet.

Firstly, I thank Marilena (Eleni), you were my partner in research and I doubt if I would have managed this much without you. We did almost all our *in vivo* experiments together, including the analysis by ELISA (sometimes 60 plates per day!) or by FACS. During the last animal studies of my PhD research we worked from the early mornings till late in the evenings for several months to finish all our experiments. We both shared the frustration (escaping or biting mice; power failure during surgery; broken FACS machines...) but also many fun times (for example, when we were drawing cartoons or got mummified when we had to wait for two hours for the animals to wake up) as well as the excitement and happiness when we obtained good results. I am also very glad that you are my Paranympth to stand at my side during my defense.

Stefan, jij bent altijd zeer bescheiden geweest, maar ook belangrijk voor het tot stand komen van dit proefschrift. Jij stond altijd klaar om mij te helpen en hebt ook bij elke *in vivo* studie (soms tot in de avonduren) geholpen. Ook hebben we vaak gediscussieerd over van alles en nog wat. Bedankt!

Ook mag ik Raphaël niet vergeten voor alle keren dat ik met spoed naar hem ben gegaan om een apparaat aan te passen of om pleisters/reservoirs te maken voor microneedlebehandelingen. Ook

door de goede samenwerking met jou, de discussies over chemisch inerte materialen en het ontwerpen en ontwikkelen van onder andere coatingsapparaten en micronaald-applicatoren zijn mijn studies goed verlopen.

Daarnaast wil ik Karen bedanken voor alle keren dat ze mij geholpen heeft met de (oppervlak)chemie. Ik heb in het begin van mijn promotieonderzoek veel van jou geleerd, en heb in mijn proefschrift uiteindelijk vijf hoofdstukken gewijd aan de (oppervlak)chemie.

Verder wil ik Jaques niet vergeten voor de hulp en uitleg van de ellipsometer en de leuke koffiemomenten. Aansluitend wil ik respectievelijk Alexander en Gideon bedanken voor het kritisch lezen van de eerste oppervlakchemie- en polio hoofdstukken, Ferry Ossendorp voor de FACS discussies en Robert Poole voor zijn hulp met de NMR-analyse. Ook wil ik Jeroen bedanken voor zijn hulp met de statistiek van de proefdierstudies en de gezellige pauzemomenten.

Also, I would like to mention the four Master students (Huixin, Jasmine, Emine, and Romain) who did their research internship under my supervision and contributed to five of my chapters.

Ook wil ik Bas en Heiko apart vermelden. Onze goede samenwerking heeft geleid tot een gezamenlijke publicatie. Ik denk met vreugde terug aan de avond dat we onze eerste holle micronaald gefabriceerd hadden (die we vervolgens op de grond terug moesten zoeken), wat we daarna gingen vieren met een maaltijd en wat biertjes.

Pim, ik ken je al heel lang (vanaf de eerste dag van het introductiekamp van de studie Farmacie). We kwamen daar allebei als een van de laatste aan voor het eten, omdat we er niet van houden om in een rij te staan wachten. We werden goede vrienden en hebben de afgelopen tien jaar veel samen meegemaakt, geleerd en gediscussieerd. Ik ben dan ook zeer verheugd dat jij aan mijn zijde staat als Paranimf tijdens de verdediging van mijn proefschrift.

Connie, jij zorgt er altijd voor dat afspraken goed geregeld zijn en als er een probleem is (zoals de helpdesk bijvoorbeeld) dat er actie ondernomen wordt. Ook zorg jij dat de kleine dingetjes, zoals formulieren/handtekeningen voor publicaties, zaken omtrend mijn promotie, goedkeuring van bestellingen/declaraties die te lang op zich laten wachten, geregeld worden en had je altijd een luisterend oor (en een goede kop koffie).

Verder wil ik iedereen van DDT bedanken voor de kritische vragen en opmerkingen tijdens presentaties en koffie- en lunchpauzes en de goede tijd die ik de afgelopen vier jaar tijdens mijn promotieonderzoek heb gehad.

Daarnaast wil ik Tim bedanken voor alle tijd en moeite die hij genomen heeft om dit proefschrift er zo mooi, stijlvol en uniek uit te laten zien.

Ten slotte mag Hanna hier niet ontbreken. In het laatste jaar was ik vaak in de avonden en weekenden of op het lab aan het werk of zat ik thuis alleen maar gefocust achter mijn laptop te schrijven. Naast dat je hebt meegholpen/meegedacht met de opmaak van enkele plaatjes en figuren van mijn proefschrift, ben ik zeer dankbaar dat je mij altijd gesteund hebt.

4-FBDA	4-formyl-1,3-benzenedisulfonic acid disodium salt
4-PCA	4-pyridinecarboxaldehyde
AFM	atomic force microscopy
APTES	(3-aminopropyl)triethoxysilane
AR	analytical grade reagent
BSA	bovine serum albumin
CD	circular dichroism
CLSM	confocal laser scanning microscopy
CMC	carboxymethylcellulose
CPTA	(3-carboxypropyl)trimethylammonium chloride
DCC	N,N'-dicyclohexylcarbodiimide
DLS	dynamic light scattering
EDTA	ethylenediaminetetraacetic acid
ELISA	enzyme-linked immunosorbent assay
FNAA	fluorescent nanoparticle adhesion assay
H&E	hematoxylin and eosin
HEPES	(4-(2-hydroxyethyl)-1-piperazineethanesulfonic acid
HPLC	high-performance liquid chromatography
HRP	horseradish peroxidase
i.d.	intradermal
i.m.	intramuscular
IMDM	Iscove's modified Dulbecco's medium
IPV	inactivated polio vaccine
IR	infrared
LbL	layer-by-layer
LU	Leiden University
MEA	Microenhancer array
MQ	deionized water produced by a Millipore water purification system
NHS	N-hydroxysuccinimide
OPV	oral polio vaccine
PBS	phosphate buffered saline
PCPP	poly[di(carboxylatophenoxy)phosphazene]
PCTFE	polychlorotrifluoroethylene
PDI	polydispersity index
PE	penetration efficiency
PEM	polyelectrolyte multilayer
pI	isoelectric point

PLGA	poly(lactic-co-glycolic acid)
POM	polyoxymethylene
PTH	parathyroid hormone
rhGH	recombinant human growth hormone
rpHPLC	reversed-phase HPLC
s.c.	subcutaneous
SA	succinic anhydride
SAM	self-assembling monolayer
sIEP	surface isoelectric point
SC	stratum corneum
SEM	scanning electron microscopy
THF	tetrahydrofuran
TMB	3,3',5,5'-tetramethylbenzidine
TMC	N-trimethyl chitosan chloride
UN	U-Needle
VN	virus neutralizing